Assessment and Mitigation of Overheating Risks in Archetype and Existing Canadian Buildings under Recent and Projected Future Climates

Fuad Baba

A Thesis

In the Department

of

Building, Civil & Environmental Engineering

Presented in Partial Fulfillment of the Requirements

For the Degree of

Doctor of Philosophy (Building Engineering) at

Concordia University

Montreal, Quebec, Canada

July 2022

CONCORDIA UNIVERSITY

This is to certify that the thesis prepared

By: Fuad Baba

Entitled: Assessment and Mitigation of Overheating Risks in Archetype and Existing Canadian Buildings under Recent and Projected Future Climates

and submitted in partial fulfillment of the requirements for the degree of

Doctor of Philosophy (Building Engineering)

complies with the regulations of the University and meets the accepted standards concerning originality and quality.

Signed by the final examining committee:

Dr. Sebastien Le Beux	Chair
Dr. Zhiqiang (John) Zhai	External Examiner
Dr.Pragasen Pillay	External-to-program Examiner
Dr.Radu Zmeureanu	BCEE Examiner
Dr. Ali Nazemi	BCEE Examiner
Dr. Hua Ge	BCEE Supervisor

Approved by

Dr. Mazdak Nik-Bakht, Graduate Program Director

07/7/2022

Dr. Mourad Debbabi, Dean

Gina Cody School of Engineering and Computer Science

ABSTRACT

Assessment and Mitigation of Overheating Risks in Archetype and Existing Canadian Buildings under Recent and Projected Future Climates

Fuad Baba, Ph.D.

Concordia University, 2022

This research aims to develop a framework to assess and mitigate the overheating risks under projected future climates for both archetype and existing buildings. More specific objectives are to 1) determine the contribution and correlation of individual building envelope parameters to the change in indoor temperature in conjunction with ventilation, therefore, to determine whether high energy-efficient buildings required by Canadian building codes to reduce heating consumption in new buildings are at lower or greater overheating risk compared to old buildings; 2) develop an automated calibration procedure to calibrate a building simulation model based on the indoor hourly temperature to achieve high accuracy to be used overheating studies in existing buildings; 3) assess overheating risks under current and future extreme years and recommend effective mitigation measures; and 4) provide an optimal design for retrofitting existing buildings to achieve lowest heating energy demand and highest thermal and visual comfort in new building design. To achieve these objectives, a robust sensitivity analysis (SA) and calibration method, a systematic framework for evaluating overheating and passive mitigation measures, and an optimization methodology are developed and applied to an archetype detached house and existing school buildings.

The results showed that the archetype and existing Canadian buildings have experienced overheating under current climates and the overheating risks will increase dramatically under future climates. Due to the positive contribution of lower U-values of windows, walls, and roofs and SHGC, high energy-efficient houses have a lower overheating risk than old buildings if adequate ventilation (>2.2 ACH) is provided. Natural ventilation in the high energy-efficient house is sufficient to reduce the overheating risk under the recent climate but will require adding interior and exterior shading under future climates. For existing school buildings, the calibrated model achieved high accuracy. The results also showed that the use of exterior blind roll or a combination of night cooling and other mitigation measures that reduce solar heat gain is required under the recent climate and adding a cool roof will be required in future extreme years. For optimization design, the applied optimization methodology can generate several optimal building design solutions based on Window-Wall-Ratio.

Acknowledgements

During my Ph.D. studies, many people generously helped and supported me. I would first like to thank my supervisor, Dr. Hua Ge, who has been a role model of endless learning, research, and perseverance. Dr. Ge did not skimp on any support, assistance, or guidance during my period of work with her, she also provided me with many job opportunities to develop my knowledge and skills by joining many research projects, workshops, and conferences. There are not enough words to thank her for her wonderful efforts, cooperation, patience, support, and excellent work ethic with me. This quality can be demonstrated by my outstanding research productivity in terms of journal publications, conferences, and technical reports. Up to now, I have with Prof. Hua more than 15 published papers

I would also like to thank Dr. Leon Wang and Dr. Radu Zmeureanu for their efforts in supervising the project "*Assessment and Mitigation of Summertime Overheating Conditions in Vulnerable Buildings of Urban Agglomerations*", Which was a major part of my Ph.D. thesis. Through our bi-weekly meetings, Dr. Wang, and Dr. Zmeureanu, who have excellent academic and research capabilities, have contributed to increasing my scientific knowledge, improving my research performance, and developing my analytical capabilities. I also appreciate all of my colleagues and friends who worked with me on this project.

I would like to thank my family, my parents, my wife, my children, brother, sisters, and friends, who have stood by me and supported me " **Without you, nothing would be possible**". This success is your success and the fruit of your hard work all these years. Thank you with all my heart

I would like to acknowledge the financial support from the FRQNT scholarships, the Natural Sciences and Engineering Research Council (NSERC) of Canada through the Advancing Climate Change Science in Canada Program, the NSERC Discovery Grant, and the Gina Cody School of Engineering and Computer Science of Concordia University.

TABLE OF CONTENT

LIST OF FIGURES

LIST OF TABLES

NOMENCLATURE

CV(RMSE)	Coefficient of Variation Of Root-Mean-Square Error (%)
He	Hours of Exceedance (hr)
MAD	Maximum Absolute Difference (°C)
N_m	Minimum number of samples
NMBE	Normalized Mean Bias Error (%)
N_r	Number of samples required to achieve a sum of sensitivity indices equal to 1,
RMSE	Root-Mean-Square Error (°C)
S_{Ti}	Total-order Sensitivity Index for a parameter
$\overline{T_m}$	Average of a number of n observations (°C)
T_{mrt}	Indoor hourly mean radiant temperature of the zone (°C)
T_{op}	Indoor operative temperature (°C)
$T_{pma(out)}$	Prevailing mean outdoor air temperature of seven days
T_r	Indoor hourly air temperature (°C)
T_s	Indoor simulation temperature data (°C)

T_{upp}	Upper Limit Temperature (°C)
V(Y)	Total variance of the model output (variance of all parameters with all interactions)
$V_{X\sim i}$	Measures the effect of all parameters except a parameter X_i on the model output.
We	Daily Weighted Exceedance (°C/day)

ABBREVIATION

AL	Acceptable Limit
ANOVA	ANalysis Of VAriance
AOS	Accurate Optimal Solutions
BEP	Building Envelope Parameters
CMIP	Coupled Model Inter-comparison Project
FOS	Final Optimal Solution
GCM	Global Climate Model
GSA	Global Sensitivity Analysis
HEEB	High Energy-Efficient Buildings
LSA	Local Sensitivity Analysis
MBCn	Multivariate Bias Correction-Normal probability density function
MM	Mitigation Measures
MOGA	Multi-objectives Genetic Algorithm
NV	Natural Ventilation
OAT	One-At-a-Time

OB	Old Buildings
OR	Overheating Risk
PDF	Probability Density Function
RCM	Reginal Climate Model
RCP	Representative Concentration Pathways
RSWY	Reference Summer Weather Year
SI	Sensitivity Indices
WOFA	Window Opening -To-Floor Area

CHAPTER 1: INTRODUCTION

1.1 BACKGROUND

With continuous human activities, the world has been becoming hotter over time. Statistics show that the average global temperature on Earth has increased by about 0.8 ° C since 1880 (GISS, 2022). Two-thirds of this warming has occurred since 1975, with an average of 0.15-0.20 °C per decade. According to NASA's Goddard Institute for Space Studies (GISS, 2022), the global mean temperatures are rising faster with time, and the hottest four years were 2016, 2020, 2019 and 2017 respectively. Also, 17 out of the 18 warmest years in the 136 years' records were since 2001. According to the latest IPCC AR6 Report (2022), the Earth's surface temperature is expected to continue to rise until at least mid-century under all emissions scenarios. The Earth's surface temperature will rise by 1.5°C to 2°C during this century unless there are significant reductions in emissions of carbon dioxide and other greenhouse gases in the coming decades. With a global surface temperature rise of 1.5°C, 14% of the world's population will experience extreme heatwaves at least once every five years and about 40% of the world's population if the global temperature rise reaches 2°C (IPCC, 2022).

Across Canada, climate change has an even greater impact with the average annual temperature has risen by 1.7 ° C since 1948, more than twice the global average temperature rise. Similarly, the average annual rainfall has increased by 30% in the northernmost regions of Canada (Zhang et al., 2019). In 2021, British Columbia-Canada recorded the highest ever temperature of 49.6 °C in Lytton city (Uguen-Csenge and Lindsay, 2021). In May 2020 and in July 2018, Quebec-Canada recorded the hottest day (36.6°C) since records began 147 years ago in Montreal (The Weather Network, 2020). In 2018, 2020 and 2021, the province of British Columbia issued an emergency warning after hundreds of wildfires that destroyed buildings and forced people out of their homes because of high temperatures (British Columbia, 2021).

Despite the different definitions, the heatwave is usually measured according to the usual weather in the region and relative to the average seasonal temperatures (IPCC, 2012). According to the World Health Organization (WHO) (McGregor et al., 2015), a heatwave is a period (typically three to five consecutive days) when the daily maximum temperature is higher than the average daily maximum temperature by 5°C in reference to the historical norm throughout 1961-1990. In the

U.K., the heatwave is defined as the period when the temperature reaches the threshold temperatures in one or more regions on one day and the following night; and it is very likely (90% confidence) that temperatures on the next day will be above the daytime threshold (Public Health England, 2018). Environment Canada defines heatwaves as periods of at least three consecutive days during which temperatures reach or exceed 30 °C during the day (Li et al., 2018; Ville de Montréal, 2017).

In 2017, there were 18 million more people exposed to heatwaves than that in 2016 (Watts et al., 2018). Exposure to extreme heat increases the risk of death for those having pre-existing medical conditions (Watts et al., 2018). The danger of extreme heat to humans ranges from extreme thirst to death. Statistics indicate that excessive heat is responsible for more weather-related deaths than any other weather phenomenon such as hurricanes or tornadoes (NOAA, 2020; Gagnon, et al., 2015; Borden and Cutter, 2008). In 2021, British Columbia (BC) Chief coroner (Lapointe, 2021) reported that during the heatwave period from June 23-30, 570 out of 815 (70%) sudden deaths were related to extreme heat. They also confirmed that 79% of them were 65 years of age or older and that some of them died in their chair in the living room without opening the windows, as the indoor temperature reached 35 °C (Lapointe, 2021). In 2018, the regional director of public health in Montreal-Canada (Drouin, 2018) confirmed that during the heatwave from June 30 to July 8, there were 66 heat-related sudden deaths and 88% of them died in their homes. In 2010, Quebec province-Canada was struck by high temperature and heatwaves in July and August with daily maximum and minimum temperatures of 31-33 °C and 16-20 °C, respectively, over 4 to 6 days (Lebel et al., 2017). These heatwaves increased the excess deaths above 1360 for the province, with 383 in Montreal (Lebel et al., 2017). In the summer of 2009, British Columbia was hit by an eight-day heatwave with temperatures increasing to 34.4 °C causing 90 heat-related deaths (Kosatsky, 2010). In the summer of 2005, Toronto experienced 41 hot days with temperatures exceeding 30°C in 30 days causing 60 heat-related deaths (HC, 2011b). In European countries, the consequences of rising temperatures under future climate could be more devastating than the European heatwave that occurred in August 2003, which led to 70,000 additional deaths compared to the reference period 1998-2002 (Robine et al., 2007). Due to climate change, the number of deaths resulted from excessive heat could be three times higher by 2050 than in 2003 (Zero Carbon Hub, 2015). Public Health England (2015) predicts that European summer 2003 temperatures may become the norm by the 2040s. In the United States, excess heat is responsible for the highest

number of deaths between 1992 and 2001, with 2190 deaths compared with 880 deaths from floods and 150 deaths from hurricanes (Basu and Samet, 2002).

Mora et al. (2017) studied 1949 mortality cases in 164 cities in 36 countries from 1980 to 2014. They found the relation between the mean daily air temperature, relative humidity, and lethal heat events, as shown in Figure 1-1. "Lethal" is used when referring to climatic conditions that cause excess human death (mortality), and "Deadly" is used when referring to the climatic conditions that are expected to cause death.

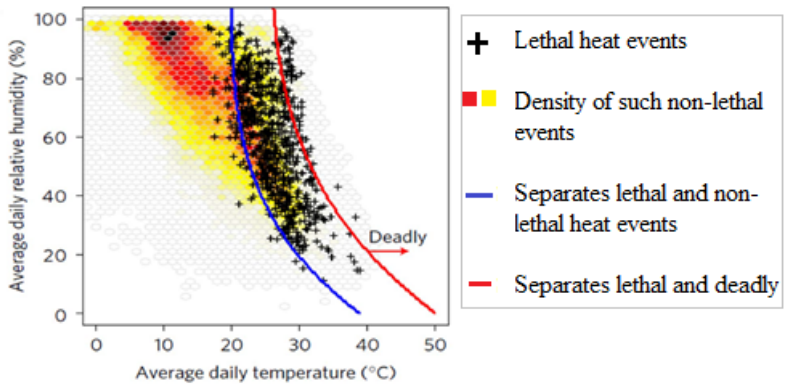

Figure 1-1. Mean daily air temperature and relative humidity during lethal heat events (Mora et al., 2017)

Since we spend more than 65-90% of our time in buildings (Klepeis et al., 2011; Leech et al., 2002), the main impact of climate change will be on the occupants of buildings. Therefore, the literature review focuses on the impact of climate change on the thermal condition and comfort of residential buildings.

1.2 RESEARCH OBJECTIVES

The indoor overheating risk during the summer may increase in cold climates, such as Canada, where the buildings are designed for the heating season only with the cooling or mechanical ventilation being not required by building codes. Statistics Canada showed that in 2020, 61% of residential buildings and 75% of commercial buildings have air conditioning (Statistics Canada, 2021a), while in 2012, 42% of residential buildings and 69% of commercial buildings had air conditioning (NRCa/n, 2012 and 2013). The excessive use of air conditioning in buildings to

reduce overheating under heatwave events could cause sudden power outages, which in turn will exacerbate the overheating and health risks of occupants (Ville de Montréal, 2017). The problem of overheating will be more severe if occupants are elderly, children, or suffering from pre-existing health problems. In 2021, over 18.5% of Canada's population were aged 65 or older (Statistics Canada, 2021b). By 2030, is expected that there will be 9.5 million seniors, which is 23% of Canadians(Government of Canada, 2021b).

To safeguard the public's health and safety under the changing climates and mitigate the effect of climate change, the Canadian government is making efforts to include climate change in the upcoming building codes. Buildings built or retrofitted today need to be designed and optimized based on projected future climates but not the historical data. The thermal conditions of buildings over the next 50-year need to be evaluated to ensure acceptable indoor conditions to avoid thermal discomfort and heat-related health issues. Buildings also need to be adaptive to climate change and remain resilient under extreme weather conditions. There is limited research on evaluating the indoor thermal conditions of buildings under projected future climates within a Canadian context. To address the knowledge gap, this thesis aims to achieve five objectives:

1) determine the contribution and correlation of individual building envelope parameters to the change in indoor temperature in conjunction with ventilation, therefore, determine whether high-energy-efficient buildings required by Canadian building codes to reduce heating consumption in new buildings are at lower or higher risk of overheating compared to old buildings
2) develop an automated calibration procedure to calibrate a building simulation model based on the indoor hourly temperature to achieve high accuracy so that the building model can be used to assess indoor overheating risks in existing buildings
3) assess overheating risks under recent and future extreme years
4) provide recommendations on effective mitigation measures under recent and future extreme years
5) provide the optimal design for retrofitting existing buildings to achieve the lowest heating energy demand and highest thermal and visual comfort in new building design.

1.3 OUTLINE OF THE THESIS SCOPE

This thesis is organized into five chapters with chapter 1 introducing the context and research objectives.

Chapter 2 includes a detailed review of previous studies on: 1) the effect of building envelope parameters on indoor overheating risk studies using sensitivity analysis (Section 2.1); 2) calibration methods used to calibrate the building simulation model based on field monitored data (Section 2.2); 3) the overheating studies using either indoor simulation or measured data, thermal comfort criteria that are used to determine indoor overheating risks, future climate generation scenarios and methods, and methods for detecting the future reference summer year (Section 2.3), 4) mitigation measures for reducing the overheating risks (Section 2.4); and 5) optimization strategies to achieve lowest heating energy demand and highest thermal and visual comfort in new building design. At the end of this chapter (Section 2.5), a summary identifying the research gaps and research questions is provided (Section 2.6).

Chapter 3 presents the developed methodologies and master frameworks to achieve the main objective of this research work, which is to assess the overheating risks and develop effective mitigation measures under recent and projected future climates for both archetype (Section 3.1) and existing buildings (Section 3.2). More specific objectives are described in 1) Section 3.1.1: a sensitivity analysis methodology that is developed to find the contribution of each building envelope parameters to the change of indoor temperature; 2) Section 3.2.1: a robust automated calibration methodology that is developed to calibrate a building simulation model based on the indoor hourly temperature with high accuracy; 3) Sections 3.1.3 and 3.2.3: thermal comfort criteria that are used to assess overheating risk in both archetype and existing buildings respectively, and methods that are used to generate the future weather data and to select future reference summer weather years (extreme years); 4) Sections 3.1.4 and 3.2.4: the mitigation measures that are evaluated to improve indoor thermal comfort in summer for both archetype and existing buildings; and 5) Section 3.2.5: optimization strategies developed by applying a multi-objective genetic algorithm to generate optimal building design solutions considering heating energy efficiency, summer thermal comfort and visual comfort in building design At the end of this chapter, a summary table of all simulation scenarios (Section 3.3) is provided.

Chapter 4 presents the results of these frameworks and methodologies that have been developed and applied to an archetype detached house (Section 3.1) and an existing school building (Section 3.2) in Montreal. An extensive discussion of the findings and recommendations is also provided. Chapter 5 is the conclusion and future work.

CHAPTER 2: LITERATURE REVIEW

2.1 SENSITIVITY ANALYSIS OF BUILDING ENVELOPE PARAMETERS

Greenhouse gases (GHG) are one of the main causes of climate change (UN-Environment, 2017). The building sector produces 39% of greenhouse emissions in the world and 23% in Canada (UN-Environment, 2017). Therefore, governments have been increasing their efforts to make all new buildings to be net-zero energy, such as Canada (BC Energy Step Code, 2018), the European Union (EU) (2022), USA (Nadel, 2020) through the use of a high energy-efficient building envelope, especially in cold climate zones. However, the trend toward a high energy-efficient building envelope may increase the overheating risk in buildings as concluded by previous studies (BC Housing, 2019; Maivel et al., 2015; Ibrahim and Pelsmakers, 2018; Goia et al., 2015; Hooff et al., 2014; Peacock et al., 2010; Stazi et al., 2010; Psomas et al., 2017). BC (British Columbia-Canada) Energy Step Code (BC Housing, 2019), which incentivizes or requires a high level of energy efficiency in new construction, predicted that the high wall and roof thermal insulation and/or high building airtightness increase indoor overheating by retaining internal heat gain. Maivel et al. (2015) conducted field measurements of indoor temperatures in more than 100 Estonian apartments for three months. They found that the average room temperature in the new buildings was consistently 1ºC higher than that in the older buildings, and there was no overheating in the old residential buildings, while 14% of apartments in new buildings suffered from overheating. They indicated that the reason might be a larger glazing area in new buildings (Maivel et al., 2015). Ibrahim and Pelsmakers (2018) studied the summer thermal comfort of an existing residential building, which uses mechanical ventilation (MV) (0.9 ACH) to improve the indoor thermal condition in winter and summer, before and after retrofit in northern England in 2018 and future climate through simulations. They found that increasing the wall's thermal resistance would increase the overheating risk, while reducing the window SHGC would reduce the overheating risk. However, increasing the roof thermal resistance would not have a significant effect on the risk of overheating. They also found that the future climate has a greater impact on Passive House (PH), where the overheating increased by up to 100% compared to the pre-retrofit house (Ibrahim and Pelsmakers, 2018). Goia et al. (2015) studied the effect of the wall thermal resistance level on the overheating risk in a Norwegian detached single-family house that relied on 0.8 ACH to ventilate the building in summer. They found that increasing the wall thermal resistance would

increase the overheating risk in summer. Similar results were obtained by Hooff et al. (2014) Peacock et al. (2010) in the cold climate and Chvatal et al., [33], Stazi et al. (2010) and Psomas et al. (2017) in the Mediterranean climate.

Baniassadi and Sailor (2018) studied the effect of a high wall/window thermal resistance and the window's SHGC on the temperature of a single-family detached house in Houston and Phoenix (warm and hot climate) in the USA in summer with fixed and movable windows providing 4.8 ACH natural ventilation (NV). In contrast to the results presented before, they found that with movable windows, the use of high energy-efficient walls and windows was more beneficial to provide passive survival and improve indoor temperature compared to a low energy-efficient house that rapidly reached dangerous levels during heatwave events. But with fixed windows, the overheating risk in a high energy-efficient house is lower than in a low energy-efficient house. Fosas et al. (2018) tried to identify parameters that have a significant effect on the indoor overheating risk including building location, thermal mass, building envelope insulation level (all building envelope parameters are changed at the same time), infiltration, shading, window wall ratio and with 1.5 ACH ventilation rate in cold and warm climates. They found that the insulation level would reduce the risk of building overheating but not have a significant effect on indoor overheating as the location of a building, orientation or infiltration rate. However, they did not study the significance or contribution of each building envelope parameter to the change in indoor overheating, or whether the ventilation rate affects the thermal performance of building envelope parameters.

Table 2-1 provides a summary of studies reported in the literature on the effect of building envelope thermal characteristics on indoor overheating risk. The building envelope parameters (BEP), climate, ventilation type and rate and the results of each study are listed in Table 2-1. Except for reference (Fosas et al., 2018) which uses the regression sensitivity analysis method (RSA), all references use the One-At-Time local sensitivity analysis (OAT). In addition, all references in Table 2-1 used NV as a constant without any specific schedule except for Hooff et al. (2014), which used the Airflow Network method to calculate the ventilation rate and used 24 °C as the natural ventilation setpoint to open the windows. No shading devices were included in these studies

Table 2-1. Previous studies related to the effect of building envelope parameters (BEP) on indoor overheating

References	BEP studied	Climate	Ventilation type and rate	Results
Ibrahim and Pelsmakers (2018), Goia et al. (2015), Hooff et al. (2014)	Wall U-value	Cold climate	NV constant (0.8-0.9ACH)	Low wall U-value increases overheating
Ibrahim and Pelsmakers (2018),	- Roof U-value - Window SHCG	Cold climate	MV constant (0.9ACH)	- Low roof U-value had a negligible effect. - Low SHGC reduces overheating
Chvatal et al. (2009), Stazi et al. (2010)	Wall U-value	Warm climate	NV constant (0.7-0.8ACH)	Low wall U-value increases overheating
Baniassadi and Sailor (2018)	- Wall U-value - Window U-value - Window SHCG	Hot climate	NV constant (4.8 ACH)	- Low wall and window U-values reduce overheating - Low SHGC reduces overheating
Fosas et al. (2018)	Building envelope U-value	Warm and Cold climate	NV constant (1.5 ACH)	Low U-value reduces overheating.

As shown in Table 2-1, previous studies (Maivel et al., 2015; Ibrahim and Pelsmakers, 2018; Goia et al., 2015; Chvatal et al., 2009; Hooff et al., 2014; Peacock et al., 2010; Stazi et al., 2010; Psomas et al., 2017; Baniassadi and Sailor, 2018; Fosas et al.,2018) examined the effect of increasing the thermal performance of some building envelope parameters, such as the U-value of the wall and SHGC of the window, on the indoor temperature using the local sensitivity analysis method (it is discussed in more details in Section 2.1.1) that can help determine the importance of each parameter. This method is one of the most commonly used, simple, and has the least computational time and cost (Delgarm et al., 2018). However, this method cannot determine the effect of

changing several input parameters simultaneously on the change in indoor temperature. Most previous studies (Ibrahim and Pelsmakers, 2018; Chvatal et al., 2009; Fosas et al.,2018; Baniassadi and Sailor, 2018) showed that the effect of the building envelope parameters on indoor overheating risk is not influenced by the exterior climatic conditions. As shown in Table 2-1, these studies all had a low ventilation rate of less than 1 ACH, while with a ventilation rate of 1.5 ACH (Fosas et al., 2018), the low wall U-value reduced overheating but the impact of it was small. Reference (Baniassadi and Sailor, 2018) studied the effect of building envelope thermal characteristics with varying ventilation rates and different conclusions were arrived depending on the different levels of ventilation rates. The question is whether the ventilation rate has an interactive effect on the thermal properties of the building envelope and does the contribution and correlation between building envelope parameters and indoor overheating risk change with the ventilation rate?

Sensitivity analysis methods can be divided into Local Sensitivity Analysis (LSA) and Global Sensitivity Analysis (GSA) (Saltelli et al., 2008). These methods are discussed in more detail in Sections 2.1.1 and 2.1.2, respectively.

2.1.1 Local Sensitivity Analysis

Local Sensitivity Analysis (Screening techniques) is a simplified approach to maintaining a small number of assessments at a computationally high speed. One of the simplest and most common approaches in LSA is One-At-a-Time (OAT) (Czitrom, 1999. In this method, the input parameters are changed one by one by keeping the other inputs fixed at a baseline and monitors changes in the output. Despite its simplicity, this approach does not fully explore the input space since it does not consider the simultaneous variation of input variables (Tian, 2013). Based on the OAT sampling method, Morris (Morris, 1991) developed an effective screening method called the Elementary Effects (EE) method. This method determines input factors that have direct and indirect essential impacts on the outputs by identifying several sequences of step-by-step parameter changes, which are called trajectories. The EE method classifies the input parameters into three different groups: 1) Negligible; 2) linear and additive effect; 3) non-linear and interaction effects, based on standard deviation (σ) and the mean value (μ). Screening approaches can provide a qualitative measure of the parameter arrangement according to their effect on the model outcome, but do not quantify exactly the relative importance of the input. It gives a quick look at the effect

of parameters with a small number of models, but it does not evaluate or distinguish between nonlinear effects. This approach is not valid for non-linear models. Global methods should be used instead. As a precursor to GSA, the Morris method may identify parameters that can be removed from the study (Campolongo et al., 2007; Tian, 2013).

2.1.2 Global sensitivity analysis

Global sensitivity analysis (GSA) has the ability to find the sensitive parameters and to determine the contribution of each input parameter by quantifying the variance of input parameters that caused all the variance of the output. It can also consider the interaction effects among parameters. Global sensitivity analysis can be found by the Regression-based method or Variance-based method. Regression methods are used for a linear regression model between input and output. Input variables can be set as random values from their potential range according to sampling techniques. Then each entry variable can be considered a vector, which contains random values, and random output values can be calculated accordingly. This method uses Standard Regression Coefficients SRC as direct measures of sensitivity (Iman and Helton, 1991). If the input variables are independent (uncorrelated), the absolute value of SRC provides a measure of the significance of the variable. The input parameter with a larger SRC has higher importance than that with a smaller SRC.

The sign of the SRC indicates whether the output variable increases (positive SRC) or decreases (negative SRC) with the corresponding input variable. Another indicator to find the linear regression analysis between inputs and output is the Partial Correlation Coefficient (PCC), which can be calculated based on the correlation coefficient (Helton, 1993). PCC refers to the linear relationship between one input and output after removing the non-linear effects of the remaining input variables on the output. To be reliable with PCC and SRC, the model must be linear. However, if the relations between input and output are nonlinear but monotonic, the Partial Ranked Correlation Coefficient and Standardized Ranked Regression Coefficient should be used to improve the linear relationship between the input and output (Helton and Davis, 2002). The regression method is most appropriate when the response of the model is indeed linear (linearity can be confirmed if the coefficient of determination "R squared" is close to one). However, this method cannot analyze the variance model's output to fractions to find the contribution of each

input variable to the output. The advantages of regression analysis are that it is simple and has a low computational cost.

Another form of global sensitivity analysis is called Variance-based sensitivity (Saltelli et al., 2008) which was derived from the ANalysis Of VAriance (ANOVA) technique (Sobol, 2001; Archer et al., 1997). Variance-based sensitivity is attractive because it measures sensitivity across the entire input area, as it can handle nonlinear and non-monotonic models, and the effect of interactions can be measured. The sum of the sensitivity indices will be equal to 1 when the model is purely additive, as there is no correlation between the input data (Rabitz, 2010). For that, sensitivity indices can be interpreted directly as percentages. The SOBOL method is one of the most common and effective methods developed to decompose the ANOVA technique for sensitivity analysis is the SOBOL method (Sobol, 2001; Xu and Gertner, 2011; Saltelli et al., 2008). SOBOL finds the sensitivity index for various inputs by calculating the "First-order Sensitivity Index" which essentially measures the contribution of one input to the variance in output, and the " Total-order Sensitivity Index " which gives the total uncertainty in output caused by one input and its interactions with any of the other input variables. Monte Carlo integration is used to calculate the SOBOL indices by evaluating the integrals in the decomposition.

Compared to local sensitivity analysis, there is a limited number of studies that have used this method, to explore the contribution of building parameters to the energy performance of buildings (Zeferina, et al., 2021; Tian et al., 2018; Shen and Tzempelikos, 2012; Burhenne et al., 2010; Hopfe et al., 2011) and thermal (Concalve et al., 2021; Yang et al, 2021). Burhenne et al. (2010) used a regression-based method with random sampling to analyze the influence of six parameters (natural ventilation, infiltration, temperature setpoint, the efficiency of the heat exchanger of the air handling unit, shading, and operating schedule for heating pumps) on the energy performance of the building. They found that the most significant influential input parameter was natural ventilation, followed by the temperature setpoint, and the pump operating schedule as the third most influential input. The effect of the rest was small. Hopfe et al. (2011) used a regression-based method with a Latin hypercube sampling technique to find the most influential parameters on the energy efficiency of buildings among six inputs; infiltration rate, internal gain (occupant, lighting, and equipment), room size, and window type. They concluded that the infiltration rate and room size had a greater effect on the energy performance of buildings. Garcia Sanchez et al. (2012) tried

to classify 24 building parameters into three Morris groups (Morris, 1991). They found that all parameters are non-linear influences and/or interactions with other parameters (the third group in Morris classification), except occupant load (linear). Setpoint temperature, ventilation rate, and insulation thickness can be classified as significant influences, while occupants' load, solar gains, and surrounding climate can be classified as secondary but non-negligible (Garcia Sanchez et al., 2012).

There are minimal studies that attempt to find building parameters that have a significant impact on indoor summer thermal conditions through sensitivity analysis. Concalve et al. (2021) used the SOBOL variance-based sensitivity analysis method to find the effect of the uncertainty of internal heat gain, infiltration rate, thermal transmittance of building envelope and other building parameters on the indoor temperature. They found that the uncertainty in internal heat gain could cause a 57% change in indoor temperature followed by a 14% from infiltration rate, 13% from building envelope U-value and 16% from other parameters. Yang et al.(2021) used global sensitivity analysis to find out which parameter of Building-integrated Photovoltaics BIPV has a significant effect on indoor overheating risk. Although this method is effective, the disadvantage of the global sensitivity analysis is the high computational cost and its inability to determine the type of correlation between the inputs and the outputs. Amoako-Attah and B-Jahromi (2016) used the sensitivity analysis (regression-based method) to find the most critical outdoor weather variables in the indoor temperature using different weather files (historical, recent, and future projection climate for London). They found that the outdoor dry temperature and solar radiation are the most influencing weather factors that affect the indoor temperature of dwellings in London. The other weather variables of wind direction, wind speed, humidity, and cloud cover have a relatively small impact on the indoor temperature. Encinas and Herde (2013) studied the effect of six parameters, i.e., infiltration rate, night ventilation, exposition of the thermal mass, internal gain, the solar and light transmittance of solar protection devices, and orientation, on the indoor temperature in a reinforced concrete apartment building in Santiago-USA. One hundred forty samples are selected using Latin Hypercube sampling. Global (Regression-based Method) and local sensitivity approaches were used to provide information about the most sensitive input parameters on indoor temperature. The results indicated that the presence of solar protection devices represents a high priority, which is especially noticeable in the case of living rooms, due to their extensive glazing surfaces. Night ventilation also constitutes a very significant input

parameter for all the spaces, especially for the bedrooms, which may generally provide more possibility of night ventilation in comparison to the living rooms. Hopfy et al. (2007) Studied the effect of seven different parameters (thermal mass, infiltration rate, internal gain, wall thermal permeability, window wall ratio (WWR), orientation, and SHGC) on overheating hours (based on PMV standards) using regression-based sensitivity method. They found that the internal gain, SHGC, WWR, and thermal transmittance of the wall had a significant effect, while others had little effect.

2.2 CALIBRATION OF BUILDING MODEL

Building Energy Modeling (BEM) is commonly used to model the archetype and existing buildings to assess their energy and thermal performance. For existing buildings, calibrating of building model is an important process of improving the accuracy of BEM simulation to reflect the as-built status and actual operating conditions. For energy studies, calibrated building models are used to track the performance of buildings during the commissioning and operation stages (Samuelson et al., 2016; Coakley et al., 2014) or to identify and analyze opportunities to improve the energy performance of existing buildings during the retrofit stage (Johnson, 2017). The metered energy consumption (Ascione et al., 2017; Yang et al., 2016) is usually used in the energy calibration process for a specific time scale (hourly or monthly). For thermal studies, calibrated building models are used to track the thermal condition of buildings during the commissioning and operation stages for overheating assessment studies (Baba et al. 2019a). Calibrated building thermal model helps to study the thermal condition of buildings under future climates (Baba et al. 2019b), or/and to analyze different mitigation measures to improve the thermal comfort during the retrofit stage (McLeod et al. 2013). Usually, indoor air temperature monitoring data (Penna et al., 2015b) or/and CO2 concentration (Montazami et al., 2012) are typically used in the thermal calibration process for a specific time scale (hourly or sub-hourly). Although calibration with a short timescale (sub-hourly or hourly) is more complicated and takes more time than that with a large scale (monthly or yearly), it can provide a better understanding of the physical phenomenon and produce good results with low errors. Reddy (2006) found that an existing building can be modelled by a set of calibrated models instead of only one single model.

There are two main methods for calibrating the building simulation model (Coakley et al., 2014): 1) manual and 2) automated methods.

2.2.1 Manual calibration

Manual calibration relies on a trial-and-error procedure or data gathering (building audit processes) of all input variables by performing field measurement, monitoring, and physical examination in order to reduce the error between the measured data and simulation results. Manual calibration requires high skills and practices from a designer who mainly adjusts input variables based on his experience. Regardless of skill, this process usually takes a long time to complete due to repeated trial and error processes or as a result of data collection. To better understand the trial-and-error process, the input variables are changed one at a time in each simulation run. For each simulation, the output has to be compared with the original model.

Several studies in the literature used the manual calibration method (Coakley et al., 2011; Westphal, and Lamberts, 2005; Pan et al., 2007). Cornaro et al. (2016) calibrated a model of a complex historical building using the manual calibration method. Indoor air temperatures were used for calibration by comparing monitored data and simulation results. They used the field survey to determine some parameters such as window properties, internal gain, and occupancy load. In contrast, they used the trial-and-error procedure to determine other parameters, such as the properties of partitions. Assumptions were made for infiltration and thermal bridges due to the high complexity of the structure.

Similarly, Raftery and Keane (2011) calibrated the EnergyPlus model for a new office building consisting of over 100 thermal zones. They calibrated the building manually using hourly sub-utilities measured data. Pan et al. (2007) calibrated the energy performance of a high-rise commercial building in Shanghai manually. They were able to achieve an energy model with high accuracy in predicting the actual energy use of the specific building. Overall, due to the amount of manual information transformation currently involved in the calibration of a model, the process takes considerable time and resources (Pan et al., 2007). The main advantage of manual calibration is that it combines human intelligence and experience with a trial-and-error process and often makes the calibrated model more reliable and closer to the actual building (Pan et al., 2007).

2.2.2 Automated calibration

Automated calibration relies on mathematical and statistical methods to minimize the difference between measured and simulated data. Automated procedures often include sensitivity analysis to

reduce the number of inputs to the optimization tool and speed up the computing time. There are two main approaches for automated calibration; 1) Bayesian approach, and 2) Evolutionary algorithms.

Bayesian approach

Bayesian analysis (Rasmussen, C.E., Williams, 2006; Bakir, 2007; Woodward, 2011; Bolstad, 2010) is a statistical inference method in which unknown input variables are treated as random variables. In this method, Bayesian probability theory can be applied not for finding "best-fit" models, but rather to compute a posterior probability distribution of input variables. The Bayesian approach relies on choosing a prior distribution that represents initial beliefs about the distribution of uncertain inputs. This belief could be derived from a pool of sources, such as experiments, surveys, expert knowledge, and industry standards. The Bayesian calibration based on Kennedy and O'Hagan (2001) mathematical framework is the basis for nearly all subsequent work in the field of building energy modelling. Gaussian process, a flexible class of stochastic functions, provides information about likelihood distribution as well as the uncertainty surrounding this value. Bayes' theorem calculates the posterior probability of an event based on likelihood data as well as prior data (Matthew and Muehleisen, 2014; Pavlak et al., 2013). Markov Chain Monte Carlo algorithms are the most prevalent sampling method for Bayesian inference. Markov Chain Markov Chain Monte Carlo algorithms also explore the geometry of the posterior density by drawing a random sample and returning a sample sequence (i.e., Markov chain) of the posterior density (Jaynes, 2003). Finally, a posterior distribution function of each uncertain parameter is assessed.

Heo et al. (2012 and 2015) used the Bayesian calibration approach to calibrate models of office buildings in the U.K. and the USA. They calibrated the model by adjusting four parameters that were found to be the most influential on energy use using Morris sensitivity analysis with the Latin Hypercube Sampling method. Prior (triangular) distributions of four parameters (infiltration, heating set-point, appliance, and lighting power densities) were updated to a posterior distribution by taking monthly natural gas measurements into account. The posterior distributions were then used to quantify uncertainties resulting from potential energy conservation measures. They achieved 17% of the CV(RMSE) for hourly temperature. Booth et al. (2012) used a sensitivity analysis with the Bayesian calibration process in order to quantify uncertain of six parameters

(internal heating setpoints, the fraction of space heating, air leakage, heating system coefficient of performance, window U-value, and window-to-wall ratio) in London housing stock models. In the same context, Kristensen et al. (2017), Li et al. (2015), Kang and Krarti (2016) Berger et al. (2016) used the Bayesian method to calibrate unknown input variables and retrofit analysis. Several studies addressed the computational cost of auto-calibration, which has slowed the adoption of such techniques. Notably, the computational cost can be reduced by fitting a statistical emulator or meta-model, to replace the physical model. Meta-models are often adopted in combination with Bayesian calibration approaches (Kristensen et al. 2017; Kim and Park 2016). Manfren et al. (2013) successfully produced the meta-model with the Bayesian calibration process. They confirmed that this method reduced computational cost without sacrificing much accuracy. However, Bayesian calibration quality is influenced by the quantity and quality of building energy data. More research is needed to define the amount of data required for accurate Bayesian calibration and how to distinguish usable and useless data (Tian et al., 2016).

Evolutionary algorithm

The evolutionary algorithm was introduced in the 1960s by Rechenberg (1960). Evolutionary algorithms are a heuristic-based approach to solving problems that cannot be easily solved or would take far too long to process (Bäck et al., 1997). Evolutionary algorithms are a family of population-based optimization algorithms inspired by Darwinian evolution. One of the evolutionary algorithms that are commonly used to generate high-quality solutions to optimization and search problems is a **Genetic Algorithm GA** (Bäck, 1996; Banzhaf et al., 1998; Mitchell, 1996). Holland (1975) was the first to propose a genetic algorithm as an optimization technique. GA has gained an increasing relevance due to its ability to work with a population of individuals that converges to non-dominated solutions (Pareto optimal solutions) by relying on biologically inspired operators such as mutation, crossover, and selection (Banzhaf et al., 1998). However, the GA method can not deal with multi objectives since objectives often conflict with each other, which can cause unbalanced results output (Bäck, 1996). For that, in 1985, the GA method is developed to be a Multi-objectives Genetic Algorithm (MOGA) by Schaffer (1985). For multi-objective optimization problems, no single solution exists that simultaneously optimizes each objective. Therefore, there exist many Pareto optimal solutions. All Pareto optimal solutions are considered equally good. Researchers study multi-objective optimization problems from different

viewpoints and, thus, there exist different solution philosophies and goals when setting and solving them. Pareto optimal sets can reduce production time and cost. Hamdy et al. (2016) compared the performances of seven commonly-used multi-objective optimization algorithms 1) NSGA-II: non-dominated sorting genetic algorithm with a passive archive, 2) MOPSO: a multi-objective particle swarm optimization; 3) PR_GA: a two-phase optimization using the genetic algorithm; 4) ENSES: an elitist non-dominated sorting evolution strategy; 5) evMOGA: a multi-objective evolutionary algorithm based on the concept of epsilon dominance; 6) spMODE-II a multi-objective differential evolution algorithm; and 7) MODA: a multi-objective dragonfly algorithm. They found that evolutionary algorithms needed 1400–1800 simulations to find the optimization results of the building energy model instead of 10,600,000 possible evaluations. They found that the PR_GA algorithm had high repeatability to explore a large area of the solution-space and achieved close-to-optimal solutions with good diversity, followed by the NSGA-II, evMOGA, and spMODE-II. The following points explain the steps involved in making a multi-objective genetic algorithm:

1. Treat each parameter as a "chromosome" that contains a certain number of genes.
2. Create the first population randomly (called the first generation) from a certain number of chromosomes,
3. Choose the best chromosomes from the current population after running the simulation and place them in the mating pool.
4. Carry out Selection, Mating/Crossover, and Mutation process in the mating pool
5. Sort the resulting set and pass the best chromosomes to the new generation.
6. Set the highest-ranked Pareto non-dominated from all generations.

MOGA has become a new trend in recent research in **calibration and optimizing** machining process parameters. NSGA-II is one of the most popular multi-objective optimization algorithms with three unique characteristics, i.e., fast non-dominated sorting approach, fast crowded distance estimation procedure, and simple crowded comparison operator (Deb et al., 2009; Kodali et al., 2008; Jianling, 2009; Mitra, 2009). NSGA-II was developed by Deb et al. (2002). Lara et al. (2017) state that the use of calibrated energy simulation models is considered as a key to the success of operation management or building improvements. They used Genetic Algorithm (NSGA II) optimization methods to calibrate a large educational building model in the north of Italy. The total design space consists of about 72,000 EnergyPlus building models. The genetic algorithm only

needed 137 generations to find the best results. Hong et al. (2017) calibrated the energy model automatically using the genetic algorithm (NSGA-II) with the optimization objective of approaching the minimum CV(RMSE). The CV(RMSE) was reduced from 18.10% to 12.62%. Roberti et al. (2015) calibrated a historical building in Italy using a particle swarm optimization algorithm. A sensitivity analysis was performed to identify significant parameters affecting the errors between simulated and monitored indoor air temperatures in this study. The model was calibrated on the hourly indoor air temperatures where temperature root means square errors ranged from 0.4 to 0.8 K. Several studies have used the GA algorithm for auto-calibration such as Nagpal et al. (2018); Pezeshki (2018); Arida et al. (2017); Banihashemi et al. (2017); Ramos et al. (2016) and Andrade-Cabrera et al. (2016 and 2017).

There are two commonly used calibration methods (Reddy, 2006, Samuelson et al. 2016): 1) Manual calibration and 2) Automated calibration. Manual calibration relies on a trial-and-error procedure or data gathering (building audit processes) of all input variables by performing field measurement, monitoring, and physical examination to reduce the error between the measured data and simulation results. Manual calibration requires high skills and practices from a user who mainly adjusts input variables based on her/his experience or by measuring some parameters, such as infiltration rate (Lozinsky and Touchie, 2018). Regardless of skills, this process usually takes a long time to complete due to repeated trial and error processes or as a result of data collection. To better understand the trial-and-error process, the input variables are changed one at a time in each simulation run. For each simulation, the output has to be compared with the original model. Several studies in the literature used the manual calibration method (Lozinsky and Touchie, 2018; Coakley et al., 2011; Pan et al., 2007; Cornaro et al., 2016; Raftery et al., 2011)

2.2.3 Model calibration based on the hourly indoor temperature

There is a limited number of studies on model calibration based on the hourly indoor temperature and most of them used the manual calibration method (Donovan et al., 2019; Royapoor and, Roskilly, 2015; Coakley et al., 2012; Paliouras et al., 2015; and Cacabelos et al., 2015). O' Donovan et al. (2019) calibrated a university residence building located in the U.K. by using the indoor measured temperature. They calibrated the model parameters manually, such as shading, internal gain, and the amount of natural ventilation. They considered the model calibrated when the discrepancy in CV(RMSE) and Normalized Mean Bias Error (NMBE) between hourly

measured and simulated data was less than 20 % and 10%, respectively. They achieved an RMSE of 0.8 °C in the occupied summer week and 1.1 °C in the occupied autumn season with 6% of the CV(RMSE) and 5% of NMBE. Royapoor and Roskilly (2015) manually calibrated the EnergyPlus office model by measuring parameters in the building such as HVAC system, infiltration rates, building envelope thermal properties, and internal gain. They were able to predict hourly space air temperatures with an accuracy of ±1.5 °C for 99.5% and an accuracy of ±1 °C for 93.2% of the time and achieved 3% of the CV (RMSE) and 1.5% of NMBE. Coakley et al. (2012) achieved 14% of the CV (RMSE) and 4% of NMBE from the calibrated HVAC system and internal gain in the Nursing at the National University of Ireland. Paliouras et al. (2015) considered the model calibrated based on indoor temperature when the discrepancy of CV(RMSE) was less than 5%, and they achieved 4% of the CV (RMSE). Cacabelos et al. (2015) calibrated a library simulation model in northwest Spain. They collected all necessary data, such as the building envelope thermal proprieties, occupancy levels, hours of use, lighting schedules, ventilation, and HVAC system, to obtain an accurate calibration. The average CV(RMSE) error of the indoor temperature was around 10%. Roberti et al. (2015) calibrated a historical building in Italy using the measured data for all uncertain parameters based on the hourly indoor air temperatures. To increase the accuracy, the particle swarm optimization algorithm was used for calibrating a narrow range of parameters representing uncertainties in the measurement equipment or method. The calibrated model based on the measurement data achieved an RMSE of 0.96 ºC, while with further adjustment, the RMSE was reduced to 0.66 ºC. Martínez-Mariño et al. (2021) found the multi-objective genetic algorithm does not reduce temperature prediction errors (CV (RMSE)) compared with the initial model.

All previous studies (Donovan et al., 2019; Royapoor and, Roskilly, 2015; Coakley et al., 2012; Paliouras et al., 2015; and Cacabelos et al., 2015) used the Verification Protocol (IPMVP) (1997) and/or the ASHRAE Guideline 14 (2014) to calibrate indoor air temperatures, although these standards provide the criteria for determining whether a model is calibrated based on energy use only (Table 2-2). Some researchers have found that these acceptable ranges can be achieved even though there is a significant difference in the hourly distribution between the simulated and measured temperature data (Donovan et al., 2019; Royapoor and, Roskilly, 2015; Coakley et al., 2012; Paliouras et al., 2015; and Cacabelos et al., 2015). The calibration errors based on indoor temperature from these existing studies are summarized in Table 2-2.

Table 2-2. Calibration benchmark values based on energy consumption and indoor temperature.

		Calibration Type	CV-RMSE (%)	NMBE (%)
Based on energy consumption	ASHRAE 14 (2014)	Hourly	30	10
	IPMVP (1997)	Hourly	20	-
Based on indoor temperature	Literature review*	Hourly	5-14	2-6

*(Donovan et al., 2019; Royapoor and, Roskilly, 2015; Coakley et al., 2012; Paliouras et al., 2015; and Cacabelos et al., 2015).

2.3 OVERHEATING RISK ASSESSMENT

Researchers aim to find the relation between the outdoor climate and the indoor thermal condition of buildings. Hamdy et al. (2017) found that the indoor air temperature in houses is often higher than the outdoor air temperature by 6 ° C during summertime in Netherland due to the internal heat gain and solar gain. White-Newsome et al. (2012) conducted hourly field measurements in 30 houses built between 1919 and 1987 in the summer of 2009 in Detroit-USA. The field measurements included outdoor temperature, dewpoint temperature, and solar radiation. They found that the indoor temperature was 13.8 °C higher than the outdoor temperature, and the indoor temperature reached up to 34.8 °C. The study also concluded that houses with wood siding were more sensitive to outdoor temperature changes than brick homes (Newsome et al., 2012).

To understand the effect of indoor thermal conditions on the thermal comfort of occupants, researchers in previous studies (Section 2.3.1) attempted to assess the indoor overheating risks using different thermal comfort criteria (Section 2.3.2) and under future climate. Section 2.3.2 describes the future climate scenarios and methods that can be used to generate future climates. This work focused on studying the overheating risk in free-running buildings, especially buildings housing vulnerable populations, such as residential and school buildings, because their occupants are more susceptible to heat stress or heat-related death (Section 2.3.1).

2.3.1 Overheating risk in buildings

2.3.1.1 Residential buildings

Gamero-Salinas et al. (2020) monitored indoor temperature in a free-running apartment building in Central USA during Spring (March to May) 2018. They found that the building experienced 66 hours of overheating, which was determined using the adaptive ASHRAE 55 method. The maximum indoor temperature reached 32 °C (Gamero-Salinas et al., 2020). Mitchell et al. (2019) assessed the level of overheating risk in 62 detached houses and 20 low-rise residential buildings in the U.K. using field-measured temperature data in these buildings. They used both the Passivhaus Planning Package (PHPP) criteria to assess the overheating risk. These buildings use natural ventilation in summer (window opening, especially at night) for improving indoor air quality and for cooling purposes. They found that 40% and 17%of bedrooms in low-rise residential buildings and detached houses, respectively, were overheated based on PHPP criteria. Hughes et al. (2019) evaluated the indoor thermal condition in senior houses in the U.K using simulation data in 2017 and 2018. They found, based on CIBSE TM59 criteria, that 57% of houses were overheated in 2017, while in 2018, which was a more extreme year, this number increased to 94%. This underlines the importance of assessing the risks of overheating under the most severe and intense weather, especially in the homes of vulnerable people (Hughes et al., 2019). Quigley and Lomas (2018) monitored indoor temperature in fifteen rooms in the student accommodation building in North U.K. during the summer of 2014. The building was constructed in 2012 with Light-gauge steel. The building was designed with centralized exhaust systems in apartments with outlets in shower rooms, kitchen, and hall. The window opening was restricted to 15 cm. Analysis of field measurements showed that 44% of nighttime hours were overheating based on CIBSE Static criteria in all rooms. That means the sleep of occupants could be severely disrupted for a prolonged period. They also found that the rooms on the seventh floor and higher suffered from overheating, while those on lower floors did not. Also, results showed that the mechanical ventilation system in apartments was also ineffective. McGill et al. (2017) found that 75% of living rooms and 57% of bedrooms in 60 new houses aged less than ten years in England experienced overheating in the summer of 2012 and 2014. They did not provide details on building envelope properties or ventilation rates to explain the causes of this overheating. Touchie et al. (2016) conducted field measurements and a survey to assess overheating risk in Sixty-five suites in seven

multi-unit residential buildings in Toronto, Canada in 2015. The average suite's temperature during summer was 27.7°C with a peak temperature of over 34°C. During the heat alert, the temperature exceeded 30 ° C in 80% of suites. Loenhout et al. (2016) conducted a questionnaire and field measurements to examine the effect of one week of outdoor heatwave on elderly people in 113 homes in the Netherlands in 2012. They found that during a one-week heatwave, the maximum outside temperature was about 30 °C for five days and reached 35 °C on the two extreme days. While the average maximum indoor temperature in 113 living rooms (31-32 °C during the week) was1 to 2 °C above the maximum outdoor temperature on five days but 2 °C lower in the two extreme years (Loenhout et al., 2016). According to their questionnaire results, these high temperatures made 43% of the elderly feel very thirsty, 41% suffer from sleep disturbances and 40% sweat excessively (Loenhout et al., 2016). Baborska et al. (2017), Pathan et al. (2017) and Beizaee et al. (2013) carried out occupant surveys and field measurements in dwellings and apartments in different climate zones in the U.K. They found that the overheating occurred in 21-44% of bedrooms and 28-29% of living rooms according to the overheating criteria established by CIBSE and BS EN 15251 (2007). In Estonia, Simson et al. (2017) measured the indoor temperatures in 16 apartment buildings during the summer of 2014. They carried out an energy simulation for 25 buildings using Test Reference Year (TRY) to identify the critical parameters that affect the overheating, such as the orientation of the room, lack of shading and window wall ratio. The apartment buildings of this study were built in the year 2009 and later with more than four floors above ground using precast concrete structures. The buildings in this study used either a central mechanical exhaust ventilation system or a mechanical supply-exhaust system. The field measurements showed that in many cases, the average room temperature reached up to 32 °C, and most of the apartments had temperatures higher than 27 °C, which indicated clear evidence of overheating. The simulation results also revealed that 68% of the studied apartment buildings do not comply with the summer thermal comfort requirements of Estonian regulation. They also emphasized the significant difference between the measured temperature (real year) and simulated temperature (reference year climatic data). With climate change, increased attention has been paid to investigating the thermal condition of existing and new buildings under future climates, to ensure these buildings can adapt to changing climates during their expected service life. Based on the heatwave definition by Environment Canada, Li et al. (2018) found that 35-44 heatwave events with 5.5 to 10.2 consecutive days may occur in Ontario cities from 2071 to 2100. In the

Netherlands, Hamdy et al. (2017) simulated many types of dwellings under the worst future scenario in 2100, which considered an increase in the average temperature of 4 °C due to a global warming effect and 1.4 °C further temperature rises due to the urban heat island effect. Under this scenario, they found that the maximum indoor operative temperature in dwellings may reach 38 °C, and the minimum indoor operative temperature would also increase significantly from 14 °C to 20 °C. The problem of overheating will be more severe if occupants are elderly, children, or suffering from pre-existing health problems. According to overheating survey carried out by the Zero Carbon Hub (2015) in the U.K., 53 (91%) of 58 Housing Provider organizations reported at least one case of overheating from 2009 to 2014 in their housing stock.

The overheating risk affects not only the comfort and health of occupants but also affects the productivity and performance of occupants. Ohnaka and Takeshita (2005) found that high temperature during the night increases alertness and interrupted sleep, causing a decrease in the productivity and performance of occupants. Moreover, overheating may cause HVAC failure due to overload, power outage, increase operating and maintenance costs, and increase CO_2 emissions by increasing the use of air conditioners (Plokker et al., 2009; IOM, 2011, Littlefair, 2005; CIBSE, 2014). The use of household air conditioners in the U.K. may increase by 8% annually (Daly et al., 2014). This phenomenon could lead to an additional six million tons by 2030 (Daly et al., 2014).

2.3.1.2 School buildings

There are about 600 million school students worldwide (UNESCO, 2017), and children spend about 30% of their lives in school buildings (Valeria et al., 2012). Therefore, research efforts have been made to evaluate the effect of the indoor thermal condition of classrooms on students' comfort (Mohamed et al., 2021; Jindal, 2018; Giuli et al., 2012), health (Liang et al., 2012), and academic performance (Wargocki and Wyon, 2017; Sarbu and Pacurar, 2015). Mohamed et al. (2021) monitored the indoor temperature of free-running two school buildings that were built after 2010 in the U.K. They found that the indoor temperature for 60% of the occupied periods was over the indoor overheating threshold. Jindal (2018) conducted a questionnaire during the summer of 2015 to investigate thermal comfort in free-running Indian classrooms. Jindal (2018) found that 90% of the 650 students felt hot that year and required a cooler indoor environment. Giuli et al. (2012) conducted a questionnaire to assess the indoor environmental conditions of seven free-running

Italian primary schools in the summer of 2009, their behaviour towards discomfort and what was their level of interaction with the environment, such as opening windows, using the shading and/or turning off the light. They found that 19% of students complained mostly of thermal conditions in warm seasons as they felt too hot in schools. They also found that teachers did not react to improve the indoor thermal condition, where they kept indoor shading open, and windows closed during lesson time. Liang et al. (2012) found that the indoor temperature in four classrooms in Taiwan reached 33 °C, and 5% of the occupied hours per year was above 31 °C, causing students to have headaches and fatigue. Uncomfortable classroom environments affect students' health and academic performance. Wargocki and Wyon (2017) conducted a questionnaire to find out the effect of indoor temperature on the educational performance of students learning language and math skills. They found that the educational performance of students could be 30% lower at indoor temperatures of 30°C compared to their performance at 20 °C. Sarbu and Pacurar (2015) found that the students' optimal academic performance was at an indoor temperature of 25 to 26 °C, while at 27 °C the performance could be 30% lower than their performance at 25 °C based on a questionnaire conducted over a period of 36 days. Wargocki and Wyon (2013) found that increasing the ventilation rate from 5 to 9 L/s.person improved the logical thinking, concentration, and speed of performance of a task in children. Huang et al. (2015) studied the thermal condition of a free-running education building in Taiwan, which was designed with a green roof, cross ventilation, and overhangs, by a questionnaire and measuring indoor temperature during the summer of 2013. They found that the severity, which measures how far and how long the temperature rises above the upper limit of the comfort temperature of the indoor thermal condition, is 18% lower than outdoor thermal conditions.

In Canada, there are 5.3 million students (15% of the population) spread over 15,500 school buildings (Council of Ministers of Education Canada, 2021). In 2021, for the first time ever, dozens of schools were forced to close due to a severe heatwave in June as the outside temperature was 41.5 °C in British Columbia–Canada (British Columbia, 2021). Canadian education buildings consume around 13% of the total energy consumption of commercial buildings (Natural Resources Canada (NRC, 2019). The Space cooling consumption in educational buildings across Canada accounted for about 5.5% of total energy consumption in 2000, while this proportion rose to 8.6% in 2018, an increase of 56% (NRC, 2019). In Toronto-Canada, about 80% (455 out of 583) of schools relied on natural ventilation to cool the building, which increases the risk of students and

staff being exposed to significant heat stress and encourages parents to keep their children at home and away from school more often (Flanagan, 2018). Re-equip these schools with air conditioners would cost nearly $750 million, which would dramatically increase CO2 emissions (Flanagan, 2018). In Quebec-Canada, Schools that were built before 1970 represent 64% of the province's total schools (Gouvernement du Québec, 2021). According to Quebec Public Infrastructure (Gouvernement du Québec, 2021), 40% of these buildings have poor indoor conditions.

Despite the previous studies (Council of Ministers of Education Canada, 2021; Gouvernement du Québec, 2021; British Columbia, 2021; NRC, 2019; Flanagan, 2018; Mohamed et al., 2021; Jindal, 2018; Giuli et al., 2012; Liang et al., 2012; Wargocki and Wyon, 2017; Sarbu and Pacurar, 2015) that emphasize the importance of providing appropriate indoor conditions for children in schools, studies on the thermal conditions and overheating risks in Canadian school buildings are still rare, especially studies based on actual observation of the performance of existing buildings that were built before the 1970s, compared to other buildings such as residential buildings (Fletcher et al., 2017; Sameni et al., 2015; Stazi et al., 2017; Psomas et al., 2017) and office buildings (Nguyen et al., 2021; Fedorczak-Cisak et al., 2020; Virk et al., 2020; Brambilla et al., 2018). Furthermore, the large stock of existing buildings provides great opportunities to increase or decrease the consumption of energy consumed to achieve indoor thermal comfort.

Therefore, this work aims to evaluate the current thermal condition of an existing and archetype Canadian building using simulation and field measurement data, to assess the extreme future climate data using a calibrated simulation model, and to provide passive mitigation solutions to provide appropriate indoor conditions for building occupants, especially vulnerable populations such as the elderly and children without adding cooling loads to them.

2.3.2 Thermal comfort criteria

Many thermal comfort criteria have been developed in this field to determine the severity and occurrence of overheating. Thermal comfort standards can be divided into two major groups: standards related to 1) mechanically heated/cooled spaces; and 2) free-running buildings. This thesis work focuses on the free-running building without a mechanical system. For free-running buildings, the metrics determine the level of thermal comfort by calculating the overheating hours, either using a static threshold, such as CIBSE-Guide A (2011), adaptive threshold, such as ASHRAE 55- Adaptive (2017) and BS EN 15251 (2007), as shown in Section 2.3.2.1. Based on

these thermal comfort standards, various building guidelines have developed acceptable limits for overheating risks, as shown in Section 2.3.2.2.

2.3.2.1 Thermal comfort standards

2.3.2.1.1 ASHRAE 55: Adaptive comfort model

ANSI/ASHRAE-55 (2017) standard allows the adaptive comfort method to be used in naturally conditioned zones that do not have a mechanical cooling or ventilation system but are equipped with operable external windows controlled by the occupants. This optional method also requires the occupants of these zones to be free to change their clothes according to indoor and outdoor thermal conditions. The acceptable indoor operative temperatures for these zones are calculated based on Equations 2-1 to 2-5. The 90% acceptance limits are for sensitive and fragile people with special requirements, while the 80% acceptance limits are for typical applications. If the average monthly outdoor temperature is less than 10 ° C or greater than 33.5 ° C, this method cannot be used. According to ASHRAE 55-2017, the acceptability limits have already considered the effect of humidity, clothing discomfort, metabolic rate, and air speed. The prevailing mean outdoor air temperature ($T_{pma(out)}$) is defined as the arithmetic average of the mean daily outdoor temperatures calculated over 7 to 30 days. Overheating occurs when the operative temperature (T_{op} in Equation 2-6) is greater than the upper threshold temperature (T_{up}) in Equations 2-1 or 2-2.

$$\text{Upper 80\% acceptable limit } T_{up} = 21.3 + 0.31 * T_{pma(out)} \quad (2\text{-}1)$$

$$\text{Upper 90\% acceptable limit } T_{up} = 20.3 + 0.31 * T_{pma(out)} \quad (2\text{-}2)$$

$$\text{Optimal Comfort Temperature} = 17.8 + 0.31 * T_{pma(out)} \quad (2\text{-}3)$$

$$\text{Lower 80\% acceptable limit } T_{lower} = 14.3 + 0.31 * T_{pma(out)} \quad (2\text{-}4)$$

$$\text{Lower 90\% acceptable limit } T_{lower} = 15.3 + 0.31 * T_{pma(out)} \quad (2\text{-}5)$$

$$T_{op} = (T_r + T_{mrt})/2 \quad (2\text{-}6)$$

Where $T_{pma(out)}$ is the prevailing mean outdoor air temperature of seven days. T_r is the indoor hourly air temperature (°C), and T_{mrt} is the hourly mean radiant temperature of the zone (°C)

2.3.2.1.2 BS EN15251: Adaptive comfort method

European Standard EN 15251 (2007) defines the indoor comfort limits based on the predicted mean vote (PMV), the predicted percentage of dissatisfied (PPD), and the adaptive comfort method developed from the European Smart Controls And Thermal comfort (SCATS) project. This standard contains three acceptable categories for the adaptive comfort model:

1. Category I threshold applies to zones that are occupied by very sensitive and fragile persons with special requirements, such as the disabled, sick, very young, and the elderly. The acceptance limit for this category is calculated by Equations 2-7 and 2-11.

2. Category II threshold applies to new buildings and renovations. The acceptance limit for this category is calculated by Equations 2-8 and 2-12.

3. Category III applies to existing buildings. The acceptance limit for this category is calculated by Equations 2-9 and 2-13

$$\text{Upper limit Category I} = 0.33 \cdot T_{rm} + 18.8 + 2 \quad (2\text{-}7)$$

$$\text{Upper limit Category II} = 0.33 \cdot T_{rm} + 18.8 + 3 \quad (2\text{-}8)$$

$$\text{Upper limit Category III} = 0.33 \cdot T_{rm} + 18.8 + 4 \quad (2\text{-}9)$$

$$\text{Optimal Comfort Temperature} = 0.33 \cdot T_{rm} + 18.8 \quad (2\text{-}10)$$

$$\text{Lower limit Category I} = 0.33 \cdot T_{rm} + 18.8 - 2 \quad (2\text{-}11)$$

$$\text{Lower limit Category II} = 0.33 \cdot T_{rm} + 18.8 - 3 \quad (2\text{-}12)$$

$$\text{Lower limit Category III} = 0.33 \cdot T_{rm} + 18.8 - 4 \quad (2\text{-}13)$$

$$T_{rm} = \frac{(T_{od-1} + 0.8T_{od-2} + 0.6T_{od-3} + 0.5T_{od-4} + 0.4T_{od-5} + 0.3T_{od-6} + 0.2T_{od-7})}{3.6} \quad (2\text{-}14)$$

Where T_{rm} is the exponentially weighted running mean of daily mean outdoor temperatures (°C), and $T_{od\text{-}n}$ is the daily mean outdoor temperature of the nth day before the day in question (°C)

2.3.2.1.3 CIBSE Guide A criteria

CIBSE Environmental Design Guide A (CIBSE-Guide A, 2011) recommends keeping the indoor temperature below 25 ° C, as people begin to feel uncomfortable above 25 ° C. According to this standard, overheating in living rooms occurs if the operative temperature exceeded 28 °C. At the same time, a low temperature of 26 ° C is recommended in bedrooms, as the ability of people to help themselves to cool down during sleep is more limited than daytime.

2.3.2.1.4 Humidex

Humidex is a Canadian invention that was first used in 1965. It describes how an average person feels in the outdoor hot and humid weather. The Humidex combines the temperature and humidity into one number to reflect the perceived temperature using Equation 2-15 (Environment Canada, 2018). Degree of comfort (OHSCO, 2007): 1) < 20 is comfort; 2) 20 to 29 is little discomfort; 3) 30 to 39 is some discomfort; 3) 40 to 45 is great discomfort; avoid exertion; 4) Above 45: Dangerous; heatstroke possible.

$$Humidex = T_{op} + (5/9 \cdot (e - 10)) \quad (2\text{-}15)$$

Where T_{op} is an operative temperature (°C) calculated using Equation 2-6, and e is an actual vapour pressure in millibars (mb).

2.3.2.2 Building thermal comfort guidelines

2.3.2.2.1 BC Energy Step Code guide

BC Energy Step Code (BCESC) (2019) developed the acceptable limit for overheating hours based on the ASHRAE-55 adaptive comfort model (2017). The building must not exceed 200 hours per year to accept the design of the building based on ASHRAE-55 with 80% acceptance limits. For buildings occupied by vulnerable people, the overheating hours that are calculated based on ASHRAE-55-80% must not exceed 20 hours per year.

2.3.2.2.2 CIBSE TM52

CIBSE TM52 (2013) developed three criteria based on EN15251 thresholds to evaluate the thermal performance of any type of building. The building must exceed two of the three criteria to be accepted. These criteria are:

1. **Hours of Exceedance (He):** Number of hours that its operative temperature (Top) exceeds the Tmax by 1 K or more, as shown in Equations 2-16 and 2-17, must not exceed 3% of occupied hours during summertime (1 May to 30 September).

$$He = \sum hr \; \forall \; \Delta T \geq 1 \text{ °C} \tag{2-16}$$

$$\Delta T = T_{op} - T_{max} \tag{2-17}$$

   Where T_{op} is the hourly indoor operative temperature (°C), T_{max} is the overheating threshold for any EN15251 Category (see Section 2.3.2.1.2).

2. **Daily Weighted Exceedance (We):** Sum of ΔT that is higher than 1 K during the day should not exceed 6 degree-hours (°C · hr/day) on any one day, as shown in Equation 2-18**.** This criteria measures how far and how long the temperature rises above the upper limit of the comfort temperature.

$$We = \sum hr \cdot \Delta T < 6/\text{day} \qquad \text{when } \Delta T > 0 \tag{2-18}$$

3. **Upper Limit Temperature (T_{upp}):** Operative temperature should not exceed Tmax by 4 K or more at any time.

2.3.2.2.3 Building Bulletin BB101 Guide

Building Bulletin BB101 (2016 and 2018) was developed by the U.K. Government to provide recommendations for schools' ventilation, thermal comfort and indoor air quality. For thermal comfort, BB101 used the adaptive thermal comfort threshold EN15251 (2007) to determine the overheating risk in the schools.

BB101 (2018) used three criteria to assess thermal comfort in the school. BB101 requires Criterion 1 to be met as a minimum to pass or fail, but Criteria 2 and 3 mainly measure short-term discomfort and for information reporting only. If a school design fails to meet Criterion 2 or Criterion 3 then

designers should consider potential overheating mitigation measures and indicate which are viable for the project. The three criteria are the same as CIBSE TM52 with different acceptance ranges:

- Criterion 1 - Hours of Exceedance (He)-Equations 2-16 and 2-17: must not exceed 40 occupied hours during the period 1st May to 30th September
- Criterion 2 – Daily Weighted Exceedance (We)-Equation 2-18: should not exceed 6 on any one day
- Criterion 3 - Upper Limit Temperature (Tupp): operative temperature should not exceed Tmax by 4K or more at any time

These criteria must be applied on the period Monday to Friday from 09:00 AM to 04:00 PM, from May 1 to September 30, including the summer holiday period as if the school was occupied normally. The goal of applying these criteria during the summer holidays is to achieve thermal comfort in the hottest months, thus ensuring that May, June and September will be more comfortable in the coming years or under extreme years. Including the hottest months in the study also reduces the uncertainty of future climate generation.

2.3.2.2.4 CIBSE TM59

CIBSE TM59 - Design Methodology for the Assessment of Overheating Risk in Homes (2017) developed two criteria to predict overheating risk in **domestic dwellings** with natural and mechanical ventilation. These criteria combine guidance from CIBSE TM52 (EN15251) and CIBSE Guide A to provide temperature limits in both living rooms and bedrooms. These criteria are:

1. **Criterion A:**

   In living rooms and kitchens, the "Hours of Exceedance" of CIBSE TM52 (Criterion 1) should not exceed 3% (60 hr) of the daytime (9 am to 10 pm) in the non-heating season that has been defined from 1 May to 30 September.

   In bedrooms, the "Hours of Exceedance" of CIBSE TM52 (Criterion 1) should not exceed 3% (113 hr) of all-time (24 pm) in the non-heating season.

2. **Criterion B**:

   In bedrooms only, the operative temperature shall not exceed 26°C (CIBSE Guide A) for more than 1% (33 hr) hours of annual hours

2.3.2.2.5 PHPP standard

The Passivhaus Planning Package PHPP (Feist et al., 2015) requires that the percentage of the total time in the year that exceeds 25°C (CIBSE Guide A) not exceed 5-10% of occupied hours. If the value exceeds 10% of the annual hours (876 hr), more summer protection must be added (Feist et al., 2015). The PHPP provides a range of criteria: exceedance of 25°C more than; 1) 15% of the time is Catastrophic; 2) 10–15% is Poor; 3) 5–10% is Acceptable; 4) 2–5% is Good, and 5) 0– 2% is Excellent.

2.3.2.2.6 LEED Credit IPPC100–Passive Survivability and Functionality During Emergencies

The U.S. Green Building Council (USGBC) (Wilson, 2015) adopted new pilot credits on resilient design to ensure that buildings will maintain reasonably during emergencies. One of these credits is addressing thermal resilience and maintaining the building's interior environment's "livable temperatures" during a power outage that lasts seven days during the peak summertime and wintertime conditions of a typical year. USGBC has adopted the Standard Effective Temperature (SET) from ASHRAE 55 (2017) as a measuring tool for determining "livable temperatures".

According to ANSI/ASHRAE Standard 55-2017, SET is *the temperature of an imaginary environment at 50 percent [relative humidity], less than 0.1 meters per second air-speed, and [the mean radiant temperature equals the air temperature], in which the total heat loss from the skin of an imaginary occupant with an activity level of 1.0 met and a clothing level of 0.6 cloth is the same as that from a person in the actual environment, with actual clothing and activity level*". SET is essentially a comprehensive comfort index that endeavours to incorporate all six basic physical factors of thermal comfort (Four Environmental factors: Air temperature, Radiant temperature, Air velocity, and Humidity. And two personal factors: Clothing Insulation, and work rate/Metabolic heat) as well as physiological considerations.

"Livable temperatures" are defined as a SET that does not exceed 30 C. Deviations from this range are limited to a certain number of degree-days (or degree-hours) using SET resultants during peak summer conditions. For residential buildings (single-family and multi-family) during the one week during the summer peak, the building may not exceed 30°C SET (86°F SET) for more than 9 SET °F degree-days (9 SET °F degree-days) (120 SET °C degree-hours (216 SET °F degree-hours)).

2.3.3 Future climate

2.3.3.1 Emission scenarios

In 1988, the World Meteorological Organization (WMO) and the United Nations Environment Program (UNEP) established the Intergovernmental Panel on Climate Change (IPCC) that continues to make significant efforts to identify the causes of climate change by assessing scientific, technical and socio-economic information relevant to understanding the risks of climate change, predicting its effects on the future climate, and preventing it. The IPCC has produced a series of comprehensive assessment reports since 1990 on the state of understanding the causes of climate change, its potential impacts, and options for response strategies. The reports concluded that human activities are estimated to have caused approximately 1.0°C of global warming above the pre-industrial level (IPCC, 2018).

The IPCC aims not only to understand the causes of climate change in the past but also to forecast future climate by developing global scenarios that influence the future. The IPCC issued its first global scenarios in 1990 in the First Assessment Report. In 1995, the IPCC released a new set of emissions scenarios in the Second Assessment Report (SAR) (IPCC, 1996). Then they released the Third and Fourth Assessment Report in 2001 (IPCC, 2001) and 2007 (IPCC, 2007), respectively, with Special Report on Emissions Scenarios (SRES). The SRES scenarios cover the key causes of future greenhouse gas emissions, such as social, economic, environmental and technological assumptions. The three main scenarios were: 1) B1 which assumes that the world will move towards high social and environmental sustainability leading to lower levels of carbon dioxide emissions; 2) A1B, which assumes that the world will move toward intermediate social and environmental sustainability resulting in intermediate CO2 emissions, and 3) A2 assumes that the world will move toward a high level of fossil fuel use resulting in high CO2 emissions.

The Fifth Assessment Report (AR5) was released in 2013, which relied on RCP scenarios (Representative Concentration Pathways). The RCPs (IPCC, 2014) primarily depend on the concentrations of greenhouse gas and the climate forcing determined by the approximate radiative forcing (W/m^2) reached at the end of the 21^{st} century. Radiative forcing is the difference between solar radiation absorbed by the Earth and energy radiated back to space. These Pathways are combined with reasonable socio-economic pathways to provide complete scenarios. RCP includes four paths: RCP2.6, RCP4.5, RCP6.0, and RCP8.5, as described in Table 2-3.

Table 2-3. The differences among RCP scenarios

	RCP8.5 **(Riahi et al., 2011)**	RCP6 **(Masui et al., 2011)**	RCP4.5 **(Thomson et al., 2011)**	RCP2.6 **(Vuuren et al., 2011)**
Radiative Forcing	8.5 W/m^2 in 2100 Equivalent to 1370 ppm CO_2	6 W/m^2 post-2100 Equivalent to 850 ppm CO_2	4.5 W/m^2 post-2100. Equivalent to 650 ppm CO_2	3 W/m^2 before 2100, declining to 2.6 W/m^2 by 2100. Equivalent to 490 ppm CO_2
Temp anomaly	4.9 °C	3.0 °C	2.4 °C	1.5 °C

The IPCC is constantly updating climate change scenarios in line with observational data and to provide multi-model future projections based on different scenarios of greenhouse gas emissions and socioeconomic development. In August 2021, IPCC released the sixth assessment report AR6 report (IPCC, 2021) which relied on Shared Socioeconomic Pathways SSP scenarios that explore the effect of societal choices on greenhouse gas emissions. The SSPs (IPCC, 2021) are complementary to RCPs-radiative forcing (IPCC, 2014) by adding multiple socio-economic scenarios based on the Paris Agreement climate targets. SSPs scenarios are mainly based on focusing on the changing paths of education & population growth, technological progress, urbanization, economic development and environmental conditions SSP includes five paths: SSP1-1.9, 2.6, 4.5, 7.0, and SSPP 8.5, described in Table 2-4. Figure 2-1 shows the future global surface temperature resulting from the use of different scenarios of AR4 (IPCC, 2007), AR5 (IPCC, 2014), and AR6 (IPCC, 2021)

Table 2-4. The differences among RCP scenarios

SSP	Scenario	Mean projected global temperature rise (°C)		Very likely range (°C)
		(2041–2060)	(2081–2100)	(2081–2100)
SSP1-1.9	Sustainability of the road- achieving the Paris Agreement climate targets by reducing CO2 emissions to net-zero by 2050	1.6 °C	1.4 °C	1.0 – 1.8
SSP1-2.6	Sustainability of the Road- achieving the Paris Agreement climate targets by reducing CO2 emissions to net-zero by 2070	1.7 °C	1.8 °C	1.3 – 2.4
SSP2-4.5	Middle of the Road- CO2 emissions remained close to current levels until 2050, then declined by 2100 but not net-zero	2.0 °C	2.7 °C	2.1 – 3.5
SSP3-7.0	A Rocky Road - CO_2 emissions double by 2100	2.1 °C	3.6 °C	2.8 – 4.6
SSP5-8.5	Taking the Highway- CO_2 emissions triple by 2075	2.4 °C	4.4 °C	3.3 – 5.7

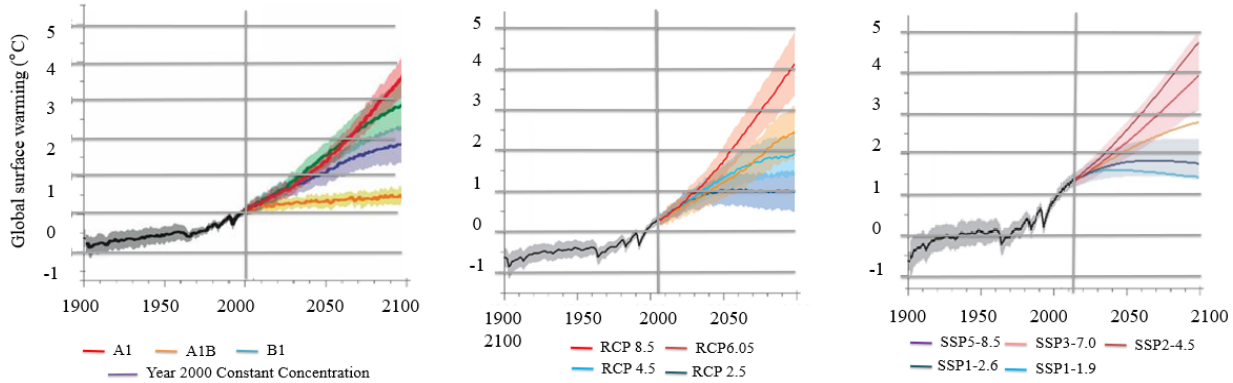

Figure 2-1. Future global surface temperature using different scenarios from AR4 (IPCC, 2007), AR5 (IPCC, 2014), and AR6 (IPCC, 2021)

2.3.3.2 Global Circulation Model (GCM)

Climate models are one of the main ways for scientists to understand what caused climate change in the past and how it might change in the future. GCM is a numerical model for representing physical processes in the components of the climate system (NOAA, 2016). The climate system processed in a climate model consists of: 1) the atmospheric component that simulates aerosols and clouds that have a significant contribution to heat transfer around the world; 2) the component of the land surface that studies surface properties such as vegetation, soil, rivers, and snow cover; 3) the ocean component that analyzes the movement and biochemistry of the oceans that constitute the largest reservoir of heat and carbon in the climate system, and the sea ice component that modulates solar radiation (NOAA, 2016).

In 1995, the Coupled Model Inter-comparison Project (CMIP) was initiated under the auspices of the Working Group on Coupled Modeling (WGCM, 2014) in order to provide a community infrastructure to support diagnostics, validation and documentation of the climate model. This infrastructure allows bringing together a diverse group of scientists from around the world to systematically analyze and improve GCMs to understand the past, present and future climate changes caused by non-forced natural fluctuations or changes in radiative forcing. The outputs of the first climate models collected by CMIP were based on constant values of solar energy and CO2 and then the outputs were collected from the idealized forcing which assumes a 1% increase in CO2 per year. The Spatial resolution of the GCMs in this CMIP phase was about 500 km. CMIP (Hausfather, 2019) continues to develop experiments and models to have a high spatial resolution with new biogeochemical and physical processes to represent climate change. In CMIP Phase Three (CMIP3), the 'realistic' scenarios developed were included in the Fourth Assessment Report of IPCC (AR4) to examine past and present climate impacts. The spatial resolution of the GCMs in CMIP3 reached about 100 km. Based on the IPCC Fifth Assessment Report AR5, CMIP5 climate models are presented. CMIP5 includes 20 climate modelling groups from around the world who have modelled 43 GCMs to consider 4 representative concentration pathways (RCPs). The outputs of CMIP5 include simulated data for historical climate from 1850 to 2005, short-term from 2006 to 2035 and long-term to 2100 and beyond for 4 RCPs. In this CMIP phase, they included the radiative forcing estimation in the past with the idealized forcing in the integrations forcing to estimate future changes. The newest phase of CMIP is CMIP6 (WCRP, 2021). To date, 10

Scenario Model Comparison Projects (Scenario MIPs) (O'Neill, 2016) provide future projections based on SSP scenarios from IPCC AR6. However, CMIP5 is used in this study due to limited model availability in CMIP6.

The GCMs in CMIP5 depict the climate using a three-dimensional grid over the globe with a horizontal resolution between 50 and 300 km, and 10 to 20 vertical layers in the atmosphere and sometimes as many as 30 layers in the oceans (IPCC, 2019 and NOAA, 2019). These predictions (predictors) have a low spatial and temporal (daily or monthly) resolution. Therefore, the downscaling technique is required to convert the predictions from-coarse scale to fine-scale (local scales) to obtain local weather data predictors.

2.3.3.3 Downscaling techniques

The downscaling approach is the derivation of local regional-scale (10-50 km) information from larger-scale modelled. There are two main approaches: dynamical downscaling and statistical downscaling (CIESIN, 2014; GIS climate change UCAR, 2019 and NOAA, 2019). According to Moazami et al. (2019), 71% of researchers in previous studies used a statistical downscaling to generate future years, 15% used dynamical downscaling and 14% used observational data.

2.3.3.3.1 Dynamical downscaling

Dynamical downscaling relies on the use of a regional climate model (RCM), similar to a GCM in its principles but with higher resolution. RCMs take the large-scale atmospheric information supplied by GCM output at the lateral boundaries and incorporate more complex topography, the land-sea contrast, surface heterogeneities, and detailed descriptions of physical processes to generate realistic climate information at a spatial resolution of approximately 1–25 km and a temporal resolution of approximately 5 -120 minutes. Since the RCM is nested in a GCM, the overall quality of dynamically downscaled RCM output is tied to the accuracy of the large-scale forcing of the GCM and its biases (Seaby et al., 2013).

The Coordinated Regional Climate Downscaling Experiment (CORDEX) (Giorgi et al., 2009) was developed and validated by the WCRPR to develop a framework to generate regional-scale climate projections according to GCMs of CMIP5 across multiple regions around the world. CORDEX divided the world into 10 main domains, namely North America (NAM), Central America (CAM), South America (SAM), Europe (EUR), Australia (AUS), Africa (AFR), West Asia (WAS), East

Asia (EAS), Central Asia (CAS) and Southeast Asia (SEA). CORDEX adopted the REMO2015 regional climate downscaling method which was developed for the Europe domain and then spread to several domains around the world such as North America (Cerezo-Mota et al., 2016), Africa (Haensler et al., 2011 and Haensler et al., 2011b), South Asia (Kumar et al., 2014) and South America (Solman, et al. 2013). With REMO2015, CORDEX was able to increase the spatial resolution of regional climate data from 50 km to at least 25 km for all domains and 12.5 km for the Europe domain (Jacob, et al., 2014). The time accuracy is up to 3 hours for all domains and 1 hour for Europe domains during the historical period (1976-2005) and the future period (2006-2100). Data on seven climate variables, called near-surface air temperature, near-surface relative humidity, near-surface specific humidity, near-surface wind speed, surface air pressure, surface downwelling shortwave radiation, and total cloud fraction, are available for the RCP4.5 and/or RCP8.5 scenarios. CORDEX data is freely available and accessible in the Earth System Grid Federation (ESGF). CORDEX selected three GCM models for the North American domain, called NorESM MPI-ESM and HADGEM2ES, that represents a wide spread of sensitivity of global equilibrium climate (ECS). Equilibrium climate sensitivity (ECS) (Armour, 2017) is a quantity that describes how sensitive the climate is to Earth system models (ESMs) by estimating the eventual steady-state mean surface temperature when CO2 doubles. NorESM GCM has low ECS sensitivity at 1.5 °C, MPI-ESM GCM has medium sensitivity at 3 °C and HADGEM2ES has high sensitivity at 4° C (Giorgi, 2019). According to Georgi (2019), the main reasons for these differences lie in hypotheses underpinning climate models, such as their representation of the physical climate interactions. This uncertainty will increase in climate models when it downscales from FCM to RCM, which can increase to range from 3 °C up to 10 °C, especially in regions in northern high latitude regions.

Data Bias in Regional Climate Data

There is often a relative difference (not in absolute values) between weather data generated by regional climate models during a particular historical period and observational data for the same period, and this difference is called bias. Most of the data on the CORDEX models has not been adjusted, therefore, it is important to know whether or not this data has bias-adjusted before using it. Various techniques exist for making a model bias-adjusted, called bias adjustment methods. In these methods, the correction factor is usually calculated by comparing the simulation data from

the regional model with measurements data in the reference period and then applied to both the historical and future climate, which results in historical bias-adjusted and future-bias-adjusted data.

Many researchers and scientists, such as Michelangeli et al. 2009, Piani et al. 2010 and Hempel et al. 2013, have contributed to the development of various types of bias correction algorithms, such as rank matching, histogram equalizing and quantile mapping (QM) methods. The majority of these methods rely on cumulative distribution functions (CDFs) to account for bias correction between the simulated and observed climate variables (Piani et al. 2010; Wilcke et al., 2013). Quantile mapping is one of the most popular correction methods in climatology (Wilcke et al., 2013). This method, like most other methods, is used to correct the bias for individual variables (univariate method), which means that it ignores the interrelationships that exist between climate variables (Wilcke et al., 2013).

For the effectiveness of the quantile mapping method, it was developed by several researchers, such as Vrac and Friederichs (2015), Cannon (2016) and Mehrotra and Sharma (2016), to be able to correct for multivariate bias, called multivariate bias correction (MBC). According to Cannon (2018), "*MBCn method transfers all aspects of an observed continuous multivariate distribution to the corresponding multivariate distribution of variables from a climate model using the N-dimensional probability density function transform, not as other methods (such as Pearson or Spearman rank correlation) that neglect the dependence between different variables"*. Cannon (2018) compared the MBCn approach to other univariate bias correction methods to describe wildfire weather across North America. He found that the MBCn method was more accurate in describing wildfire weather. This method was adopted to correct for bias for all aspects of the climatic continuum of the CanRCM4 simulation.

2.3.3.3.2 Statistical downscaling

Statistical downscaling refers to generating high-resolution climate data by developing the relationships between local climate variables (e.g., surface air temperature and precipitation) and large-scale predictors (e.g., pressure fields) statistically.

There are three main methods to perform statistical downscaling (NARCCAP, 2019):

1. **Linear Methods:** This approach, such as the Delta method, and the Simple and multiple linear regression method, is used to establish linear relationships between predictors and predict. It is the simplest and easiest method, but it is suitable for spatial downscaling only.

- **Stochastic weather generation**: This method generates synthetic weather data having statistical data similar to the observed data for unlimited periods of time. This approach is used for spatial downscaling by creating time series of weather at the location from which the observed data were obtained. Meteonorm software (Meteonorm, 2021) uses the statistical interpolation method to create future climate weather files based on the A2, A1B and B1 scenarios from IPCC AR4. They used the average of data that obtained from 18 of GCMs to provide data for future ten-year periods up to 2100 by generating six weather variables, i.e. the minimum, maximum and mean temperature, solar radiation, wind and precipitations.
- **Morphing**: this method is adopted by Belcher et al. (2005). The morphing approach uses the observed climate as the baseline climate, which is reliable, instead of GCM monthly averaged climate variables for a baseline period (Berardi, 2017). This method achieves spatial downscaling since the present-day weather series is used from observations at a real location (Berardi, 2017). The morphing method was compared with RCM from UKCIP02 by heating degree days HDD, and it was found that the morphing method can provide very similar results to RCM (Belcher et al., 2005). CIBSE (Chartered Institution of Building Services Engineers) selected this method rather than the weather generation method because it is the most reliable (Berardi, 2017).

  Morphing involves three generic operations (Jentsch, 2018): 1) shift, such as relative humidity, atmospheric pressure, and total sky cover; 2) linear stretch (scaling factor), such as Global horizontal radiation, Diffuse horizontal radiation, wind speed; and 3) combination of shift and a stretch, such as Dry bulb temperature (°C) shifted by the mean temperature value and stretched by the predicted change (Jentsch, 2012)

The Sustainable Energy Research Group (Jentsch, 2013) used the Morphing method to develop the Climate Change World Weather Generator (CCWeatherGen) excel tool to generate the future typical year from reference weather climate. The developers analyzed 29 models of GCMs and chose the HadCM3 climate model because it was the only model that contained all the necessary climate variables at the time. They also chose the A2 socio-economic scenario to generate future

nine weather variables, i.e. the maximum, mean and minimum daily temperatures, the relative humidity, the daily total solar irradiance, the cloud cover, the wind speed, the precipitations and the atmospheric pressure. The tool provides three future weather profiles: 2011-2040, 2041-2070, and 2071-2100. This tool provides three future weather profiles, 2011-2040, 2041-2070, and 2071-2100, in EnergyPlus Weather (EPW) format to make the data available for building simulation studies.

Arup and Argos Analytics developed the WeatherShift tool (Dickinson and Brannon, 2016), which uses the morphing method to generate future typical years from 14 GCMs with two scenarios, RCP4.5 and 8.5. The cumulative distribution functions (CDF) are generated from the outputs of these fourteen models. The percentile distribution, such as the 10th and 90th distributions, obtained from CDF represents the percentage of GCM models above and below the percentile (Troup and Fannon, 2016). For example, if a 4°C temperature change in CDF is at the 70th percentile, this means that 70% of 14 global models predict a temperature change above 4°C, while the other 30% predict a lower temperature change temperature by 4 °C. This tool provides three future weather profiles, 2026-2045, 20456-2075, and 2081-2100, in EnergyPlus Weather (EPW) format with generating future eight weather variables, i.e. the maximum, mean and minimum daily temperatures, the relative humidity, the total solar irradiance, the wind speed, the precipitations and the atmospheric pressure.

Table 2-5 shows the advantages and disadvantages of Morphing and CORDEX downscaling methods.

Table 2-5. Advantages and disadvantages of downscaling methods (Moazami et al., 2019; Jentsch et al., 2013)

	Statistical (Morphing)	Dynamical (CORDEX)
Advantages	This method - Requires low computational time, cost and power - Generates EnergyPlus Weather (EPW) files for building simulation studies in a simple and easy way - Does not need to bias-adjusted	This method - Develops a physical data set between different weather variables and climate components - Detects years with extreme heatwaves
Disadvantages	- Represents climate change through the change in monthly averages without any physical correlation between weather variables - Creates typical years into the future which makes it difficult to detect extreme events in the future	- Requires high storage capacity to download weather data - Needs to analyze the data either to determine the data for the desired location or to work on increasing the time resolution to 1 hour or less, where the weather data is available for 3 hours as in CORDEX - Requires time and knowledge to convert the data to an EPW file - Requires bias-adjusted for most data on the CORDEX

2.3.3.4 Reference Summer Weather Year

Most researchers use typical future climate data to evaluate the impact of climate change on building thermal performance. Moazami et al. (2019) found that 52% of researchers used typical future years to represent future climate change and 38% of them used extreme future years. This typical year may be suitable to assess the energy consumption of the building studies but not the overheating studies. To reduce the risk of overheating, buildings should be designed and operated to be resilient under such extreme climatic conditions. Therefore, the researchers aimed to develop a Reference Summer Weather Year (RSWY) that was selected from multi-year climate data with various types of extreme heat events to represent the extreme weather. The development of such

reference years requires the use of proper metrics to rank and select representative years that contain periods of extreme heat events. Furthermore, the metrics should take into account not only the climate variables but also the human factors and building properties that are exposed to such extreme heat events to assess their thermal comfort and heat-related health stress.

There is no universal consensus on the definition of RSWY. Several have attempted to determine RSWY either by temperature distribution, by including other weather variables, such as relative humidity and solar radiation, or by detecting the heatwaves. The Chartered Institution for Building Services Engineers (CIBSE, 2002) developed the Design Summer Year (DSY). The DSY is the third hottest summer within a 21year climate data set based on the average air temperature from April to September (Levermore and Parkinson, 2006). Jentsch et al. (2015) developed a near-extreme Summer Reference Year (SRY) by modifying the selection criteria of DSY or Test Reference Year TRY. SRY is the year that has the highest degree hours and direct solar radiation. However, The DSY or SRY process can result in the selection of years that are warm on average but do not contain extreme heatwave events, so the problem with DSY is that it ignores heatwaves that are usually the cause of heat stress or heat-related death. Therefore, CIBSE TM49 (2014) has adopted the DSY to the probabilistic Design Summer Year pDSY as the RSWY. The pDSY method was developed to detect years when the weather is severe, intensive, or has the longest period of severe weather. The severe year is detected by finding the year that has the highest Weighted Cooling Degree Hours (WCDH). WCDH is the cumulative square of the hourly difference between the outside temperature and the adaptive thermal comfort temperature EN15251 (2007). The intensive year is detected by finding the year that has the highest Static Weighted Cooling Degree Hours (SWCDH). SWCDH is the cumulative square of the hourly difference between the outside temperature and the Static thermal comfort temperature determined for each region in the U.K. by CIBSE TM49 (2014). The intensive year is detected by finding the year that has the highest Threshold Weighted Cooling Degree Hours (TWCDH). TWCDH is the sum of WCDH and SWCDH. This method uses a threshold designed to be suitable for the London climate to determine the overheating which could make it unsuitable for other weather conditions.

Some researchers have developed the RSWY detection method by adding climatic variables other than temperature (such as solar radiation, humidity, and wind speed) and/or adding thermo-physiological parameters (such as clothing and human activities). Jentsch et al. (2015) added the

solar radiation weather variable to detect SRY. Liu et al. (2016) Use the same requirements as pDSY but use physiological equivalent temperature (PET) rather than air temperature to determine. PET (Hoppe, 1999) is defined as "*the air temperature at which, in a typical indoor setting (without wind and solar radiation), the heat budget of the human body is balanced with the same core and skin temperature as under the complex outdoor conditions to be assessed*". Laouadi et al.(2019) used the Transient Standard Effective Temperature tSET that was developed from Standard Effective Temperature SET rather than outdoor temperature to determine the RSWY. SET (ASHRAE 55, 2017)is defined as "*the temperature of an ideal indoor environment at 50% relative humidity and air temperature, in which an imaginary occupant wearing clothing standardized for the activity level has the same heat stress (skin temperature) and strain (skin wittedness) as in the actual environment*". They developed a tSET (Laouadi et al., 2019) using the approach of Schweiker et al. (2016) by considering the solar radiation, some modifications in thermo-physiological parameters, and calculation of past and present thermal conditions when calculating the SET at each hour. These methods usually rely on developing special thresholds for these methods to identify the heatwaves or overheating. These thresholds are often associated with a specific region and period, which makes them unsuitable and not appropriate for all regions and climate periods (historical and future) in the world.

Ouzeau et al. (2016) developed a method for finding RSWY based on the heatwave detection operational method that was adopted from Météo-France for climate monitoring (Ouzeau et al., 2006). This method has the advantage of being applicable to any region and time series by calculating its threshold value based on selected historical data for a selected location. This method has the advantage of using three percentile thresholds (instead of one) to combine two successive heatwave events with no significant temperature drop between them. These three percentile thresholds are calculated over the daily mean air temperatures of the 20-year historical temperatures to apply to the future air temperatures. S_{pic} threshold represents 99.5 quantiles of the daily mean temperature during the historical period (20 years), which defines the beginning of the heatwave; 2) S_{deb} represents 97.5 quantiles, and 3) S_{int} represents 95 quantiles. To detect a heatwave, the outdoor temperature ($T_{outdoor}$) must be above the S_{pic} threshold for at least one day. The heatwave begins from the day when the daily outdoor temperature ($T_{outdoor}$) is above the S_{pic} threshold or from days before that day provided that the $T_{outdoor}$ is above the S_{deb} threshold and without interruption. The heatwave is interrupted or ends if the $T_{outdoor}$ is below S_{deb} for three

consecutive days or $T_{outdoor}$ is below S_{int} on one day. Each heatwave must be at least 5 consecutive days.

2.3.3.5 Uncertainties in weather data generation

There are many uncertainties in climate generation starting from climate models and ending to the bias correction factor. In this section, the main causes of various uncertainties are presented. According to Hawkins and Sutton (2009, 2011), there are three main categories of uncertainty in global climate models that may relate to 1) the emissions scenario, 2) the climate model, and 3) meteorological. Uncertainty in emissions scenarios relates to uncertainties about assumptions associated with socio-economic development and climate change mitigation policies. Climate model uncertainty relates to uncertainties in predictions, representations of climate variables and boundary conditions that can vary from one model to another. Meteorological uncertainty is related to the natural fluctuations of the climate from year to year. For example, the trend in ten years may be warming but the weather in one of ten years may be abnormally extreme hot or cold.

There are also uncertainties associated with downscaling methods. For the statistical method, the uncertainties are related to 1) the spatial scale, 2) the time factor, and 3) the equations of the morphing method (Jentsch et al, 2013). The uncertainty in the spatial scale is related to the significant difference between the spatial resolution of GCM data ranging from 100 to 250 km and the observed data ranging from 1 to 12 km. Uncertainty in the time factor is associated with a lack of information about daily or hourly climate changes due to the use of monthly averages of future climate change resulting in an inability to detect extreme events. Uncertainties in the equations of the morphing method are related to the independence (lack of correlation) between climate variables. Uncertainties in the RCM are related to uncertainty in the GCM and emissions scenarios (Georgi, 2019). According to Georgi (2019), the uncertainty in the model increases when the scale is downscaled from global to regional.

In addition, there is uncertainty in the main assumption of the correction factor in bias-adjustment methods which states that the correction factor is a constant that does not change over time, i.e. it will be the same in the future. But it is not certain whether this factor will change in the future or not (Cannon, 2018).

2.4 OVERHEATING MITIGATION MEASURES

Grussa et al. (2019) found that using the exterior shutter shading and night ventilation in detached houses in the U.K. was effective in mitigating indoor overheating in the 2016 climate. However, they state that based on current U.K. building practices, some types of external shading, such as shutter shading, may not be an available solution because in most cases the windows open outwards. Tink et al. (2018) applied night ventilation and internal blinds shading as mitigation measures to improve the indoor thermal condition of an existing house in the U.K.in 2015. They found that these mitigation measures reduced the indoor temperature by 2 °C and removed the overheating risk during the heatwave event in 2015. Auzeby et al. (2017) used Phase Change Materials (PCM) to improve the indoor thermal condition of U.K. residential buildings. PCM is used to absorb excess heat when the room is warm and release stored heat when the room is cold. They found that PCM kept the indoor temperature below 28 °C until 2050. Huanga and Hwang (2017) found that increasing the thermal insulation of the building envelope, reducing the window-wall ratio and adding exterior shading in the detached house in Taiwan had a great impact on reducing overheating. Hooff et al. (2014) evaluated six passive climate change adaptation measures; (1) thermal resistance of building envelope; (2) thermal mass; (3) short-wave reflectivity (albedo value); (4) green roof; (5) exterior solar shading; and (6) additional natural ventilation; to reduce the impact of climate change on house and apartment building in the Netherlands. They concluded that the exterior solar shading and the additional natural ventilation were the significant measures to reduce overheating, while the other measures had a slight effect. Peacock et al. (2010) concluded that natural ventilation significantly reduced the overheating risk, but it is not sufficient in the future climate. Peacock et al. (2010) simulated three different types of building envelopes ranging from light construction with low thermal transmittance to a massive wall with high thermal transmittance. They found that the high thermal mass and high thermal transmittance of the building envelope can reduce overheating risk by 6% in a cold and warm climate.

2.5 OPTIMIZATION OF BUILDING DESIGN

Approximately 2% of the world's buildings are newly constructed each year, a similar amount is renovated, and the rest are existing buildings (IEA, 2020). In the U.S., 88% of building stock, 54 belong to buildings over twenty years old (U.S. EIA, 2016). In most EU countries, 50% of building

stock was built before 1970, which means before the first energy regulations (European Commission, 2022). In Canada, 88% of the building stock was built the 2000s and 45% of them were before the 1980s (NRC, 2020). These buildings that are over 50 years old are a high consumer of energy and a high generator of greenhouse gases, and most of them have reached the end of their first life cycle and must be renovated. During the design stage of an existing building renovation, building and architectural engineers must attempt to achieve multiple performance aspects in a building design simultaneously. However, Some design strategies used to improve some performance aspects of building design such as reducing energy consumption have a negative impact on other aspects of building design such as thermal or visual comfort. For example, increasing the insulation level of building envelope parameters that significantly reduce the heating energy consumption of buildings may significantly increase the overheating risk during summer (BC Energy Step Code, 2019; Mulville and Stravoravdis, 2016; Baniassadi and Sailor; 2018; Fosas et al. 2018). Also, the window design strategy**,** including the Window-Wall Ratio WWR, glazing system and shading, have a significant impact on the energy consumption, lighting load and thermal comfort. The large WWR provides a great amount of indoor daylight, but this size of WWR can cause brightness and visual fatigue due to glare (Nelson et al., 1984), reduce summer thermal comfort (De Luca et al, 2019; Vanhoutteghem et al, 2015), and increase the energy demand (Ville de Montréal, 2017; Uribe et al., 2019; Hoffmann et al., 2016). De Luca et al. (2019) and Hoffmann et al. (2016) found that the use of fixed exterior shading significantly reduced the overheating risk, but it also reduced indoor daylight and increased heating energy consumption. Hoffmann et al. (2016) and Uribe et al. (2019) found that movable shading, which can be a good solution to reduce cooling load while preserving daylight and visibility, needs more instrumentation and maintenance which increases the initial and operational cost.

To find the optimal design from different building design strategies, researchers generally use two main optimization methods: 1) manual method (trial and error) (Uribe et al., 2019; Hoffmann et al., 2016), and 2) automated method using Multi-Objectives Optimization Genetic Algorithm method (MOOGA) (Hamdy et al., 2016; Ascione et al., 2019). Lakhdari et al. (2021) used the manual method to address building design, including exterior shading, WWR and window proprieties (U-value, SHGC and Visible Transmittance), to achieve daylight and thermal comfort in schools in the hot climate. They found that 60% of WWR with exterior louvre shading and window (1.1 $W/m^2.K$, 0.26 SHGC and 0.64 Visible Transmittance (Vt)) can achieve the daylight

and thermal comfort objectives. Sepúlveda et al. (2020) used the manual method to address building design, including WWR and exterior shading, to achieve thermal and visual comfort in a residential building in Estonia. They found that 40% of WWR with 0.9 m exterior overhang shading can achieve the objectives.

The MOGA method was used to find the optimization design that improves various performance aspects of building design, such as energy consumption, thermal comfort, visual comfort, initial cost and/or life cycle cost (Ascione et al., 2019; Gou et al., 2018; Zhang et al., 2017; Sepúlveda et al., 2020; Lakhdari et al., 2021; Zhai et al., 2019; Shen et al., 2019; Ferrara et al., 2018; Jafari and Valentin, 2017). Ascione et al. (2019) used this method to address building envelope design, including thermal transmittance of wall and roof, window type (U-value and SHGC), roof solar absorbance, wall thermal mass and cost of each variable, to minimize primary energy consumption, global cost and discomfort hours of a new archetype Italian residential building. They found that the thermal transmittance and thermal mass of the wall should be 0.2 $W/m^2.K$ and 220 $KJ/m^2 \cdot K$ respectively, similar values for the roof with 0.6 of solar absorbance and the window should be 1.4 $W/m^2.K$ and 0.58 SHGC to achieve their objectives. Gou et al. (2018) used this MOGA method to address building envelope proprieties, building orientation, WWR, roof solar absorbance, exterior shading and wall thermal mass, to reduce energy demand and thermal comfort of a new residential building in Shanghai, China. They found that the optimal design should have the long façade facing south, 18% of WWR with 1.3 m overhang exterior shading, window properties 2.2 W/m2.K and 0.50 SHGC, 0.24 W/m2.K for wall and 0.20 W/m2.K for the roof, and the solar absorbance of a roof should be 0.1. Zhang et al. (2017) used the MOGA method to address WWR, window proprieties (U-value, SHGC and Visible Transmittance) and exterior shading, to improve the thermal and daylight performance of a new school building in China. They found that WWR should be 35%, 0.78 $W/m^2.K$, 0.48 SHGC and 0.66 Visible Transmittance (Vt) for windows and blind roll for exterior shading.

In Quebec, Canada, 85% of school buildings are over 50 years old and 44% are over 70 years old (Després et al, 2017), making them a high consumer of heat energy and a high generator of greenhouse gases. 80% of these schools also relied on natural ventilation and indoor shading only to cool the building in the summer, which made them more vulnerable to overheating risks, especially with climate change and global warming (Flanagan, 2018). With these buildings

reaching the end of their first life cycle, the Quebec government decided to renovate and repair nearly 60% of these buildings at a cost of $1.8 billion over the years 2017-2027 (Gouvernement du Québec, 2021) to improve energy efficiency, reduce greenhouse gas emissions, and improve thermal and visual comfort. Thermal and visual comfort has a significant impact on the satisfaction, performance, health and well-being of building occupants (Ko et al. 2017; Liu, 2017; Wargocki and Wyon, 2017). Daylight and direct sunlight are critical to human health and their circadian rhythms and to reduce energy lighting load (Tabadkani et al, 2021; Ramasoot and Panyakeaw, 2015).

2.6 SUMMARY OF LITERATURE REVIEW

According to this literature review, the following research gaps and questions are identified:

- Contradictory findings are reported in the literature showing that new high energy-efficient residential buildings (HEEB) have either higher or lower overheating risks compared with older buildings, as shown in Section 2.1. Most of the sensitivity analysis of building envelope studies used the local sensitivity analysis method that cannot determine the effect of changing several input parameters simultaneously on the change in indoor temperature and the contribution of each parameter. Most of these studies examined sensitivity analysis with a low ventilation rate of less than 1 ACH. The question is whether the ventilation rate has an interactive effect with the thermal properties of the building envelope and does the contribution of thermal properties of the building envelope to indoor overheating risk change with the change of the ventilation rate?
- There are limited studies on model calibration based on the hourly indoor temperature for overheating studies compared to many calibration studies for building energy performance, as shown in Section 2.2. Most of the calibration studies based on the hourly indoor temperature used the manual calibration method to determine unknown parameters, and it is often calibrated for a single room in the building by calibrating the unknown parameters in this room without considering the impact of unknown parameters in other rooms, which neglects the effect of heat transfer between rooms in the calibration process. In addition, there are no specific evaluation criteria and acceptance range for the indoor temperature calibration in building overheating studies. The assessment of overheating or thermal risk

requires a more accurate prediction of indoor temperatures since one- or two-degree differences may cause a major difference in thermal risk, especially for vulnerable people. The questions are, can a robust methodology be developed to obtain a highly accurate calibrated EnergyPlus model for multi-room indoor temperature prediction to reduce the discrepancy in the overheating risk assessment? What evaluation criteria should be developed to evaluate the EnergyPlus model compared to indoor measured temperature?

- There is not much information available to researchers and decision-makers about the indoor thermal conditions of Canadian buildings under present climates and extreme future years, where most researchers used a typical future year to study the impact of climate change on buildings, as shown in Section 2.3. The question is how existing and archetype Canadian buildings have thermally performed under recent climates and how they will be performing under extreme future climates.
- There are limited studies on the effective overheating mitigation measures in cold climates, as shown in Section 2.4. The question is how to effectively mitigate overheating risks for Canadian buildings?
- There are limited studies on optimization strategies that are required to find the optimal building design solutions if the existing building is to be completely renovated, as shown in section 2.5. The questions are, what optimization strategies should be developed when retrofitting existing Canadian buildings to consider heating energy consumption, thermal and visual comfort aspects of building performance.

CHAPTER 3: RESEARCH METHODOLOGY

The developed systematic frameworks shown in Figures 3-1 and 3-2 outline the steps needed to assess and mitigate the overheating risk in Canadian archetype and existing buildings, respectively, under recent and future climates by addressing the knowledge gap described in Section 2.6

For archetype buildings, the developed framework (Figure 3-1) includes:

1) Determination of the contribution of each building envelope parameter to the change in indoor temperature to determine whether old buildings have lower or higher overheating risk than HEEB buildings. To achieve that, a new **Sensitivity Analysis Methodology** is developed based on global and local sensitivity analysis to determine the sensitivity, contribution and correlation between building envelope parameters (BEP) and indoor temperature with and without natural ventilation (Section 3.1.1).
2) Assessment of the impact of climate change on the indoor thermal conditions of archetype Canadian buildings. To achieve that, the **overheating risk** (OR) in archetype buildings is assessed; 1) with different thermal properties of the building envelope representing buildings at different ages to determine the effect of the building envelope on the indoor overheating risk (Section 3.1.2); 2) under different weather generations using different climate scenarios to determine the thermal performance of these buildings under recent and future climates (Section 3.1.3), and 3) with different ventilation rates to determine the effectiveness of ventilation in mitigating the indoor overheating and to determine the minimum ventilation rate that makes new HEEB buildings perform better than old buildings (OB)
3) Finding effective passive and emergency cooling **mitigation measures** (MM) for the building if the overheating risk is higher than the Acceptable Limit (AL). To achieve that, the potential mitigation measures parameters are identified, and the Global Sensitivity Analysis (GSA) is carried out to find sensitive and effective mitigation measures. The overheating risk in a building is assessed with sensitive mitigation measures under recent and future climates to provide recommended overheating mitigation measures under different climate generations (Section 3.1.4).

To illustrate the process of assessment and mitigation of overheating conditions in archetype building under recent and future climates, in the following Section 3.1, the proposed framework is implemented and demonstrated by an **Archetype detached house** for each major step in Figure 3-1.

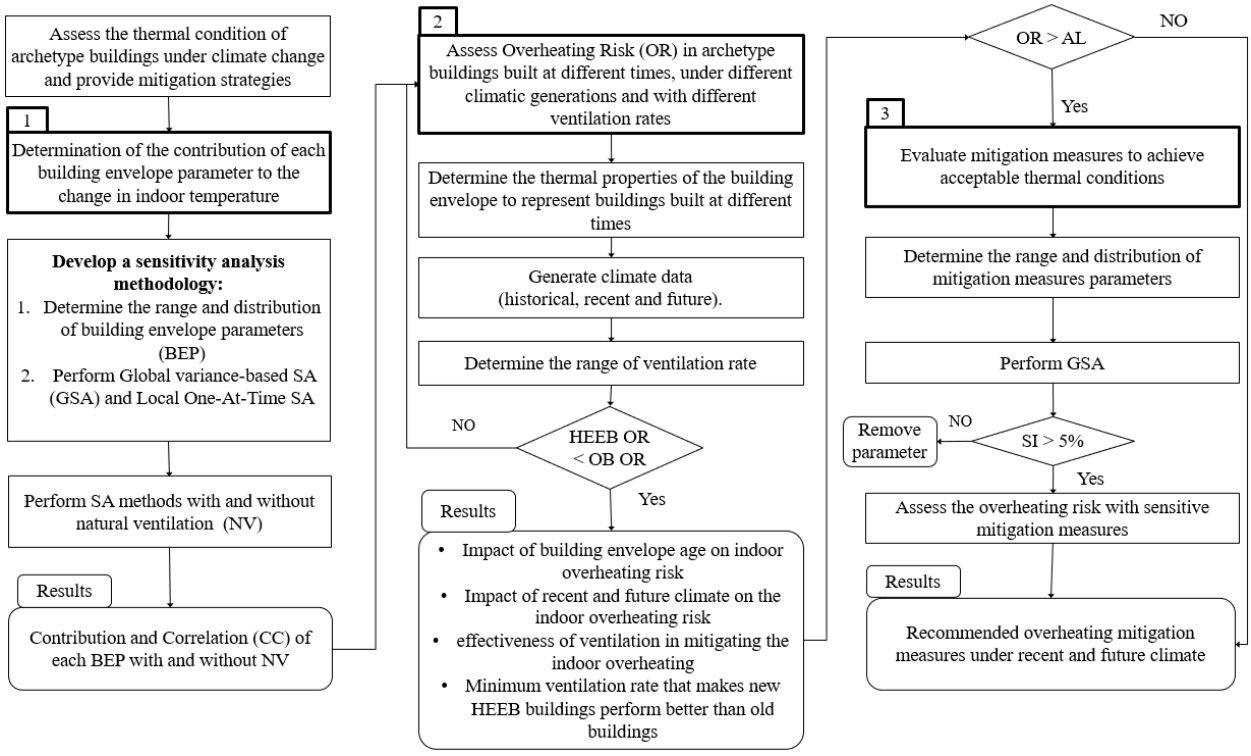

Figure 3-1. Proposed framework to assess overheating risk and mitigation measures in archetype buildings

For existing buildings, the developed framework (Figure 3-2) includes:

1. Calibrating EnergyPlus models for existing buildings to achieve high-accuracy prediction of indoor air temperature compared to indoor air temperature measurement. To achieve that, a **Calibration Methodology** is developed based on a Multi-Objective Genetic Algorithm (MOGA), global sensitivity analysis, and new evaluation and selection criteria (Section 3.2.1).
2. Assessment of the impact of climate change on the indoor thermal conditions of existing Canadian buildings. To achieve that, **overheating risk** (OR)in an existing school building (Section 3.2.2) is assessed using the calibrated building model under different climate

generations to determine the performance of these buildings under recent and future climates (Section 3.2.3).

3. Finding effective passive and emergency cooling **mitigation measures** for the building if the overheating risk is higher than the Acceptable Limit (AL) specified by building guidelines. To achieve that, the potential mitigation measures parameters are identified, and the Local Sensitivity Analysis is performed to find sensitive and effective mitigation measures. The overheating risk in a building is assessed with sensitive mitigation measures under recent and future climates to provide recommended overheating mitigation measures under different climate generations (Section 3.2.4).
4. Finding the **optimization building design** if the existing should be completely renovated. To achieve that, optimization strategies are developed based on MOGA to achieve three building performance aspects (objectives), i.e. lowest heating energy demand and highest thermal and visual comfort in new building design (Section 3.2.5).

To illustrate the process of assessment and mitigation of overheating conditions in an existing building under recent and future climates, in the following Section 3.2, the proposed framework is implemented and demonstrated by an **existing school building** for each major step in Figure 3-2.

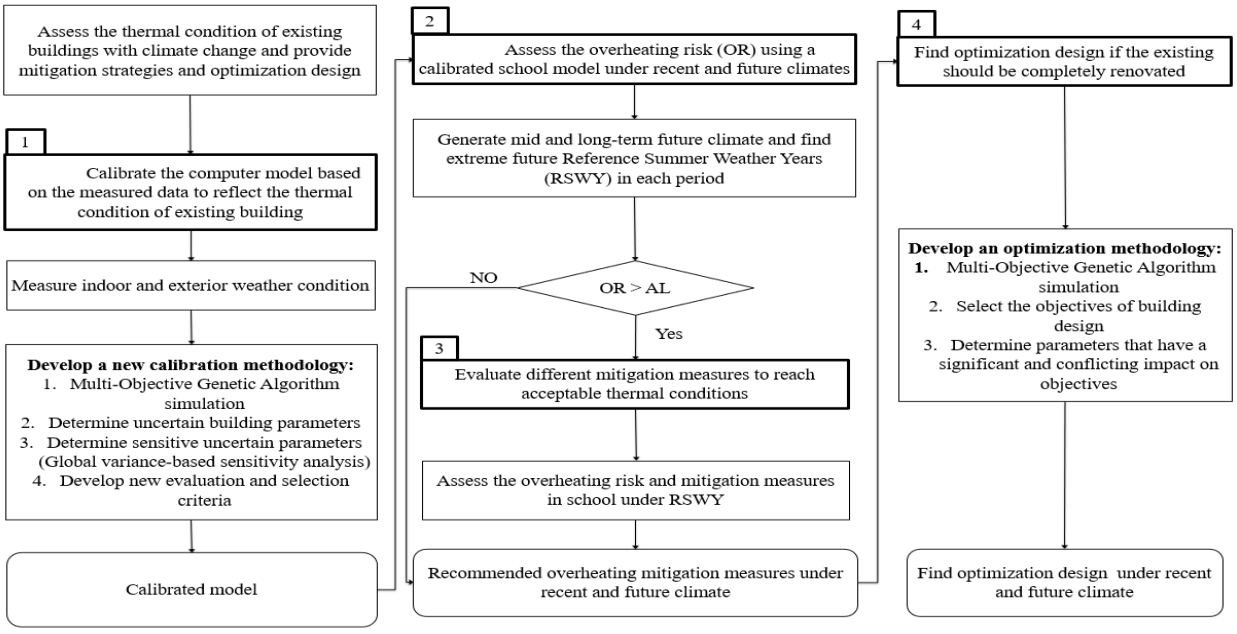

Figure 3-2. Proposed framework to assess overheating risk and mitigation measures in existing buildings

The research activities are organized as follows:

3.1 ARCHETYPE BUILDING

3.1.1 Sensitivity analysis methodology

To determine the sensitivity, contribution and correlation between building envelope parameters and indoor temperature, the global variance-based method and local OAT method are proposed as shown in Figure 3-3. Global and local sensitivity analysis methods used in this work are illustrated in Sections 3.1.1.1 and 3.1.1.2, respectively. To determine whether the contribution and correlation of the building envelope are affected by the amount of ventilation rate in the building, the global and local sensitivity analyses are performed with and without natural ventilation. If there is a change in the contribution and correlation results based on the ventilation rate, the minimum ventilation rate (threshold) that makes the new HEEB buildings perform better than the old buildings should be determined.

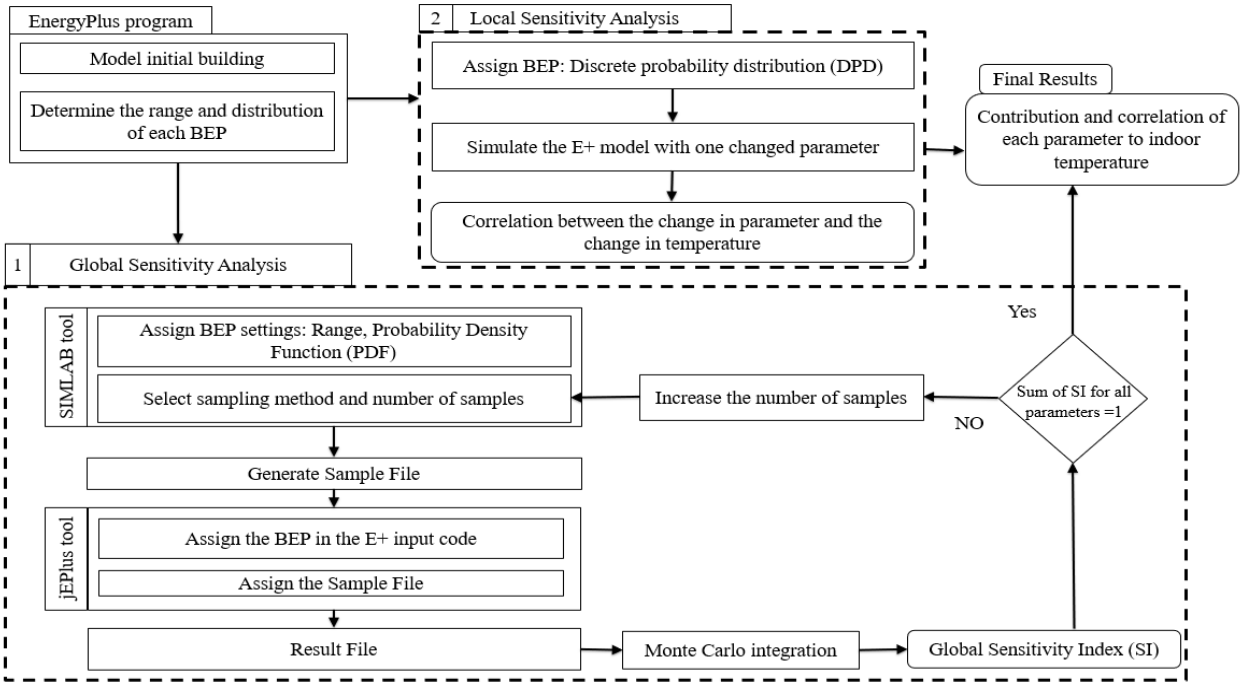

Figure 3-3. Proposed workflow to calculate the contribution of each building envelope parameter

3.1.1.1 Global sensitivity analysis

A Global Sensitivity Analysis (GSA), SOBOL variance-based, is carried out to determine the contribution of building envelope parameters to buildings' indoor operative temperature. The SOBOL method (Rabitz, 2010) is chosen in this study because of its ability to deal with non-linear and non-monotonous correlations between input and output, measure the effect of interactions between input parameters, and calculate the contribution of each input to the output.

Figure 3-3 shows the proposed workflow that is used to determine the contribution of each building envelope parameter to indoor operative temperature using EnergyPlus, SIMLAB and jEPlus tools. EnergyPlus program is used to model an initial building with all details except the thermal properties of the building envelope, which are defined as variables. SIMLAB program (Joint Research Centre, 2015) is used to generate a sample file that is generated by assigning the range and probability density function (PDF) of the thermal properties of the building envelope parameters and specifying the sampling method and number of samples. The Sample File that contains all sampled cases are simulated using the jEPlus tool (Zhang, 2012), which provides a Graphical User Interface (GUI) for defining the building envelope parameters, editing the EnergyPlus input model, managing simulation samples in EnergyPlus, and collecting results of the average indoor operative temperature. jEPlus generates the Result File that contains one result value (average indoor operative temperature in summer) for each sampled case. Monte-Carlo integration is then used to calculate the sensitivity indices (SI) based on Sample File and Result File. The sum of sensitivity indices should be 1 when the model is purely additive (i.e. no correlation among the inputs) and there are enough samples, therefore, the SI can be presented as ratios. The minimum sample numbers required in the SOBOL method can be determined from Equation 3-1, and if the total sensitivity indices are not 1, then the number of samples must be increased using Equation 3-2. "Total-order Sensitivity Index (S_{Ti})" that gives the total contribution of one input and its interactions with other input variables to the output is calculated using Equations 3-3.

$$N_m = 16 \cdot (2k + 2) \tag{3-1}$$

$$N_r = 2^{(r-1)} \cdot N_m \ , \quad r = 1 \dots 9 \tag{3-2}$$

$$S_{Ti} = 1 - \frac{V_{X\sim_i}}{V(Y)} \quad (3\text{-}3)$$

Where N_m is the minimum number of samples, where each sample contains one value from the range of each parameter. N_r is the number of samples required to achieve a sum of sensitivity indices equal to 1, which is the multiple of the minimum number, V(Y) is the total variance of the model output (variance of all parameters with all interactions), and $V_{X\sim_i}$ measures the effect of all parameters except X_i on the model output.

3.1.1.2 Local sensitivity analysis

Local sensitivity analysis (LSA), the one-time method (OAT), is used to determine whether the correlation between the change in the building envelope parameter and the change in indoor temperature is positive or negative. A positive correlation is defined as when a decrease in the thermal characteristic values of the building envelope parameters leads to a decrease in the indoor temperature in the summer, and a negative correlation is defined as when a decrease in the thermal characteristic values of the building envelope parameters leads to an increase in the indoor temperature in the summer. For example, a decrease in the thermal characteristic values, such as a decrease in the U-value of walls, roofs and windows means higher thermal insulation values and more energy-efficient building envelopes. In this method, one parameter is changed at a time (OAT) and others are kept at their baseline value to see what effect this has on the output.

3.1.2 Study building: Single-family detached house

Single-family detached houses represent 53.6% of residential buildings in Canada (Statistics Canada, 2019). Montreal ranked second in the number of single-family detached houses in Canada (Statistics Canada, 2019). Single-family detached houses consumed 17% of total energy use and contributed to 10% of Canada's greenhouse gas emissions (NRCan, 2014). Therefore, a free-running archetype Canadian single-family detached house is selected as a representative building in Montreal in this study. The proposed sensitivity analysis methodology is applied to this building with typical Canadian building construction practices, i.e. the building envelope construction was wood-frame construction with the brick veneer external wall, to determine the effect of building envelope parameters representing different building ages on the indoor operative temperature. The overheating risk in this building is also assessed under historical, recent and future climates. Figure

3-4 shows the first and second-floor plans and 3D model in the DesignBuilder program. The total floor area is 85 m^2 for each floor, the window wall ratio WWR is 17% of the external wall area, the length to width ratio is 1.5:1, and it has a ventilated attic with a roof slope of 4/12.

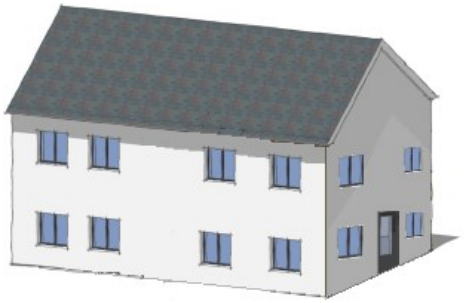

a)

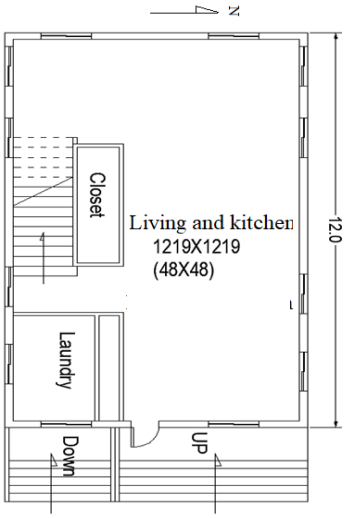

b)

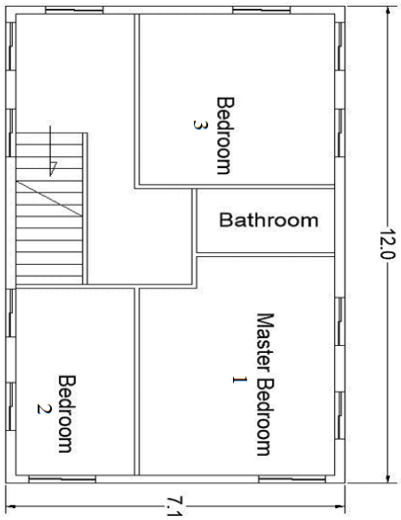

c)

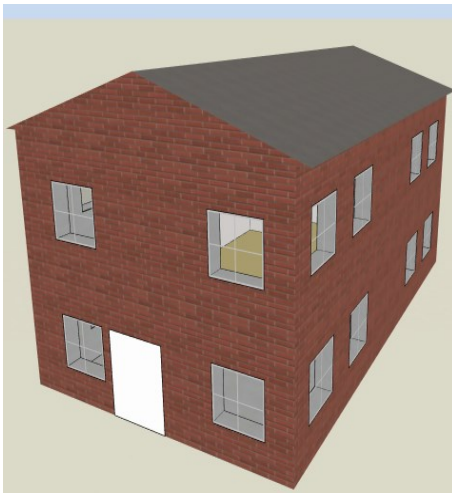

d)

Figure 3-4. a) Sketch up; b) First-floor plan; c) second-floor plan; and d) 3D model of the single-family detached house. Dimensions are in m

3.1.2.1 Building envelope components

Four generations of building envelope thermal characteristics representing buildings built at different times are included to determine the contribution of each building envelope parameter to indoor operative temperature. These generations are: 1) 1950-old building, representing building envelope built from 1945 to 1955. These buildings represent about 17% of all recent homes in

Canada (NRC, 2020); 2) the 1990 building, representing the building envelope built from 1985 to 1995. These buildings represent about 28% of all recent homes in Canada (NRC, 2020); 3) NECB building, representing building envelope in compliance with the National Energy for Buildings NECB-2017 prescriptive requirements; and 4) HEEB-new building, representing building envelope meeting Passive House energy performance requirements (International Passive House Association, 2021). The building envelope's thermal properties listed in Table 3-1 represent the average value of those properties over the age of the buildings. Values for 1950 and 1990 buildings are the average values calculated using the data provided by the CanmetENERGY Natural Resources Canada guide (Parekh, 2012a and 2012b). Based on these four generations of the building envelope, the range of each building envelope parameter is created with a uniform distribution as shown in Table 3-1. This uniform distribution range for each parameter is used in the global sensitivity analysis.

Table 3-1. Building envelope thermal characteristics in buildings built at different ages (Parekh, 2012a and 2012b)

Building Age	Wall	Roof	Windows		**Airtightness**
	U-value ($W/m^2.K$)		U-value ($W/m^2.K$)	SHGC	ACH50 (1/h @50Pa)
1950	0.80	0.60	3.80	0.75	8.0
1990	0.45	0.25	2.50	0.68	4.0
NECB	0.24	0.18	1.50	0.56	2.5
HEEB	0.10	0.08	0.68	0.26	0.6
Uniform distribution range	0.1-0.8	0.08-0.6	0.68-3.80	0.26-0.75	0.6-5.0

3.1.2.2 Key settings in EnergyPlus simulations

The free-running building without any mechanical ventilation system is studied in this work. for two reasons: 1) 58% of residential buildings in Canada do not have air conditioning (NRCan, (2012; and 2013) most heatwaves were accompanied by power outages (Ville de Montréal, 2017;

IOM, 2011). Two scenarios are assumed; 1) the building is designed with horizontal sliding operable windows (natural ventilation (NV) scenario), and 2) with fixed windows (without natural ventilation (NNV) scenario) to represent the situation if the occupant can not open the window for any reason (Lapointe, 2021). The existing survey found that 46% of occupants in north England do not open their windows when they are out of the house or at night due to a security concern (Baborska-Marozny et al., 2017). While 30% of the occupants keep their windows open 5-10 cm of the window during "heatwaves," the outdoor conditions during "heatwaves" may not be favourable for the cooling effect of natural ventilation by keeping windows open (NRCan, 2013; Quigley and Lomas, 2018). Also, some building codes in some countries, such as the UK (DCLG, 2021), have restrictions on windows to open no more than 10 cm for safety reasons A study in New York City found that 30% of seniors were unaware of heat warnings in 2011 and took no action to protect themselves from the dangers of extreme temperatures (Lane et al., 2014). Therefore, in the operable window scenario, four window opening size options are included to represent the behaviour of the occupants, 1%, 3%, 5%, and 10% of the floor area being the window opening size (Window Opening -to-Floor Area WOFA). These values represent 7, 15, 25 and 50 cm (5, 12, 20 and 40% of window area) of the horizontal window opening, respectively, multiplied by the height of the window (1.5 m) in the building. The window design in this building, including window area, window opening ratio and window location, complies with the current provisions of the Québec Construction Code and Safety Code (RdbQ, 2018), where these codes require at least one window with an area not less than 2.3 m^2 for each bedroom and living room to provide ventilation and emergency exit. The window will be opened if the indoor temperature is higher than the natural ventilation setpoint (NV setpoint) and the outdoor temperature. According to the EnergyPlus Airflow Network Model that is used to calculate the natural ventilation rate through the windows, these opening ratios provide 78, 141, 230, 350 L/s (1.5, 2.2, 3.6, 5.5 ACH) average airflow rate during the summer months from May 1st to Sep. 30th. The minimum ventilation rate that is required by ASHRAE 62.2 (2019) is 40 L/s (0.8 ACH) to satisfy indoor air quality requirements for 4 persons. The Airflow Network Model is also used to calculate the air infiltration through the cracks in the building envelope. Other main settings inputs in EnergyPlus simulations are listed in Table 3-2. To find the direct effect of window parameters on the indoor temperature and to evaluate the natural ventilation on the indoor overheating, the absence of indoor shading devices was assumed.

Table 3-2. Inputs in E + program related to this study

Building envelope components	Units	Value	Notes and references
Heating setpoint	°C	21	NBC 9.36.5.4. (5)
Heating setback	°C	18	NEBC Table A-8.4.3.2.(1)
Appliances & plug loads	W/m^2	2.5	NEBC Table A-8.4.3.3 (2) A.
Lighting density	W/m^2	5	NEBC8.4.4.6.
Target Illuminance	Lux	125	NEBC Table A-8.4.3.3 (2) A.
Natural ventilation (NV) set point	°C	24	When $T_{NVset\ point} < T_{inside} < T_{cooling\ setpoint}$ Natural ventilation will be activated

3.1.3 Overheating assessment under recent and future climate

To study the effect of climate change on indoor thermal conditions of Canadian buildings, the overheating risk is assessed in the archetype detached house under recent observational weather (Section 3.1.3.1) and future climate that methods for generating future climate and detecting extreme future years are described in Section 3.1.3.2. Thermal standards and building guidelines used to assess the overheating risk in this building are described in Section 3.1.3.3.

3.1.3.1 Observational weather data

Weather data from 2015 to 2020 were collected from a weather station installed at the Concordia-EV building in Montreal. This weather station records hourly dry-bulb temperature, relative humidity, global solar radiation, wind speed and direction. To identify the recent extreme observational year, the overheating risk in the NECB building with 40% of the window area open is evaluated based on the E+ simulated indoor operative temperature for each year from 2015 to 2020. It is found that the building in 2020 experienced the highest overheating risk with 282 hours, followed by 274, 245, 225, 207 and 177 hours in 2016, 2019, 2017, 2015 and 2018, respectively. Therefore, the 2020 year is selected to represent the recent extreme observational year in this study.

3.1.3.2 Future weather data

To generate future climates for Montreal, the statistical downscaling method, which is commonly used for building studies, is used to generate typical future years, and the dynamical downscaling

method is used to generate the future years. Sections 3.1.3.1.1 and 3.1.3.1.2 illustrate the methods used to generate future climate using statistical and dynamical downscaling respectively.

3.1.3.2.1 Statistical downscaling method

Based on the statistical downscaling technique, the WeatherShift™ program (Moazami et al., 2017 and WeatherShift, 2016) was developed by Arup and Argos Analytics LLC to generate typical future weather files based on RCPs scenarios using the morphing method for downscaling (Belcher et al., 2005). WeatherShift™ program transforms 'present-day' EPW weather files into EPW weather files for future years. It uses 14 GCMs to generate future weather files. Cumulative distribution functions (CDF) blend these 14 GCMs and create the percentile distribution, such as 10^{th} to 95^{th}. The percentile distribution represents the percentage of GCM models above and below the average (Troup and Fannon, 2016). In this work, the 50^{th} percentile of RCP4.5 and 8.5 is used to generate the 2030 and 2090 typical years based on the historical year (1961-1990). The sensitivity analysis of the building envelope and mitigation measures are performed under the recent and the typical future year. The overheating is assessed for the buildings under recent and the typical and extreme future years to study the difference between the effect of typical and extreme future years generated by RCM models.

3.1.3.2.2 Dynamical downscaling

The Global Climate Model (GCM) of Max-Planck Institute for Meteorology - Earth-System Model (MPI-ESM) from the Coordinated Regional Climate Downscaling Experiment (CORDEX) (Cerezo-Mota et al., 2016) data is used to generate the 20 years of future mid-term (2041-2060) and long-term (2081-2090) climatic data based on the RCP8.5 scenario for Montreal, Canada. MPI-ESM is chosen because it has a medium Equilibrium climate sensitivity (ECS) (Armour, 2017; Giorgi, 2019). Seven climate variables are used to generate the weather file, including near-surface air temperature, near-surface relative humidity, near-surface specific humidity, near-surface wind speed, surface air pressure, surface downwelling shortwave radiation, and total cloud fraction. The driving model MPI-M-MPI-ESM-LR provides data for the North American domain with a spatial resolution of 0.22°/25 km and 3 hours time frequency for the seven weather parameters over 150 years each (1950-2100). Weather observational data for Montreal during the historical period from 2001 to 2020 were obtained from EU Watch Forcing Data ERA-Interim reanalysis (Machard et al., 2020; Gaur, 2019; Weedon et al., 2014).

These observation data are used to calculate the bias-correction factor based on the Multivariate bias correction (MBCn) method. MBCn is selected for bias-correction because it showed climate data that was more accurate than data corrected by other univariate bias-correction approaches according to Cannon (2018). The bias adjustment data are downscaled to 1 hour using polynomial regressions for the dry-bulb temperature and the global solar radiation. Linear regression is used for the other weather variables. Figure 3-5 shows the workflow used to generate the future climate data from CORDEX.

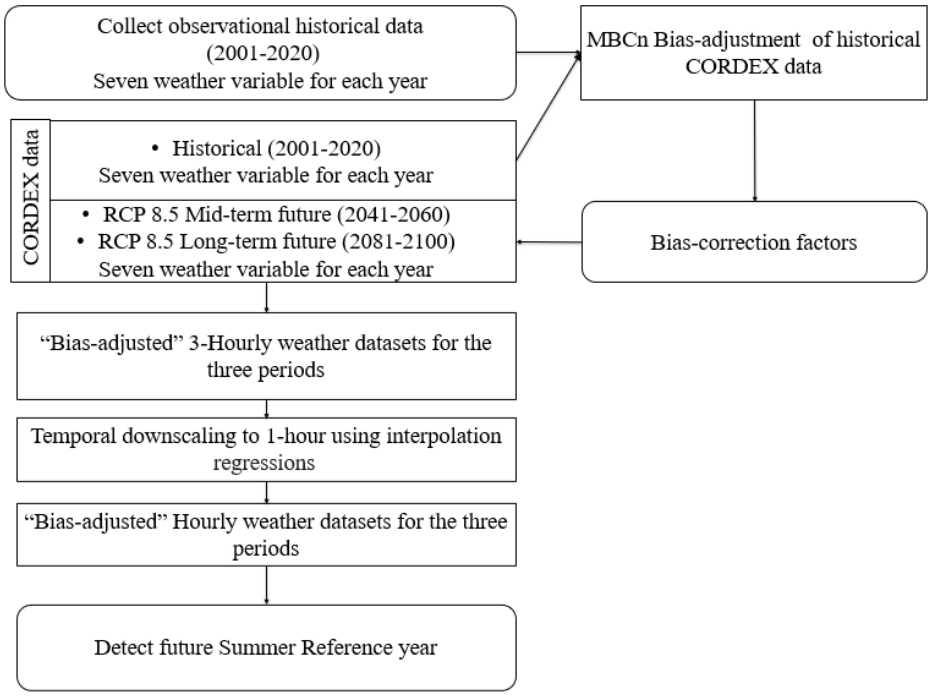

Figure 3-5. Workflow to generate future weather data

Reference summer weather year (RSWY)

To determine the Reference summer weather year (RSWY), which represents the extreme year, the heatwave detection operational method that was developed by Ouzeau et al. (2016) is used. Three percentile thresholds are calculated over the daily mean temperatures of the 20 years historical (2001-2020) temperatures and then used to detect heatwaves for 20 years of bias-adjusted mid and long-term future temperatures. These three percentile thresholds are: 1) S_{pic} threshold represents 99.5 quantiles of the daily mean temperature during the historical period (20 years), which defines the beginning of the heatwave; 2) S_{deb} represents 97.5 quantiles, and 3) S_{int}

represents 95 quantiles. To detect a heatwave, the outdoor temperature ($T_{outdoor}$) must be above the S_{pic} threshold for at least one day. The heatwave begins from the day when the daily outdoor temperature ($T_{outdoor}$) is above the S_{pic} threshold or from days before that day provided that the $T_{outdoor}$ is above the S_{deb} threshold and without interruption. The heatwave is interrupted or ends if the $T_{outdoor}$ is below S_{deb} for three consecutive days or $T_{outdoor}$ is below S_{int} on one day. Each heatwave must be at least 5 consecutive days. Figure 3-6 shows the characteristic of the heatwave (duration, intensity and severity) recorded in Montreal in the summer of 2020 with three percentile thresholds (S_{pic}, S_{deb} and S_{int}), as an example. The duration of a heatwave (days) is the number of days of a heatwave. Intensity (°C) is the maximum daily mean temperature of a heatwave. Severity (°C.day) is the cumulative temperature above the S_{deb} threshold. Based on this method, RSWY is the year that has the longest (Duration), most severe, or most intense heatwave.

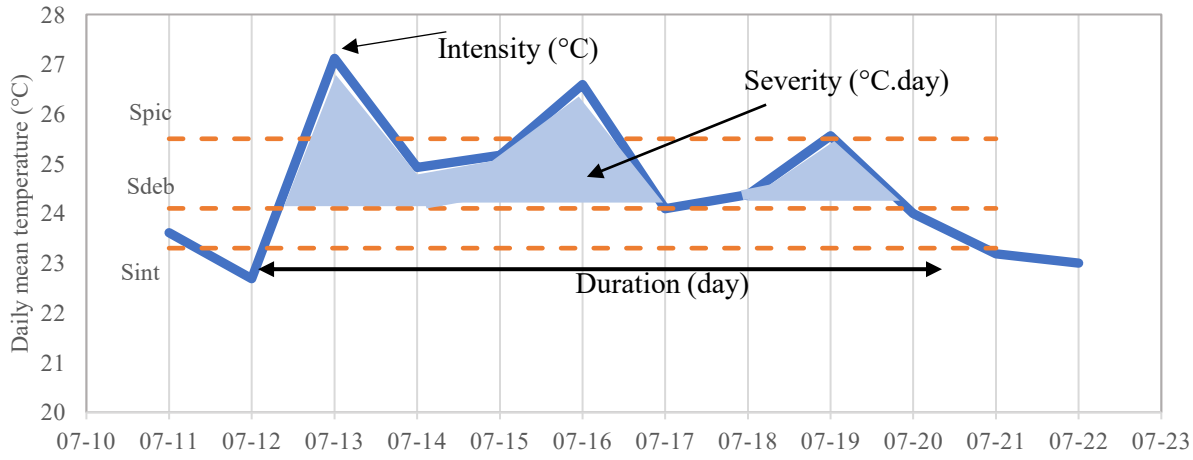

Figure 3-6. Daily mean temperature of Montreal with three thresholds during the heatwave in 2020

The developed Python codes for downloading the weather data from CORDEX, calculating bias-correlation and for detecting RSWY are attached in Appendix A.1.

3.1.3.3 Building guidelines and thermal comfort criteria

BC Energy Step (2019) guideline is used to determine the acceptable limit for the detached house (Section 2.3.2.2.1). The indoor thermal condition of the building is considered acceptable if the number of overheating hours is less than 200 hours (5% of summer from May to September). The overheating hours are calculated according to ASHRAE 55-80% overheating threshold (Equation

2-1 in Section 2.3.2.1.1) using simulated indoor operative temperature. The prevailing mean outdoor air temperature ($T_{pma(out)}$) is calculated over seven days

3.1.4 Overheating mitigation measures

Mitigation measures are evaluated against recent and expected future climates. This procedure will contribute to developing appropriate building codes and guidelines to mitigate the expected impacts of global warming in new houses. Several mitigation measures are proposed to minimize overheating risks in archetype single-family detached houses under recent and projected future climates. These passive mitigation strategies include building envelope parameters, natural ventilation, movable interior and fixed exterior shading. Interior roll shading will be deployed if the solar radiation on the window is higher than 100 W/m^2. Global sensitivity analysis is carried out to determine the significance of these mitigation measures on the overheating risk for existing buildings. The range of mitigation measures to perform the global sensitivity analysis is listed in Table 3-3. The range for building envelope parameters covers the values in old buildings built-in 1950 to new HEEB buildings. To reduce the excess heat, sensitivity analysis of mitigation measures is carried out under 2020 and 2090-RCP8.5 with a total of 2048 samples for each year.

Table 3-3. Range of mitigation measures with building envelope thermal properties in the range representing building ages from 1950 to HEEB for global sensitivity analysis

	Parameters	Unit	Uniform distribution range
P1	**Natural ventilation rate**	ACH	1.5-5.5
P2	**Window proprieties**	W/m^2. K	0.68-3.8
P3		SHGC	0.26-0.75
P4	**Wall U-values**	W/m^2. K	0.1-0.8
P5	**Roof U-values**	W/m^2. K	0.08-0.6
P6	**Solar reflectance of interior shading**	(-)	0.2-0.9
P7	**Exterior overhang**	m	0-1.5

3.2 EXISTING BUILDINGS

3.2.1 Calibration methodology

The auto-calibration methodology proposed in this work (shown in Figure 3-7) includes:1) creating a building simulation model in a simulation program using available information about the existing building, such as building geometry and dimensions, orientation, building envelope, internal gain, HVAC system, and/or outdoor weather data; 2) determining all uncertain building parameters, such as infiltration rate, internal gain, and/or shading; 3) using global sensitivity analysis to reduce the number of uncertain parameters by selecting significant uncertain parameters that affect the indoor room temperature to be used in the calibration process (Section 3.2.1.1); 4) removing any insensitive parameters from calibration process and assigning a specific value to these parameters in E+ initial model by setting the average value of their range; 5) defining Multi-Objective Genetic Algorithm (MOGA) simulation settings and assigning the sensitive uncertain parameters in input E+ code, measured hourly temperature data, and evaluation criteria for each room in MOGA simulation (Section 3.2.1.2); 6) determination of the Pareto optimal solutions in each iteration based on the three evaluation criteria (Section 3.2.1.3) established for each room; 7) selecting the final Pareto optimal solutions if Pareto solutions do not change for 10 generations (100 iterations); and 8) determination of the final optimal solution from Pareto optimal solutions list based on the new selection criteria (Section 3.2.1.3). After the building model is calibrated during the calibration period, the validation is carried out for a different period to ensure that the set of calibrated parameters is working correctly under different weather conditions.

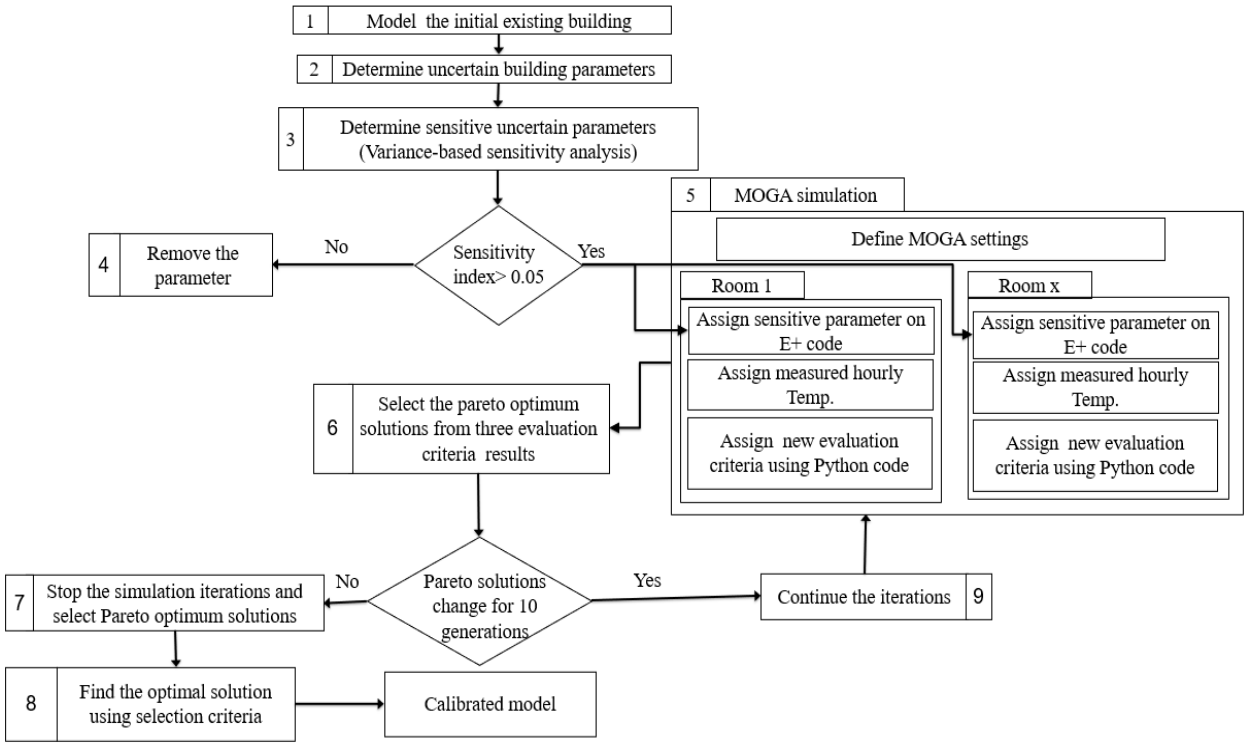

Figure 3-7. Flowchart of the proposed automated calibration model based on hourly indoor air temperature of multi-rooms.

The developed Python codes for determining the objectives (evolution criteria) and calculating the three evaluation criteria are attached in Appendix A.2.

3.2.1.1 Global Sensitivity Analysis of uncertain building parameters

To identify the sensitive parameters affecting the indoor temperature, the global variance-based sensitivity (SOBOL) method that illustrated in Section 3.1.1.1. SOBOL sensitivity index computes the "Total-order Sensitivity Index", which calculates the contribution of each input parameter and its interactions with any of the other input parameters on the output for nonlinear and non-monotonic models, as shown in Equations 3-1 to 3-3. Figure 3-3 (Part 1-Global sensitivity analysis) shows the proposed workflow chart to calculate the SOBOL sensitivity indices.

3.2.1.2 Multi-Objective Genetic Algorithm method

The Multi-Objective Genetic Algorithm (MOGA) NSGA-II auto-calibration method is used. The main challenge in calibration based on indoor temperature is that when more than one room is monitored, these rooms need to be calibrated simultaneously since they are thermally connected.

Therefore, it is more suitable to use the MOGA calibration method instead of the manual calibration. jEPlus+EA program 1.7 (Zhang, 2012; Zhang and Korolija 2020) is used in this study to apply this MOGA method. In the MOGA, E+ model code, the significant uncertain parameters, measured indoor air temperature, genetic algorithm setting, and the objective evaluation criteria need to be assigned. A Python script (as shown in Appendix A2) is written to calculate the evaluation criteria. Following the recommendations by (Lara et al., 2017; Nagpal et al., 2018; Pezeshki, 2018; Arida et al., 2017; Banihashemi et al., 2017) for the setting in the GA method, the population size is set to 10 individuals in order to ensure enough variability in creating new solutions, and the maximum number of generations is fixed at 200. Simulations are run on a desktop computer with 8 GB RAM and E-1280 V2 CPU. Simulations stop when all Pareto solutions do not change within 100 simulations with ten generations.

3.2.1.3 New evaluation and selection criteria

Most previous studies relied on energy consumption calibration requirements (CV (RMSE) and NMBE) to calibrate buildings based on the measured indoor temperature, as listed in Table 2-2. However, these requirements can be achieved even though there is a significant discrepancy between simulation and measurement temperature data distribution (Donovan et al., 2019; Royapoor and, Roskilly, 2015; Coakley et al., 2012; Paliouras et al., 2015; and Cacabelos et al., 2015). In this work, the Maximum Absolute Difference (MAD), NMBE, and RMSE are used as the objective functions in MOGA for each room. MAD is to find the maximum absolute difference between simulation and measured hourly indoor temperature during the calibration period, as shown in Equation 3-4. The RMSE shows how close the simulated values are to the measured values and how similar the distribution is, while NMBE captures the average bias between them. However, these two criteria cannot show how significant the discrepancy is between the measured and simulated air temperature in some hours, therefore, MAD is also used. The RMSE and NMBE are calculated according to Equations 3-5 and 3-6, respectively.

MOGA produces a set of feasible non-inferior solutions called Pareto Optimal Solutions. Since this method calibrates multiple rooms simultaneously, MOGA will produce different Pareto Optimal solutions for each room, thus no one perfect solution can be found for all objectives in all rooms. Therefore, one additional new metric, the 1°C Percentage Error criterion, is developed to find the Final Optimal Solution (FOS) among the top five Accurate Optimal Solutions (AOS).

AOS is defined as a solution that achieves the highest accuracy on a third or more of the objectives and achieves a close number (10% difference) to the highest accuracy number in other objectives. The 1 °C Percentage Error criterion calculates the percentage of the number of hours over the calibration period having the error between simulated and measured indoor air temperature higher than 1 °C. The lowest MAD does not necessarily mean it is the best solution. Therefore, the 1 °C Percentage Error criteria are established to find the best solution among the five Pareto solutions with the lowest RMSE and NMBE. According to adaptive criteria for overheating assessment, such as ASHRAE 55 (2017) or EN15251 (2007), the difference between the acceptable limits is 1°C, which indicates that the 1°C difference can lead to a significant difference in the calculation of overheating hours. Therefore, the 1 °C Percentage Error criterion is important to reduce the discrepancy in assessing the overheating risk using the simulation and the measured data. Meanwhile, a 0.5 °C Percentage Error criterion is also used in this work as an indicator to demonstrate the level of accuracy the model can achieve.

$$MAD\ (°C) = Max\ (abs(T_{sj} - T_{mj})), \quad j = 1 \dots n \tag{3-4}$$

$$RMSE\ (ºC) = \left[\frac{1}{n-1} \cdot \sum_{j=1}^{n} (T_{sj} - T_{mj})^2\right]^{0.5} \tag{3-5}$$

$$NMBE\ (\%) = \frac{100}{\overline{T_m}} \cdot \frac{\sum_{j=1}^{n} (T_{sj} - T_{mj})}{n-1} \tag{3-6}$$

Where j is a specific hour during the calibration period, T_s is the simulated data, T_m is the measured data, n is the number of observations, and $\overline{T_m}$ is the average of a number of n observations.

3.2.2 Monitored study buildings

This methodology is applied to calibrate two school buildings and a multi-unit residential building in Montreal. Specifications of instruments that have been used to measure indoor and outdoor thermal conditions are described in Section 3.2.2.1 and the description of the three school buildings, two schools and one multi-unit residential building, monitored in Montreal, is described in Section 3.2.2.2.

3.2.2.1 Field Measurement

In all monitored study buildings, the indoor wireless sensors, HOBO MX1101 (Figure 3-8), are used to measure the indoor dry-bulb air temperature (Accuracy: ±0.2 ºC), relative humidity (Accuracy: ±2% RH).

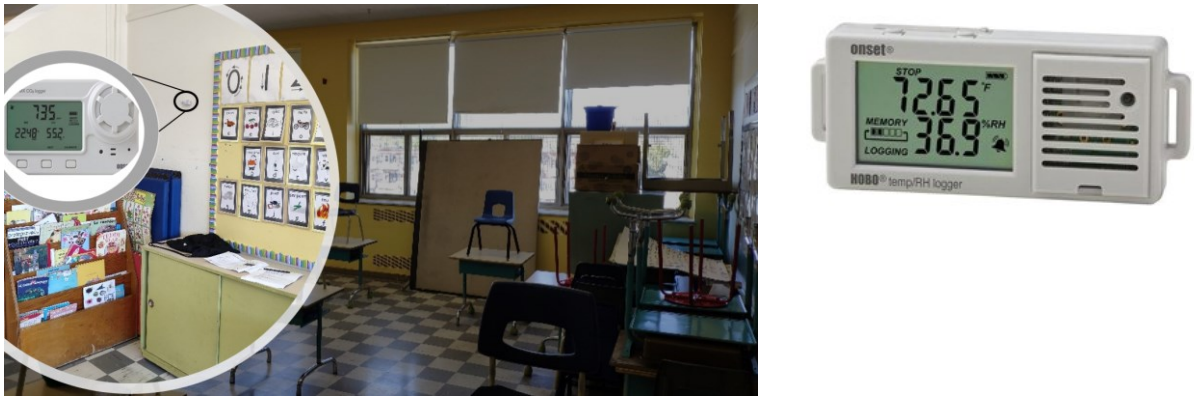

Figure 3-8. Indoor RH/T wireless sensor in classrooms

The weather station (HOBO RX3000 Data Logger, as shown in Figure 3-9) was installed on top of the roof to record dry-bulb temperature (Accuracy: ±0.2 ºC), relative humidity (Accuracy: ±2% RH), global solar radiation (Accuracy: ±10 W/m^2), wind speed (Accuracy: ±0.20 m/s) and direction (Accuracy: ±1.4 degrees), and rainfall intensity (Accuracy: ±0.2 mm). All measurements are collected at 5-minute intervals. Hourly data are obtained by arithmetically averaging indoor and outdoor five-minute data.

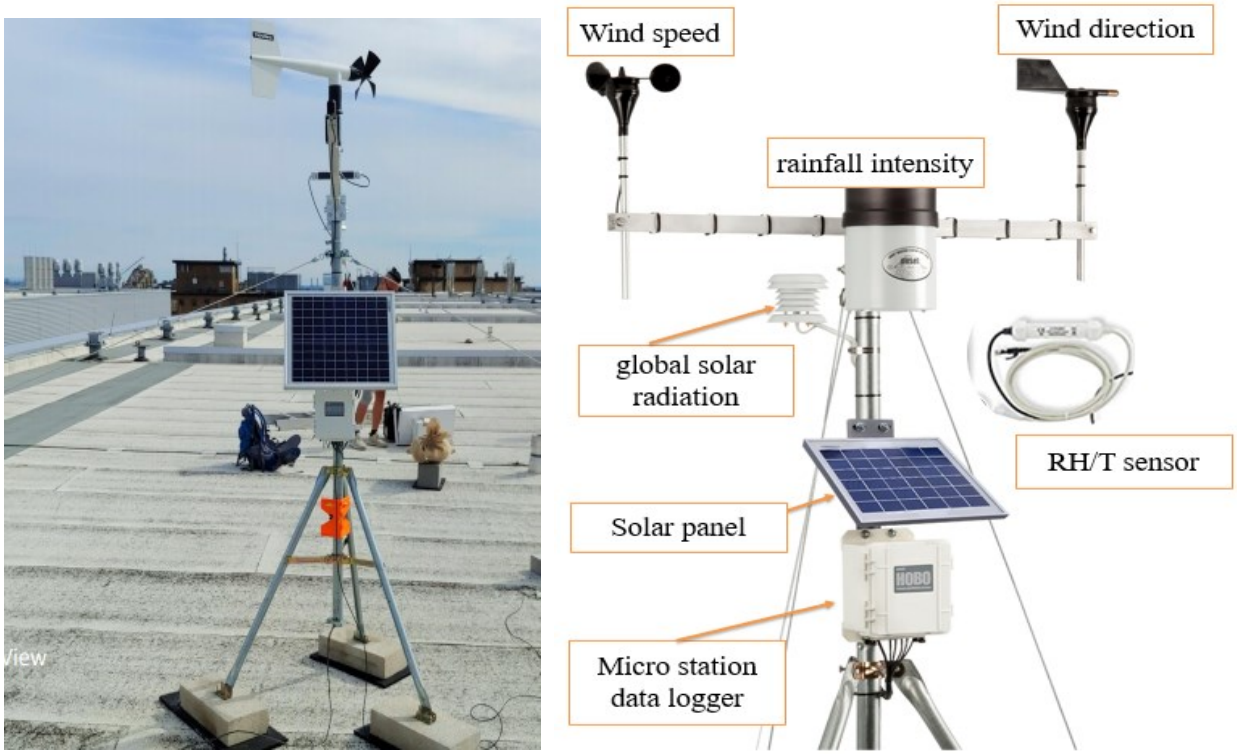

a) b)

Figure 3-9. a) Weather station on school roof; b) Weather station component

3.2.2.2 School building 1

This building was built in 1958 with concrete block-brick veneer exterior wall, block partitions, concrete floor, concrete roof with insulation, and two-layer single glazed windows. Figure 3-10 shows the building photos and second-floor plan. The orientation of the front façade is 210º from the North.

Four classrooms, shown in Figure 3-10c, located on the second floor (i.e., rooms 200, 203, 208 and 212) were selected according to different orientations for comparison purposes. Moreover, according to our questionnaire survey and site visits conducted in September 2019, the rooms with the highest overheating complaints in recent years were selected. The four rooms have the same dimensions (8.84 × 7.12 × 3.2 m) and 60% of the window-wall ratio. The indoor measured temperatures collected from May 23rd to Oct. 15th are used in this study for calibration, except for data from June 5th to July 2nd, and from August 4th to 6th 2020 because of renovation work. All rooms on the first floor and second floor are modelled in DesignBuilder to generate the IDF file. the school was closed from March to September 2020, for that the calibration is divided into two

periods: 1) school closed period from May 23rd to Aug. 20th; and 2) school open period from Sep. 12th to Oct. 15th.

EN 15251 (2007)-Category I and II of overheating threshold is used for determining the overheating hours in the existing using measured air temperature. The indoor thermal condition of the building is considered acceptable if the number of overheating hours is less than 40 hours (5% of summer from May to September), which is defined by the BB101 (2018) code as the acceptable limit.

a) Front façade

b) Back façade

c) Second-floor plan with classrooms monitored

Figure 3-10. a) Photo for school front façade; b) Photo for school back façade; c) Second-floor plan with classrooms monitored

The first step in the calibration is to identify the uncertain parameters in the building. Sections 3.2.2.2.1 and 3.2.2.2.2 show the uncertain parameter during the closed and opened periods, respectively.

3.2.2.2.1 Uncertain building parameters during the closed period

During the closed period, there were no internal gain, no air-conditioning, and no natural ventilation (because windows were closed). This period is used to calibrate the uncertain building parameters, which include thermal transmittance of wall and roof, airtightness, window SHGC and U-value, the thermal mass of wall and roof, and the interior shading. A uniform distribution is assumed for each parameter, and the ranges are determined according to the level of uncertainty. For example, wall and roof thermal transmittance and airtightness have a high degree of uncertainty as there is no information about them except that we know the building was built in 1958. Therefore, two wide ranges are used. The first range assumes that the wall and roof were in compliance with the building practice at the time of construction and have never been renovated, while the second range assumes that the wall and roof were renovated at some point. On the other hand, the ranges of the window thermal properties and thermal mass of the wall and roof were narrow because of the information we collected through the questionnaire survey and site visits (Table 3-4). Depending on the building age, the first range of each parameter (Table 3-4) is determined according to archetype buildings developed by Natural Resources Canada (Parekh, 2012a) and presented in (Parekh and Chris, 2012b). The second range is assigned from the minimum value in the first range to the current NECB building code (2017) requirements assuming that the building was renovated in recent years. During the site visits, we noticed that the interior blinds attached to all windows were completely closed. While the solar reflection coefficient of the interior shading is unknown, this factor can be included in the blind opening ratio, which represents the combined effect of actual shading material properties or/and shading opening ratio. The orientation and window wall ratio are known parameters. The sensitivity analysis and building model calibration are performed twice, one with the first range of building envelope characteristics and other parameters, and the second with the second range of these unknown building envelope characteristics and other parameters listed in Table 3-4.

Table 3-4. Range of building parameters used in the global sensitivity analysis for the period when school was closed (May 23rd to Aug. 20th) and opened (Sep. 12th to Oct. 15th, 2020).

	Parameters	Range	
		First range	Second range
School closed period	**Wall U-Value (W/m²·K)**	0.40-0.70	0.20-0.40
	Roof U-Value (W/m²·K)	0.23-0.33	0.15-0.23
	Air Infiltration (@ACH 50)	3.5-8.5	1.5-3.5
	Window U-Value (W/m²·K)	2.20-3.00	
	Window SHGC	0.60-0.76	
	Solar reflectance of interior diffusing roll blinds	0.3-0.9	
	Thermal mass of exterior wall (KJ/m²·K)	150-350	
	Thermal mass of internal floors and roof (KJ/m²·K)	150-350	
School open period	**Occupancy load (Number of students)**	20-25	
	Lighting load (W/m²)	9-16	
	Equipment load (W/m²)	2-5	
	Maximum air change rate from NV (ACH)	0-15	
	NV Setpoint (°C)	20-24	
	Interior shading opening ratio in all northwest rooms (%)	10-90	
	Interior shading opening ratio in all southeast rooms (%)	10-90	

3.2.2.2.2 Uncertain building parameters during the school opening period

The school opened on Aug. 26, 2020; therefore, the internal gain, opening of windows, and interior shading are included in the model as uncertain parameters. There is no mechanical cooling or ventilation in the building. The range of internal gain, according to the information collected during the site visit and survey, is listed in Table 3-4. The amount of natural ventilation defined as the input data in E + is the maximum air change rate and is adjusted according to the natural ventilation setpoint (when the indoor temperature is higher than the setpoint), outdoor temperature (when the indoor temperature is higher than the outdoor temperature), and the operation schedules. The range of the maximum air change rate from the natural ventilation (NV) is selected based on the E+ Airflow Network method (DOE, 2021b), which considers the wind direction and speed, stack effect and interior window/door openings, and with a 25% of exterior window opening area. This range is also compatible with WHO Natural Ventilation Guideline results (Atkinson et al., 2009) and measured air change rate in U.K. classrooms (Jones and Kirby, 2012). The range of the NV setpoint is determined based on the analysis of measurement data. To take into account the effect of orientation, shading opening level parameters are set separately for NW and SE rooms with the same values for all rooms in the same orientation.

3.2.2.2.3 Calibration of the four rooms separately

Building model calibration based on the indoor air temperature in four selected rooms separately can only achieve a high-accuracy calibration for one or two rooms, not all four rooms together; or a high-accuracy calibration can be achieved in each room but with different calibrated building envelope parameters. Moreover, calibrating the four rooms separately may neglect the effect of heat transfer between rooms and thus the effect of some parameters in other rooms on the room to be calibrated. To confirm, each room is calibrated separately during the school closed period from May 23rd to Jun. 4th. Table 3-5 shows the calibrated parameters values and RMSE for each room using the first range (Table 3-4). The results confirmed that the high accuracy of the calibrated model could be achieved for each room separately (with an RMSE in the range of 0.5 to 0.7°C) but with different calibrated parameter values. Also, if one room is calibrated and its calibrated parameters are applied to the other rooms, the accuracy of calibration for other rooms is reduced. For example, if the calibrated parameters of room 203 are used for other rooms, room 203 can achieve 0.4 of RMSE, while the RMSE is increased to 0.6, 1.1and 1.3 for rooms 200, 208, and

212, respectively. Figure 3-11 shows the difference between the measured and simulated indoor air temperature in rooms 203 and 212 resulting from calibrating room 203 separately during the closed period.

In addition, the results of sensitivity analysis (Section 4.2.1.1.1) confirm the effect of heat transfer between rooms. For example, the level of shading in the south-facing rooms has a significant influence on the indoor temperature in the north-facing rooms.

To achieve high accuracy for all four rooms, the whole building with all rooms is modelled and the four rooms are calibrated simultaneously. Results are provided in section 4.2.1.1.

Table 3-5. Calibrated model parameters and RMSE results for each room during the school closed period when each room is calibrated separately for a period from May 23rd to Jun. 4th.

Parameters	R 200	R 203	R 208	R 212
Shading	0.9	0.7	0.5	0.3
Infiltration rate (@ACH50)	3.8	3.5	4.2	4.5
Wall U-value (W/m²·K)	0.68	0.76	0.45	0.5
Roof U-value (W/m²·K)	0.26	0.24	0.26	0.26
Accuracy				
RMSE for R 200 (ºC)	0.5	0.6	1.3	1.4
RMSE for R 203 (ºC)	0.6	0.4	1.1	1.3
RMSE for R 208 (ºC)	0.8	0.6	0.5	0.6
RMSE for R 212 (ºC)	1.0	0.9	0.7	0.7

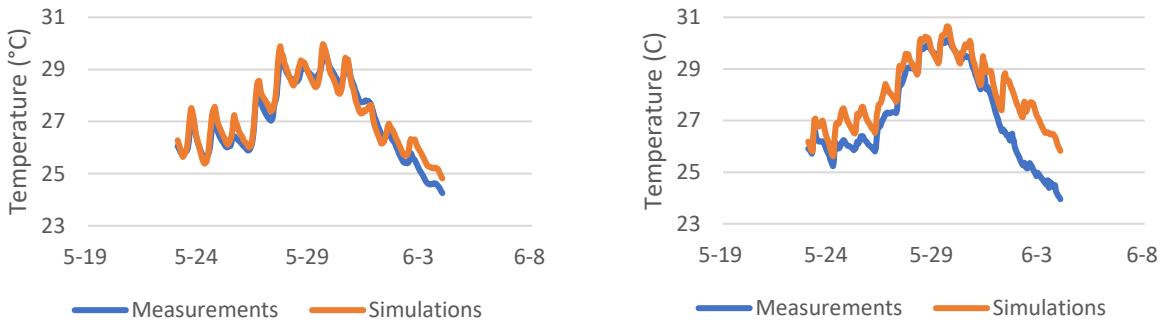

R 203-RMSE 0.4 R212-RMSE 1.3

Figure 3-11. Comparison of indoor air temperature between measurements and simulation results from the calibrated 203 room separately during the closed period.

3.2.2.3 School building 2

This school building is located in the urban area of Montreal. This building was built in three different periods. As shown in Figure 3-12a, Block 1 was built in 1948, Block 2 in 1990, and Block 3 in 2014. The building envelope construction was steel with brick veneer external wall, and block partitions. Figures 3-12 show the building plan, school photo and 3D model. According to Google Earth, The orientation of the front façade is 87º from the North. According to our questionnaire survey and site visits conducted in Sept. 2019, there are overheating complaints in recent years, especially in the West and East and Southside.

Two classrooms (room 109, 114) and the Gym in Block1 and two classrooms (room 168, 173) in Block 2 are selected, as shown in Figure 3-12b. The internal dimensions and window-wall ratio are measured for each room. The weather station was installed on top of the roof to monitor outdoor conditions, including temperature, relative humidity (RH), solar radiation, wind speed and direction, and rainfall intensity. The indoor temperatures are measured from June 30th to Oct. 10th. The school building blocks are modelled in DesignBuilder separately, as shown in Figure 3-12c&d, since each block has different building age and there is no thermal connection between them.

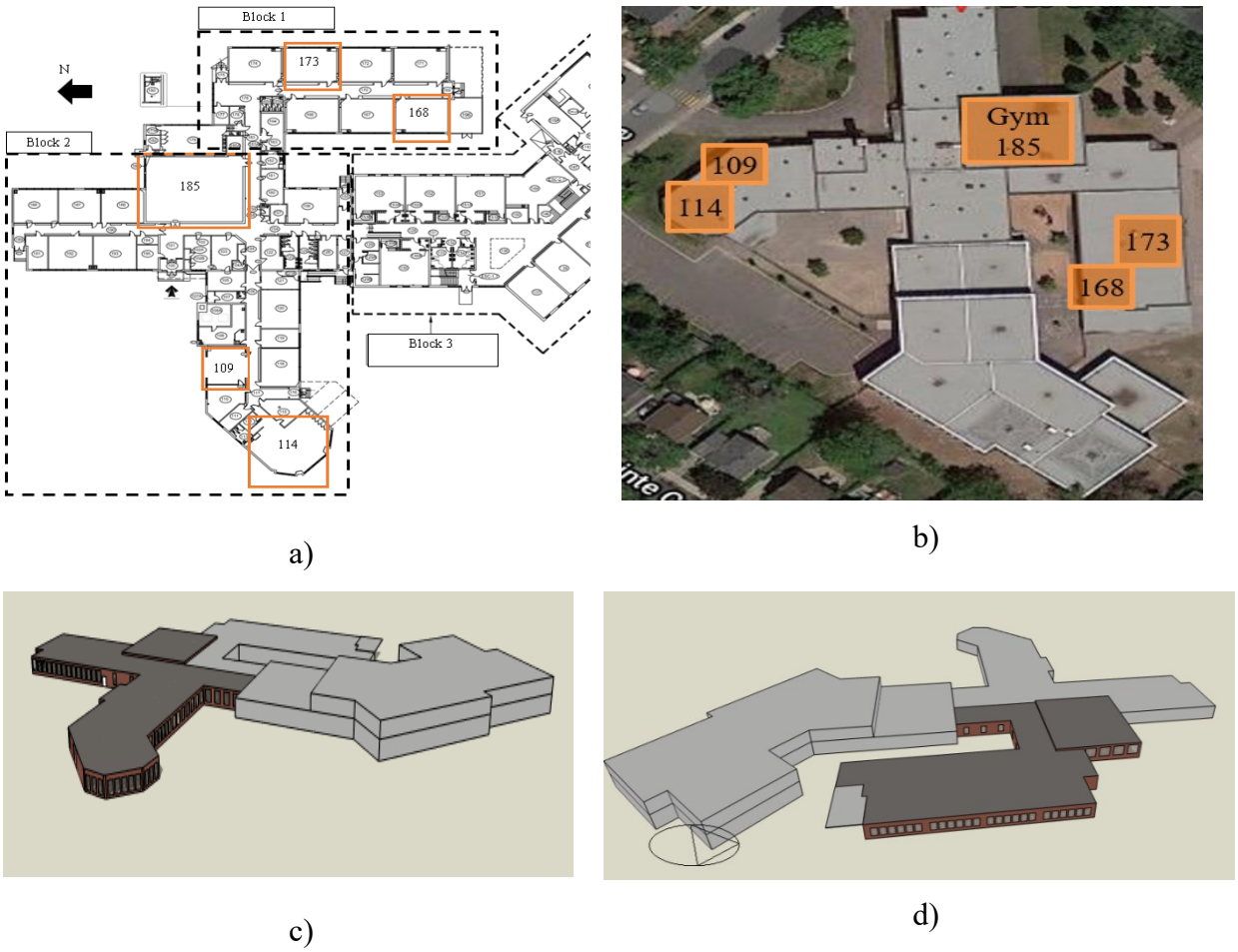

Figure 3-12. a) School photo; b) School plan with classrooms monitored; c) 3D Block 1 model; d) c) 3D Block 2 model in DesignBuilder

3.2.2.3.1 Uncertain building parameters during the closed period

Block 1 (built-in 1950)

The uncertain building design parameters studied include thermal transmittance of wall and roof, airtightness, window SHGC and U-value, the thermal mass of wall and the interior shading. A similar uniform distribution range is assumed for each parameter, and the ranges are determined according to the level of uncertainty, as shown in Table 3-4.

Block 2 (built-in 1990)

Depending on the building age and the level of uncertainty, the range of each parameter (Table 3-6) is determined according to archetype buildings developed by Natural Resources Canada (Parekh, 2012a) and presented in (Parekh and Chris, 2012b).

Table 3-6. Range of building design parameters used in the global sensitivity analysis

Parameters	Range-uniform distribution
Wall U-Value (W/m^2·K)	0.20-0.40
Roof U-Value (W/m^2·K)	0.15-0.30
Air Infiltration (ACH 50)	0.6-3.0
Window U-Value (W/m^2·K)	1.5-2.5
Window SHGC	0.35-0.76
Solar reflectance of interior diffusing roll blinds	0.4-0.9
Thermal mass in the wall (KJ/m^2.K)	60-150
Thermal mass in the floor and roof (KJ/m^2.K)	60-150

3.2.2.3.2 Uncertain building parameters during the closed period

On Sept. 1st, 2020, the school started, and therefore, the internal gain (occupant load, lighting load, and equipment load), natural ventilation (NV) quantity, and shading opening level are now uncertain parameters. There is no mechanical cooling or ventilation in the building. A similar uniform distribution range is assumed for each parameter, and the ranges are determined according to the level of uncertainty, as shown in Table 3-4.

3.2.2.4 Multi-unit residential building

This building was built in 1958 and it is in the operation since 1992. The building envelope construction was wood-frame construction with the brick veneer external wall. Three bedrooms (rooms 1, 2, and 3) and the living room on the third floor are selected, as shown in Figure 3-13. The interior dimensions and window-wall ratio are measured for each room. The indoor temperatures are measured from Sep.16th to Oct. 15th for the bedrooms and after Dec 15th for the living room, therefore, three bedrooms are calibrated only. The building with surrounding buildings is modelled in DesignBuilder, as shown in Figure 3-13c.

a)

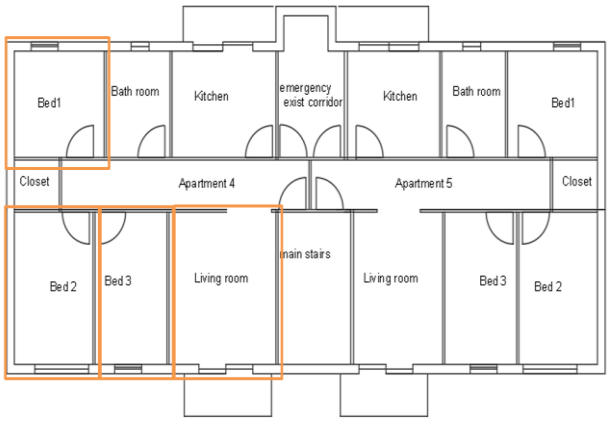

b)

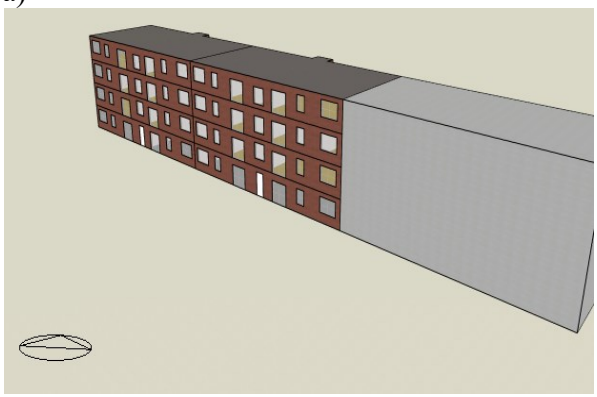

c)

Figure 3-13. a) building photos; b) apartment plan with monitored rooms; c) 3D model in DesignBuilder

Uncertain building parameters

The uncertain building design parameters studied include thermal transmittance of the wall, airtightness, window SHGC and U-value, interior load, natural ventilation, and interior shading. A uniform distribution range is assumed for each parameter, and the ranges are determined according to the level of uncertainty. For example, internal gain, wall thermal transmittance and airtightness have a high degree of uncertainty as there is no information about them except that we know the building was built in 1958, but it was probably renovated in 1992 when it came into use from the office municipal d'habitation de Montreal. Therefore, similar two wide ranges of building envelope parameters in Table 3-4 are used. The range of building operation parameters is listed in Table 3-7. The amount of all operation parameters defined as the input data in E+ is the maximum value and the operation schedules. The initial operational schedule for each parameter is created

according to NECB (2017) and ASHRAE-90.1 (2016) codes. the maximum value and the operation schedules are calibrated according to the measured data distribution using MOGA.

Table 3-7. Range of building design parameters used in the global sensitivity analysis

Parameters	**Range- uniform distribution**
Solar reflectance of interior diffusing roll blinds	0.4-0.9
Lighting load W/m^2	5-10
Equipment load W/m^2	5-10
Maximum air change rate from NV (ACH)	0-2.5
NV Setpoint	22-25

3.2.3 Overheating assessment under recent and future climate

To study the effect of climate change on indoor thermal conditions in Canadian buildings, the overheating risk is assessed in the existing School Building 1 under recent and future climates. The future climate generation and extreme future years methods are illustrated in Section 3.1.3.1. BB101 (2018) guideline is used the determine the acceptable limit for the school (Section 2.3.2.2.3). The indoor thermal condition of the building is considered acceptable if the indoor overheating hours and indoor operative temperature are passed the three criteria. The overheating hours are calculated according to BS EN15251- Category I and II overheating thresholds (Equations 2-7 and 2-8 in Section 2.3.2.1.2). These criteria are applied to the period of Monday to Friday from 09:00 AM to 04:00 PM, from May 1 to September 30, including the summer holiday period as if the school was occupied normally, this option will not be available with measured indoor air temperatures during the summer holiday. Therefore, the predicted indoor operative temperature from the calibrated model is used to evaluate the indoor thermal condition. According to BB101 (2018), the goal of applying these criteria during the summer holidays is to achieve thermal comfort in the hottest months, thus ensuring that May, June and September will be more comfortable in the coming years or under extreme conditions.

3.2.4 Overheating mitigation measures

Mitigation measures are evaluated against recent and expected future climates. This procedure will contribute to developing appropriate building codes and guidelines to mitigate the expected impacts of global warming on existing buildings. Passive mitigation measures that can be added to the building with minor renovation are studied to improve indoor operative temperate without increasing cooling consumption. These mitigation measures are listed in Table 3-8. Local sensitivity analysis is used to evaluate these mitigation measures and the combination between them under 2020. Significant mitigation measures resulting from sensitivity analysis are used under future extreme years.

Table 3-8. Mitigation measures for existing school building 1

	Parameters	Value	Description
P1	**Night cooling**	Opening 25% of window opening area	It is opened if the indoor temperature is higher than the outdoor temperature and higher than the ventilation setpoint (23 °C)
P2	**External overhang**	1.5 m	Applied to the southeast side with keeping the internal shading
P3	**Blind external roll (Solar reflectance)**	0.8	It is used instead of the current inside blind roll. It is activated when the solar on the window surface is higher than 120 W/m^2
P4	**Cool Roof- shortwave reflectivity (albedo**	0.8	the solar reflectance of the roof changes from 0.3 to 0.8
P5	**Window SHGC**	0.3	by using electrochromic film (Hoseinzadeh, 2017), or Dark Shading window Tinted film
P6	**Green Roof**		the leaf area index (LAI) of 5.0 and an average height of 0.1 m in the soil. The maximum volumetric moisture content of the soil layer is 0.5.0-1.5

3.2.5 Optimization of building design

3.2.5.1 Optimization design methodology

The auto-optimization methodology proposed in this work (shown in Figure 3-14) includes:1) creating a building simulation model in a simulation program; 2) determining the performance aspects (called objectives) that must be achieved in the design of the building, such as minimizing the heating energy demand and minimizing the overheating risk; 3) determining building parameters (called Selected Parameters) that have the impact on each objective, such as building envelope thermal characteristics, infiltration rate, Window Wall Ratio WWR, and/or shading; 4) performing sensitivity analysis (Section 3.2.5.2.3) to reduce the number of selected parameters by selecting parameters that has a significant and contradictory impact on objectives, if the number of possible solutions is high than 2 million. Since MOGA is a heuristic (selection) method that can find the optimal solution among a large number of possibilities, using MOGA without using sensitivity analysis will be more efficient with probabilities of less than 2,000,000; 5) defining Multi-Objective Genetic Algorithm MOGA simulation settings and assigning the selected parameters in input E+ code, and objectives; 6) determining the Pareto optimal solutions in each iteration based on the objectives determined; 7) selecting the final Pareto optimal solutions if Pareto solutions do not change for 10 generations (100 iterations), and determining designs that achieve objectives from Pareto optimal solutions list.

To illustrate the process of developing the optimization strategies in recent and future climates, the proposed framework (Figure 3-14) is implemented and demonstrated by the existing School Building 1 for each major step in the framework, as shown in Sections 3.2.5.2-3.2.5.4

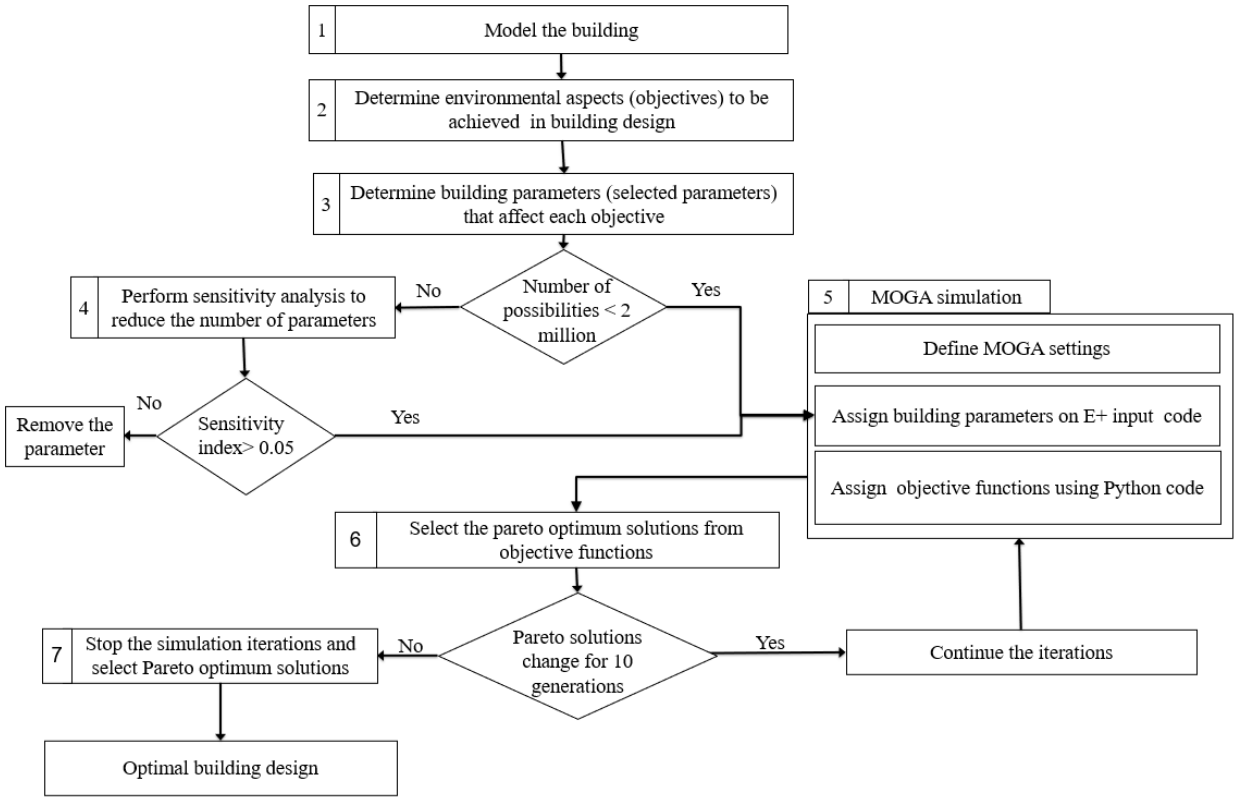

Figure 3-14. Framework of the proposed automated model optimization

3.2.5.2 Study building: School Building 1

In this school, it is assumed the building will be completely renovated.

3.2.5.2.1 Objectives of optimal building design

The building should provide comfort to its occupants all year round, therefore, three objectives are determined that the new design must achieve:

1) Summer thermal comfort that can be achieved by keeping the number of overheating hours in school that is evaluated based on the Building Bulletin BB101 Guideline (2018) lower than 40 hours
2) Winter thermal comfort that can be achieved by using a heating system with a setpoint of at least 22 ºC and 18 ºC for the setback based on NECB (2017) requirements. In addition, a mechanical ventilation system should be added to the building with 5.0 L/s/person and 0.6 L/s/m^2 capacity according to ASHRAE 62.1 (2019). The objective is to achieve winter thermal comfort while keeping the school's heating energy demand below 15 kWh/m^2 per year as is the PH requirement. (Passive House Guidelines, 2022).

3) Visual comfort during the year. The level of visual comfort depends on the indoor Daylight Factor, which measures the ratio of indoor horizontal illuminance to outside horizontal illuminance, (International WELL building institute, 2019; Pierson et al., 2018; Valitabar et al., 2018) and the level of glare (Chaloeytoy et al., 2020; European Commission, 2018; Narisada and Schreuder, 2004; Boyce, 2003). In this work, the minimum indoor illuminance required in the classroom (400 Lux according to NECB (2017)) is achieved by either using daylight or artificial lighting and daylight glare is avoided by using interior shading when the glare exceeds the Maximum Allowable Discomfort Glare Index for the classroom threshold (20 according to EnergyPlus documentation (DOE, 2021a)). This means the effective use of daylight while avoiding glare will reduce the artificial lighting load. Therefore, the light-dimming control strategy (EN 15193-1, 2017) is used to control indoor artificial lighting based on the availability of daylight while maintaining the minimum required illumination and without glare. The EnergyPlus Daylighting Controls (Detailed Method) (DOE, 2021a) is used to calculate the space daylighting illuminance levels and then used to determine how much the electric lighting can be reduced. In the EnergyPlus model, one or two sensors are assigned in rooms based on the room size to calculate the glare index and daylight factor. For Glare Index calculation, the angle between occupant view direction and the direction of the window is determined by 45-90 degrees. The daylight illuminance factor in a space depends on many variables, some of which are related to outdoor weather, such as sun position and cloud condition; and some are related to the building, such as location, size and type of window, interior surface reflectance, and shading devices. In our case, all of these variables are fixed except the size and type of window and exterior and interior shading devices.

The optimal design must not only exceed the minimum requirement of heating demand, overheating hours and lighting load, but also be close to the lowest achievable values for each objective (lowest heating demand, overheating hours, and lighting load). Therefore, the best design (Section 4.2.4.1) that achieves the best achievable values for each objective while not necessarily achieving the minimum requirements for the other two objectives is determined.

3.2.5.2.2 Building design parameters

According to previous studies (Ascione et al., 2019; Gou et al., 2018; Zhang et al., 2017; Sepúlveda et al., 2020; Lakhdari et al., 2021; Zhai et al., 2019; Shen et al., 2019; Ferrara et al., 2018; Jafari and Valentin, 2017), 10 building parameters that have an effect on the three objectives are selected, as shown in Figure 3-15. These parameters are:

- **Building envelope parameters**

  The building envelope must meet at least the current National Energy code (NECB-2017) requirements. Each building envelope parameter (wall and roof thermal transmittance, window and infiltration rate) has four options, as shown in Figure 3-15, starting with the current building situation, which is Low Energy-Efficient Building (LEEB), NECB that meets the current NECB prescriptive requirements, NECB+, whish is 30% better than NECB requirements, and then PH (high energy efficiency option) that meets the Passive House Guidelines and 60% better than NECB requirements (2017).

  The low thermal transmittance of the building envelope and low infiltration favourably affect the heating demand in buildings by preventing heat loss through the building envelope. However, this improvement in the energy efficiency of the building envelope will retain the heat gain inside the building in summer, which may increase the overheating risk, especially without adequate ventilation. A window's solar heat gain coefficient (SHGC) affects the amount of solar heat entering a building. Windows with a lower SHGC help reduce the overheating risk, but this will increase the heating energy demand in winter when it is desirable to increase solar heat gain indoors. Also, the low SHGC reduces the Visible Light Transmittance (VLT) through the window making spaces darker and requiring additional lighting (Sbar et all., 2012). Four window products are selected from Abritek Manufacture-National Fenestration Rating Council (NFRC 201, 2020) to represent the current building with windows that meet NECB (, NECB+ and PH requirements.

- **Exterior and interior shading**

  The current building has an interior shading blind roll but without exterior shading. Therefore, 5 and 3 options for exterior and interior shading are selected respectively. The exterior options are no shading, 0.5 m, 1 m. 1.5 m overhang (fixed shading) and screen shading (fixed or movable option based on the season).

The interior shading options selected have variability in the solar reflectance (Sr) and visible transmittance factor (Vt) values. The first option representing the current situation has high solar reflectance (Sr=0.7) with a low visible transmittance factor (Vt=0.4). The second option has a medium solar reflectance (Sr=0.4) and medium visible transmittance factor (Vt=0.6), and the third option has low solar reflectance (Sr=0.1) and high visible transmittance factor (Vt=0.8). The interior shading will be controlled by the Maximum Allowable Discomfort Glare Index instead of controlled by the occupants (schedule).

Solar shading devices can significantly reduce solar heat gain through windows, especially exterior shading, which reduces the risk of overheating but will increase the heating energy demand in winter. Shading devices also reduce daylight which increases the lighting load.

- **Window Wall Ratio (WWR) and Window Opening Ratio (WOR)**

  The building in the current situation has 60% WWR with 25% of WOR. Four options of WWR are selected, i.e. 25% which is a lower value that can be used in the building (CIBSE, 2017), 40%, 60%, and 80%. Lower WWR helps reduce the heating energy consumption of the building, however, it also reduces daylight. A lower WWR decreases the overheating risk by decreasing solar heat gain but at the same time decreasing WOR (the natural ventilation amount) which increases the overheating risk.

  Four options for Window Opening Ratio WOR are selected: 25% as the current situation, 30%, 40% and 50%. The windows are opened if the indoor temperature is higher than 23 ºC (which represents the current situation) and higher than the outdoor temperature. Cross ventilation is achieved in the current situation of the building by opening internal doors and internal windows and will keep it in the future design. The Airflow Network Model method in EnergyPlus is used to calculate the natural ventilation into the building (DOE, 2021b).

- **Night cooling**

  Three options are selected for the operation of night cooling: 0 ACH representing the current situation, 2.5 ACH representing the minimum Mechanical ventilation amount to meet IAQ requirements of 180 L/s or by opening 25% of the window opening area, and 5 ACH which can be achieved by opening 50% of window opening area. Nighttime ventilation is assumed by opening windows. If for any reason it is not possible to open windows at night, the ventilation rate can be achieved by mechanical ventilation, in which

case an excess mechanical load must be added. Therefore, night cooling is chosen as the last option to remove indoor excess heat. Nighttime ventilation allows buildings to be passively pre-cooled in preparation for the next day.

- **Cool Roof**

  Four solar reflectance values are selected to reduce the heat gain from the roof. These values are 0.2, which represents the current situation, 0.4, 0.6, and 0.8, which represents a -Cool Roof to reflect the solar irradiance to reduce heat gain and thus lower the indoor temperature. Moreover, a Cool Roof that reflects sunlight helps reduce maximum and mean ambient temperature by up to 4°C and 0.5°C and reduces mean ambient temperature during heatwave by 0.3 °C (Macintyrea and Heaviside, 2019). However, decreasing the solar gain will increase the heating demand in winter.

These options create about 291,600 potential optimal building designs to achieve three objectives simultaneously. These potential optimal designs do not include the current situation options of the building envelope (wall, roof, window and infiltration rate) because the building must at least meet current NECB requirements in any major building renovation.

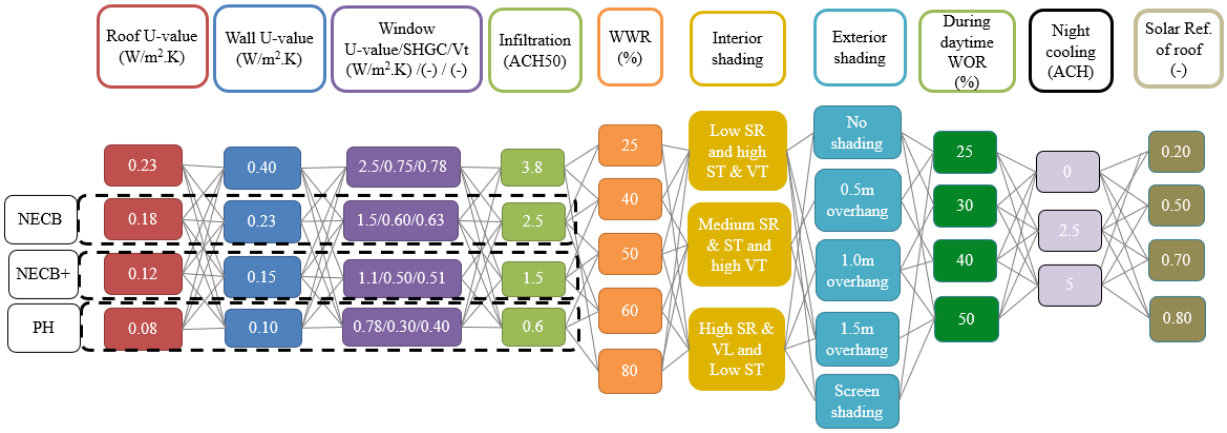

Figure 3-15. Building design parameters (Selected parameters)

3.2.5.2.3 Sensitivity analysis of selected building parameters

To identify the parameters that have a significant and contradictory effect on the heating energy demand, indoor temperature and lighting load, the global and local sensitivity analyses are used, as shown in Figure 3-16.

The global sensitivity analysis method should be performed to find the sensitivity index (SI) for each parameter to each objective. A parameter with a sensitivity index greater than 0.05 is considered a significant parameter, as is explained in Section 3.1.1. The local One-at-Time (OAT) method should be performed to determine the correlation between each sensitive parameter and each objective. If the correlation between a sensitive parameter and an objective is positive and negative for another objective, this parameter is considered a sensitive and contradictory parameter. These parameters should be used in the optimization analysis.

In this case, the possible solutions resulting from 10 building parameters are 291,600 which is less than 2 million, so sensitivity analysis is not used.

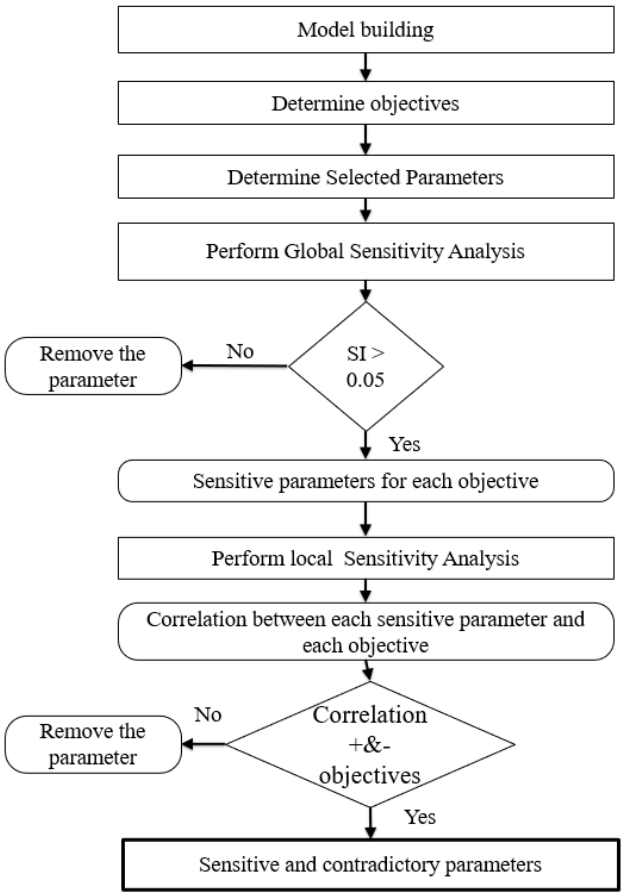

Figure 3-16. Proposed workflow to find the sensitive and contradictory parameters.

3.2.5.2.4 MOGA sittings

The jEPlus+EA-1.7 (Zhang, 2012; Zhang and Korolija 2020) program is used to implement the Multi-Objective Optimization Genetic Algorithm NSGA-II. In the MOOGA, E+ model code, the

objectives functions, the selected building parameters, and the genetic algorithm setting need to be assigned. The GA settings used to find the optimal design is similar to that in Section 3.2.1. Simulations stop when all Pareto solutions do not change within 100 simulations with ten generations.

3.3 SUMMARY OF SIMULATION SCENARIOS

This work aims to assess overheating risks and mitigation measures in Canadian archetype and existing buildings. More specific objectives are to 1) develop the sensitivity analysis methodology to determine the contribution of each building envelope parameter to the change in indoor temperature to determine whether old buildings have lower or higher overheating risk than HEEB buildings; 2) develop the robust calibration methodology to calibrate EnergyPlus model for an existing building with a high-accuracy prediction of indoor air temperature compared to measured indoor air temperature; 3) assess the indoor overheating risk under recent and future climates; 4) provide effective mitigation measures to mitigate overheating risk in the buildings; 5) develop the optimization strategies by applying a multi-objective genetic algorithm to provide the optimal design for retrofitting existing buildings considering heating energy efficiency, summer thermal comfort and visual comfort in the new building design.

To perform a global sensitivity analysis for the archetype detached house, 3072 simulations are needed. This number of simulations or samples (3072) is determined by applying Equations 3-1 and 3-2, where the minimum number of samples (N_m) for the five parameters listed in Table 3-1 is 196 and the number of samples (N_i) required to achieve the sum of sensitivity indices of 1 is $196 \times 2^2 = 1536$ simulations for each ventilation scenario (with and without ventilation). To determine the correlation, 40 simulations (from Table 3-1, 5 parameters × 4 options= 20) simulations for each ventilation scenario (with and without ventilation) are needed. To assess overheating risk in the archetype detached house, 85 simulations (4 building ages × 5 ventilation scenarios× 8 weather generations (historical, recent, two typical future years and 4 extreme future years) are needed. To find overheating mitigation measures for the detached house, a global sensitivity analysis is performed using 2048 simulations to find significant mitigation measures under the recent and future climate. 54 cases (3 building ages × 3 mitigation measures× 6 weather

generations) are simulated to evaluate the sensitive mitigation measures under the recent and future climate.

To calibrate the school building 1 model, 4354 simulations are required, which is determined by applying Equations 3-1 and 3-2 on the parameters listed in Table 3-4, to perform the global sensitivity analysis to find the significant uncertain parameter (2304 simulations during the closed period and 2048 simulations during the opened period), and 3550 simulations (1670 simulations during the closed period and 1880 simulations during the opened period) are simulated to calibrate the uncertain building parameters. The Des Grands- Êtres school model has calibrated 5030 cases (1640 cases during the closed period for each block (block 1 and 2) and 1750 cases during the opened period) are simulated to calibrate the uncertain building parameters. The multi-unite residential building model is calibrated using 1920 simulations to calibrate uncertain building parameters.

To assess the overheating risk in the existing school building 1 under different future generations, 5 simulations are required. To find overheating mitigation measures for school building 1, local sensitivity analysis is performed using 18 simulations (6 mitigation measures×3 weather generations) under the recent and future climate. To find the optimal building design for Canadian existing buildings, the optimization methodology is applied to the existing school building 1. Each optimal building design needs 1100 cases under each climate generation to find it.

In total, **25548** cases are modelled in the DesignBuilder (EnergyPlus) program, as shown in Table 3-9, to achieve the five objectives in this work.

Table 3-9. Simulation scenarios to achieve the five objectives in this work.

Objectives	**Scenarios**			
	Building parameters	**Mitigation measures**	**Weather data**	**# of simulat.**
Archetype building				
Objective 1: Sensitivity analysis methodology				
- Global sensitivity analysis	Detached house: - Wall, roof, window proprieties and infiltration rate (Range-Table 3-1)	NV: 0 and 10% WOFA	2020	3072
- Local sensitivity analysis	1950, 1990, NECB and HEEB			40
Objective 2: Overheating assessment				
Overheating risk	1950, 1990, NECB and HEEB	NV: 0%, 1%, 3%, 5% and 10% WOFA	2020, Typical: 2030, 2090 Extreme: 2042,2044 2059,2090	160
Objective 3: Mitigation measures				
- Global sensitivity analysis	7 parameters listed in Table 3-8	NV: 10% WOFA	2020, 2090-RCP8.5	4096
- Overheating risks assessment with the significant mitigation measures	1950, NECB and HEEB	NV, interior and exterior shading	2020, Typical: 2030-RCP4.5, 8.5, 2090-RCP4.5, 8.5 Extreme: 2044, 2090	54
Existing building				
Objective 1: Calibration methodology				
- Global sensitivity analysis	Existing buildings: - Uncertain building parameters (Table 3-4)		2020	4352

- MOGA analysis for calibrating sensitive uncertain building parameters for:	- School building 1 (Tables 3-4) - School building 2 (Table 3-6) - residential apartment (Table 3-7)		2020 2020 2020	3550 5030 1920
Objective 2: Overheating assessment				
Overheating risk	School building 1		2020, 2042, 2044, 2059, 2090	5
Objective 3: Mitigation measures				
- Local sensitivity analysis is performed for the parameters listed in Table 3-7	School building 1		2020	6
- Overheating risks assessment with the significant mitigation measures		Night cooling, blind roll, cool roof, combinations of them	2044, 2090	12
Objectives 4: Optimization design				
MOGA methodology	School building 1	10 parameters are shown in Figure 3-16	2020 2044 2090	3300
Total cases				**25548**

CHAPTER 4: RESULTS AND DISCUSSION

4.1 ARCHETYPE DETACHED HOUSE

4.1.1 Sensitivity analysis of building envelope parameters

4.1.1.1 Global sensitivity analysis

Figure 4-1 shows the global sensitivity indices that reflect each parameter's contribution and significance to the indoor temperature variance. It can be seen that without natural ventilation, the window SHGC contributes by 42% to the change in the indoor temperature, the U-value of the wall by 27%, airtightness by 18% and the U-value of windows by 13% (Figure 4-1a).

The smaller U-values of walls and windows and airtightness in HEEB buildings prevent the transfer of excess heat to the outside and thus increase the indoor temperature. Therefore, old buildings provide more comfortable indoor conditions because they are able to release the excess heat from solar heat gain and internal loads through infiltration, which is an uncontrolled form of ventilation, walls and windows (low thermal resistance) when the outdoor conditions are favourable. This study does not compare the energy use of these buildings over ages.

In contrast, with adequate natural ventilation (10% WOFA), SHGC of windows becomes the most important factor with an 87% contribution to the change of indoor temperature. Although the U-value of walls is the second, its contribution is much smaller, i.e. 9%, compared to the SHGC of windows, as shown in Figure 4-1b. The U-value of windows is the 3rd most significant parameter having a contribution of 4%. Similar trends were found under the historical, recent or future climatic conditions.

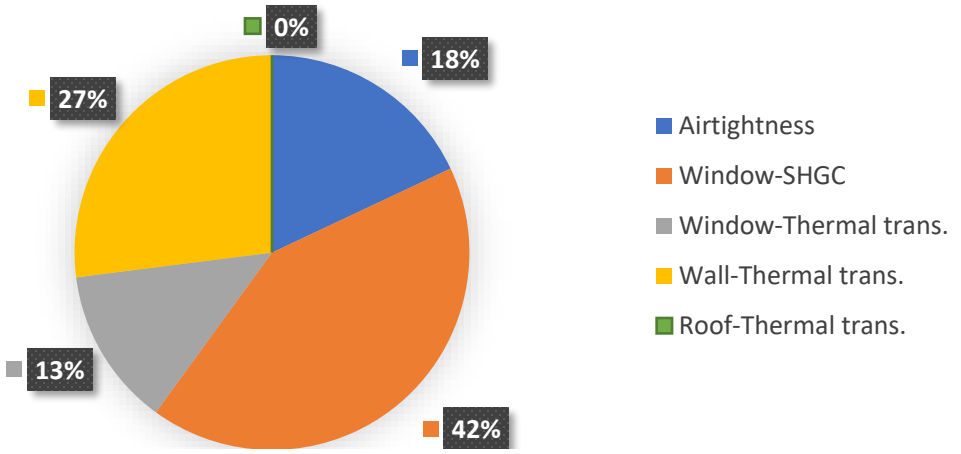

a)

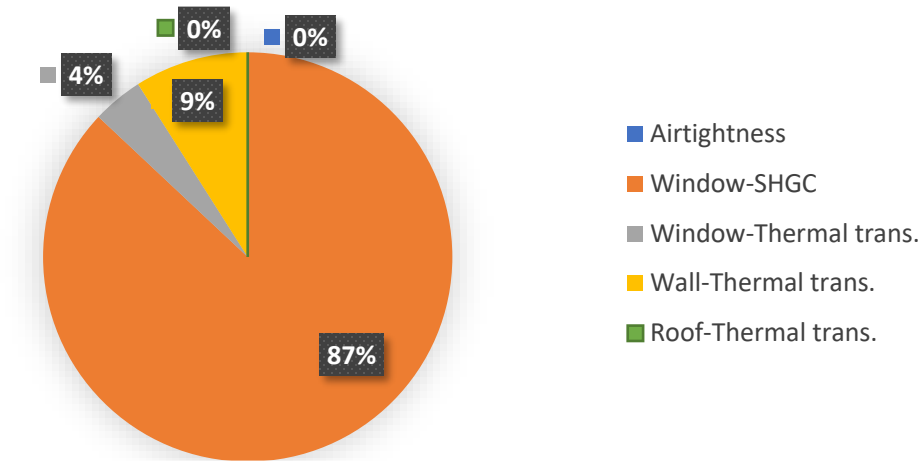

b)

Figure 4-1. Global sensitivity index of building envelope parameters; a) NNV; and b) NV (10% WOFA)

4.1.1.2 Local sensitivity analysis

The results of the OAT sensitivity analysis (Figure 4-2) show that the ventilation rate changes the influence of building envelope parameters on the indoor operative temperature, where without natural ventilation the effect of changing the parameters is higher than with natural ventilation, indicated by the narrower variation of indoor temperatures. For example, without natural ventilation, the maximum indoor operative temperature in summer decreases from 46.4 °C to 34 °C (12 °C) by reducing the window SHGC from 0.75 to 0.26, while with natural ventilation, it decreases from 30.8 to 25.6 °C (5 °C).

The OAT results show that without natural ventilation (Figure 4-3a-NNV) the correlation between (i) the average indoor operative temperature in summer, and (ii) wall and window U-values and air infiltration is negative, while the correlation between indoor temperature and the window SHGC is positive. These results also confirmed the results from the global sensitivity analysis, where the SHGC ranked as the most important parameter. The effect of SHGC is a temperature change by up to 8.6 °C, followed by the wall U-value by 6.4 °C, infiltration rate by 4.8 °C and window U-value by 4 °C. With adequate natural ventilation, the correlation between indoor temperature and wall U-value (Figure 4-3b-NV) and U-value of windows becomes positive, the same as for window SHGC (Figure 4-3b-NV). Similar to the results of the global sensitivity analysis, the SHGC parameter ranked the most important parameter with temperature change up to 4.5 °C followed by the U-value of the wall by 1.7 °C, infiltration rate by 0.4 °C and window U-value by 1.1 °C. The contribution of each building envelope parameter is not as significant as the case without NV and the contribution of infiltration is much smaller. As shown in Table 3-1, HEEB building has the lowest SHGC, wall U-value and window U-value, which explains why HEEB building performs the best when natural ventilation is applied.

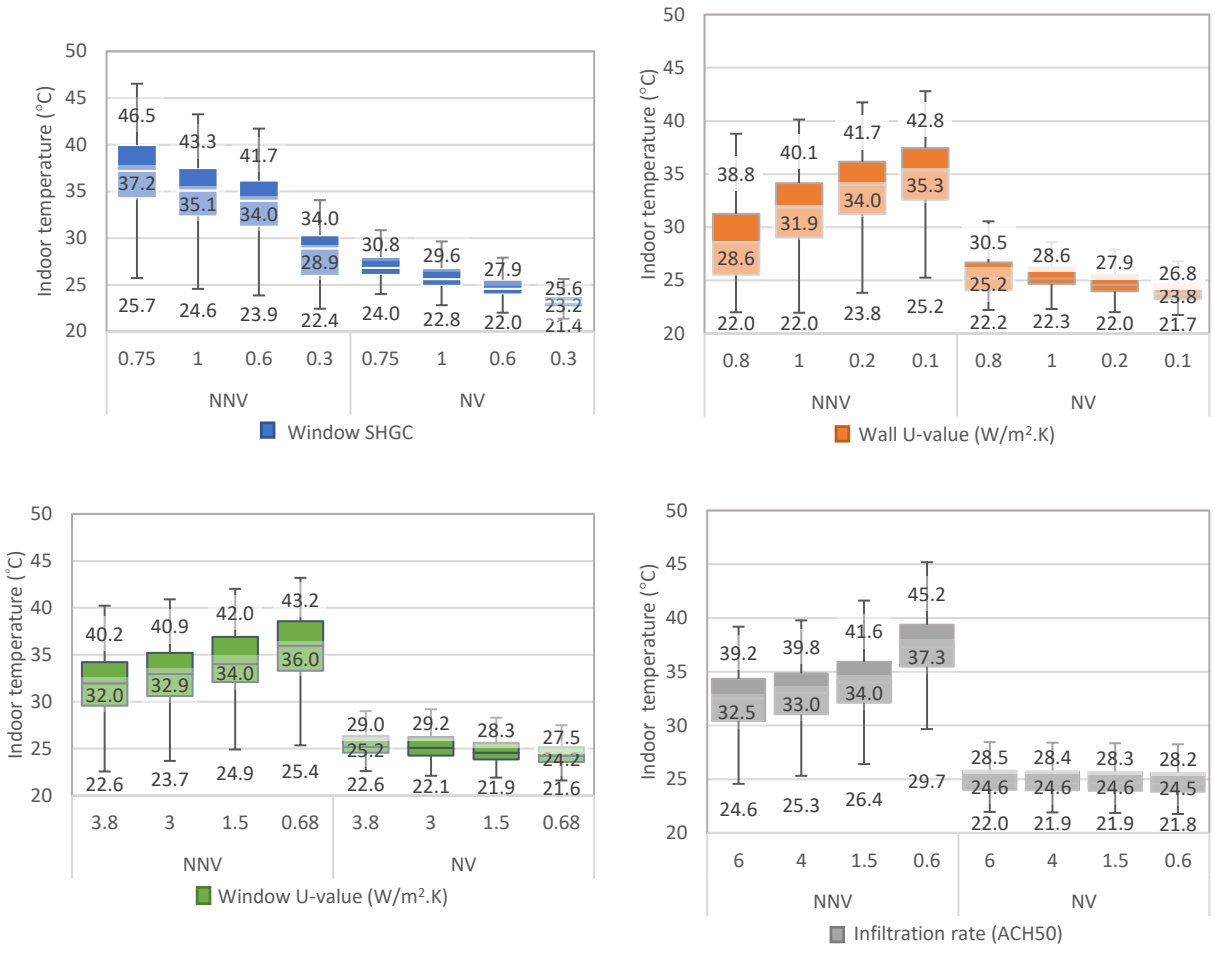

Figure 4-2. Indoor operative temperature percentile distribution from May to September-local sensitivity (OAT) results

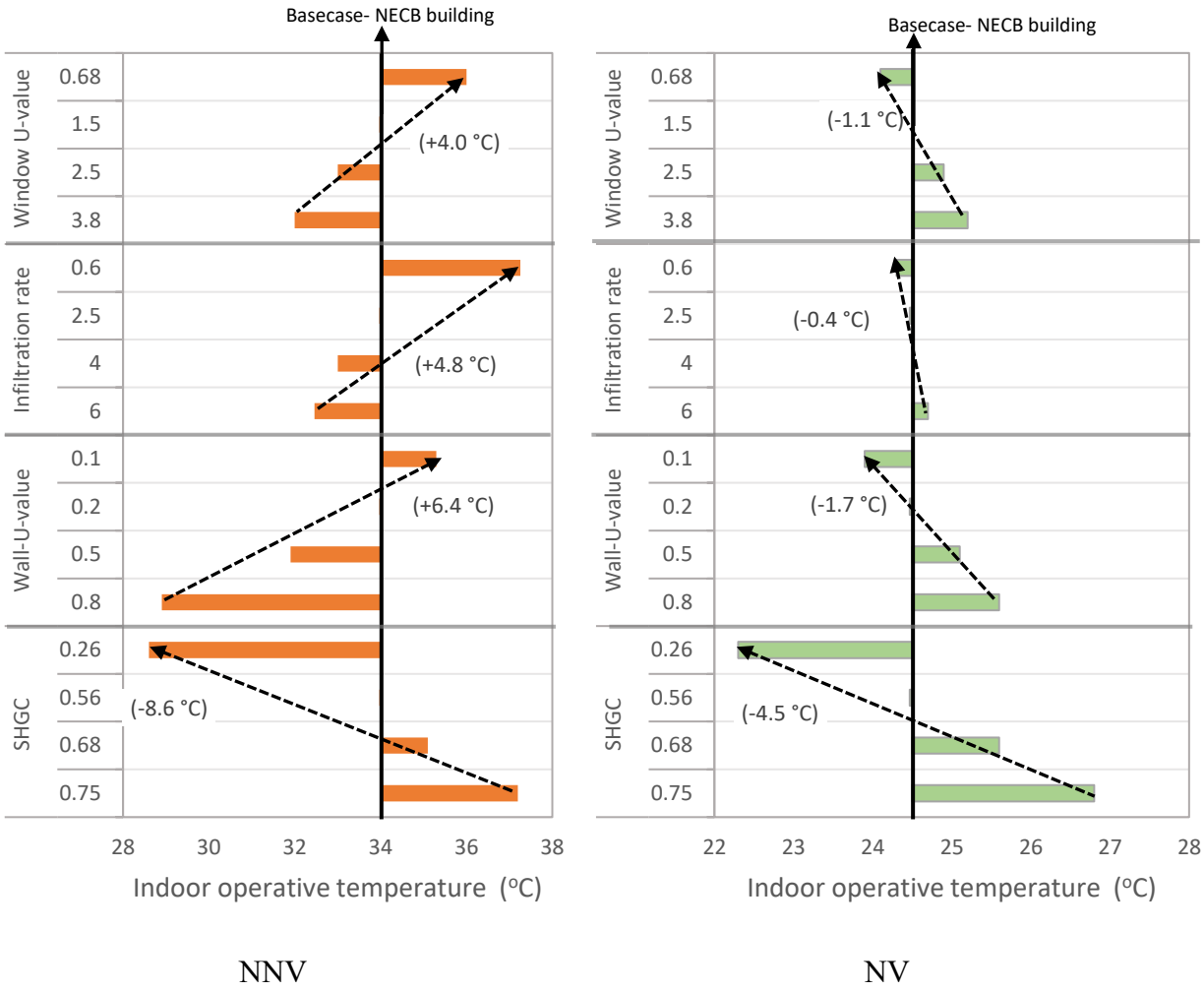

Figure 4-3. Local sensitivity (OAT) results of sensitive building envelope parameters with and without natural ventilation

4.1.2 Overheating assessment

Usually, thermal comfort and energy consumption of buildings are performed by using the historical TMY year (1961-1990). This approach neglects the effect of climate change on indoor thermal conditions. Therefore, this section focuses on determining how these buildings with different natural ventilation rates perform under the recent observation and projected typical future years compared to the historical TMY year. Also, it focuses on determining the ventilation rate required for the HEEB building to provide lower indoor overheating risk than old buildings. As shown in Figure 4-4, the minimum ventilation rate that makes HEEB buildings perform better than the old building (1950) is 3% WOFA, equivalent to 2.2 ACH, which is higher than the

ASHRAE ventilation rate requirement (0.8 ACH for indoor air quality purposes). With 1% WOFA, overheating hours increase with the better-insulated building envelope. The overheating hours in the HEEB building are about 200 and 300 hours higher than that in the 1950 building under historical TMY and RCM 8.5-2090, respectively. With 3% WOFA or higher, overheating hours decrease with the better-insulated building envelope. The overheating hours in the HEEB building are about 350 hours lower than in the 1950 building under all climatic scenarios.

Figure 4-6 also shows the effect of recent and future climate on the indoor overheating risk in different buildings and with different ventilation rates. Under TMY historical weather, old buildings can't achieve the acceptable overheating hours limit (200 hr) even with 10% WOFA (equivalent to 5.5ACH), while NECB and HEEB buildings can achieve an acceptable overheating limit with 10% and 5% WOFA, respectively. Under the 2020 observational year, the overheating hours in all buildings increased and no building can achieve the acceptable overheating hours limit (200 hr) except for HEEB. HEEB building with 10% WOFA has 207 overheating hours. The increase in overheating hours ranges from 170 to 440 hrs in the 1950 building and from 78 to 415 hrs in the HEEB building. Under the projected 2030, 2090-RCP8.5 climate, no buildings can achieve the acceptable overheating hours limit. The results also show that HEEB buildings are more resilient to global warming, especially with adequate ventilation (10% WOFA), where the overheating hours are about 300 hr lower than that of 1950 buildings in recent and future climates. However, Canadian single-family detached houses can no longer rely on natural ventilation only to remove indoors excess heat, and other mitigation measures are becoming necessary under projected future short and long-term climates.

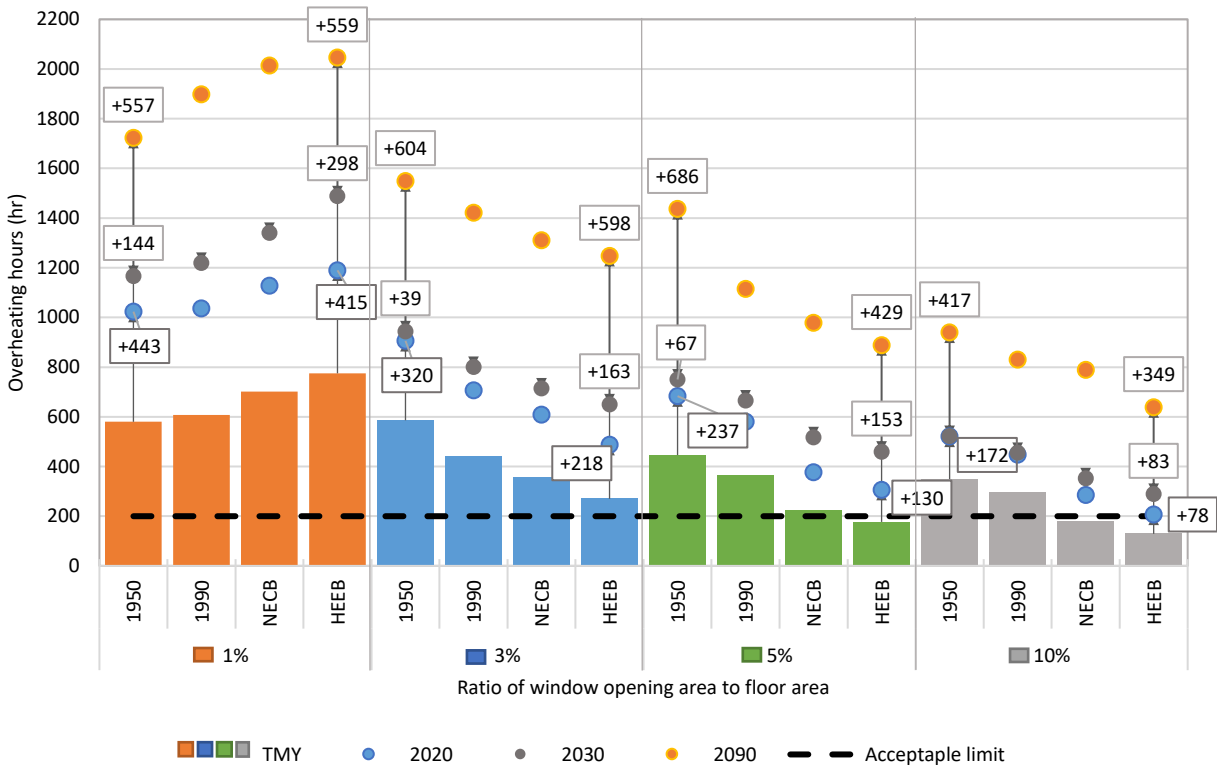

Figure 4-4. Overheating risk for four building ages with different ratios of window opening area to floor area under Historical TMY, 2020, 2030-8.5 and 2090-8.5. Values in the rectangles represent the increase in overheating hours between each two successive climate

For a more detailed overheating risk assessment under the future extreme year, the RSWY should be detected from individual future years (2041-2060 and 2081-2100) generated using CORDEX data. Based on the heatwave detection operational method, the three heatwave thresholds are 25.5 ºC for Spic, 24.1 ºC for Sdeb and 23.3 ºC for Sint threshold. Figure 4-5 shows the daily average temperature during 20 years of historical (2000-2001), bias-adjusted mid- and long-term future summer temperatures (May to September) with three thresholds. Based on these three heatwave thresholds, four heatwave events were detected over the historical period (Figure 4-6a), 38 heatwave events in the future mid-term (Figure 4-6b), and 88 in the future long-term period (Figure 4-6c). The bubble center values in Figures 4-6b–c represent the duration and intensity of the heatwave event and the bubble size represents the heatwave severity. Figure 4-6d shows in which year the longest, most intense and severe heatwave occurred during the historical period (2001-2020), future mid-term (2041-2060) and long-term period (2081-2100).

During the historical period, the extreme year (RSWY) is 2020 as it has the most intense, severe and longest heatwaves. During the future mid-term, three extreme RSWY years are selected: 2059 as it has the most intense heatwave, 2042 as it has the most severe heatwave, and 2044 as it has the longest heatwave. During the future long-term, the extreme RSWY year is 2090 as it has the longest, most intense and most severe heatwave. Therefore, the indoor thermal condition of the school is assessed in 2020 with observational weather data, and future years 2042, 2044, 2059 and 2090 with projected future weather data.

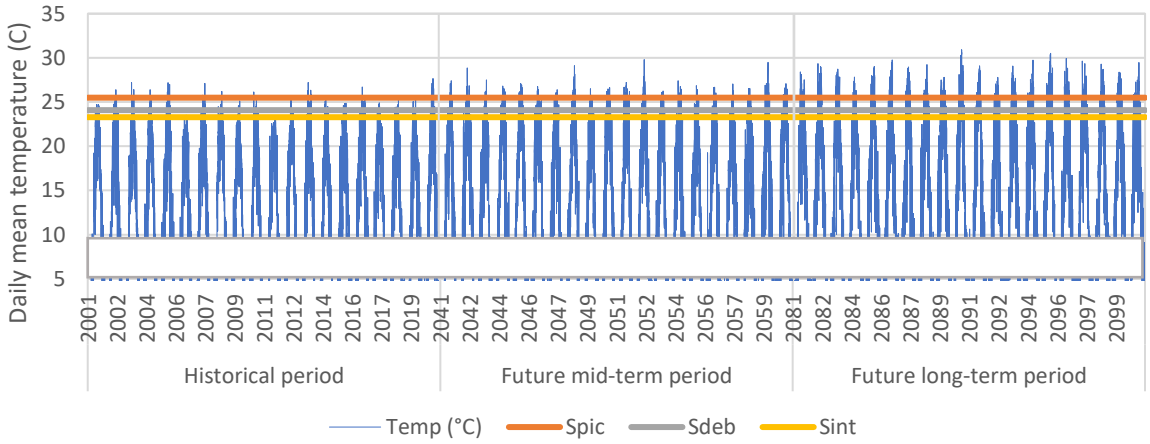

Figure 4-5. Daily mean temperature of Montreal with three thresholds during three periods, b) Extreme heatwave events during three periods.

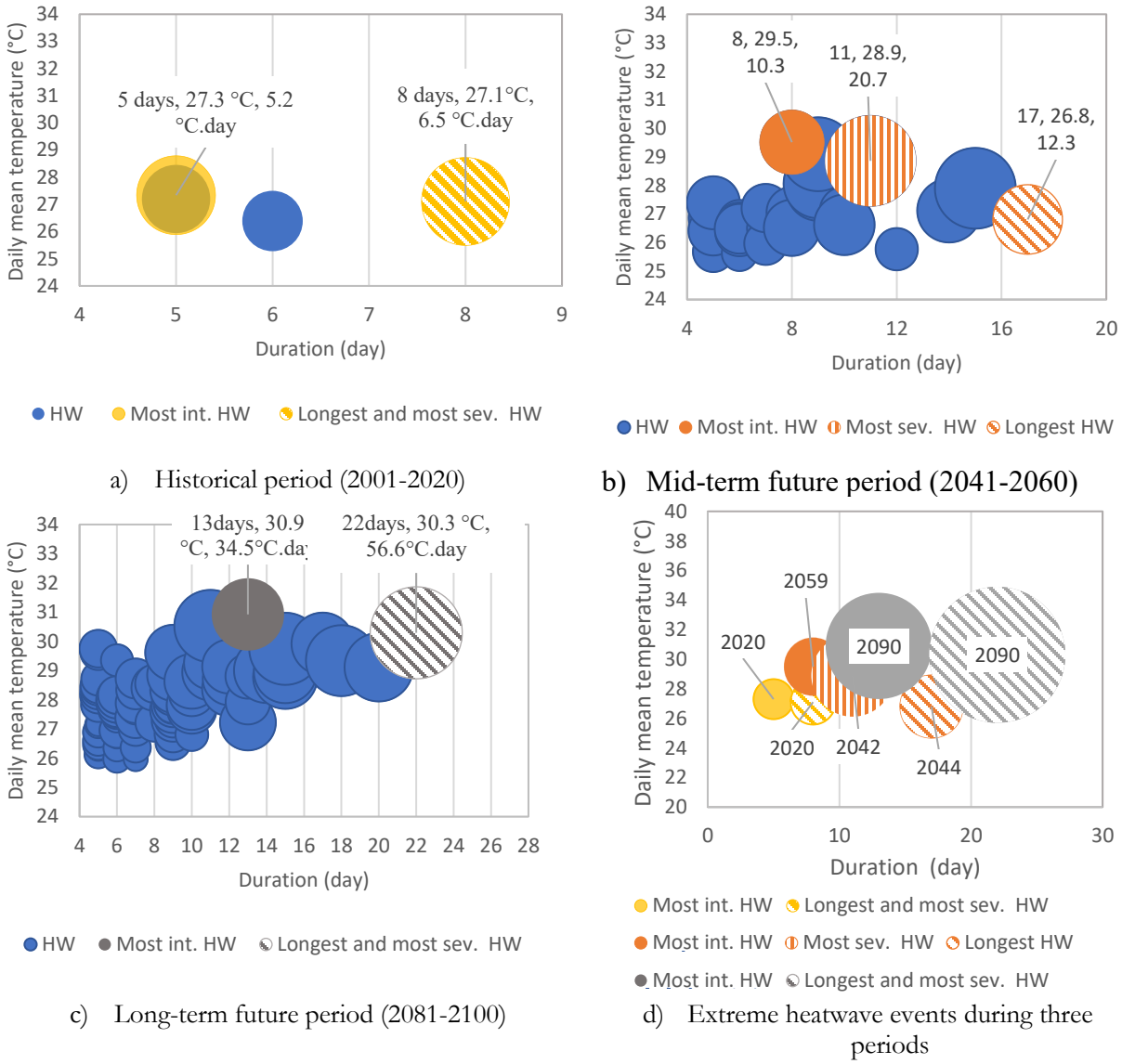

Figure 4-6. Heatwave events during a) historical period, b) mid-term, c) long-term future period. Values at the top of bubbles represent duration (days), intensity (˚C), and Severity (˚C·day); d) extreme heatwave events during three periods (value at the bubbles represents the year in which the heatwave occurred)

The overheating risk is assessed under four future extreme years, i.e. 2042, 2044, 2059, and 2090, and their results are compared to the future typical years generated using WeatherShift software. The results in Figure 4-7 show that the average overheating hours in the house will be 481 hrs in 2044with a difference of about 66% compared to the results of the 2030 typical year, 422 hrs in 2059 with a difference of about 10% compared to the results of the 2050 typical year, and 764 hrs

422 hrs in 2090 with a difference of about 19% compared to the results of the 2090 typical year. Therefore, 2020, 2044 and 2090 years are selected to conduct more detailed studies on mitigation measures in these years.

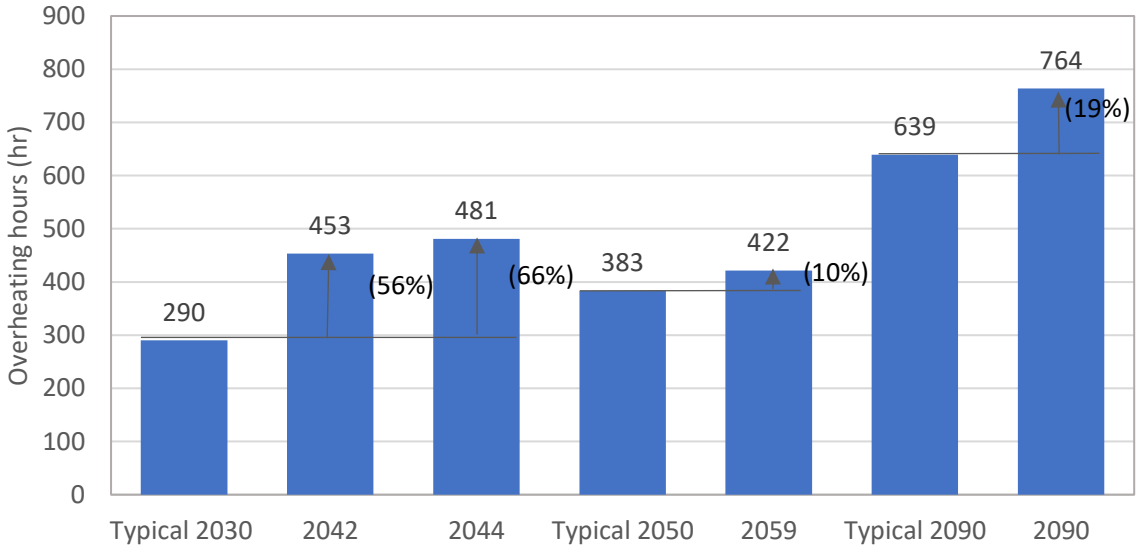

Figure 4-7. Overheating risk in HEEB under future extreme and typical years based on RCP8.5 scenario

4.1.3 Mitigation measures

The high natural ventilation rate (10% WOFA, 5.5 ACH) with a high energy-efficient building envelope can achieve the BCESC and ZEBP requirements (less than 200 hrs) in 2020 and without interior shading. However, with climate change, the natural ventilation will not be sufficient to remove the overheating under 2030-RCP8.5 or 2090, as shown in Figure 4-8. Therefore, additional mitigation measures are required. Global sensitivity analysis is performed to find the contribution and significance of each mitigation measure to the indoor temperature variance under 2020 and 2090 weather and the results are shown in Figure 4-8.

Under 2020, it can be seen that among all the mitigation measures, natural ventilation is the most significant parameter with a sensitivity index of 0.51, followed by window SHGC (0.17), interior shading (0.13), wall thermal transmittance (0.08) and exterior shading (0.07). These results can help decision-making in retrofitting existing buildings to mitigate overheating risks. The priority should be given to ensuring adequate natural ventilation in design and operation, followed by good solar control to reduce solar heat gain by upgrading windows to lower SHGC; however, it needs

to be balanced with considering winter heating demand or implementing interior shading and the exterior shading. Under 2090, the three most significant factors are the same as under 2020 weather (Figure 4-8b); however, the contribution of natural ventilation is reduced and the contributions of interior shading and window SHGC become greater. These results confirm that natural ventilation as a mitigation measure will not be as effective in the future as it is now since higher outdoor temperatures will be expected and less favourable for natural ventilation, as shown in Figure 4-8.

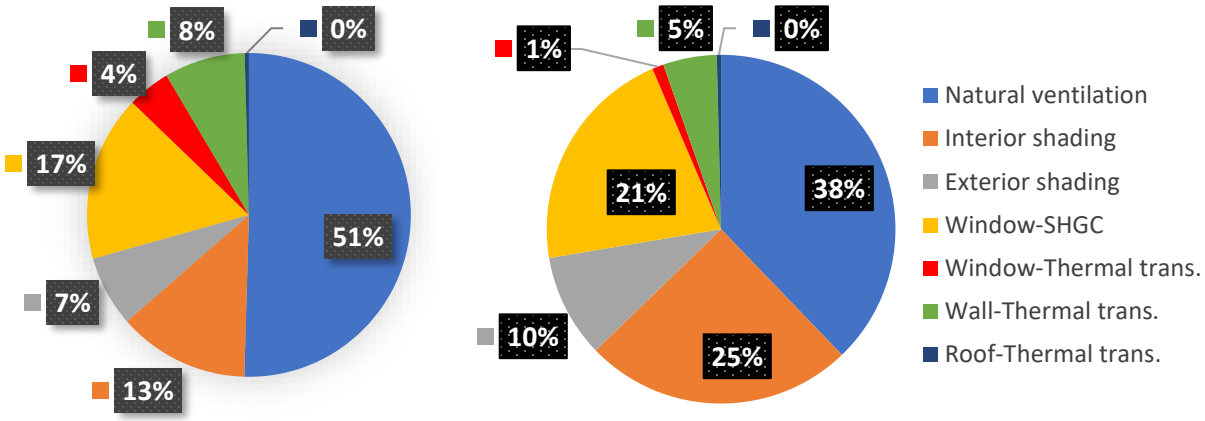

a) 2020 b) 2090-8.5

Figure 4-8. Global sensitivity index of various mitigation measures under 2020 and 2090-RCP8.5

According to SA results, interior roll shading (0.8 of solar reflectance and used if the solar radiation on the window is higher than 100 W/m2) and exterior overhang (1.5 m) are added to the 1950 and HEEB buildings as additional mitigation measures The improvement on indoor overheating hours is assessed and the results are shown in Figures 4-9 and 4-10. The 1950 building is over 70 years old by 2020 bringing it to the end of its first life cycle and needs major renovation. For such a renovation, the building envelope needs to meet at least the NECB requirements. Therefore, the overheating risk in the 1950 building is studied with mitigation measures under 2020 only, and then under the future climate, the overheating risk is studied in the NECB and HEEB buildings.

Figure 4-9 shows the quantile of indoor operative temperature distribution from May to September for 1950, NECB and HEEB buildings with mitigation measures under 2020 and 2030 and 2090-RCP8.5 years. The results show that the median and max temperature of three buildings is

significantly reduced with the addition of interior shading for natural ventilation compared to the addition of exterior shading for interior shading, which confirmed the importance of interior shading as shown in Figure 4-8. The results also show that 75 percentiles of the indoor operative temperature of the NECB and HEEB buildings is about 26 °C in recent and future climates and the max temperature does not exceed 28 °C until 2030 and 30 °C until 2090.

Figure 4-10 shows the overheating hours in the buildings under recent and future climates. In 2020, natural ventilation was sufficient to keep the overheating hours in NECB or HEEB lower than the acceptable limit. The addition of the interior shading to the NECB and HEEB buildings, and both the interior and exterior shading in the 1950 building is required to keep the overheating hours in these buildings lower than or close to the acceptable limit. In the near-future 2030, natural ventilation and interior shading will be still sufficient to have an acceptable thermal condition in NECB or HEEB buildings. However, under the 2090 scenario, the NECB building will need to have additional exterior shading added to maintain overheating hours below the acceptable limit. For the HEEB building, under RCP8.5, additional exterior shading is required to reduce the overheating hours to 159 hrs.

These results confirm the importance of improving the thermal condition of the building envelope to mitigate the overheating risk.

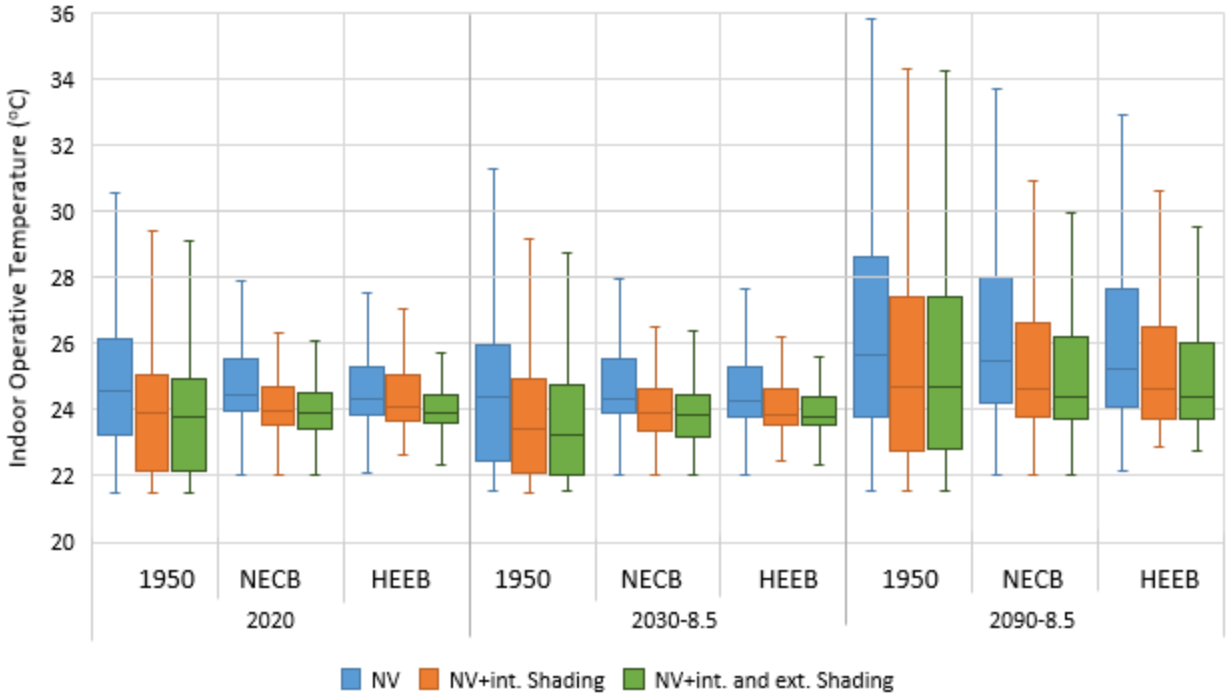

Figure 4-9. Indoor operative temperature percentile distribution from May to September for 1950, NECB and HEEB buildings with mitigation measures under recent and future years

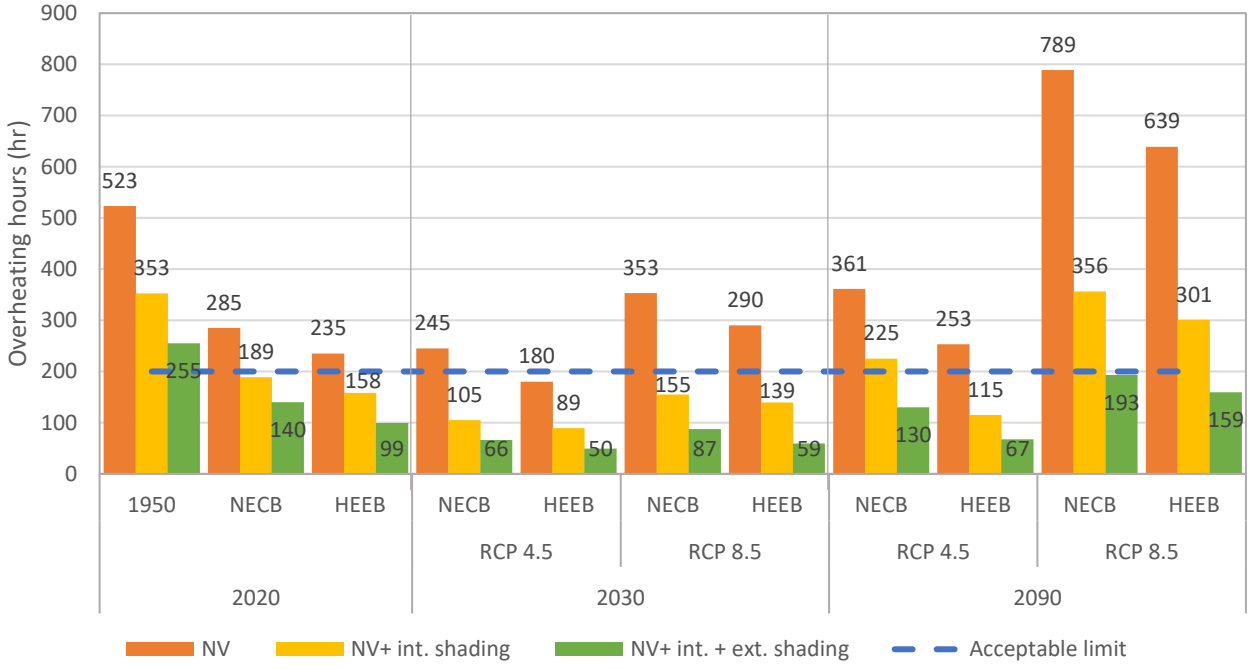

Figure 4-10. Overheating hours for 1950, NECB and HEEB buildings with mitigation measures under recent and future typical years

For a more detailed mitigation measures assessment under the recent and future extreme years, the overheating risk in the HEEB house rooms is assessed using ASHRAE 55 as shown in Figure 4-11. In 2020, natural ventilation and interior shading in the HEEB house are sufficient to keep the overheating hours lower than the acceptable limit in all rooms. In 2044, it is necessary to add exterior overhang shading (1.5 m) to keep the overheating hours lower than the acceptable limit in all rooms. In 2090, it is necessary to use exterior blind roll shading with interior shading and natural ventilation (combination 3) to keep the overheating hours lower than or close to the acceptable limit in all rooms. These results confirm that under extreme years, more additional mitigation measures are required compared to those used under typical years.

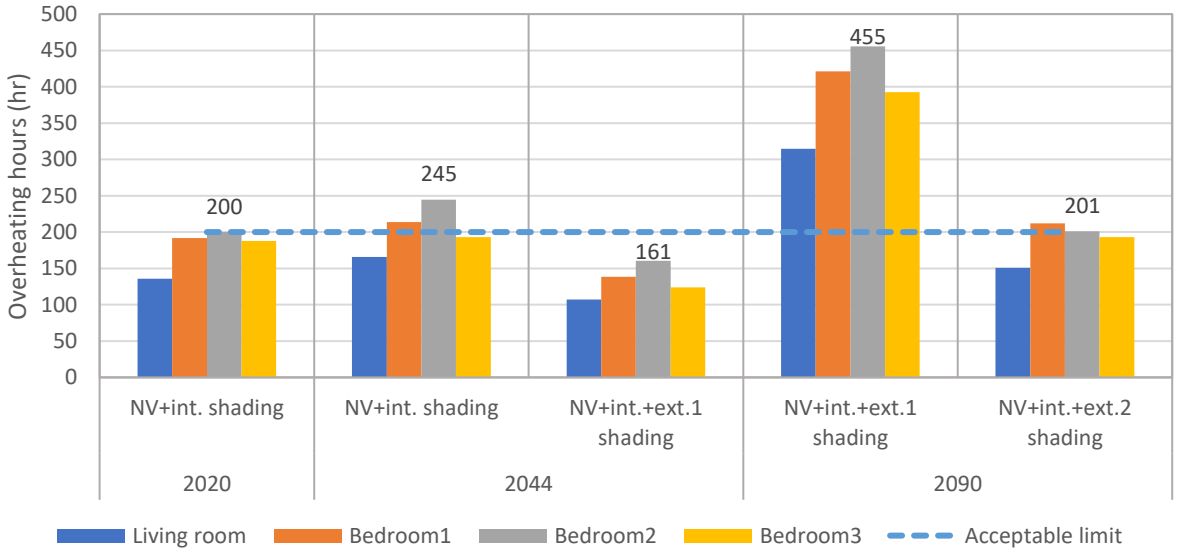

* Ext. 1 is exterior 1.5 m overhang shading, Ext. 2 is exterior blind roll (screen) shading

Figure 4-11. Overheating hours for rooms in HEEB building with mitigation measures under recent and future extreme years using ASHRAE 55

4.2 EXISTING BUILDINGS

4.2.1 Calibration Model

4.2.1.1 School building 1

4.2.1.1.1 Sensitivity analysis of uncertain building parameters

Global variance-based sensitivity index that reflects each parameter's contribution and significance to the indoor temperature variance under summer 2020 weather has been calculated for uncertain building parameters during the closed and opened periods (Figure 4-12, room 200 as an example). A number of 2304 samples are used to calculate the sensitivity index. This number of samples was enough to make the sum of the total sensitivity indices equal to 1. The significant parameters that influence the indoor temperature are the shading solar reflectance (0.59), followed by the infiltration rate (0.22), wall thermal transmittance (0.09), and roof thermal transmittance (0.06). The impact of wall and roof thermal transmittance on the indoor temperature was greater than window variables because the windows have more certain values with a narrower range set, compared to the range of wall and roof thermal transmittance (shown in Table 3-1). Since the type of construction in the wall, interior floor, and the roof is known, this parameter was more certain than others causing its contribution to decrease as well. The results are similar for the second range with a slightly greater contribution of shading solar reflectance. The results of this sensitivity index are similar for the four rooms.

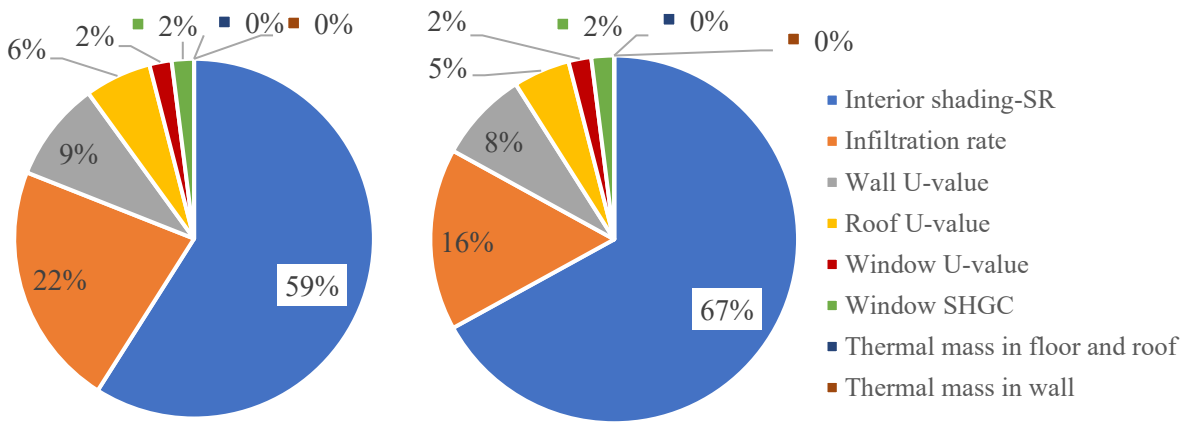

a) b)

Figure 4-12. Global total sensitivity index of building envelope parameters obtained from: a) the first range of building parameters; and b) the second range during the closed period; for room 200 as an example.

Table 4-1 shows the sensitivity index for the building operation parameters during the opened period. Sensitivity analysis of the building operating parameters is performed after the building envelope parameters have been calibrated during the closed period. A number of 2048 samples are simulated and used for the calculation of the sensitivity index. The results show that the shading opening level in southeast rooms has a significant effect not only on the temperature of southeast rooms (R 200 and 203) but also on the northwest rooms (R 208 and 212), which confirms that calibration should be carried out for all rooms together, not separately. It can be seen that significant parameters that influence the indoor temperature after the shading opening level are natural ventilation rate and setpoint, followed by the lighting load. The impact of lighting load on the indoor temperature was greater than the occupancy and equipment load

Table 4-1. Global sensitivity index of building parameters after school was opened.

Parameters		R 200 (SE)	R 203 (SE)	R 208 (NW)	R 212 (NW)
Interior shading opening ratio	**Southeast rooms on the second floor**	0.85	0.86	0.53	0.48
	Northwest rooms on the second floor	0.00	0.00	0.23	0.26
Max air change rate from NV		0.05	0.04	0.10	0.12
NV Setpoint		0.08	0.08	0.08	0.08
Lighting load		0.04	0.04	0.04	0.04
Occupancy load		0.01	0.01	0.01	0.01
Equipment load		0.01	0.01	0.01	0.01

4.2.1.1.2 Calibration and validation results during the closed period

Based on the sensitivity analysis, seven parameters, i.e., four interior shadings, air infiltration, wall thermal transmittance and roof thermal transmittance parameters have been defined in the calibration model; 1) two shading parameters for all rooms facing southeast; and 2) two shading parameters for all rooms facing northwest, one for the first floor and one for the second floor. In total, there are 1,300,000 possibilities of solutions resulting from these seven parameters. There are twelve objective functions, three for each room, i.e., NMBE, RMSE, and MAD. Two weeks of data from May 23rd to Jun. 4th is used for calibration of the four classrooms simultaneously. Data from Jul. 3rd to Aug. 20th is used for validation of the calibrated model. The Pareto solutions have been achieved after 167 generations with 1670 simulations for the first range and 155 generations with 1550 simulations for the second range. As an example, Figure 4-13 shows the distribution of solutions in the objective function space (RMSE for room 200 and MAD for room 208). The cyan point in Figure 4-13 represents the optimal solution that has been selected. Table 4-2 shows the value of each parameter of the optimal solution from the two ranges, which will be used in the calibrated model. The values of parameters from the two ranges are almost the same, as shown in Table 4-2, but the first range gives more accurate results than the second range based on the MAD, RMSE, and NMBE criteria, as shown in Table 4-3. Therefore, the calibrated model based on the first range is selected.

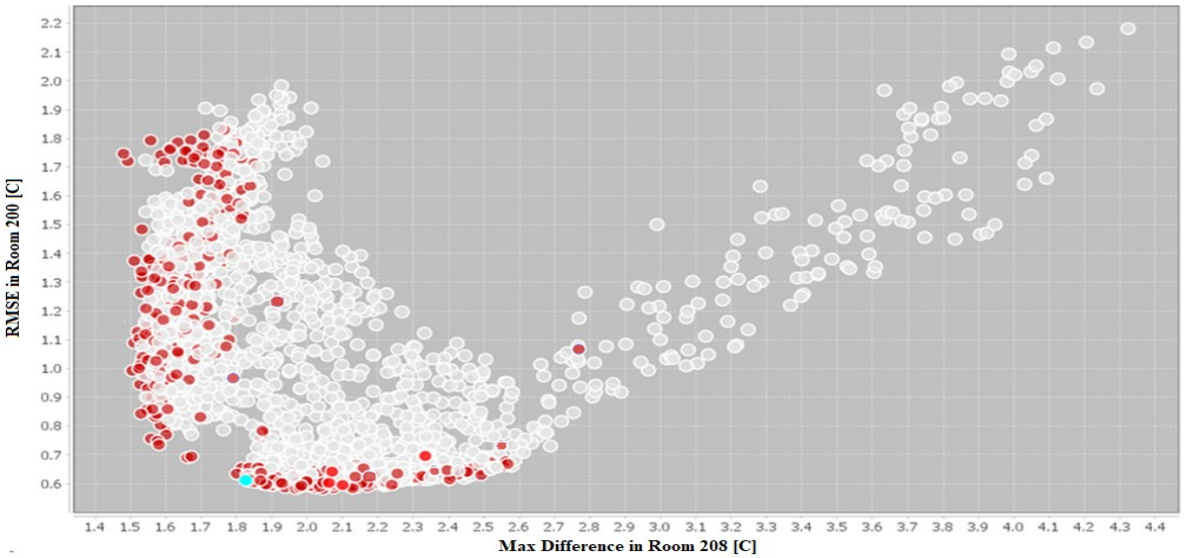

Figure 4-13. Gray points are all simulations; red points are the Pareto front solutions from MOGA calibration; the cyan point is the selected optimal solution**.**

Table 4-2. Calibrated model parameters from the optimal solution for the school closed period.

Parameters		Values from the First range	Values from the Second range
Shading solar reflectance	**Second floor-SE**	0.9	0.9
	Second floor- NW	0.5	0.3
	First floor-SE	0.8	0.8
	First floor- NW	0.5	0.5
Infiltration rate (@ACH50)		3.9	3.0
Wall U-value (W/m^2·K)		0.43	0.40
Roof U-value (W/m^2·K)		0.23	0.23

Figure 4-14 shows the comparison of indoor temperature between measurements and simulations over the period from May 23rd to Jun. 4th (calibration period) and over the period from Jul. 3rd to Aug. 20th (validation period) for the four classrooms. The results clearly show that the simulated data has a similar pattern to the data measured at most hours and also show that the indoor temperature follows the variation pattern of the outdoor measured temperature.

Table 4-3 shows the calibration results for both calibration and validation periods. For the calibration period, the calibrated model achieved an RMSE in the range of 0.3-0.6 ºC, NMBE of -1-1%, MAD of 1.0-1.5 ºC, the 1 °C Percentage Error criteria of 0-10%, and 0.5 ºC Percentage Error criteria of 8-35% for the four rooms. Similar accuracy is achieved for the validation period. They are an RMSE of 0.3-0.5 °C, NMBE of -1-0%, MAD of 1.1-1.6 °C, the 1 °C Percentage Error criteria of 0-9% and 0.5 °C Percentage Error criteria of 11-22%.

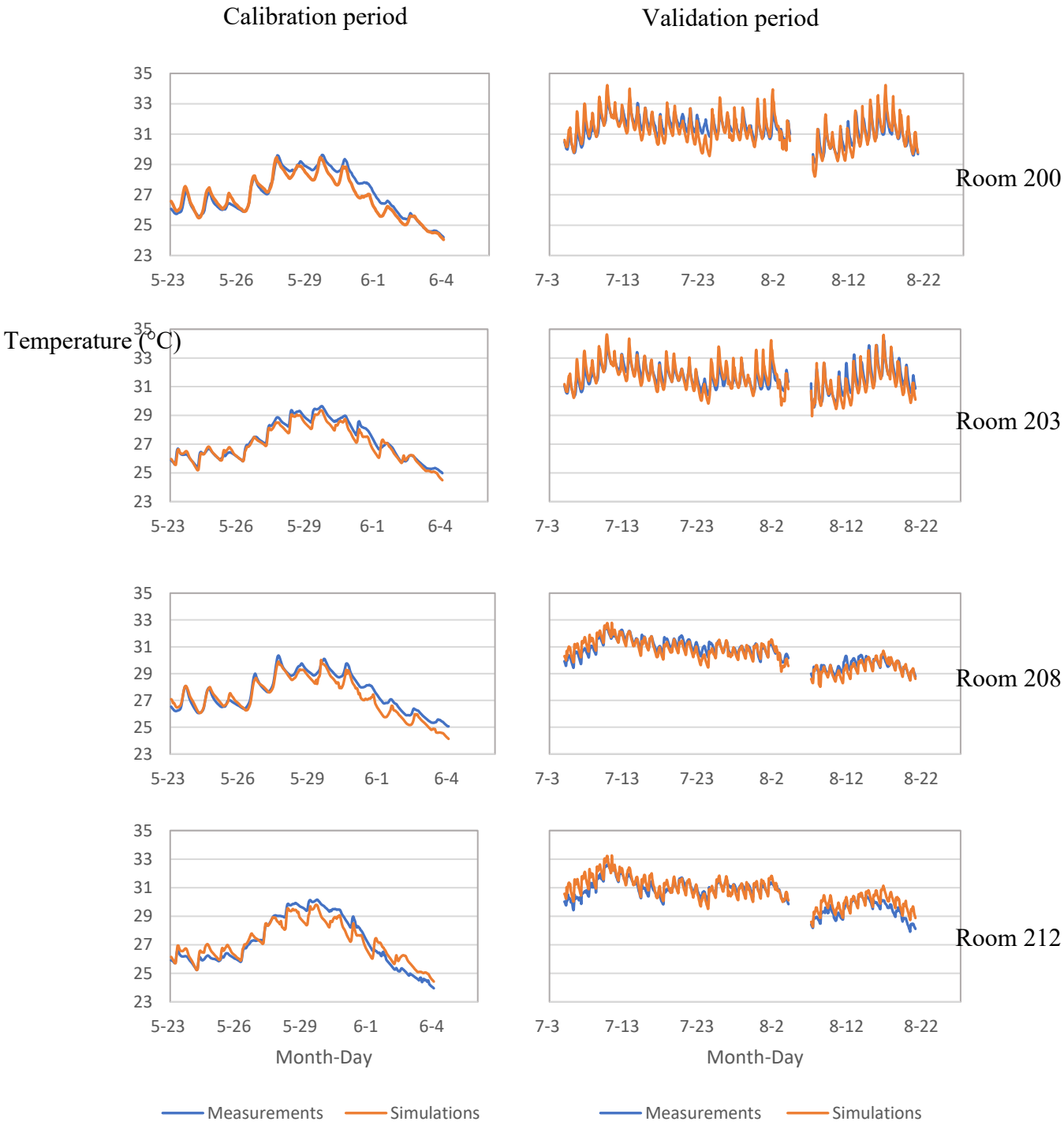
Calibration period
Validation period
Temperature (°C)
Room 200
Room 203
Room 208
Room 212
35
33
31
29
27
25
23
5-23
5-26
5-29
6-1
6-4
7-3
7-13
7-23
8-2
8-12
8-22
Month-Day
Measurements
Simulations

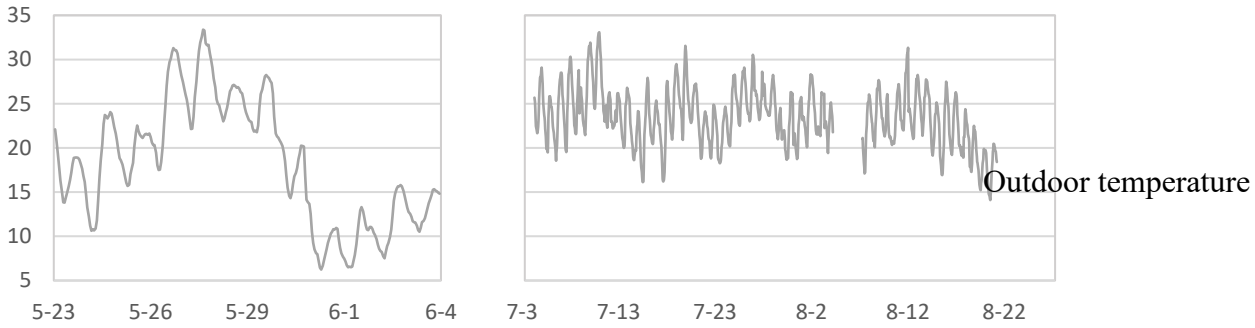

Figure 4-14. Comparison of indoor air temperature between measurements and simulation results from the calibrated model during the closed period for four rooms over the calibration and validation period.

Table 4-3 Model calibration results for the first (FR) and the second (SR) range.

Evaluation criteria	Calibration								Validation			
	R 200		R 203		R 208		R 212		R 200	R 203	R 208	R 212
	FR	SR	FR	SR	FR	SR	FR	SR				
RMSE (ºC)	0.5	0.6	0.4	0.4	0.3	0.4	0.6	0.5	0.5	0.5	0.3	0.5
NMBE (%)	-0.6	-0.7	-0.5	-0.6	0.1	0.1	-0.6	-0.8	0.3	0.2	0.1	-0.5
Max Diff (ºC)	1.3	1.5	1.2	1.3	1.0	1.0	1.5	1.5	1.8	1.8	1.1	1.4
1 °C Percent. Error (%)	6	8	3	4	0	0	10	9	9	5	0	4
0.5 °C Percent. Error (%)	31	33	21	24	8	11	35	34	22	19	11	16

4.2.1.1.3 Calibration and validation results during the opened period in 2020 and 2021

After the building envelope parameters are calibrated during the closed period, 10 parameters, including 2 parameters for shadings, 4 for NV amount, 2 for NV setpoint and 2 for lighting load, are selected for calibration of the four classrooms simultaneously during the opened period. The

initial operation schedule for lighting load is set based on the lighting fraction in the NECB-2017 code, and the NV rate as a result of the window opening ratio is set based on the occupancy fraction in the NECB-2017 code.

The Pareto front solutions have been achieved after 188 generations, with 1880 simulations. Figure 4-15 shows the comparison between measured and simulated indoor air temperature over the period from Sep. 12th to Oct. 5th (calibration period) and over the period from Oct. 6th to Oct. 15th (validation period) for the four classrooms. In 2021, the model is also validated using the data from May 14th to Jun. 19th. The results clearly show that the simulated data has a similar pattern to the data measured at most hours. The calibrated parameter values are listed in Table 4-4. Table 4-5 shows the calibration results after the school opened during the calibration and validation period.

For the calibration period, the calibrated model achieved an RMSE in the range of 0.5 ºC, NMBE of 0.2%, MAD of 1.5-1.9 ºC, 1 °C Percentage Error criteria of 5-6%, and 0.5 ºC Percentage Error criteria of 30-35% for the four rooms. Similar accuracy is achieved for the validation period from Oct. 6th to Oct. 15th, 2020. The calibrated model achieved an RMSE of 0.3-0.5 °C, NMBE of -1-0%, MAD of 0.8-1.6 °C, 1 °C Percentage Error criteria of 0-9% and 0.5 °C Percentage Error criteria of 12-40%. Similar accuracy is achieved for the validation period from May 14th to Jun. 19th, 2021. The calibrated model achieved an RMSE of 0.5-0.6 °C, NMBE of 0.1-0.2%, MAD of 1.6-1.7 °C, 1 °C Percentage Error criteria of 6-9% and 0.5 °C Percentage Error criteria of 30-45%.

The results showed that a calibrated model with an overall high accuracy has been achieved over the whole period (closed and open period), however, at some interval times, a slightly higher discrepancy is observed. This is because the unknown parameters calibrated represent the average over the entire period, for example, occupancy profile or natural ventilation rate due to window opening. However, in real operation, these operational parameters are dynamic and change over time.

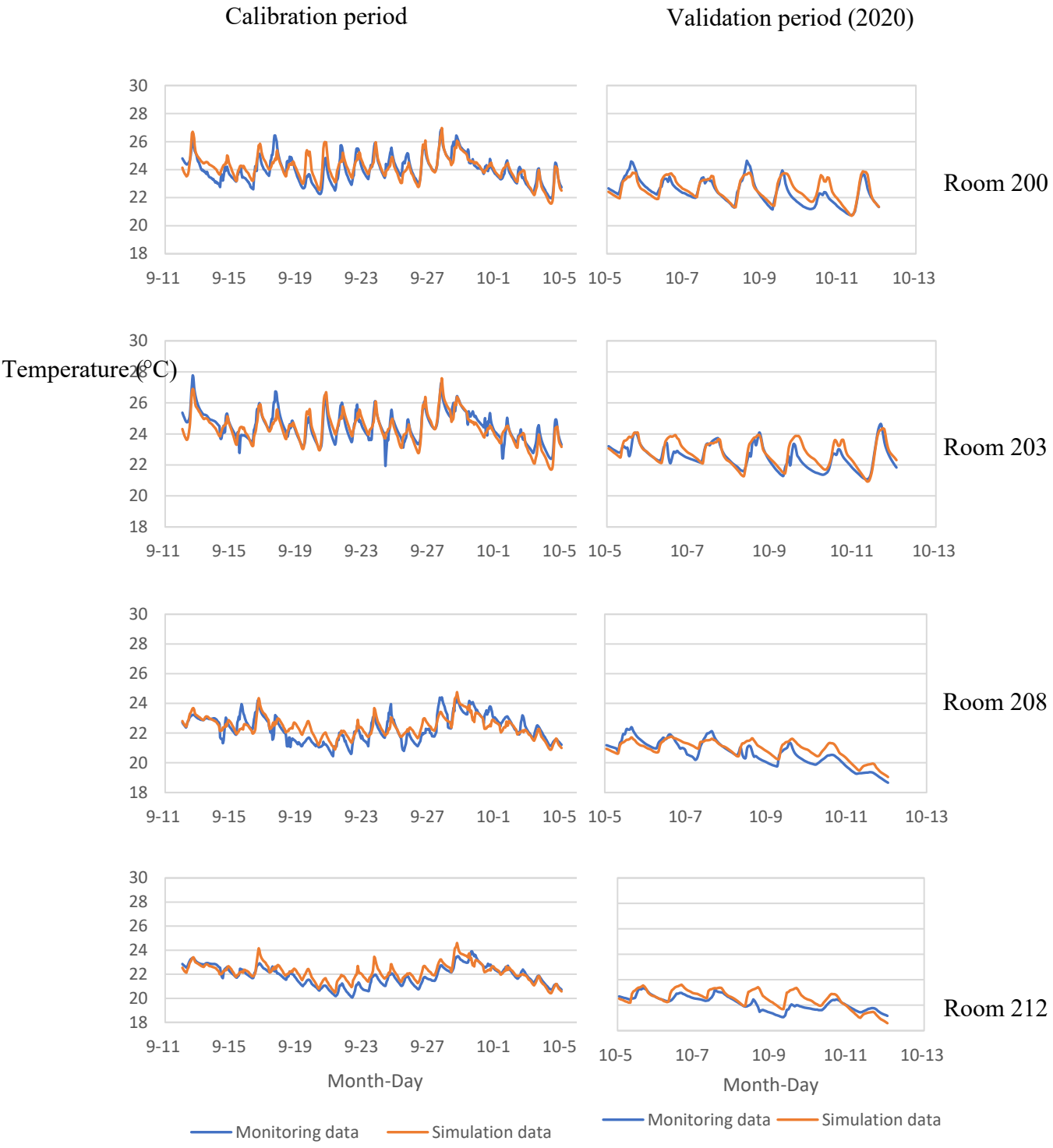
Calibration period
Validation period (2020)
Room 200
Room 203
Room 208
Room 212
Temperature(℃)
30
28
26
24
22
20
18
9-11
9-15
9-19
9-23
9-27
10-1
10-5
10-7
10-9
10-11
10-13
Month-Day
Monitoring data
Simulation data

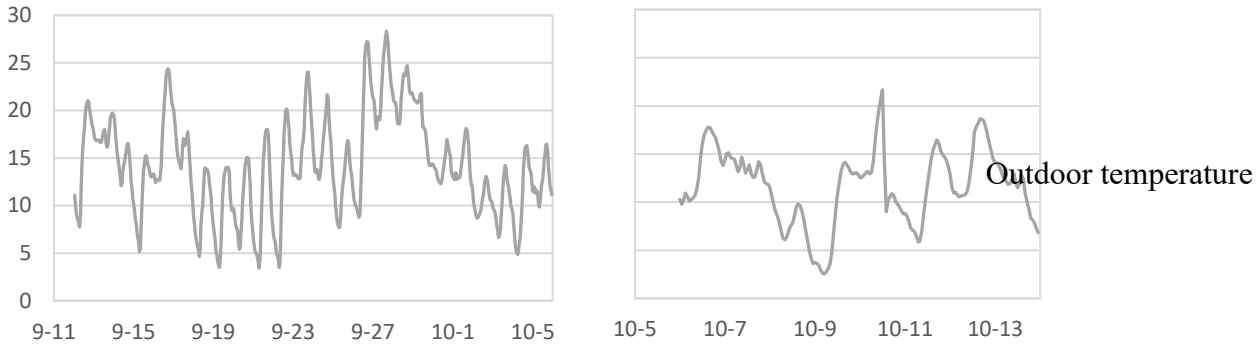

Validation period (2021)

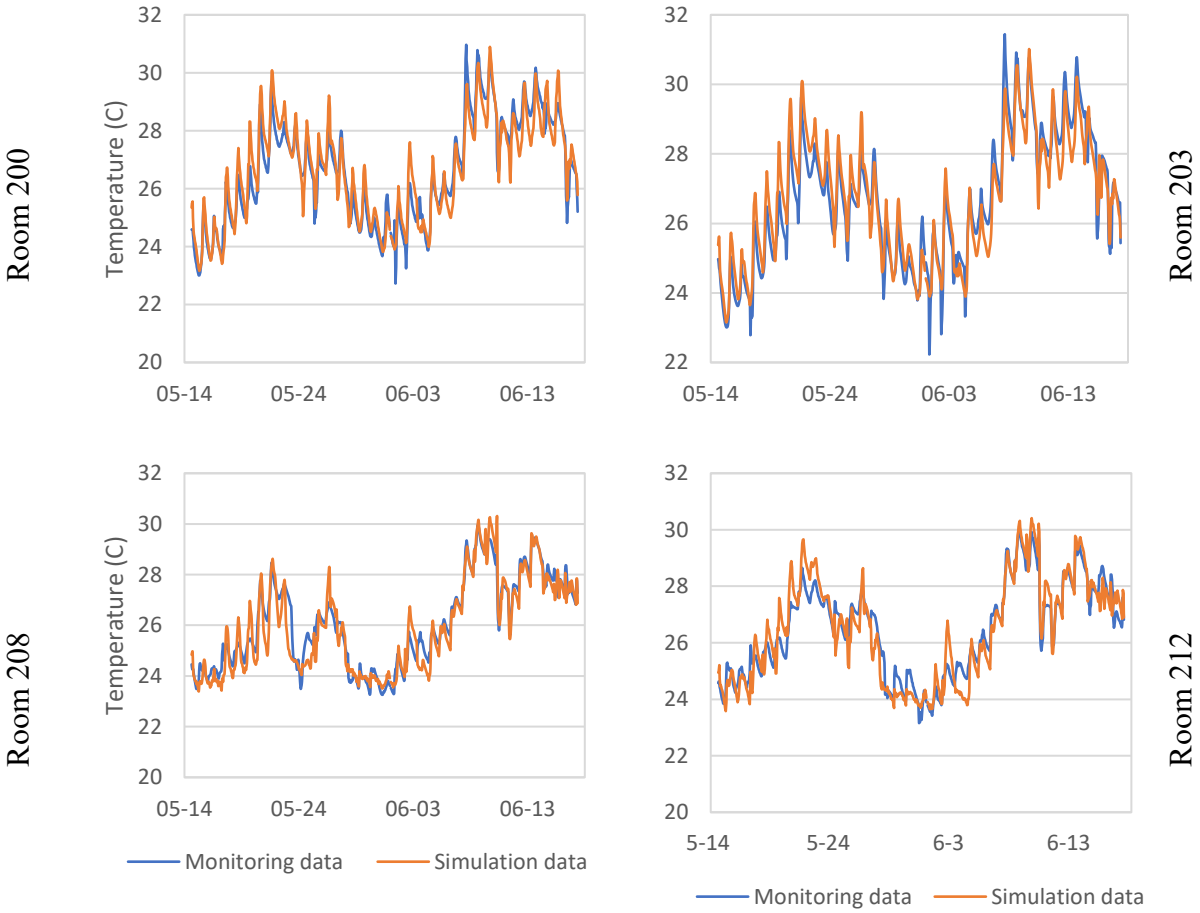

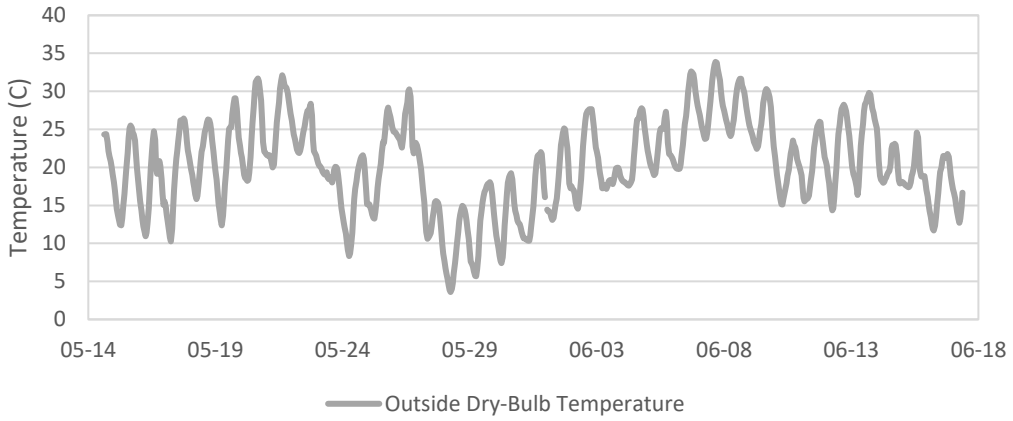

Figure 4-15. Comparison of indoor air temperature between measurements and simulation results from the calibrated model during the opened period for four rooms over the calibration and validation period in 2020 and 2021.

Table 4-4 Calibrated parameters and the achieved accuracy during calibration and validation period after the school is opened.

Parameters	R 200	R 203	R 208	R 212
Max NV amount (ACH)	9	9	10	10
NV setpoint (ºC)	24	23	21	21
Maximum lighting load (W/m^2)	10	10	12	12
Shading solar reflectance	0.8	0.9	0.5	0.6

Accuracy achieved

Evaluation criteria	Calibration				Validation (2020)				Validation (2021)			
	R 200	R 203	R 208	R 212	R 200	R 203	R 208	R 212	R 200	R 203	R 208	R 212
RMSE (ºC)	0.5	0.5	0.5	0.5	0.5	0.5	0.5	0.3	0.5	0.6	0.5	0.6
NMBE (%)	0.2	0.4	0.2	0.2	-0.8	-0.5	-0.6	0.1	0.1	0.1	0.2	0.1
Max Diff. (ºC)	1.9	1.8	1.6	1.5	1.5	1.7	1.1	0.8	1.4	1.7	1.6	1.8
1 °C Percentage Error (%)	5	5	6	5	6	7	1	0	6	8	8	9
0.5 °C Percentage Error (%)	34	30	35	35	29	25	40	12	35	45	30	35

The overheating risk that is calculated based on the measured and simulated indoor temperature, respectively, according to ASHRAE 55 80% acceptable limit over the calibration period May 23rd – Oct. 15th is shown in Table 4-5. The absolute difference between the overheating hours based on the measured and simulated indoor temperature is about 1% for all rooms, which confirms the efficacy and robustness of this methodology.

Table 4-5 Overheating hours based on simulated and measured indoor air temperature.

	Measurement (hr)	**Simulation (hr)**	**Abs. Diff. (hr)**	**Abs. Diff. (%)**
R200	1371	1383	17	1%
R203	1305	1322	12	1%
R208	1262	1244	18	1%
R212	1227	1212	15	1%

Similar results have been obtained for both school building 2 and the multi-unit residential building.

4.2.1.2 School Building 2

4.2.1.2.1 Calibration and validation results during the closed period

Data from Jun. 30th to Jul. 28th is used for calibration of the four classrooms simultaneously. Data from Jul. 29th to Aug. 25th is used for validation of the calibrated model. Table 4-6 shows the calibrated value of each parameter obtained from the optimal solution from two ranges of Block1, and the range of Block2. The values of parameters from the two ranges are almost the same except for the wall and infiltration parameters, as shown in Table 4-6. The calibrated parameters from the first range give more accurate results than the second range based on Maximum Difference, RMSE and NMBE criteria, as shown in Table 4-7. Therefore, the calibrated model based on the first range is selected. Figure 4-16 shows the comparison of indoor temperature between measurements and simulations over the period from June 30th to Aug. 25th for all classrooms and gym.

Tables 4-7 and 4-8 show the accuracy of the calibrated model during the validation period for classrooms in block 1 and block 2 respectively. High accuracy of the calibration is achieved for all classrooms and the gym in block1 and block 2. The calibrated model can predict the indoor air temperature for the four classrooms in blocks 1 and 2 in the range of 0.5 °C of RMSE, 0.1-1.2% of NMBE, 1.2-1.7 °C of Maximum Difference, 1-10% of 1 °C Percentage Error criteria, and 14-

45% of 0.5 °C Percentage Error criteria. The error between measured and simulation temperature in the gym is a little bit higher than in classrooms, where the RMSE is in the range of 0.7-0.8 °C, -0.8-0.1% of NMBE, 1.9-2.2°C of Maximum Difference, 6-10% of 1 °C Percentage Error criteria, and 42-46% of 0.5 °C Percentage Error criteria.

Table 4-6. Calibrated model parameters from the optimal solution before school opening for rooms in Block 1 and Block2

Parameters		**Block 1**		**Block 2**
		Values from the First range	**Values from the Second range**	
Infiltration rate (ACH50)		6.0	3.0	2.8
Shading solar	Room 109	0.6	0.6	-
	Room 114	0.7	0.7	-
	Gym	0.8	0.6	-
	Room 167			0.6
	Room 173			0.7
Wall U-value (W/m^2.K)		0.4	0.30	0.30
Roof U-value (W/m^2.K)		0.27	0.23	0.20

Table 4-7. Model calibration results for first (FR) second (SR) range, and validation result for the first range for classrooms and gym in Block 1

Measurement criteria	**Calibration**						**Validation**		
	R. 109		**R. 114**		**Gym**		**R. 200**	**R. 203**	**R. 208**
	FR	SR	FR	SR	FR	SR			
RMSE (ºC)	0.5	0.6	0.5	0.7	0.8	1.0	0.5	0.5	0.7
NMBE (%)	0.1	0.1	0.5	0.7	-0.1	-0.1	-0.1	0.5	-0.8
Max Diff (ºC)	1.4	1.7	1.4	1.6	2.2	2.6	1.2	1.3	1.9

1 °C Percent. Error (%)	1	12	3	17	10	12	4	3	6
0.5 °C Percent. Error (%)	37	42	36	47	46	66	27	35	42

Table 4-8. Model calibration results for classrooms in Block 2

Measurement criteria	**Calibration**		**Validation**	
	R. 167	**R. 173**	**R. 167**	**R. 173**
RMSE (ºC)	0.4	0.5	0.4	0.5
NMBE (%)	0.2	-1.2	0.1	-0.1
Max Diff (ºC)	1.7	1.5	1.4	1.5
1 °C Percent. Error (%)	1	6	2	10
0.5 °C Percent. Error (%)	14	45	17	40

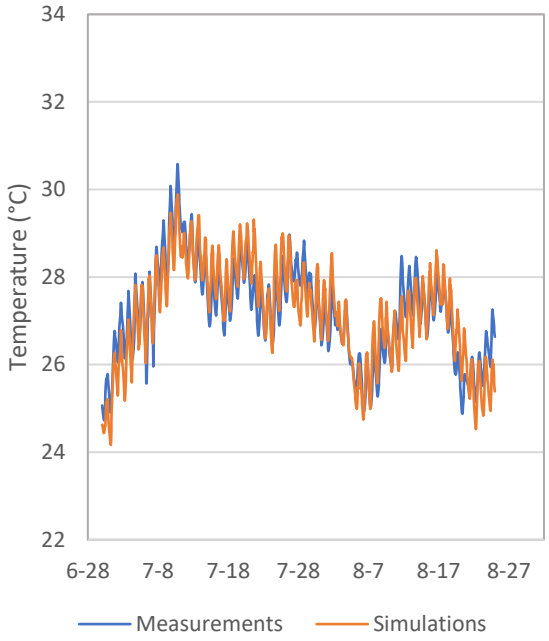

a) Classroom 109

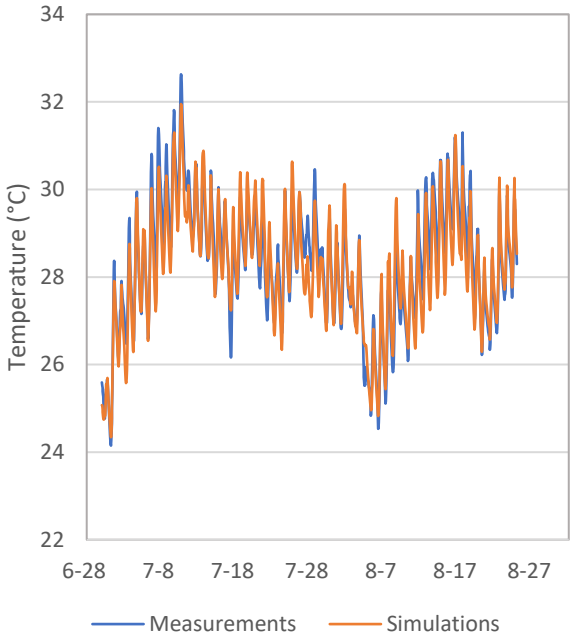

b) Classroom 114

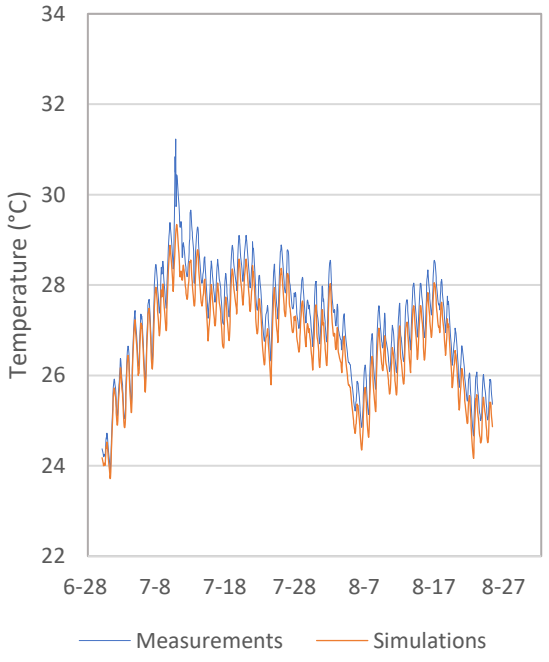

c) Gym

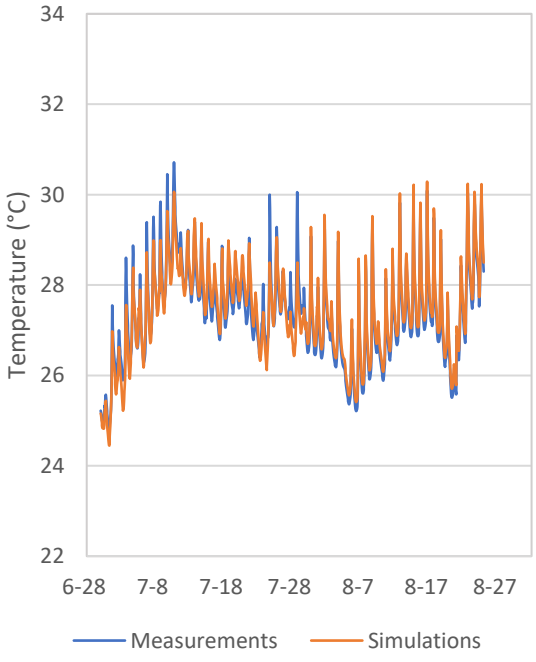

d) Classroom 167

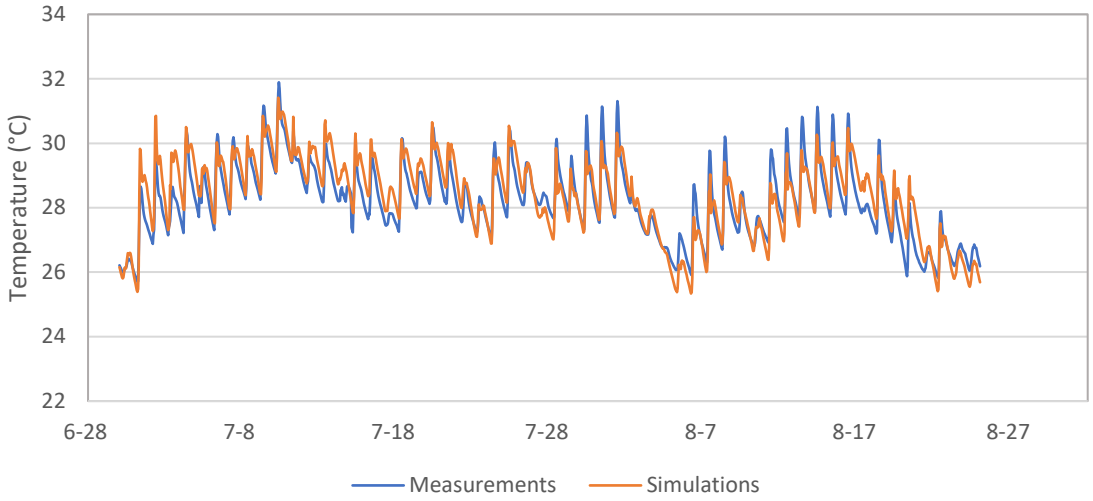

e) Classroom 172

Figure 4-16. Comparison between measurement and simulation results from the calibrated model

4.2.1.2.2 Calibration and validation results during the opened period

The calibrated parameter values are listed in Table 4-9. The lighting load is controlled by the daylight amount to achieve 400 lux. However, there are some hours when a sudden change occurs due to human behaviour, such as forgetting to close a window before leaving. Therefore, the evaluation criteria achieved are less accurate than the calibration model without occupants. Table 4-10 shows the evaluation results that have been achieved from the calibration process after school beginning during the calibration period (Sep. 1st to October. 1st) and validation period (October. 2nd to October. 12th). The calibrated model in calibration and validation periods has a discrepancy range from 0.5 °C of RMSE, 0% of NMBE, 1.4-1.9 °C of Maximum Difference, 5-7% of 1 °C Percentage Error criteria, and 30-35% of 0.5 °C Percentage Error criteria., as shown in Table A-5.

Table 4-9. Calibrated model parameters from the optimal solution after school opening

Parameters	Room 109	Room 114	Room 167	Room 173	Gym
Lighting load	8	11	9	8	13
Equipment load	2	4	3	2.5	2.5
Maximum air change rate from NV	8	6	9	7	8
NV Setpoint	22	23	22	23	22
Interior shading opening ratio	0.5	0.8	0.8	0.7	0.7

Table 4-10. Model calibration results re-opened

	Calibration period					Validation period				
Measurement criteria	**R. 109**	**R. 114**	**R. 167**	**R. 173**	**Gym**	**R. 109**	**R. 114**	**R. 167**	**R. 173**	**Gym**
RMSE (ºC)	0.5	0.5	0.5	0.6	0.7	0.4	0.5	0.5	0.6	0.7
NMBE (%)	-0.2	-0.3	0.4	-0.4	1.0	0.3	-0.4	0.3	-0.4	1.2
Max Diff (ºC)	1.6	1.5	1.8	1.6	2.2	1.7	1.4	1.7	1.6	2.1
1 °C Percent. Error (%)	8	5	5	11	15	8	5	8	7	13
0.5 °C Percent. Error (%)	26	35	34	35	49	39	30	37	45	50

4.2.1.3 Multi-unit residential building

Data from Sep. 16th to Oct. 1st is used for calibration of the three bedrooms simultaneously. Data from Oct. 2nd to Oct. 15th is used for validation of the calibrated model. Table 4-11 shows the value of each building envelope and operation parameter that has achieved the optimal solution, which will be used in the calibrated model. The values of parameters from the two ranges are completely different, as shown in Table 4-12. The calibrated parameters from the first range give lower accurate results than the second range based on Maximum Difference, RMSE and NMBE criteria. Therefore, the calibrated model based on the second range is selected.

Table 4-12 shows the accuracy of the calibrated model during the calibration and validation period. High accuracy of the calibration is achieved during both periods. The calibrated model is able to predict the indoor air temperature for the two classrooms in the range of 0.5-0.6 °C of RMSE, 0.1-0.5% of NMBE, 1.5-1.8 °C of Maximum Difference, 3-9% of 1 °C Percentage Error criteria, and 31-50% of 0.5 °C Percentage Error criteria. Figure 4-17 shows the comparison of indoor temperature between measurements and simulations over the period.

Table 4-11. Calibrated model operation parameters from the optimal solution

Parameters		**Bed 1**	**Bed 2**	**Bed 3**
Infiltration rate (ACH50)	**Values from the First range**		0.3	
	Values from the Second range		1.5-2.5	
Wall U-value ($W/m^2.K$)	**Values from the First range**		0.4	
	Values from the Second range		0.25-0.3	
Roof U-value ($W/m^2.K$)	**Values from the First range**		0.25	
	Values from the Second range		0.20	
Shading solar		0.4	0.4	0.4
Lighting load		8-10	5-8	5-8
Equipment load		8-10	6-8	6-8
Maximum air change rate from NV		0.5	1	1
NV Setpoint		26	26	26

Table 4-12. Model calibration results for first (FR) second (SR) range, and validation result

Measurement criteria	Calibration						Validation		
	Bed 1		Bed 2		Bed 3		Bed 1	Bed 2	Bed 3
	FR	SR	FR	SR	FR	SR			
RMSE (ºC)	1.1	0.5	0.9	0.6	0.8	0.5	0.5	0.6	0.6
NMBE (%)	3	0.4	1	0.2	2	0.2	0.6	0.1	0.5
Max Diff (ºC)	3.4	1.3	2.5	1.8	2.3	1.4	1.7	1.8	1.7
1 °C Percent. Error (%)	40	3	35	6	28	5	5	9	9
0.5 °C Percent. Error (%)	80	31	75	41	65	37	35	50	47

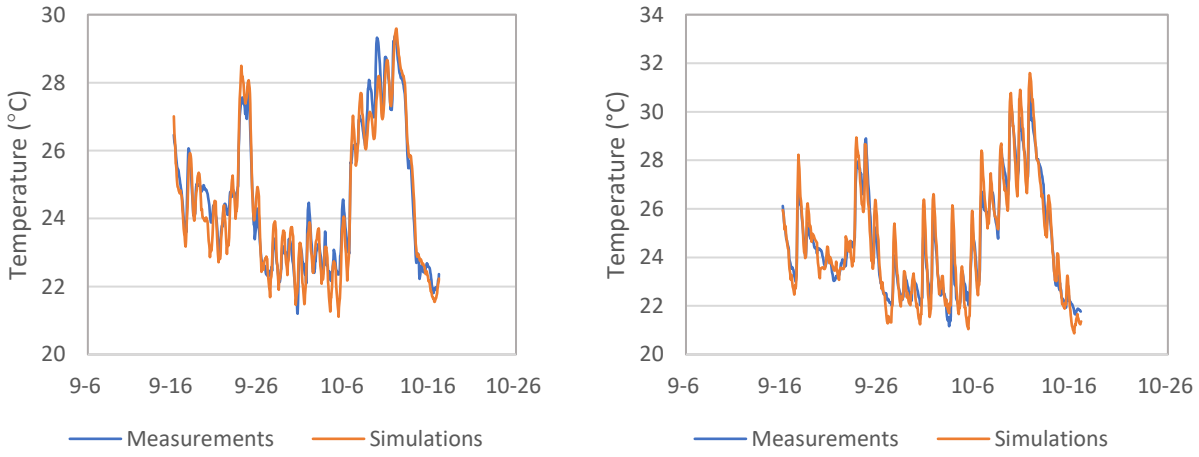

a) Bedroom 1 b) Bedroom 3

Figure 4-17. Comparison between measurement and simulation results from the calibrated model

4.2.2 Overheating assessment

4.2.2.1 Overheating hours under the historical RSWY year

The EN 15251-Category II limit is used first to find the duration of overheating in each classroom in the school during the summer period from May 1 to September 30, 2020 (observational data), Monday to Friday and 09 to 16 h using simulated indoor operative temperature. The results listed in Table 4-13 show that with the current operational situation (original case), represented by natural ventilation by opening 25% of the external window area and by using interior shading with high solar reflectance, the number of overheating hours can maintain to less than 40 hrs that meets the requirement of BB101-Criterion 1 in all classrooms. The classrooms on the second floor have up to four times overheating hours compared to the first floor due to heat transfer from the roof. In addition, the rooms on the southeast side on the second floor have around 2.5 times more overheating hours than those in the northwest rooms due to the direct solar gain. Classroom 200, located in the southeast corner of the building on the second floor (as shown in Figure 3-10), recorded the highest temperature and had 38 overheating hours during the summer. To find the CORDEX weather data accuracy, the overheating hours in classrooms are calculated under 2020 (CORDEX data adjusted for bias) and compared with those calculated under 2020 (observation data). The results showed that the overheating hours are slightly higher in 2020 (observation data) than those in 2020 (CORDEX data adjusted for bias) 2-20 hours depending on the location of the room. Therefore, the 2020 monitoring data is used to assess and mitigate the overheating risk, as shown in Table 4-13.

However, applying EN 15251-Category I the overheating hours increased significantly by up to 72 hrs, which made the indoor thermal conditions in all classrooms on the second floor unacceptable, as shown in Table 4-13. These results emphasize the importance of selecting the correct category to be used in evaluating the thermal performance of the building. The average overheating hours of all classrooms are 104 hrs on the southeast side and 44 hours on the northwest side. Classroom 200 also had the highest overheating hours of 110 hours. Therefore, room 200 is selected for further analysis on the impact of climate change on indoor thermal conditions and mitigation measures.

Table 4-13. Overheating hours in all classrooms based on the first BB101 Criterion using Cat. I and II threshold under recent and future RSWY (green means passed BB101 requirement and red failed)

			2020 (Obs.)		2020 (CORDEX)	2042	2044	2059	2090
		Room	Cat II	Cat I	Cat. I	Cat I	Cat I	Cat I	Cat I
			(hr)	(hr)	(hr)	(hr)	(hr)	(hr)	(hr)
First floor	Northwest	Room3	2	20	18	80	105	70	152
		Room4	1	21	18	86	115	73	162
	Southeast	Room7	2	30	20	115	135	108	222
		Room8	6	32	22	120	140	111	222
		Room9	5	28	25	112	132	105	218
		Room10	1	28	24	110	130	100	213
Second floor	Northwest	Room212	8	42	30	185	185	121	265
		Room211	11	45	33	183	186	125	266
		Room210	11	45	34	181	182	124	265
		Room209	10	44	34	187	188	120	270
		Room208	11	44	33	185	186	117	268
		Room207	8	41	33	181	184	119	264
		Room206	11	44	33	185	186	121	272
	Southeast	Room205	35	102	92	290	303	217	412
		Room204	36	104	93	300	309	219	416
		Room203	35	102	92	290	306	217	412
		Room202	35	104	93	280	290	212	412
		Room201	35	102	92	290	312	218	416
		Room200	38	110	98	310	333	252	436

Figure 4-18a shows the correlation between the indoor hourly operative temperature in room 200 and the running mean of daily mean outdoor temperatures (5 days) and BB101 criteria 1 and 3 limits. The result shows that the overheating risk increases significantly when the running mean outdoor temperature of 5 days is higher than 23 °C. The indoor operative temperature in this room has not exceeded (passed) BB101-criterion 3 (Upper Limit Temperature-intensity of overheating) at any hour. Figure 4-18b shows the severity (daily weighted temperature) of temperature in room 200. The results show the Daily Weighted Exceedance (We) in room 200, which was calculated based on Cat. II, has not exceeded the acceptance limit, while We calculated based on Cat. I has

exceeded the acceptance limit by three times, on May 27th, June 20th, and the highest one on July 9th and 10th with 6.2, 6.7 and 8 and 12 °C/day.

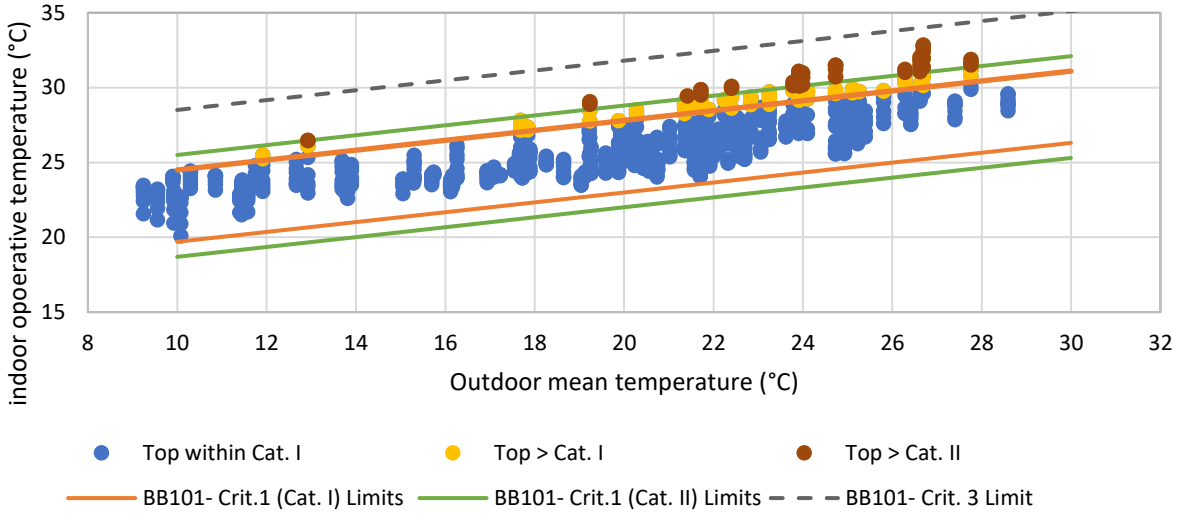

a)

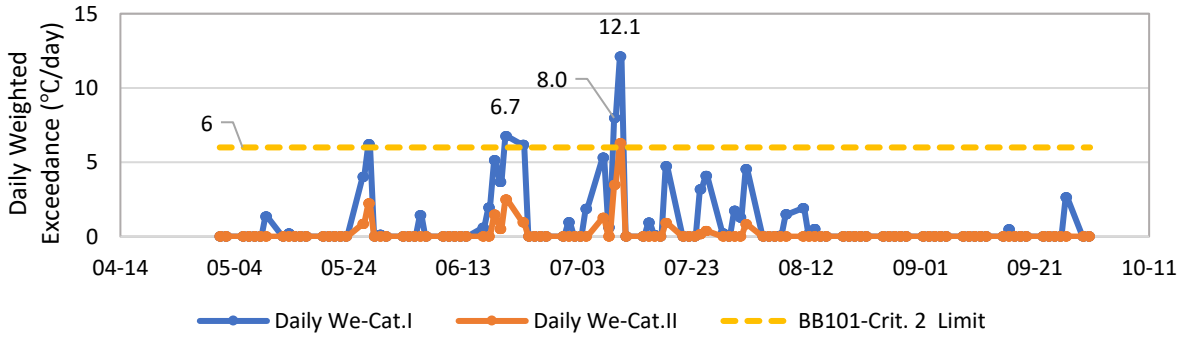

b)

Figure 4-18. Thermal condition of room 200 under 2020 based on; a) BB101 criteria 1&3 limits b) BB101 criterion 2 limit

4.2.2.2 Overheating hours under future RSWY years

The overheating hours of all classrooms under 2042, 2044 and 2059 for mid-term future climate, and 2090 for long-term future climate are also calculated based on Cat. I, as shown in Table 4-13. The results showed that the 2044 year, which has the longest heatwave event, has the highest effect on the indoor thermal conditions compared to years that have the most intense and longest heatwaves. Under 2044, the overheating hours in the hottest and coldest northwest classrooms are 188 and 182 hrs respectively, confirming that there was no significant difference between the indoor thermal condition of northwest classrooms on the second floor. While in the southeast

classroom, the difference between the overheating hours in the hottest and coldest room can be around 40 hours with 333 and 290 hours, respectively. Therefore, the average overheating hours, which are calculated based on categories I and II, in all the southeast and northwestern rooms, and in the hottest classroom (room 200), and the increase in overheating hours in the hottest room compared to the results for 2020 are presented in Figure 4-19. All rooms will not have acceptable conditions in future extreme years except the northwest rooms (206-212) under 2059 using Cat. II criteria. Due to climate change, the overheating risk in the hottest room will increase by 165 and 223 hrs under 2044 using Cat. II and I, respectively. The risk of overheating risk will increase up to 327 hr in 2090 compared to overheating risk in 2020.

The southeast rooms (200-205) will suffer much more overheating than the northwest rooms. The average overheating hours in the southeast rooms (without the hottest room- room 200) are 121, 140, 185, and 290 hours, while in the northwest rooms are 35, 57, 67, and 134 hours in 2059, 2042, 2044 and 2090 years, respectively.

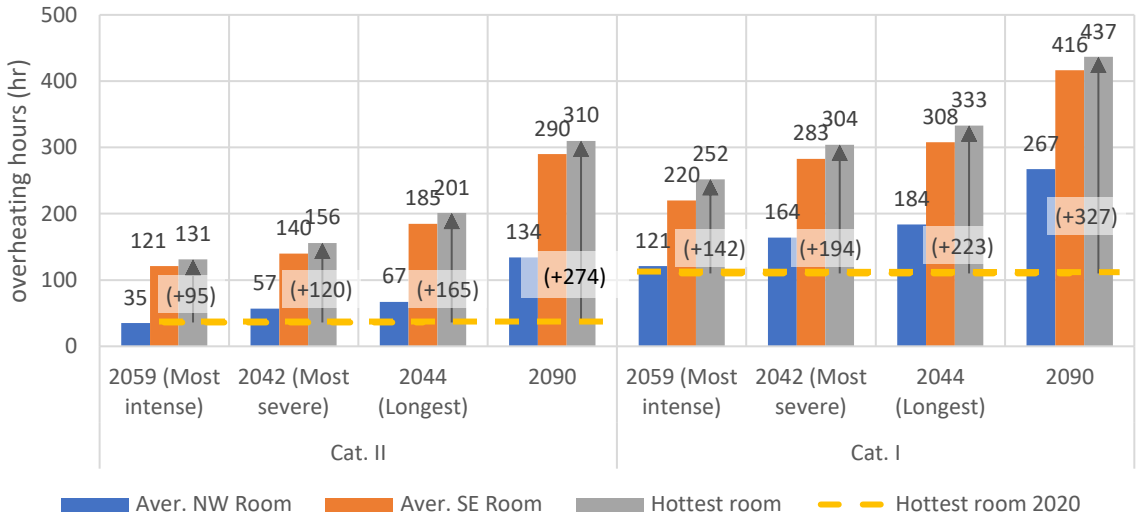

Figure 4-19. Overheating hours based on BB101 Criterion 1(Cat. I & II threshold) under future RSWY compared to overheating hours in hottest room under recent RSWY

4.2.3 Mitigation measures

Mitigation measures are evaluated for the classrooms under current and future RWSY during the summer period from May 1st to Sept. 20th and during heatwave periods using the parametric analysis method.

4.2.3.1 Current observational and future RWSY climate

Under 2020 (Figure 4-20), the addition of the green roof to the original case reduces the overheating hours by 4% in the hottest classroom and a similar reduction in all other rooms. Adding the cool roof to the original case reduces overheating hours, especially for the northwest rooms where the main source of solar heat gain for these rooms is reduced. With the cool roof, the overheating hours in northwest rooms (206-212) are reduced to about 20 hrs, while to 144 hrs (-28%) in the hottest room. The night cooling, overhang shading, and reducing SHGC reduced the overheating hour significantly to 68, 60 and 56 hr, respectively, in the hottest room. The use of overhang shading or low SHGC measures can be sufficient to meet the BB101 requirement for all rooms except the hottest room (room 200). The use of exterior screen shading (blind roll) can be the best solution to mitigate overheating, where it reduces the overheating hours to 16 hr in the hottest room and almost 0 hr in the north rooms. The effect of a combination between night cooling (NC) and cool roof (CR), overhanging shading (OH) or lower SHGC on the indoor thermal condition has also been studied. The results show that the overheating hours were reduced to 39 hr by using night cooling and cool roof, 25 hr by using night cooling and overhang shading, and 18 hr by using night cooling and lower SHGC in the hottest classroom.

Figure 4-21a shows the correlation between the indoor hourly operative temperature in classroom 200 with various mitigation measures and the outdoor running mean temperature under 2020, 2044 and 2090. The purple and yellow dots in Figure 4-21a represents the hours for which indoor operative temperature exceeded the acceptable limit after adding the night cooling and cool roof (35 hrs) and exterior blind roll (16 hrs), respectively. These mitigation measures can achieve BB101 criteria 2 (daily weighted exceedance), as shown in Figure 4-21b.

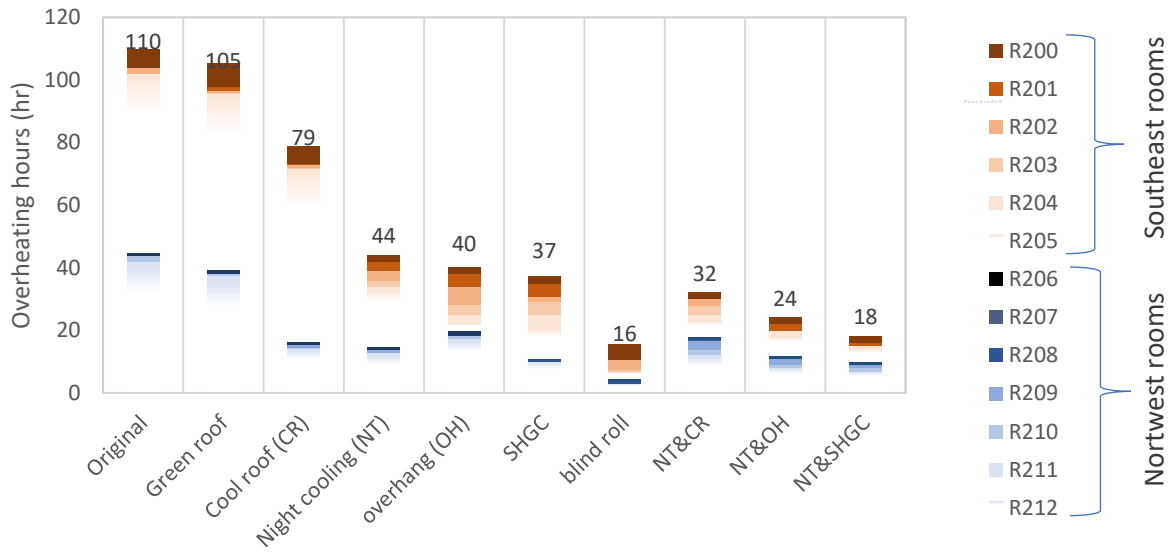

Figure 4-20. Overheating hours (Cat. I) in all classrooms on the second floor with different mitigation measures under summer 2020.

Under 2044, blind shading will be able to reduce the overheating hours from 330 hours (orange dots in Figure 4-21c) to 100 (yellow dots in Figure 4-21), but still above the requirements of BB101. Therefore, the addition of night cooling to blind shading can reduce the overheating hours to 15 hrs (green dots in Figure 4-21c) in the hottest room based on Cat. I and can achieve BB101 criteria 2 (daily weighted exceedance).

Under 2090, the combination of blind roll and night cooling will reduce the overheating hours to 84 hrs based on Cat. I, as shown in Figure 4-21d. Therefore, cool roof measures are applied with blind roll and night cooling. This combination will be able to reduce the overheating hours based on Cat. I to 39 hrs in the hottest room and can achieve BB101 criteria 2.

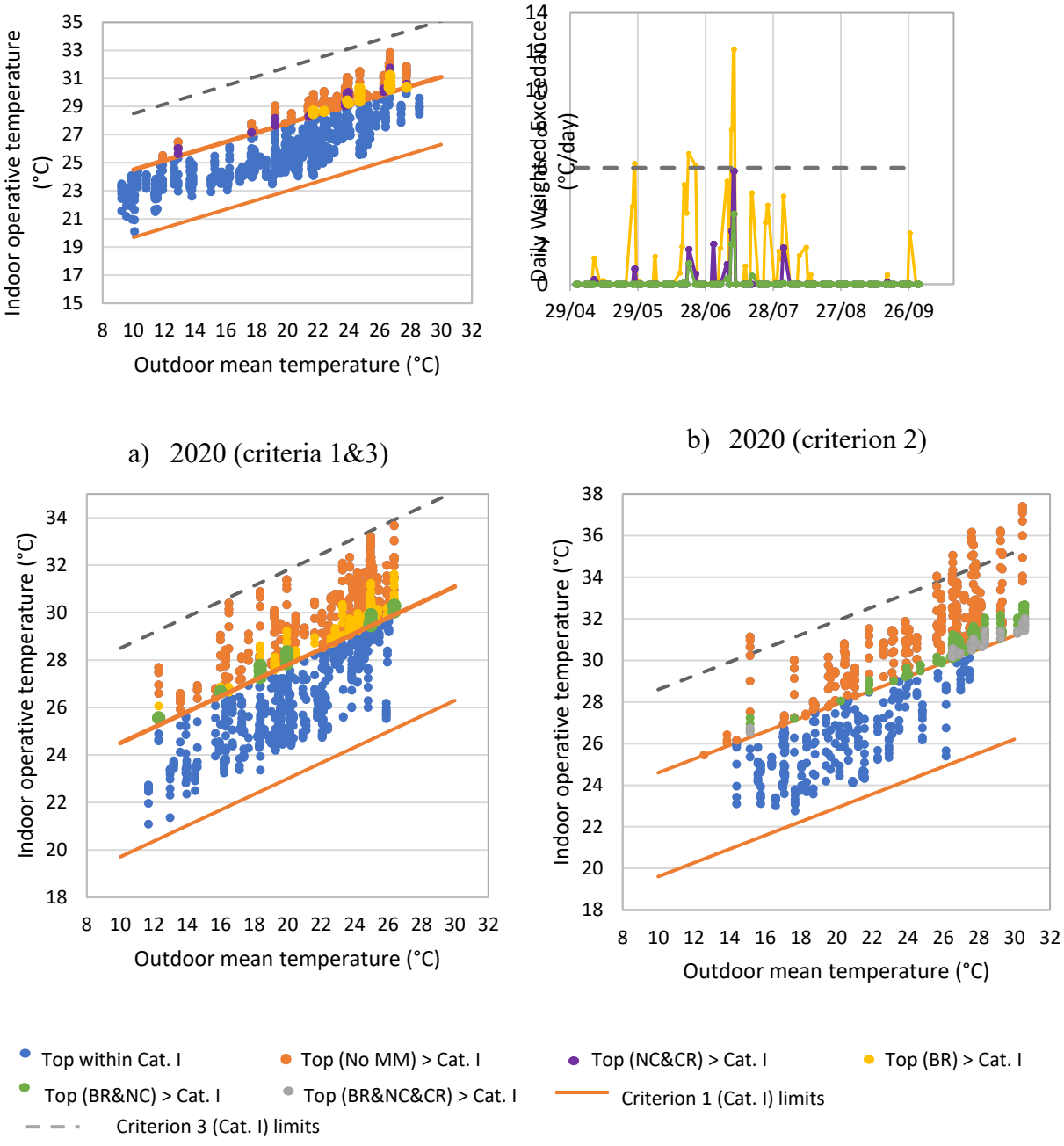

a) 2020 (criteria 1&3)

b) 2020 (criterion 2)

c) 2044 (criteria 1&3)

d) 2090 (criteria 1&3)

Figure 4-21. Indoor operative temperature with various mitigation measures at room 200 under summer 2020, 2044 and 2090

4.2.3.2 Current and future extreme heatwave events

Figure 4-22 shows the boxplot for indoor operative temperature and overheating hours (represented by dots in the Figure) in the original case and with various mitigation measures during the heatwaves in 2020, 2044 and 2090 in classroom 200.

During this 6 days heatwave from June 17th to June 23rd in 2020, the indoor temperature in room 200 under the current operation (original case) reached 32 °C and the temperature was lower than 30 °C in 75% of the time causing overheating in 23 hrs out of 40 occupied hours, which are represented by green dot points in Figure 4-22a. While the outdoor temperature reached 32 °C and the temperature was lower than 28 °C in 75% of the time. The use of exterior blind roll remains the effective measure even during the heatwave, where the maximum temperature drops to 30.5 °C and overheating hours to 4 hrs and 75% of the period is less than 28.5 °C.

During the heatwave from July 10th to 24th in 2044 (Figure 4-22b), the outdoor temperature reached 34.1 °C and the temperature was lower than 30 °C in 75%. Using the exterior blind roll and night cooling reduces the maximum temperature to 30.3 °C and overheating hours to 7 hours.

During the heatwave from July 7th to Aug. 11th in 2090 (Figure 4-22c), the outdoor temperature reached 38.6 °C and the temperature was lower than 33 °C within 75% of the time. Using exterior blind roll, night cooling and cool roof reduces the maximum temperature to 32.0 °C and overheating hours to 30 hours. Figure 4-22d shows the outdoor temperature distribution during the three heatwave events.

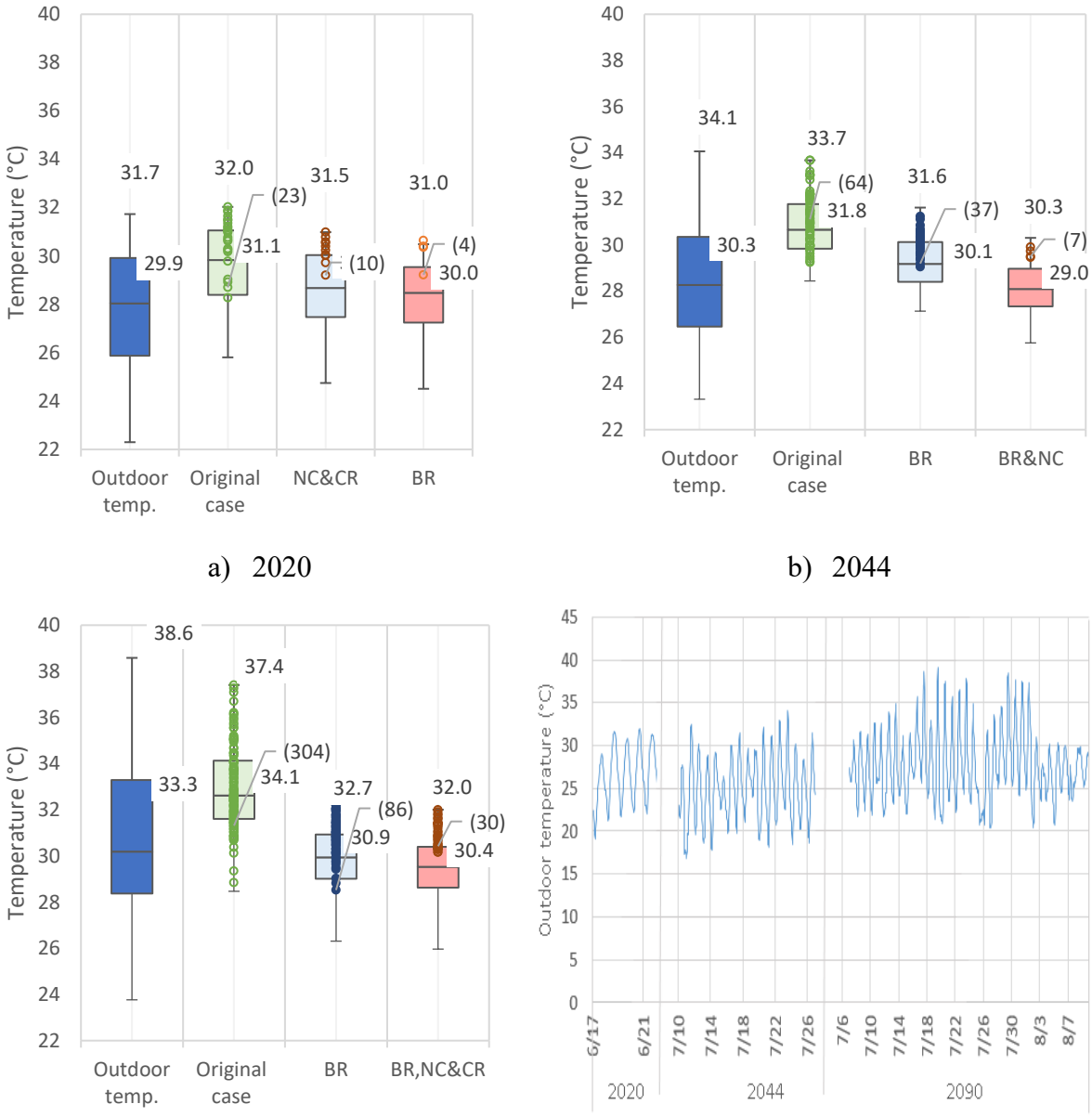

Figure 4-22. Boxplot for outdoor air temperature and indoor operative temperature in room 200 with the number of overheating hours in the brackets during the heatwave in: a) 2020; b) 2044; c) 2090; d) the outdoor temperature distribution during heatwave periods.

4.2.4 Optimization of building design

4.2.4.1 Best building design to achieve each objective separately

The optimal design must not only exceed the minimum requirement of heating demand, overheating hours and lighting load, but also be close to the lowest achievable values for each objective (lowest heating demand, overheating hours, and lighting load). Therefore, the best design that achieves the best achievable values for each objective while not necessarily achieving the minimum requirements for the other two objectives is determined.

Table 4-13 shows the results of the current building design and the best building design that can achieve the lowest annual heating demand, overheating hours or lighting load. The current building has an annual heating energy demand of 91 kW/m^2, 110 overheating hours in the summer and a 6.0 kW/m^2 lighting load. To achieve the lowest heating demand, the building needs to have the lowest thermal transmittance of walls and roof (0.1 and 0.08 W/m^2.K respectively), highest energy-efficient windows (0.78 W/m^2.K and 0.3 SHGC), airtight building envelope (0.6 ACH50), and with small WWR (25%) and with low solar reflectivity exterior roofs (0.2). In addition, the interior shading should have high solar transmittance and low solar reflectance characteristics (0.7 and 0.2 respectively) and no exterior shading devices are required. The Window Opening Ratio and night cooling do not affect the heating energy demand. This design can achieve 6.3 kWh/m^2.yr of heating demand (this value includes the heating load from the baseboard and mechanical ventilation). However, the overheating in this building is 70 hr and 8.0 kWh/m^2 for the annual lighting load. This design achieved a 93% improvement in annual heating demand compared to the existing building.

To achieve the lowest overheating hours, the building should be designed with low thermal transmittance of walls and roof (0.15 and 0.08 W/m^2.K respectively) with high solar reflective roofs (0.8), high energy-efficient windows (0.78 W/m^2.K, 0.3 SHGC), airtight building envelope (0.6 ACH50), and with small WWR (25%) with 50% of WOR, and 5 ACH natural ventilation during the night. In addition, the interior shading should have low solar transmittance and high solar reflectance characteristics (0.2 and 0.7 respectively) and screen exterior shading devices are required. This design can reduce the overheating hours to 8 hr. However, the annual heating demand in this building design is 8.6 kWh/m^2.yr and 7.4 kWh/m^2 for the annual lighting load. This

design achieved a 93% improvement in summer overheating hours compared to the existing building

To achieve the lowest lighting load, the building should be designed with high WWR (80%) and windows with 0.62 visible transmittances. In addition, the interior shading should have high visible transmittance (0.7) and no exterior shading devices are required. The other parameters do not significantly affect the lighting load. This design can reduce the lighting load to 4.2 kWh/m^2. However, the annual heating demand in this building design is 18 kWh/m^2.yr and 300 hr of overheating hours. This design achieved a 31% improvement in annual lighting load compared to the existing building

Table 4-14. Building design parameters to achieve the lowest annual heating demand, overheating hours, or lighting load.

Design / Variables	Existing design	Lowest heating demand	Lowest overheating hours	Lowest lighting load
Roof U-value ($W/m^2.K$)	0.23	0.08	0.08	0.08
Wall U-value (W/m2.K)	0.4	0.1	0.15	0.15
Window type	LEEB	PH	PH	NECB
Infiltration (ACH50)	3.8	0.6	0.6	0.6
WWR (%)	60	25	25	80
Interior shading	High SR	Low SR	High SR	Low SR
Exterior shading	No shading	No shading	Screen shading	No shading
WOR (%)	25	50	50	50
Night Cooling (ACH)	0	0	5	0
Solar reflectance	0.2	0.2	0.8	0.8
Heating demand (kWh/m^2)	91	6.3	8.6	18
Overheating hours (hr)	110	70	8	300
Lighting load (kWh/m^2)	6.0	8.0	7.4	4.2
Best design compared to existing design		-93%	-96%	-31%

4.2.4.2 Optimal designs under observational 2020

The results (Figure 4-23) show that four designs can achieve the three objectives. Each design relies on a certain WWR. The four designs all require the lowest roof and wall thermal transmittance and lowest air infiltration.

- **Optimal design 1:** it has 40% of WWR. This small window area compared to the next optimal design helps reduce overheating hours and heating demand, but increases the lighting load. To reduce the lighting load, the results show that a NECB+ window that has

at least a 0.5 visible transmittance factor should be selected to increase the daylight. However, this type of window increases the overheating risk and the heating demand compared to the PH window type. To reduce the overheating risk in this optimal design, there are two options:

1. Option 1 relies on not using night cooling (in case the windows cannot be opened during the night), so a 0.5 m overhang and cool roof (0.8 SR) should be added with opening the windows to at least 50% of the window area during the day to reduce the overheating risk. These mitigation measures will increase the heating demand. Therefore, the interior shading must be changed from high solar reflectance to high solar transmittance. This optimal design still has the highest annual heating demand and lighting load compared to the other four optimal designs with 9.4 kWh/m^2.yr and 5.7 kWh/m^2, respectively, and 28 hr of overheating in the hottest room (Room 200). This design achieved a 90%, 75% and 5% improvement in heating demand, overheating hours and lighting load compared to the existing building. However, the achievements of this optimal design are 3.1 kWh/m^2, 20 hr and 1.5 kWh/m^2 of heating demand, overheating hours and lighting load higher than the lowest values achieved for the three objectives as shown in Table 4-14.
2. Option 2 relies on using night cooling (at least 2.5 ACH) by opening the windows at least 50% of the window area during the day, therefore, no overhang or cool roof is required. The interior shading should have a high solar transmittance (0.7). This optimal design can achieve 8.0 kWh/m^2.yr of annual heating demand, 22 overheating hours in the hottest room and 5.5 kWh/m^2 of the lighting load. This design achieved a 92%, 80% and 9% improvement in heating demand, overheating hours and lighting load compared to the existing building. However, the achievements of this optimal design are 1.7 kWh/m^2, 14 hr and 1.3 kWh/m^2 of heating demand, overheating hours and lighting load higher than the lowest values achieved for the three objectives as shown in Table 4-14.

- **Optimal design 2:** it has 50% of WWR. This optimal design has the same building parameters as the first optimal design with night cooling. However, this design requires at least 40% of WOR during the day. This optimal design can achieve 8.8 kWh/m^2 of annual heating demand, 25 hr of overheating in the hottest room and 5.2 kWh/m^2 of the lighting

load. The heating demand and overheating hours in this design are higher than in the first optimal design because the WWR is higher. This design achieved a 91%, 77% and 14% improvement in heating demand, overheating hours and lighting load compared to the existing building. However, the achievements of this optimal design are 2.5 kWh/m^2, 17 hr and 1.0 kWh/m^2 of heating demand, overheating hours and lighting load higher than the lowest values achieved for the three objectives as shown in Table 4-14.

- **Optimal design 3:** it has 60% of WWR. This window area increases heating demand, overheating hours and reduces light load, thus the fourth type of window that has 0.78 W/m^2.K, 0.3 SHGC and 0.4 Vt can be selected. Also, interior shading with medium solar transmittance and reflectance is used. The minimum opening area of windows can be 30% and 2.5 ACH of natural ventilation during the night. This optimal design can achieve the lowest annual heating demand by 7.1 kWh/m^2.yr among optimal designs, 35 hr of overheating in the hottest room and 5.4 kWh/m^2 of the lighting load. This design achieved a 93%, 68% and 11% improvement in heating demand, overheating hours and lighting load compared to the existing building. However, the achievements of this optimal design are 0.8 kWh/m^2, 27 hr and 1.2 kWh/m^2 of heating demand, overheating hours and lighting load higher than the lowest values achieved for the three objectives as shown in Table 4-14.
- **Optimal design 4:** it has 80% of WWR. This optimal design has the same building parameters as the third optimal design. However, we must add a 0.5 m overhang to mitigate the overheating. This optimal design can achieve 8.4 kWh/m^2.yr of annual heating demand and 28 hr of overheating in the hottest room and the lowest lighting load by 5.0 kWh/m^2. This design achieved a 92%, 75% and 17% improvement in heating demand, overheating hours and lighting load compared to the existing building. However, this design achieved a 2.1 kWh/m^2, 20 hr and 0.8 kWh/m^2 in heating demand, overheating hours and lighting load higher than the best design.

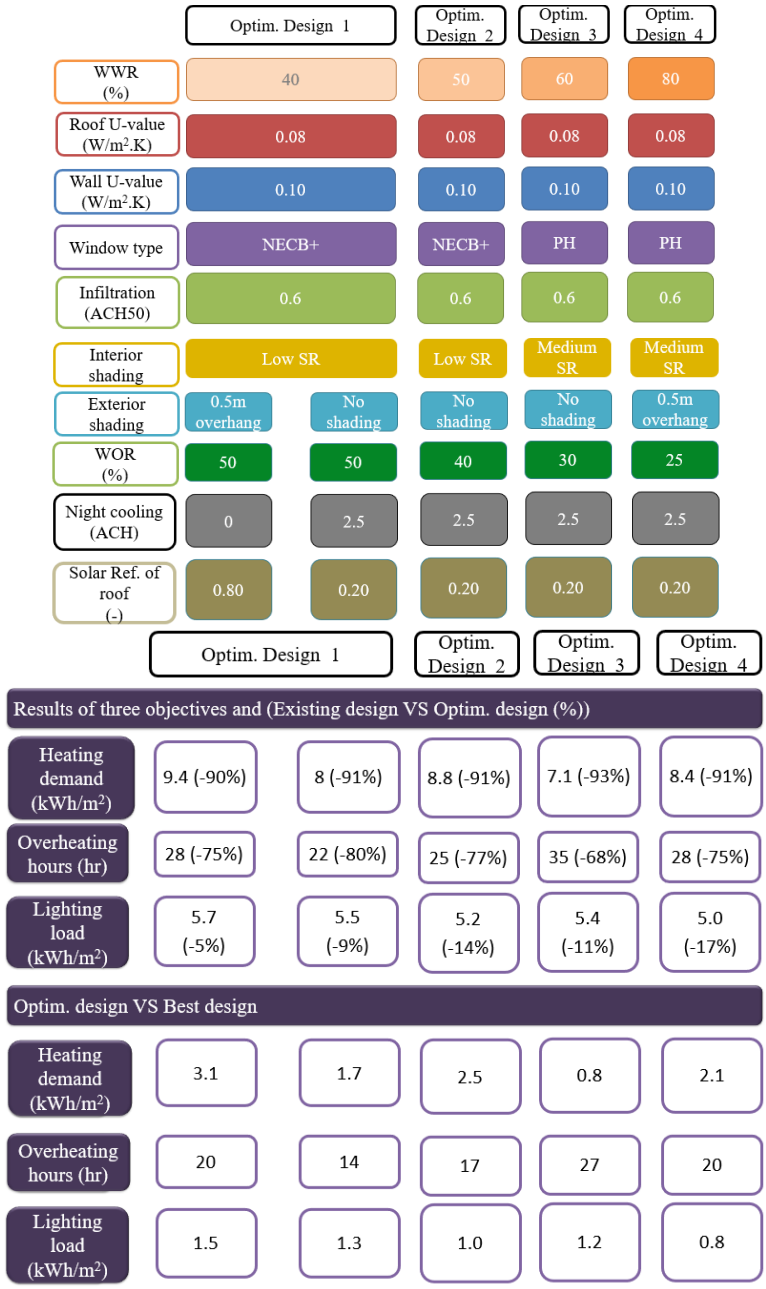

Figure 4-23. Optimal building design parameters under 2020

4.2.4.3 Optimal designs under extreme future years

Under 2044, the models, which achieved the lowest heating energy demand, overheating and lighting load in Section 4.2.4.1, have achieved higher values for three objectives by 6.7 kWh/m^2, 8 hr and 5.0 kWh/m^2, respectively. These results confirm that 2044 is more challenging than 2020 because there is a higher heating demand, overheating hours and a lighting load at the same time.

under 2090, the lowest heating energy demand, overheating and lighting load achieved from the same models in Section 4.2.4.1 is 5.1 kWh/m^2, 16 hr and 4.6 kWh/m^2, respectively

A similar approach is used to find the optimal designs in 2044 and 2090 for each WWR as in 2020, as shown in Table 4-15, are:

- **Optimal design 1:** under 2044, the overheating cannot be removed without including the night cooling. Therefore, the same building envelope design and interior shading can still be used as in 2020, but with adding the 0.5 m overhang, cool roof and increasing the night cooling to 5 ACH instead of 2.5 ACH. This optimal design can achieve 9.3 kWh/m^2 of annual heating demand and the lowest overheating by 32 hr in the hottest room and 6.0 kWh/m^2 of the lighting load. If movable overhang external shading is used, the heating demand will reduce to 8.7 kWh/m^2 and the lighting load to 5.6 kWh/m^2. This design achieved 2.5 kWh/m^2, 20 hr and 1.0 kWh/m^2 in heating demand, overheating hours and lighting load higher than the best design (lowest values).

  In 2090, the overhang (fixed option) should be increased to 1.5m to achieve 8.4 kWh/m^2 of annual heating demand, 31 overheating hours, and 6.7 kWh of the lighting load. This design achieved 3.3 kWh/m^2, 16 hr and 2.0 kWh/m^2 in heating demand, overheating hours and lighting load higher than the best design (lowest values).
- **Optimal design 2:** In 2044, we can keep the same building envelope design and interior shading as in 2020. However, we should add the 1.5 m overhang, cool roof and increase the daytime ventilation by increasing the WOR to 50% instead of 40%, and the night cooling to 5 ACH instead of 2.5 ACH. This optimal design can achieve 11.1 kWh/m^2.yr of annual heating demand and 27 hr of overheating in the hottest room and 6.3 kWh/m^2 of the lighting load. If we used movable overhang external shading, will reduce the heating demand to 10.4 kWh/m^2. This design achieved a 4.3 kWh/m^2, 15 hr and 1.2 kWh/m^2 in heating demand, overheating hours and lighting load higher than the best design (lowest values).
- In 2090, we should add the movable screen shading to the fixed overhang to achieve 9.4 kWh/m^2 of annual heating demand, 35 overheating hours, and 6.5 kWh/m^2 of the lighting load. This design achieved a 4.3 kWh/m^2, 20 hr and 1.9 kWh/m^2 in heating demand, overheating hours and lighting load higher than the best design (lowest values).

- **Optimal design 3:** In 2044, we can keep the same building envelope design and interior shading as in 2020. However, we should add the 1.5 m overhang, cool roof and increase the daytime ventilation by increasing the WOR to 40% instead of 30%, and the night cooling to 5 ACH instead of 2.5 ACH. This optimal design can achieve the lowest annual heating demand by 8.2 kWh/m^2.yr and 36 hr of overheating in the hottest room and 7.0 kWh/m^2 of the lighting load. If we used movable overhang external overheating, will reduce the heating demand to 7.3 kWh/m^2. This design achieved a 1.4 kWh/m^2, 24 hr and 2.0 kWh/m^2 in heating demand, overheating hours and lighting load higher than the best design (lowest values).

  In 2090, we should add the movable screen shading to the fixed overhang and increase the opening area to 50% to achieve 7.8 kWh/m^2 of annual heating demand, 35 overheating hours, and 7.0 kWh/m^2 of the lighting load. This design achieved 2.7 kWh/m^2, 20 hr and 2.3 kWh/m^2 in heating demand, overheating hours and lighting load higher than the best design (lowest values).

  Optimal design 4: In 2044, we can keep the same building envelope design and interior shading as in 2020. However, we should change the exterior 1.5 m overhang shading to screen shading and increase the daytime ventilation by increasing the WOR to 40% instead of 25%. If we used fixed screen shading, this optimal design can achieve 12.1 kWh/m^2.yr of annual heating demand and 36 hr of overheating in the hottest room and the lowest lighting load by 7.2 kWh/m^2. If the exterior shading is moveable based on the season (opened in the winter and closed in summer), this optimal design can achieve 8.1 kWh/m^2.yr of annual heating demand and 36 hr of overheating in the hottest room and the lowest lighting load by 6.7 kWh/m^2. This design achieved a 1.6 kWh/m^2, 24 hr and 1.7 kWh/m^2 in heating demand, overheating hours and lighting load higher than the best design. In 2090, we should add the overhang to movable screen shading to achieve 8.5 kWh/m^2 of annual heating demand, 39 overheating hours, and 7.2 kWh/m^2 of the lighting load. This design achieved a 3.4 kWh/m^2, 24 hr and 2.6 kWh/m^2 in heating demand, overheating hours and lighting load higher than the best design (lowest values).

The results confirmed that the movable overhang exterior shading was not effective as the movable screen exterior shading, where the solar angle is more horizontal on the south facade

in winter and more vertical in summer. Also, movable screen shading will be an effective method in the long-term future period.

Table 4-15. Optimal building design parameters under 2044 and 2090

Designs	Optimal 1		Optimal 2		Optimal 3		Optimal 4		
Year / Variables	2040	2090	2040	2090	2040	2090	2040		2090
Exterior shading	0.5m	1.5m	1.5m	Screen	1.5m	Screen	1.5 m overhang		Screen
WOR (%)	50	50	50	50	40	50	40		40
Night Cooling (ACH)	5	5	5	5	5	5	5		5
Solar reflectance	0.8	0.8	0.8	0.8	0.8	0.8	0.8		0.8
Results of three objectives									
Heating demand (kWh/m^2)	9.3	8.4	11.1	9.4	8.2	7.8	12.1	8.4	8.5
Overheating hours (hr)	32	31	27	35	36	35	36	36	39
Lighting load (kWh/m^2)	6.0	6.7	6.3	6.5	7.0	6.9	7.2	6.7	7.2
Best Design VS Optimal Design									
Heating demand (kWh/m^2)	2.5	3.3	4.3	4.3	1.4	2.7	5.3	1.6	3.4
Overheating hours (hr)	20.0	16.0	15.0	20.0	24.0	20.0	24	24	24.0
Lighting load (kWh/m^2)	1.0	2.0	1.2	1.9	2.0	2.3	2.1	1.7	2.6

CHAPTER 5: CONCLUSION AND FUTURE WORK

Given the lack of information about the thermal conditions of Canadian buildings with climate change, this research work aims to develop a framework to assess the overheating risks and develop effective mitigation measures under projected future climates for both archetype and existing buildings. More specific objectives to address the research gaps identified through the literature review are defined as follows: 1) determine the contribution and correlation of individual building envelope parameters to the change in indoor temperature in conjunction with ventilation; 2) develop an automated calibration procedure to calibrate a building simulation model based on the indoor hourly temperature to achieve high accuracy so that the building model can be used to assess indoor overheating risks in existing buildings; 3) assess overheating risks under recent and future extreme years and recommend effective mitigation measures; and 4) provide the optimal design for retrofitting existing buildings to achieve various performance aspects of building design.

To achieve these objectives:

1) A robust sensitivity analysis (SA) methodology is developed based on global variance-based and local one-at-time sensitivity analysis methods.
2) An auto-calibration methodology is developed to achieve a calibrated model with high accuracy. The global sensitivity analysis and the Multi-Objective Genetic Algorithm (MOGA) method is used to calibrate multiple thermal zones (rooms) in free-running buildings simultaneously. Two criteria are developed, namely the Maximum Absolute Difference and 1 °C Percentage Error.
3) A systematic framework for evaluating overheating and passive mitigation measures under recent and extreme future climates
4) Optimization strategies are developed to find the optimal building design if an existing building should be renovated under recent and extreme future climates.

The proposed frameworks are applied to an archetype detached house and an existing school building to assess and mitigate overheating conditions under recent and future climates.

The main findings from applying the proposed frameworks to <u>an archetype detached house</u> are:

- The ventilation rate plays a major role in determining whether new HEEB buildings have a higher or lower overheating risk than old buildings, where it significantly influences the contribution of the building envelope to the change in indoor operative temperature.
    - With insufficient ventilation rate, the old building has a lower overheating risk than the new HEEB building, where the variance in wall and window thermal transmittance and infiltration rate contribute significantly to the variance in indoor temperature by 58% compared to 42% due to variance in SHGC value. Based on the local sensitivity analysis, decreasing the U-values of the wall and window and the infiltration rate increases the indoor temperature, while decreasing the SHGC of the window decreases the indoor temperature over the summer period.
    - With an adequate ventilation rate, the new HEEB building has a lower overheating risk than the old building, where the variance in SHGC value contributes significantly to the variance in indoor temperature by 87%, and by 9% and 4% due to variance in the U-value of wall and window, respectively. Based on the local sensitivity analysis, decreasing the SHGC or U-values of the wall and windows decreases the indoor temperature over the summer period.
- The ventilation rate threshold that makes a HEEB building perform better than old buildings should be at least 2.2ACH, which is higher than the ventilation rate required by ASHRAE 62.2 for indoor air quality purposes, i.e., 0.8 ACH, which was used in most previous studies.
- The overheating risk in Canadian buildings will increase dramatically under projected short- and long-term future climates. To avoid overheating risk and provide thermal comfort to occupants of a typical Canadian detached house under the recent and future climate, the following strategies are recommended:
    - Ensure that adequate natural ventilation is provided by designing openable windows with an opening area of not less than 10% of the floor area (WOFA) for all climate generations.
    - Ensure that the high energy-efficient building envelope component is used by meeting NECB requirements or higher.

- Use interior shading under projected short-term typical future climate 2030 and additional exterior shading under projected future long-term climate 2090.
- Under extreme future years, additional mitigation measures are required compared to those used under typical years. For example, under 2044, an external overhang will be required, and under 2090, the exterior blind roll should be used.

The main findings from applying the proposed frameworks to <u>an existing school building</u> are:

- The auto-calibration methodology developed achieved high accuracy compared to previous studies.
    - The calibrated model achieved an RMSE in the range of 0.3-0.6 ºC, the Maximum Absolute Difference in the range of 1.0-1.9 ºC, 1°C Percentage Error in the range of 0-10% and 0.5°C Percentage Error in the range of 8-40%.
    - When there is more than one room monitored and these rooms are thermally connected, they need to be calibrated simultaneously.
    - Multi-objective Genetic Algorithms and global sensitivity analysis were able to reduce the number of simulations and the time needed to calibrate the building simulation models. The new evaluation criteria were able to improve the calibrated model and select the optimal calibrated model among many Pareto solutions.
    - The absolute difference between the overheating hours based on the measured and simulated indoor temperature is about 1% for all rooms, which confirms the efficacy and robustness of this methodology for overheating assessment studies.
- Despite the availability of natural ventilation and indoor shading, there are more than 110 overheating hours during the summer of 2020, especially in classrooms located on the Southeast side. Also, the indoor daily weighted exceedance in the hottest classroom reached 12 ° C·day, exceeding the requirement by the BB101 guide.
- The use of exterior blind roll (screen shading) or a combination of night cooling and other mitigation measures that reduce solar heat gain (such as cool roof, exterior overhang, lower window SHGC) can achieve acceptable thermal conditions by reducing overheating hours from 110 to 16 hours and the indoor daily weighted temperature from 12 to 6 ° C·day.

- The number of heatwaves will increase from four heatwaves during the historical period (2001-2020) to 38 heatwaves in the mid-term (2041-2060) and to 88 in the long-term (2081-2100) future years. Using the heatwave detection operational method, the 2020 year was the hottest in the historical period and 2044 and 2090 will be the hottest years in mid and long-term future periods, respectively. The overheating risk in the hottest classroom with the current operational situation will increase to 333 hrs and 437 hrs in 2044 and 2092, respectively, if no mitigation measures are applied.
- The use of the night cooling combined with the exterior blind roll reduces the overheating hours to 15 hrs in 2044, however, in 2090, additional measures such as adding a cool roof should be considered, which can reduce the overheating hours to 39 hrs within the acceptable limit (40 hrs).
- During the heatwaves period in the extreme years (2020, 2044, 2090), the passive mitigation measures considered in each period are still effective to achieve acceptable thermal conditions (three criteria in BB101).
- The auto-optimization methodology achieved multi-optimal designs based on WWR:
    - The WWR parameter plays the main role in determining other building parameters such as window type, interior and exterior shading, window opening area, and roof solar reflectance. Therefore, WWR should be fully considered before conducting the design optimization.
    - Under weather conditions of recent years, all optimal designs of buildings need high energy-efficient building envelope to reduce heating demand and overheating risk. Night cooling can be used to improve the indoor thermal condition in summer without adding a cool roof or external shading (except for 80% WWR where external shading must be added). Internal shading with medium or low solar reflectance with high visible transmittance should be used to reduce the heating demand and reduce overheating risk and lighting load. With a low WWR (40% or 50%), a window type with a visible transmittance of at least 0.5 to achieve good visual comfort and 0.4 with a high WWR (60% and 80%) should be used
    - In future years, overheating mitigation measures must be added. In mid-term future climate, we should add a cool roof and overhang ranging from 0.5-1.5m depending on the WWR. With 80% WWR, a movable screen shading should be added to

avoid increased heating demand and reduce the risk of overheating. In the long-term future, movable screen shading will be the best solution. The appropriate WOR during mid- and long-term future climate will be 50% of the window area.

This work concluded that under Canadian cold climates more efforts should be focused on improving the building envelope's thermal performance towards high energy-efficient buildings, which not only reduces heating energy consumption and GHG emissions but also provide resiliency to overheating risks in hot summer with adequate natural ventilation and proper solar control.

Contributions

In this research,

1. Sensitivity analysis methodology based on variance-based method and One-at-Time method is developed to find the contribution and correlation of each building envelope parameter to the change in indoor temperature with the conjunction of ventilation rate
2. Auto-calibration methodology is developed. In this methodology, 1) multiple rooms are calibrated simultaneously in free-running buildings, 2) new evaluation and selection criteria are developed to find a high accurate model, and 3) sensitivity analysis and Multi-objective Genetic algorithm are used to find the calibrated model with low numbers of simulations
3. Overheating risk in a Canadian archetype detached house using simulation data and in an existing school using measured data buildings was assessed under current and future years
4. Recommendations on effective mitigation measures were provided for archetype detached house and an existing school under current and future extreme years using local and global sensitivity analysis
5. Optimal designs were provided for retrofitting existing buildings to achieve the lowest heating energy demand and highest thermal and visual comfort in new building design using a Multi-objective Genetic algorithm

Limitations and future work

Study buildings are limited to two types of building, one location and one GCM and RCM climate model for generating future climate, which may influence the assessment and mitigation of

overheating results. To address these limitations and generalize the results, this research developed frameworks and methodologies to assess and mitigate the overheating risk in buildings under current and future climates, which can be applied to different types of buildings in different geographical locations, different future climate generation scenarios and global climate models, and to various mitigation measures.

Also, future work should include the study of the effect of nature-based (such as trees or vegetation green façades and green roofs for shading and cooling) and artificial (such as exterior solar shading for shading, and cool roofs and walls for cooling) mitigation measures not only on buildings but also on the urban micro-climate.

REFERENCE

Alcayde, A., Baños, R., Gil, C., et al. (2011). Optimization methods applied to renewable and sustainable energy: a review. Renewable Sustainable Energy Reviews. 15, 1753-1766

Amoako-Attah, J., B-Jahromi, A. (2016). The Impact of Different Weather Files on London Detached Residential Building Performance—Deterministic, Uncertainty, and Sensitivity Analysis on CIBSE TM48 and CIBSE TM49 Future Weather Variables Using CIBSE TM52 as Overheating Criteria. Sustainability. 8, 1194.

Andrade-Cabrera, C., Burke, D., Turner, N., Finn D.P. (2017). Ensemble Calibration of lumped parameter retrofit building models using Particle Swarm Optimization. Energy and Buildings. 155, 513–532

Andrade-Cabrera, C., Turner, N., Burke, D., Neu, O., Finn, D.P. (2016). Lumped parameter building model calibration using Particle Swarm Optimization. Proceedings of the 3rd Asia Conference of International Building Performance Simulation Association (ASIM 2016).

ANSI/ASHRAE Standard 55. (2017) Thermal Environmental Conditions for Human Occupancy. American Society of Heating, Refrigerating and Air-Conditioning Engineers, Inc., Atlanta.

Archer, G., Saltelli, A., Sobol, I. (1997). Sensitivity measures, ANOVA-like Techniques and the use of bootstrap. Statistical Computation and Simulation. 58, 99-120

Arida, M., Nassif, N., Talib, R., et al. (2017). Building Energy Modeling Using Artificial Neural Networks. Energy Research. 7, 24-34

Armour, K. C. (2017). Energy budget constraints on climate sensitivity in light of inconstant climate feedbacks. Nature Climate Change. 7, 331–335

Ascione, F., Bianco, N., De Stasio, C., et al. (2017). Energy retrofit of educational buildings: Transient energy simulations, model calibration and multi-objective optimization towards nearly zero-energy performance Energy and Buildings. 144, 303–319.

Ascione, F., Bianco, N., Mauro, G.M., et al. (2019). Building envelope design: Multi-objective optimization to minimize energy consumption, global cost and thermal discomfort. Application to different Italian climatic zones. Energy. 174, 359-374

ASHRAE ANSI/ASHRAE Standard 62.1. (2019). Ventilation for acceptable indoor air quality. American Society of Heating, Refrigerating and Air-Conditioning Engineers, Inc., Atlanta, GA

ANSI/ASHRAE Standard 62.2. (2019). Ventilation and acceptable indoor air quality in residential buildings. American Society of Heating, Refrigerating and Air Conditioning Engineers, Atlanta, GA.ASHRAE Guideline 14. (2014). Measurement of Energy and Demand Savings. American Society of Heating, Refrigerating and Air-Conditioning Engineers, Inc., Atlanta.

ASHRAE. ANSI/ASHRAE/IES Standard 90.1 (2016). Energy Standard For Building Except Low-Rise Residential Buildings, I-P. ASHRAE, Atlanta, GA.

ASHRAE/Technical Committee. (2002). ASHRAE Guideline 14 Measurement of Energy and Demand Savings. Vol. 8400. United States of America: ASHRAE Press

Attia S., Carlucci S., Hamdy M., et al. (2013). Assessing gaps and needs for integrating building performance optimization tools in net-zero energy buildings design. Energy and Buildings, 60, 110-124

Atkinson J., Chartier Y., Pessoa C., et al. (2009). WHO- Natural Ventilation for Infection Control in Health-Care Settings.

Auzeby, M., Wei, S., Underwood, C., et al. (2017). Using phase change materials to reduce overheating issues in UK residential buildings. Energy Procedia. 105, 4072-4077

Awada, M., Srour, I. (2018). A genetic algorithm-based framework to model the relationship between building renovation decisions and occupants' satisfaction with indoor environmental quality. Building and Environment. 146, 247-257

Baba, F., Ge, H. (2019a). Effect of climate change on the energy performance and thermal comfort of high-rise residential buildings in cold climates. Central European Symposium on Building Physics. 282, 02066.

Baba, F., Ge, H. (2019b). Effect of Climate Change and Extreme Weather Events on the Thermal Conditions of Canadian Multi-unit Residential Buildings. ASHRAE Transactions. 125, 30-33.

Baba, F. M., Ge, H., Zmeureanu, R., Wang, L. L. (2022a). Calibration of building model based on indoor temperature for overheating assessment using genetic algorithm: Methodology, evaluation criteria, and case study. *Building and Environment*, 207, 108518

Baba, F. M., Ge, H., Wang, L. L., & Zmeureanu, R. (2022). Do high energy-efficient buildings increase overheating risk in cold climates? Causes and mitigation measures required under recent and future climates. *Building and Environment*, 109230.

Baborska-Marozny, M., Stevenson, F., Grudzinska, M. (2017). Overheating in retrofitted flats: occupant practices, learning and interventions. Building and Research and Information. 45, 40-59.

Bäck, T. (1996). Evolutionary Algorithms in Theory and Practice: Evolution Strategies, Evolutionary Programming, Genetic Algorithms. Oxford Univ. Press.

Bäck, T., Fogel, D., Michalewicz, Z. (1997). Handbook of Evolutionary Computation. Oxford Univ. Press.

Bakir, G. (2007). Foundation Predicting structured data. Massachusetts Institute of Technology

Baniassadi, A., Sailor, D. (2018). Synergies and trade-offs between energy efficiency and resiliency to extreme heat – A case study. Building and Environment. 132, 263- 272

Banihashemi, S., Ding, G., Wang, J. (2017). Developing a hybrid model of prediction and classification algorithms for building energy consumption. Energy Procedia, 110, 371-376

Banzhaf, W., Nordin, P., Keller, R., et al (1998). Genetic Programming - An Introduction, Morgan Kaufmann, San Francisco

Basu, R., Samet, J. M. (2002). Relation between Elevated Ambient Temperature and Mortality: A Review of the Epidemiologic Evidence. Epidemiologic Reviews, 24 (2002); 190–202.

BB101. (2006). Building Bulletin 101: A design guide: Ventilation of school buildings. Department for Education and Skills (DfES). London.

BB101. (2016). Building Bulletin 101: Guidelines on ventilation, thermal comfort and indoor air quality in schools. Department for Education and Skills (DfES). London.

BB101. (2018). Building Bulletin 101: Guidelines on ventilation, thermal comfort and indoor air quality. Department for Education and Skills (DfES). London.

BC Energy Step Code. (2019). Design Guide Supplement S3 on Overheating and Air Quality. 40 Pages

BC Hydro Power Smart. (2014). Building Envelope Thermal Bridging Guide: analysis, application and insights. A technical report. 870 pages.

Beizaee, A., Lomas, K. J., Firth, S. K. (2013). National survey of summertime temperature and overheating risk in English homes. Building and Environment. 65, 1-17.

Belcher, S.E., Hacker, J.N., Hacker, N. (2005). Constructing design weather data for future climates. Building Service Engineering. 26, 49-61

Berardi, U. (2017). Sustainability Assessments of Buildings. Sustainability.

Berger, J., Orlande, H., Mendes, N., et al. (2016). Bayesian inference for estimating thermal properties of a historic building wall. Building and Environment. 106, 327-339,

Bolstad, W.M. (2010). Understanding computational Bayesian statistics. Wiley

Booth, A., Choudhary, R., Spiegelhalter, D. (2012). Handling uncertainty in housing stock models. Building and Environment. 48, 35–47.

Borden, K. A., Cutter, S. L. (2008). Spatial patterns of natural hazards mortality in the United States. International Journal of Health Geographics. 7; 1-13

Boyce, P. (2003). Human Factors in Lighting. 2rd ed.; Taylor & Francis/CRC Press: Boca Raton, FL, USA.

Brambilla, A., Bonvin, J., Flourentzou, F., et al. (2018). On the Influence of Thermal Mass and Natural Ventilation on Overheating Risk in Offices. Buildings. 8, 47-62

British Columbia. (2021). Statistics & Geospatial Data-Wildfire Statistics. URL: https://www.gov.bc.ca/gov/content/safety/wildfire-status/about-bcws/wildfire-statistics (accessed January 24, 2022).

British Columbia. (2021). School district boundaries. URL: https://globalnews.ca/news/7987756/first-time-ever-bc-schools-close-extreme-heat/ (accessed January 24, 2022).

BS EN 15251. (2007). Indoor environmental input parameters for design and assessment of energy performance of buildings addressing indoor air quality, thermal environment, lighting and acoustics. Standard by British-Adopted European Standard.

Burhenne, S., Elci, M., Jacob, D., et al. (2010). Sensitivity analysis with building simulations to support the commissioning process. Proceedings of the tenth international conference for enhanced building operations, Kuwait.

Cacabelos, A., Eguía, P., Luís Míguez, J., et al. (2015). Calibrated simulation of a public library HVAC system with a ground-source heat pump and a radiant floor using TRNSYS and GenOpt. Energy and Buildings, 108, 114-126

Campolongo, F., Cariboni, J., Saltelli, A. (2007). An effective screening design for sensitivity analysis of large models. Environmental Modelling & Software, 22, 1509-1518

Cannon, A.J. (2018). Multivariate quantile mapping bias correction: an N-dimensional probability density function transform for climate model simulations of multiple variables. Climate dynamics. 50, 31-49

Carlucci, S., Cattarin, G., Causone, F., et al. (2015). Multi-objective optimization of a nearly zero-energy building based on thermal and visual discomfort minimization using a non-dominated sorting genetic algorithm (NSGA-II), Energy and Buildings, 104, 378-394

Carstens, H., Xia, X., Yadavalli, S. (2017). Low-cost energy meter calibration method for measurement and verification. Applied Energy, 188, 563-575,

Center for International Earth Science Information Network (CIESIN). (2014). A Review of Downscaling Methods For Climate Change Projections Report. URL: http://www.ciesin.org/documents/Downscaling_CLEARED_000.pdf (accessed January 24, 2022).

Cerezo-Mota, R., Cavazos, T., Arritt, R., et al. (2016). CORDEX-NA: Factors inducing dry/wet years on the North American Monsoon region. International journal of climatology. 36, 824–836.

Chaloeytoy, K., Ichinose, M., Chien. S. (2020). Determination of the Simplified Daylight Glare Probability (DGPs) Criteria for Daylit Office Spaces in Thailand. Buildings. 10, 180

Chvatal, K., Corvacho, H. (2009). The impact of increasing the building envelope insulation upon the risk of overheating in summer and an increased energy consumption. Building Performance Simulation. 3, 267-282

CIBSE TM52. (2013). Limits of Thermal Comfort: Avoiding Overheating in European Buildings.

CIBSE. (2002). Weather, solar and illuminance data CIBSE Guide J. London: Chartered Institution of Building Services Engineers.

CIBSE. (2014). Design for future climate: Case studies. The Chartered Institution of Building Services Engineers. London, UK.

CIBSE. (2014). TM49-2014: Design Summer Years for London. London, UK.

CIBSE. (2017). Air Induction Unit (AIU); Air Ventilation Assessment (AVA)., 147, 162. Climate Leadership Group (C40), 47–49. Architecture, 162, 226.

CIBSE. (2017). TM 59: design methodology for the assessment of overheating risk in homes. London: CIBSE.

CIBSE. (2013). TM52: 2013 the limits of thermal comfort in European buildings. London: CIBSE

CIBSE-Guide A. (2011). Environmental design. London: Chartered Institution of Building Services England.

Coakley, D., Raftery, P., Keane, M. (2014). A review of methods to match building energy simulation models to measured data. Renewable and Sustainable Energy Reviews. 37, 123–141

Coakley, D., Raftery, P., Molloy, P. (2012). Calibration of whole building energy simulation models: detailed case study of a naturally ventilated building using hourly measured data. First Building Simulation Optimal Conference. 57-64

Coakley, D., Raftery, P., Molloy, P. et al. (2011). Calibration of a Detailed BES Model to Measured Data Using an Evidence-Based Analytical Optimisation Approach. In Proceedings of the Building Simulation, Sydney, Australia.374–381.

Concalves, V., Ogunjimi, Y., Heo, Y. (2021). Scrutinizing modeling and analysis methods for evaluating overheating risks in passive houses. Energy and Buildings. 234, 110701

Cornaro, C., Puggioni, V.A., Strollo, R.M. (2016). Dynamic simulation and on-site measurements for energy retrofit of complex historic buildings: Villa Mondragone case study. Building Engineering. 6, 17–28

Council of Ministers of Education Canada. (2021). Elementary and Secondary Education. URL: https://www.cmec.ca/299/education-in-canada-an-overview/index.html#:~:text=Schools%20and%20Enrolments,10%2C100%20elementary (accessed January 24, 2022).

Czitrom, V. (1999). One-Factor-at-a-Time Versus Designed Experiments. American Statistician, 53, 126-131.

Cukier, R.I., Fortuin, C.M., Shuler, K. (1973). Study of the sensitivity of coupled reaction systems to uncertainties in rate coefficients. Chemical physics. 59, 3814-3878

Daly, D., Cooper, P., Ma, Z. (2014). Implications of global warming for commercial building retrofitting in Australian cities. Building and Environment, 74, 86-95

DCLG. (2021). The English Housing Survey. London: Department for Communities and Local Government.

De Luca, F., Kiil, M., Simson, R., et al. (2019). Evaluating daylight factor standard through climate based daylight simulations and overheating regulations in Estonia. Proceedings of the 16th IBPSA Conference, Rome, Italy. Building Simulation.

Deb, K., Pratap, A., S. Agarwal, A. et al. (2002) A fast and elitist multi-objective genetic algorithm: NSGA-II. IEEE Transactions Evolutionary Computation, 6, 182-197

Dengel, A., Swainson, M., Ormandy, D., et al. (2016). Overheating in dwellings Guidance Document. Building Research Establishment. URL: https://www.bre.co.uk/filelibrary/Briefing%20papers/116885-Overheating-Guidance-v3.pdf (accessed January 24, 2022).

Delgarm, N., Sajadi, B., Azarbad, K., et al. (2018). Sensitivity analysis of building energy performance: a simulation-based approach using OFAT and variance-based sensitivity analysis methods. Building Engineering. 15, 181-193

Després, C., Lajoie, A., Lemieux, S., et al. (2017). Healthy Schools - Healthy Lifestyles: A Literature Review on the Built Environment Contribution. In Health and Wellbeing for Interior Architecture, edited by Dan Kopec, 123–136. New York: Routledge, Taylor and Francis Ltd.

Dickinson R, Brannon B. (2016). Generating future weather files for resilience. In: Proceedings of the international conference on passive and low energy architecture, Los Angeles, CA, USA. 11–3. URL: WeatherShift http://www.weather-shift.com/ (accessed January 24, 2022).

DOE. (2021a). EnergyPlus-Engineering Reference. Daylighting- https://bigladdersoftware.com/epx/docs/8-8/input-output-reference/group-daylighting.html (accessed January 24, 2022).

DOE. (2021b). EnergyPlus-Engineering Reference. Airflow Network Model- URL: https://bigladdersoftware.com/epx/docs/8-3/engineering-reference/airflownetwork-model.html (accessed January 24, 2022).

Donovan, A., O'Sullivan, P., Murphy, M. (2019). Predicting air temperatures in a naturally ventilated nearly zero energy building: Calibration, validation, analysis and approaches. Applied Energy. 250, 991-1010

Drouin, M. (2018). EXTREME HEAT: 66 DEATHS IN MONTRÉAL IN 2018. CIUSSS DU CENTRE SUD DE L'ÎLE-DE MONTRÉAL URL: https://santemontreal.qc.ca/en/public/fh/news/news/extreme-heat-66-deaths-in-montreal-in-2018/ (accessed January 24, 2022).

Dubrul, C. (1988). Inhabitant behavior with respect to ventilation – a summary report of lEA Annex VIII. Berks UK

Eiben, A.E., Smith, J.E. (2003). Introduction to Evolutionary Computing. Springer

Elzeyadi, I., Gatland, S.D. (2019). The impact of the exterior envelope on thermal comfort perceptions in offices. Thermal performance of the exterior envelopes of whole buildings XIV international conference, 107-114

Encinas, F., Herde A. (2013). Sensitivity analysis in building performance simulation for summer comfort assessment of apartments from the real estate market. Energy and Buildings. 65. 55-65

Environment Canada. (2018). Warm-season weather hazards. Environment Canada. URL: https://www.canada.ca/en/environment-climate-change/services/seasonal-weather-hazards/warm-season-weather-hazards.html. (accessed January 24, 2022).

European Committee for Standardization. EN 15193-1. (2017). Energy Performance of Buildings—Energy Requirements for Lighting; European Committee for Standardization (CEN): Brussels, Belgium.

European Commission. (2022). Building stock characteristics. https://ec.europa.eu/energy/eu-buildings-factsheets-topics-tree/building-stock-characteristics_en

European Commission. (2018). BS EN 17037: Daylight in Buildings https://www.en-standard.eu/bs-en-17037-2018-daylight-in-buildings/ (accessed January 24, 2022).

European Union. (2022). Nearly Zero Energy Buildings. https://energy.ec.europa.eu/topics/energy-efficiency/energy-efficient-buildings/nearly-zero-energy-buildings_en

Fedorczak-Cisak, M., Nowak, K., Furtak, M. (2020). Analysis of the Effect of Using External Venetian Blinds on the Thermal Comfort of Users of Highly Glazed Office Rooms in a Transition Season of Temperate Climate—Case Study. Energies. 13, 81-102

Feist, W., Pfluger, R., Kaufmann, B., et al. (2015). PHPP passive house planning package Version 9; the energy balance and design tool for efficient buildings and retrofits. Darmstadt: Passive House Institute.

Ferrara, M., Sirombo, E., Fabrizio, E. (2018). Energy-optimized versus cost-optimized design of high-performing dwellings: The case of multifamily buildings. Science and Technology for the Built Environment, 24, 513-528

Flanagan, R. (2018). Toronto beats temperature record as students swelter in schools without AC. URL: https://www.ctvnews.ca/canada/toronto-beats-temperature-record-as-students-swelter-in-schools-without-ac-1.4081007 (accessed January 24, 2022).

Fletcher, M.J., Johnston, D.K., Glew, D.W., et al. (2017). An empirical evaluation of temporal overheating in an assisted living Passivhaus dwelling in the UK. Building and Environment. 121, 106-118.

Fosas, D., Coley, A., Natarajan, S., et al. (2018). Mitigation versus adaptation: Does insulating dwellings increase overheating risk? Building and Environment, 143, 740–759.

Gagge, A. P., Stolwijk, J. A. J. Nishi, Y. (1986). A Standard Predictive Index of Human Responses to the Thermal Environment. ASHRAE Transactions, 92, 709–731.

Gagnon, D., Schlader, Z.J., Crandall, C.G. (2015). Sympathetic activity during passive heat stress in healthy aged humans: Ageing and MSNA during heat stress. Physiol. 593, 2225–2235

Gamero-Salinas, J., Monge-Barrio, A., Sánchez-Ostiz, A. (2020). Overheating risk assessment of different dwellings during the hottest season of a warm tropical climate. Building and Environnent. 171, 106664

Garcia Sanchez, D., Lacarrière, B., Musy, M., et al. (2012). Application of sensitivity analysis in building energy simulations: combining first and second-orderer elementary effects methods. Energy and Buildings. 68, 741-750

Gaur, A., Lacasse, M., Armstrong, M. (2019). Climate Data to Undertake Hygrothermal and Whole Building Simulations Under Projected Climate Change Influences for 11 Canadian Cities. Data-MDPI, 4, 72-83

Giorgi, F. (2019). Thirty Years of Regional Climate Modeling: Where Are We and Where Are We Going next? Journal of Geophysical Research: Atmospheres. 124, 5696–5723

Giorgi, F., Jones, C., Asrar, G. (2009). Addressing climate information needs at the regional level: the CORDEX framework. World meteorological organization. 58, 175–183

GIS climate change UCAR. (2019). Climate change scenarios- what is downscaling? URL: https://gisclimatechange.ucar.edu/question/63 (accessed January 24, 2022).

Giuli, V., Pos, O., Carli, M. (2012). Indoor environmental quality and pupil perception in Italian primary schools. Building and Environment. 56, 335-345

Goia, F., Time, B., Gustavsen, A. (2015). Impact of opaque building envelope configuration on the heating and cooling energy need of a single family house in cold climates. Energy Procedia. 78, 2626–2631.

Gou, S., Nik, V.M., Scartezzini J.L., et al. (2018). Passive design optimization of newly-built residential buildings in Shanghai for improving indoor thermal comfort while reducing building energy demand. Energy and Buildings, 169, 484-506

Gouvernement du Québec. (2021). Québec infrastructure plan 2021- 2031 Report. URL: https://www.tresor.gouv.qc.ca/fileadmin/PDF/budget_depenses/21-22/6-Quebec_Infrastructure_Plan.pdf (accessed January 24, 2022).

Government du Québec. (2021). Québec infrastructure plan 2017- 2027 Report- Appendix 2: detailed inventory school boards. (accessed January 24, 2022). URL: https://www.tresor.gouv.qc.ca/fileadmin/PDF/budget_depenses/17-18/quebecPublicInfrastructure.pdf

Government of Canada. (2014). Action for Seniors report. 27 pages: https://www.canada.ca/en/employment-social-development/programs/seniors-action-report.html#tc2a (accessed January 24, 2022).

Grussa, D., Andrews, D., Lowry, G., et al. (2019). A London residential retrofit case study: evaluating passive mitigation methods of reducing risk to overheating through the use of solar shading combined with night-time ventilation. Building Services Engineering Research Technology. 40, 385–388

Gu, L., Crawley, D. (2009). Overview of EnergyPlus development: new capabilities and applications for integrated building system design. Presented at CHAMPS 2009. Syracuse University.

Guerra Santin O., Itard, L., Visscher, H. (2009). The effect of occupancy and building characteristics on energy use for space and water heating in Dutch residential stock. Energy and Buildings. 41, 1223-1232

Gunay, H., O'Brien, W., Beausoleil-Morrison, I. (2016). Implementation and comparison of existing occupant behaviour models in EnergyPlus. Building Performance Simulation. 9, 567–588

Gupta, R., Kapsali, M. (2015). Empirical assessment of indoor air quality and overheating in low-carbon social housing dwellings in England, UK. Advances in Building Energy Research. 23 pages

Haensler, A.; Hagemann, S.; Jacob, D. (2011a). Dynamical downscaling of ERA40 reanalysis data over southern Africa: Added value in the simulation of the seasonal rainfall characteristics. International journal of climatology. 31, 2338–2349.

Hamdy, M., Carluccia, S., Hoes, P., Hensen, J. (2017). The impact of climate change on the overheating risk in dwellings-A Dutch case study. Building and Environment. 122, 307-323

Hamdy, M., Nguyen, A.T., Hensen, J.L.M. (2016). A performance comparison of multi-objective optimization algorithms for solving nearly-zero-energy-building design problems. Energy and Buildings. 121, 57-71

Hausfather Z. (2019). CMIP6: the next generation of climate models explained. Carbon brief. URL: https://www.carbonbrief.org/cmip6-the-next-generation-of-climate-models-explained (accessed January 24, 2022).

Hawkins, E.; Sutton, R. (2009). The potential to narrow uncertainty in regional climate predictions. Bulletin of the American Meteorological Society. 90, 1095–1108.

Hawkins, E.; Sutton, R. (2011). The potential to narrow uncertainty in projections of regional precipitation change. Climate dynamics. 37, 407–418

HC. (2011b). Adapting to Extreme Heat Events: Guidelines for Assessing Health Vulnerability. Prepared by: Water, Air and Climate Change Bureau Healthy Environments and Consumer Safety Branch. Health Canada, Ottawa.

Helton, J. (1993). Uncertainty and sensitivity analysis techniques for use in performance assessment for radioactive waste disposal. Reliability Engineering and System Safety. 42, 327-367.

Helton, J., Davis, F. (2002). Illustration of sampling-based methods for uncertainty and sensitivity analysis. Risk Analysis. 22, 591-622.

Heo, Y., Grazizno, D., Guzowski, L., et al. (2015). Evaluation of calibration efficacy under different levels of uncertainty. Building Performance Simulation. 8, 135-144

Heo, Y., Augenbreo, G., Choudhary, R. (2012). Calibration of building energy models for retrofit analysis under uncertainty. Energy and Buildings. 47, 550-560

Hempel S, Frieler K, Warszawski L, Schewe J, Piontek F. (2013). A trend-preserving bias correction-the ISI-MIP approach. Earth System Dynamics. 4, 219–236.

Hoffmann, S., Lee. E.S., McNeil, A., et al. Balancing Daylight, Glare, and Energy-Efficiency Goals: an Evaluation of Exterior Coplanar Shading Systems Using Complex Fenestration Modeling Tools. Energy and Buildings. 112, 279-298.

Holland J.H. (1975). Adaptation in Natural and Artificial Systems: An Introductory Analysis with Applications to Biology, Control, and Artificial Intelligence. University of Michigan Press, Ann Arbor, MI

Holland, H. (2006) Genetic Algorithms - Computer programs that "evolve" in ways that resemble natural selection can solve complex problems even their creators do not fully understand. URL: http://www2.econ.iastate.edu/tesfatsi/holland.GAIntro.htm (accessed January 24, 2022).

Hong, T., Kim, J., Jeong, J., et al. (2017). Automatic calibration model of a building energy simulation using optimization algorithm. Energy Procedia. 105, 3698–3704.

Hong, T., Kim, J., Lee, M. (2019). A multi-objective optimization model for determining the building design and occupant behaviors based on energy, economic, and environmental performance. Energy. 174, 823-834.

Hooff, T., Blocken, B., Hensen, J., Timmermans, H. (2014). On the predicted effectiveness of climate adaptation measures for residential buildings. Building and Environment. 82, 300–316.

Hoseinzadeh, S., Ghasemiasl, R., Bahari, A., et al. (2017). Type WO3 semiconductor as a cathode electrochromic material for ECD devices. Materials Science: Materials in Electronics. 28, 14446-14452.

Hopfe, C., Hensen, J. (2011). Uncertainty analysis in building performance simulation for design support. Energy and Buildings. 43, 2798-2805.

Hopfe, C., Hensen, J., Plokker, W. (2007). Uncertainty and sensitivity analysis for detailed design support. Proceedings of the 10th IBPSA Building Simulation Conference, Tsinghua University, Beijing.

Hoppe, P. (1999). The physiological equivalent temperature - a universal index for the biometeorological assessment of the thermal environment. International Journal of Biometeorology. 43, 71–75

Huang, K., Huang, W., Lin, T., et al. (2015). Implementation of green building specification credits for better thermal conditions in naturally ventilated school buildings. Building and Environment. 86, 141-150

Huanga, K., Hwang R.. (2017). Future trends of residential building cooling energy and passive adaptation measures to counteract climate change: The case of Taiwan. Applied Energy. 1230-1240.

Huanga, K., Hwang, R. L. (2016). Future trends of residential building cooling energy and passive adaptation measures to counteract climate change: The case of Taiwan. Applied Energy. 184, 1230-1240.

Hughes, C., Natarajan, S. (2019). Summer thermal comfort and overheating in the elderly. Building Services Engineering Research Technology. 40, 426–445

Ibrahim, A., Pelsmakers, S. (2018). Low-energy housing retrofit in North England: Overheating risks and possible mitigation strategies. Building services engineering research and technology. URL: https://journals.sagepub.com/doi/full/10.1177/0143624418754386 (accessed January 24, 2022).

Illuminating Engineering Society of North America (IESNA). (2013). IES LM-83-12 IES Spatial Daylight. Autonomy (sDA) and Annual Sunlight Exposure (ASE), IESNA Lighting; IESNA: New York, NY, USA

Iman, R., Helton, J. (1991). The repeatability of uncertainty and sensitivity analysis for complex probabilistic risk assessment. Risk Analysis. 11, 591-606.

International Energy Agency (IEA). (2020). Sustainable Recovery-World Energy Outlook Special Report. https://www.iea.org/reports/sustainable-recovery/buildings

Institute of Medicine (IOM). (2011). Climate Change. The Indoor Environment, and Health. Institute of Medicine of the National Academies Press, Washington, DC.

International Passive House Association. (2022). Passive House Guidelines. URL: https://passivehouse-international.org/index.php?page_id=80 (accessed January 24, 2022).

International WELL building institute. (2019). WELL Building Standard: V1 with Q1 2019 Addenda. Delos Living LLC: New York, NY, USA,

IPCC. (1996). Climate Change 1995: A report of the Intergovernmental Panel on Climate Change, Second Assessment Report of the Intergovernmental Panel on Climate Change, IPCC.

IPCC. (2001). Climate Change 2001: Synthesis Report. Contribution of Working Groups I, II and III to the Third Assessment Report of the Intergovernmental Panel on Climate Change. Geneva, IPCC Secretariat.

IPCC. (2007). Climate Change 2007: Synthesis Report. Contribution of Working Groups I, II and III to the Fourth Assessment Report of the Intergovernmental Panel on Climate Change. IPCC, Geneva, Switzerland.

IPCC. (2012). Glossary of terms. In: Managing the Risks of Extreme Events and Disasters to Advance Climate Change Adaptation. 555-569

IPCC. (2014). Climate change 2014: synthesis report. Contribution of working groups I, II and III to the fifth assessment report of the Intergovernmental Panel on climate change. IPCC.

IPCC. (2018). Global warming of 1.5°C report. An IPCC Special Report on the impacts of global warming of 1.5°C above pre-industrial levels and related global greenhouse gas emission pathways, in the context of strengthening the global response to the threat of climate change, sustainable development, and efforts to eradicate poverty

IPCC. (2019). Guidance on the use of data. What is a GCM? URL: http://www.ipcc-data.org/guidelines/pages/gcm_guide.html (accessed January 24, 2022).

IPCC. (2021). Climate Change 2021: The Physical Science Basis. Contribution of Working Group I to the Sixth Assessment Report of the Intergovernmental Panel on Climate Change. Cambridge University Press.

IPCC. (2022). Climate Change 2022: Impacts, Adaptation, and Vulnerability. Contribution of Working Group II to the Sixth Assessment Report of the Intergovernmental Panel on Climate Change

IPMVP. (2001). International Performance Measurement & Verification Protocol—Concepts and Options for Determining Energy and Water Savings, Volume I, Oak Ridge.

Jacob D, Petersen J, Eggert B. et al. (2014). EURO-CORDEX: New high-resolution climate change projections for European impact research. Regional Environmental Change. 14, 563–578.

Jafari, A., Valentin, V. (2017). An optimization framework for building energy retrofits decision-making. Building and Environment. 115, 118-129

Jaynes, E.T. (2003). Probability theory: The logic of science, Cambridge University Press, Cambridge, U.K.

Jentsch M.F., James P.A., Bourikas L., Bahaj A.S. (2013). Transforming existing weather data for worldwide locations to enable energy and building performance simulation under future climates. Renew Energy. 55, 514-524 –CCWorldWeatherGen program

Jentsch, M. F. (2012). Climate Change Weather File Generators Technical reference manual for the CCWeatherGen and CCWorldWeatherGen tools report. University of Southampton.

Jentsch, M.F., Eames, M.E., Levermore, G.J. (2015). Generating near-extreme Summer Reference Years for building performance simulation. Building Services Engineering Research & Technology. 36, 701-727

Jianling, C. (2009) Multi-objective optimization of cutting parameters with improved NSGA-II. 2009 International Conference on Management and Service Science

Jindal, A. (2018). Thermal comfort study in naturally ventilated school classrooms in composite climate of India. Building and Environment. 142, 34-46

Johnson, H., Kovats, R.S., McGregor, G., et al. (2005). Black. The impact of the 2003 heat wave on mortality and hospital admissions in England. Health Stat. Q.

Johnson, N.R. (2017). Building Energy Model Calibration for Retrofit Decision Making. Master Thesis, Portland State University. USA.

Joint Research Centre. (2015). European Commission SIMLAB: Sensitivity analysis software. URL: https:// ec.europa.eu/jrc/en/samo/simlab (accessed January 24, 2022).

Jones B., Kirby R. (2012). Indoor Air Quality in U.K. School Classrooms Ventilated by Natural Ventilation Windcatchers. International Journal of Ventilation,10, 323-337

Kang, Y., Krarti, M. (2016). Bayesian-Emulator based parameter identification for calibrating energy models for existing buildings. Building Simulation. 411-428,

Kennedy, J., Eberhart, R.C. (1995). Particle swarm optimization. In: Proceedings of the IEEE International Conference on Neural Networks. 1942–1948.

Kennedy, M. C. O'Hagan A. (2001). Bayesian calibration of computer models. Royal Statistical Society. 63, 425-464

Kenny, G. P., Yardley, J., Brown, C. (2010). Heat stress in older individuals and patients with common chronic diseases. CMAJ, 182, 1053–1060.

Kim, Y.J., Park, C.S. (2016). Stepwise deterministic and stochastic calibration of an energy simulation model for an existing building. Energy and Buildings. 133, 455–468.

Klepeis, N.E., Nelson, W.C., Robinson, J.P., et al. (2011). The National Human Activity Pattern Survey (NHAPS): A resource for assessing exposure to environmental pollutants. Exposure Analysis and Environmental Epidemiology.11, 231–52.

Ko, W., Brager, G., Schiavo, S. (2017). Building Envelope Impact on Human Performance and Well-Being: Experimental Study on View Clarity. Escholash.-CBE center for the built environment. eScholarship.

Kodali, S.P., Kudikala, R., Deb, K. (2008). Multi-objective optimization of surface grinding process using NSGA II. First International Conference on Emerging Trends in Engineering and Technology

Kosatsky, T. (2010). Hot Day Deaths, Summer 2009: What Happened and How to Prevent a Recurrence. BCMJ, 52, 261.

Kristensen, M.H., Choudhary, R., Petersen, S. (2017). Bayesian calibration of building energy models: comparison of predictive accuracy using metered utility data of different temporal resolution. Energy Procedia. 122, 277-282,

Kumar, P., Podzun, R., Hagemann, S., et al. (2014). Impact of modified soil thermal characteristic on the simulated monsoon climate over south Asia. Journal of Earth System. 123, 151–160.

Lakhdari, K., Sriti, L., Painter, B. (2021). Parametric optimization of daylight, thermal and energy performance of middle school classrooms, case of hot and dry regions. Building and Environment. 204, 108173

Lane, K., Wheeler, K., Charles-Guzman, K., et al. (2014). Extreme Heat Awareness and Protective Behaviors in New York City. Urban Health. 91, 403–414.

Laouadi, A., Bartko, M., Lacasse, M.A. (2020a). A new methodology of evaluation of overheating in buildings. Energy and Buildings. 226, 110360

Laouadi, A., Gaur A., Lacasse, M. A., et al. (2020). Development of reference summer weather years for analysis of overheating risk in buildings. Building Performance Simulation. 13, 301-319

Lapointe, L. (2021). 70% of sudden deaths recorded during B.C. heat wave were due to extreme temperatures, coroner confirms. CBC News. URL: https://www.cbc.ca/news/canada/british-columbia/bc-heat-dome-sudden-deaths-570-1.6122316 (accessed January 24, 2022).

Lara, R.A., Naboni, E., Pernigotto, G., et al. (2017). Optimization Tools for Building Energy Model Calibration. Energy Procedia. 111, 1060–1069.

Lebel, G., Bustinza, R., Dubé, M. (2017). Analyse des impacts des vagues régionales de chaleur extrême sur la santé au Québec de 2010 à 2015. Institut national de santé publique du Québec.

Leech, J.A., Nelson, W.C., Burnett, R.T., et al. (2002). It's about time: A comparison of Canadian and American time-activity patterns. Exposure Analysis and Environmental Epidemiology, 12, 427–32

Levermore, G.J., Parkinson, J.B. (2006). Analyses and algorithms for new Test Reference Years and Design Summer Years for the UK. Building Services Engineering Research and Technology. 27, 311–325

Li, Q., Gu, L., Augenbroe, G., et al. (2015). Calibration of dynamic building energy models with multiple responses using Bayesian inference and linear regression models. Building physics conference international 6th, 13-19

Li, Z., Huang, G., Huang, W., et al. (2018). Future changes of temperature and heat waves in Ontario, Canada. Theoretical and Applied Climatology. 132, 1029-1038

Liang, H., Lin, T., Hwang, R. (2012). Linking occupants' thermal perception and building thermal performance in naturally ventilated school buildings. Applied Energy. 94, 355-363

Littlefair, P.J. (2005). Avoiding air conditioning. Constructing the Future. 24, 11-20

Liu, C., Kershaw, T., Fosas. D., et al. (2017). High resolution mapping of overheating and mortality risk Building and Environment. 122, 1-14.

Loenhout, J.A.F., le Grand, A., Duijm, F., et al. (2016). The effect of high indoor temperatures on self-perceived health of elderly persons. Environmental Research. 146, 27–34.

Lozinsky, C., Touchie, M. (2018). Improving energy model calibration of multi-unit residential buildings through component air infiltration testing. Building and Environment. 134. 218-229

Machard, A., Inard, C., Alessandrini, J. (2020). A Methodology for Assembling Future Weather Files Including Heatwaves for Building Thermal Simulations from the European Coordinated Regional Downscaling Experiment (EURO-CORDEX) Climate Data. Energies. 13, 3424

Macintyrea, H.L. Heaviside, C. (2019). Potential benefits of cool roofs in reducing heat-related mortality during heatwaves in a European city. Environment International. 127, 430-441

Maivel, M., Kurnitski, J., Kalamees, T. (2015). Field survey of overheating problems in Estonian apartment buildings. Architectural Science Review. 5, 1-10

Manfren, M., Aste, N., Moshksar, R. (2013). Calibration and uncertainty analysis for computer models—A meta-model based approach for integrated building energy simulation. Applied Energy. 103, 627–641.

Martínez-Mariño, S., Eguía-Oller, P., Granada-Álvarez, E., et al. (2021). Simulation and validation of indoor temperatures and relative humidity in multi-zone buildings under occupancy conditions using multi-objective celebration. Building and Environment. 200, 107973.

Masui, T., Matsumoto, K., Hijioka, Y., et al. (2011). An emission pathway for stabilization at 6 W/m2 radiative forcing. Climatic Change. 109, 59-76.

Matthew, R., Muehleisen, R. (2014). Guide to Bayesian calibration of building energy models. 2014 ASHRAE/IBPSA-USA building simulation conference, Atlanta, GA

McGill, G., Sharpe, T., Robertson, L., et al. 2017. Meta-analysis of indoor temperatures in new-build housing. Building Research & information. 19–39.

McGregor, G. R., Bessemoulin, P., Ebi, K., Menne, B. (2015). Heatwaves and health: guidance on warning-system development. Technical Report. WMO and WHO. 96 page.

McLeod, R.S., Hopfe, C.J., Kwan, A. (2013). An investigation into future performance and overheating risks in Passivhaus dwellings. Building and Environment. 70, 189-209

Mehrotra, R., Sharma, A. (2016). A multivariate quantile-matching bias correction approach with auto and cross dependence across multiple time scales: implications for downscaling. Journal of Climate. 29, 3519–3539

Meteonorm. (2021). Handbook Part II: Theory, Version 8.0. Global Meteorological Database Version 8, Software and Data for Engineers, Planers and Education. The Meteorological Reference for Solar Energy Applications, Building Design, Heating & Cooling Systems, Education Rene. 2021. URL: https://meteonorm.com/assets/downloads/mn73_software.pdf (accessed January 24, 2022).

Michelangeli PA, Vrac M, Loukos H. (2009). Probabilistic downscaling approaches: application to wind cumulative distribution functions. Geophysical research letters. 36, 1–6.

Mitchell, M. (1996). An Introduction to Genetic Algorithms. Cambridge, MA: MIT Press

Mitchell, R., Natarajan, S. (2019). Overheating risk in Passivhaus dwellings. Building Services Engineering Research Technology. 40, 446–469.

Mitra, K. (2009). Multi-objective optimization of an industrial grinding operation under uncertainty. Chemical Engineering Science. 64, 5043-5056

Moazami, A., Carlucci, S., Geving, S. (2017). Critical analysis of software tools aimed at generating future weather files with a view to their use in building performance simulation. Energy Procedia. 132, 640-645.

Moazami, A., Nik, V.M., Carlucci, S., et al. (2019). Impacts of future weather data typology on building energy performance—investigating long-term patterns of climate change and extreme weather conditions. Apply Energy. 238, 696–720.

Mohamed, S., Rodrigues, L., Omer, S., et al. (2021). Overheating and indoor air quality in primary schools in the UK. Energy and Buildings. 250, 111291

Montazami, A., Nicole, F. (2013). Overheating in schools: comparing existing and new guidelines. Building Research and Information. 41:3, 317-329.

Montazami, A., Wilson, M., Nicol, F. (2012). Aircraft noise, overheating and poor air quality in classrooms in London primary schools. Building and Environment. 52, 129-141

Mora, C., Dousset, B., Caldwell, I.R., et al. (2017). Global risk of deadly heat. Nature Climate Chang. 7, 501–506

Morris, M.D. (1991). Factorial sampling plans for preliminary computational experiments. Technometrics. 33, 161-174

Mulville, M., Stravoravdis S. (2016). The impact of regulations on overheating risk in dwellings. Building Research and Information. 44, 520-534.

Mylona A. (2012). The use of UKCP09 to produce weather files for building simulation building services engineering research and technology. 33, 51-62

Nadel, S. (2020). Programs to Promote Zero-Energy New Homes and Buildings. American Council for an Energy-Efficient Economy (ACEEE). https://www.aceee.org/sites/default/files/pdfs/zeb_topic_brief_final_9-29-20.pdf

Nagpal, S., Mueller, C., Aijazi, A., et al. (2018). A methodology for auto-calibrating urban building energy models using surrogate modeling techniques. Building Performance Simulation. 1-16

Narisada, K.; Schreuder, D. (2004). Light Pollution Handbook: Volume 322; Springer Science+Business Media Dordrecht: Berlin, Germany.

NASA's Goddard Institute for Space Studies (GISS). (2022) Global climate change. URL: https://data.giss.nasa.gov/gistemp/ (accessed January 24, 2022).

National Ocean and Atmospheric Administration (NAOO). (2020). Weather Related Fatality and Injury Statistics-80-Year List of Severe Weather Fatalities. URL: https://www.weather.gov/hazstat/(accessed January 24, 2022).

Natural Resources Canada (NRC). (2019). National Energy Use Database-Comprehensive Energy Use Database for commercial institutional Sector report. URL: http://oee.rncan-nrcan.gc.ca/corporate/statistics/neud/dpa/menus/trends/handbook/tables.cfm?wbdisable=true (accessed January 24, 2022).

Natural Resources Canada (NRC). (2020). Residential End-Use Model-Residential Housing Stock and Floor Space sector report. URL: http://oee.rncan-nrcan.gc.ca/corporate/statistics/neud/dpa/showTable.cfm?type=HB&sector=res&juris=00&rn=11&page=0 (accessed January 24, 2022).

Natural Resources Canada (NRCan). (2011). Survey of Household Energy Use 2011. Detailed Statistical Report. Office of Energy Efficiency. Natural Resources Canada. Ottawa, Ontario.

Natural Resources Canada (NRCan). (2012). Survey of commercial and institutional energy use – buildings 2009. Detailed Statistical Report. Office of Energy Efficiency. Natural Resources Canada. Ottawa, Ontario.

Natural Resources Canada (NRCan). (2013). Energy efficiency trends in Canada 1990-2012. Office of Energy Efficiency. Natural Resources Canada. Ottawa, Ontario.

Natural Resources Canada (NRCan). (2014). Energy efficiency trends in Canada 1990-2013. Office of Energy Efficiency. Natural Resources Canada. Ottawa, Ontario.

Nelson, T.M.; Nilsson, T.H.; Johnson, M. (1984). Interaction of temperature, illuminance and apparent time on sedentary work fatigue. Ergonomics. 27, 89–101.

NFRC 201. (2020). Procedure for Interim Standard Test Method for Measuring the Solar Heat Gain Coefficient of Fenestration Systems Using Calorimetry Hot Box Methods. National Fenestration Rating Council. URL: https://www.nfrc.org/ (accessed January 24, 2022).

Nguyen, A., Rockwood, D., Doanc, M., et al. (2021). Performance assessment of contemporary energy-optimized office buildings under the impact of climate change. Building Engineering. 35, 102089

Nguyen, A.T., Reiter, S., Rigo, P. (2014). A review on simulation-based optimization methods applied to building performance analysis. Apply Energy. 113, 1043-1058

NOAA. (2016). Climate Modeling. Geophysical Fluid Dynamics Laboratory. URL: https://www.gfdl.noaa.gov/wp-content/uploads/files/model_development/climate_modeling.pdf (accessed January 24, 2022).

NOAA. (2019). Geophysical Fluid Dynamics Laboratory GFDL. Climate Modeling Report URL: https://www.gfdl.noaa.gov/wp-content/uploads/files/model_development/climate_modeling.pdf (accessed January 24, 2022).

North American Regional Climate Change Assessment Program NARCCAP. (2019). Download RCM Data. URL: http://www.narccap.ucar.edu/data/download.html (accessed January 24, 2022).

O'Neill, B.C., Tebaldi, C., Van Vuuren, D., et al. (2016). The scenario model inter-comparison project (ScenarioMIP) for CMIP6. Geoscientific Model Development. 9, 3461–3482

Oberti, F., Oberegger, U.F., Gasparella, A. (2015). Calibrating historic building energy models to hourly indoor air and surface temperatures: Methodology and case study. Energy and Buildings. 108, 236–243.

Occupational Health and Safety Council of Ontario (OHSCO). (2007). Heat stress awareness guide. URL: https://www.uwo.ca/biology/pdf/administration/heatstressguide.pdf (accessed January 24, 2022).

Ohnaka, T., Takeshita, J. (2005). Upper limit of thermal comfort zone in bedrooms for falling into a deep sleep as determined by body movements during sleep. Elsevier Ergonomics Book Series. 3, 121-126

Ouzeau, G., Soubeyroux, J.M., Schneider, M., et al. (2016). Heat waves analysis over France in present and future climate: Application of a new method on the EURO-CORDEX ensemble. Climate Services. 4, 1-12

Overbey, D. (2016). Standard Effective Temperature (SET) and Thermal Comfort. Building Enclosure. URL: https://www.buildingenclosureonline.com/blogs/14-the-be-blog/post/85635-standardeffective- temperature-set-and-thermal-comfort (accessed January 24, 2022).

Paliouras, P., Matzaflaras, N., Peuhkuri, R.H., et al. (2015). Using measured indoor environment parameters for calibration of building simulation model – a passive house case study. Energy Procedia. 78, 1227-1232

Pan, Y., Huang, Z., Wu, G. (2007). Calibrated building energy simulation and its application in a high-rise commercial building in Shanghai. Energy and Buildings. 39, 651–657.

Parekh, A. (2012a). Representative Housing Thermal Archetypes for Energy Analysis Models-Final report. CanmetENERGY Leadership in ecoInnovationm Natural Resources Canada.

Parekh, A., Chris, K. (2012b). Thermal and Mechanical Systems Descriptors for Simplified Energy Use Evaluation of Canadian Houses. Proceedings of SimBuild. 5, 279-286.

Passive House Guidelines. (2022). URL: https://passivehouse-international.org/index.php?page_id=80 (accessed January 24, 2022).

Passive House Institute. (2021). Windows components database. URL: https://database.passivehouse.com/en/components/list/window (accessed January 24, 2022).

Pathan, A., Mavrogianni, A., Summerfield, A., et al. (2017). Monitoring summer indoor overheating in the London housing stock. Energy and Buildings. 141, 361-378.

Paulos, J., Berardi, U. (2020). Optimizing the thermal performance of window frames through aerogel-enhancements. Applied Energy. 266, 114776

Pavlak, G.S., Florita, A.R., Henze, G.P., et al. (2013). Comparison of traditional and bayesian calibration techniques for gray-box modeling. Architectural Engineering. 20.

Peacock, A. D., Jenkins, D. P., Kane, D. (2010). Investigating the potential of overheating in UK dwellings as a consequence of extant climate change. Energy Policy. 38, 3277-3288

Penna, P., Cappelletti, F., Gasparella, A., et al. (2015a) A. Multi-Stage Calibration of the Simulation Model of a School Building Through Short-Term Monitoring. Information Technology in Construction. 20, 132–145.

Penna, P., Prada, A., Cappelletti, F., et al. (2015b). Multi-objectives optimization of Energy Efficiency Measures in existing buildings. Energy and Buildings. 95, 57-69

Pezeshki, Z. (2018). Energy Modeling for Estimation of Indoor Temperature of the Building on the BIM Platform. Thesis at Shahrood University of Technology, Shahrud, Iran.

Piani C, Haerter JO, Coppola E (2010) Statistical bias correction for daily precipitation in regional climate models over Europe. Theoretical and Applied Climatology. 199, 187–192

Pickup, J., de Dear R. (2000). An Outdoor Thermal Comfort Index (OUT-SET) Part I-TheModel and its Assumptions. Sydney, NSW2109 Australia: Division of Environmental and Life Sciences, Macquarie University.

Pierson, C., Wienold, J., Bodart, M. (2018). Daylight Discomfort Glare Evaluation with Evalglare: Influence of Parameters and Methods on the Accuracy of Discomfort Glare Prediction. Buildings. 8(8), 94

Plokker, W., Evers, J.J., Struck, C., et al. (2009). First experiences using climate scenarios for The Netherlands in building performance simulation. 11th IBPSA Building Simulation Conference, International Building Performance Association, Glasgow, UK, 1284-1291

PR EN 16798-1. (2015). Indoor environmental input parameters for design and assessment of energy performance of buildings addressing indoor air quality, thermal environment, lighting and acoustics. Standard by British-Adopted European Standard.

Psomas, T., Heiselberg, P., Lyme, T., et al. (2017). Automated roof window control system to address overheating on renovated houses: Summertime assessment and intercomparison. Energy and Buildings. 138, 35-46

Public Health England. (2015). Heatwave Plan for England, Protecting Health and Reducing Harm from Severe Heat and Heatwaves; Public Health England and National Health Service: London, UK.

Public Health England. (2018). Heatwave Plan for England – protecting health and reducing harm from severe heat and heatwaves. 44 pages

Quigley, E.S., Lomas, K.J. (2018) Performance of medium-rise, thermally lightweight apartment buildings during a heat wave. Proceedings of 10th Windsor Conference: Rethinking Comfort, Windsor, London, UK. 32-47.

Rabitz, H. (2010). Global Sensitivity Analysis for Systems with Independent and/or Correlated Inputs. Procedia - Social and Behavioral Sciences, 2, 7587-7589.

Raftery, P., Keane, M., O'Donnell, J. (2011). Calibrating whole building energy models: An evidence-based methodology. Energy and Buildings. 43, 2356–2364.

Raftery, P., Keane, M., O'Donnell, J. (2011). Calibrating whole building energy models: An evidence-based methodology. Energy and Buildings, 43, 2356–2364.

Ramasoot, T.; Panyakeaw, S. (2015). Prescribing the illumination levels for Thailand: A Review of Approaches and Methodologies. BTEC, 2, 200–210

Ramos, G., Fernández, C., Gómez-Acebo, T., Sánchez-Ostiz, A. (2016). Genetic algorithm for building envelope calibration. Applied Energy. 168, 691–705.

Rasmussen, C.E., Williams, C.K.I. (2006). Gaussian processes for machine learning. Massachusetts Institute of Technology.

RdbQ. (2018). Construction Code and Safety Code - Régie du bâtiment du Québec. [accessed May 05, 2022]. <https://www.rbq.gouv.qc.ca/en/laws-regulations-and-codes/construction-code-and-safety-code.html>.

RBQ. (2018). Construction Code and Safety Code - Régie du bâtiment du Québec 2018. URL: https://www.rbq.gouv.qc.ca/en/laws-regulations-and-codes/construction-code-and-safety-code.html (accessed January 24, 2022).

Rechenberg, I. (1960) Evolutions strategies. Stuttgart: Frommann-Holzboog

Reddy, T.A. (2006). Literature Review on Calibration of Building Energy Simulation Programs: Uses, Problems, Procedures, Uncertainty, and Tools. ASHRAE Transactions. Atlanta 112, 226-240

Riahi, K., Krey, V., Rao, S., et al. (2011). RCP-8.5: exploring the consequence of high emission trajectories. Climatic Change. 109, 80-98

Roberti, F., Oberegger, U., Gasparell, A. (2015). Calibrating historic building energy models to hourly indoor air and surface temperatures: Methodology and case study. Energy and Buildings. 108, 236-243.

Robine, J. M., Cheung, S. L., Roy, S. L., et al. (2007). Report on Excess Mortality in Europe During Summer 2003; European Commission, Directorate General for Health and Consumer Protection: Brussels, Belgium.

Rocha, R. (2018). Montreal Building Age Story Map. URL: https://www.cbc.ca/news2/interactives/montreal-375-buildings/ (accessed January 24, 2022).

Royapoor, M., Roskilly, T. (2015). Building model calibration using energy and environmental data. Energy and Buildings. 94, 109-120

Saltelli, A., Ratto, M., Andres, T., et al. (2008). Global sensitivity analysis: the primer John Wiley & Sons. 285 pages

Sameni, S.M., Gaterell, M., Montazami, A., et al. (2015). Overheating investigation in UK. social housing flats built to the Passivhaus standard. Building and Environment. 92, 222-235

Samuelson, H.W., Ghorayshi, A., Reinhart, F. (2016). Analysis of a simplified calibration procedure for 18 design-phase building energy models. Building Performance Simulation. 9, 17–29.

Sbar, N., Podbelski, L., Yang, H., et al. (2012). Electrochromic dynamic windows for office buildings. International Journal of Sustainable Built Environment. 1, 125-139.

Schaffer, J.D. (1985). Multiple Objective Optimization with Vector Evaluated Genetic Algorithms. The 1st International Conference on Genetic Algorithms. 93-100.

Schweiker, M., J. Kolarik, M. Dovjak, and M. Shukuya. (2016). Unsteady-state Human-Body Exergy Consumption Rate and its Relation to Subjective Assessment of Dynamic Thermal Environments. Energy and Buildings. 116, 164–180.

Seaby, L.P., Refsgaard, J.C., Sonnenborg, T.O., et al. (2013). Assessment of robustness and significance of climate change signals for an ensemble of distribution-based scaled climate projections. Hydrolog. 486, 479-493.

Sepúlveda, A., De Luca, F., Thalfeldt, M., et al. (2020). Analyzing the fulfillment of daylight and overheating requirements in residential and office buildings in Estonia. Building and Environment.180, 107036

Shen, P., Braham, W., Yi, Y., et al. (2019). Rapid multi-objective optimization with multi-year future weather condition and decision-making support for building retrofit. Energy. 172, 892-912

Shen, H., Tzempelikos, A. (2012). Sensitivity analysis on daylighting and energy performance of perimeter offices with automated shading. *Building and Environment*. 59, 303-314

Simson, R., Kurnitski, J., Maivel, M. (2017). Summer thermal comfort: Compliance assessment and overheating prevention in new apartment building in Estonia. Building Performance Simulation. 10, 378-391.

Sobol, I. M. (1967). Distribution of points in a cube and approximate evaluation of integrals. USSR Computational Mathematics and Mathematical Physics. 7, 86–112

Sobol, I. M. (2001). Global sensitivity indices for nonlinear mathematical models and their Monte Carlo estimates. Mathematics and Computers in Simulation. 55, 271-280

Solman, S.A.; Sanchez, E.; Samuelsson, P. et al. Evaluation of an ensemble of regional climate model simulations over South America driven by the ERA-Interim reanalysis: Model performance and uncertainties. Climate Dynamics. 2013. 41, 1139–1157.

Statistic Canada. (2021b). Demographic estimates by age and sex, provinces and territories. URL: https://www150.statcan.gc.ca/n1/pub/71-607-x/71-607-x2020018-eng.htm (accessed January 24, 2022).

Statistics Canada. (2013). Canadian Survey on Disability, 2012: Concepts and Methods Guide.

Statistics Canada. (2017). Census in Brief Dwellings in Canada.. URL: https://www12.statcan.gc.ca/census-recensement/2016/as-sa/98-200-x/2016005/98-200-x2016005-eng.pdf (accessed January 24, 2022).

Statistics Canada. (2019). Census in Brief Dwellings in Canada. URL: https://www12.statcan.gc.ca/census-recensement/2016/as-sa/98-200-x/2016005/98-200-x2016005-eng.pdf (accessed January 24, 2022).

Statistics Canada. (2021a). Air conditioners. URL: https://www150.statcan.gc.ca/t1/tbl1/en/tv.action?pid=3810001901 (accessed January 24, 2022).

Stazi, F., Tomassoni, E., Perna, C. (2017). Super-insulated wooden envelopes in Mediterranean climate: Summer overheating, thermal comfort optimization, environmental impact on an Italian case study. Energy and Buildings. 138, 716-732

Sarbu, I., Pacurar, C. (2015). Experimental and numerical research to assess indoor environment quality and schoolwork performance in university classrooms. Building and Environment. 93, 141-154

Tabadkani, A., Roetzel, A., Li, H.X., et al. (2021). Design approaches and typologies of adaptive facades: a review. Automation in Construction. 121, 103450

Taylor, J., Davies, M., Mavrogianni, A., et al. (2014). The relative importance of input weather data for indoor overheating risk assessment in dwellings. Building and Environment. 76, 81-91

Thomson, A., Calvin, K., Smith, S., et al. (2011). RCP4.5: a pathway for stabilization of radiative forcing by 2100. Climatic Change. 109, 77-94

The Weather Network . (2020). 36.6 ° C in Montreal: the 2nd hottest brand in history. https://www.meteomedia.com/ke/nouvelles/article/record-de-chaleur-battu-a-montreal-mai-2020 (accessed January 24, 2022).

Tian, W. (2013). A review of sensitivity analysis methods in building energy analysis. Renewable and Sustainable Energy Reviews. 20, 411-419

Tian, W., Wilde, P. Li, Z. et al. (2018). Uncertainty and sensitivity analysis of energy assessment for office buildings based on Dempster-Shafer theory. Energy Conversion and Management. 174, 705-718

Tian, W., Yang, S., Li, Z., et al. (2016). Identifying informative energy data in Bayesian calibration of building energy models. Energy and Buildings. 119. 363-376,

Tink, V., Porritt, S., Allinson, D., Loveday, D. (2018). Measuring and mitigating overheating risk in solid wall dwellings retrofitted with internal wall insulation. Building and Environment. 14, 247-261

Touchie, M., Tzekova, E., Jeffery, S., et al. (2016). Evaluate Summertime Overheating in Multi-Unit Residential Buildings Using Surveys and In-Suite Monitoring. Thermal Performance of the Exterior Envelopes of Whole Buildings XIII International Conference, ASHRAE, 135-151.

Troup, L., Fannon, D. (2016). Morphing Climate Data to Simulate Building Energy Consumption. ASHRAE and IBPSA-USA SimBuild 2016. Building Performance Modeling Conference, Salt Lake City, UT, August 8-12.

Uguen-Csenge, E., Lindsay, B. (2021). For 3rd straight day, B.C. village smashes record for highest Canadian temperature at 49.6 C. CBC News

U.S. Department of Energyr. (1997). IPMVP International Performance Measurement and Verification Protocol.

U.S. Energy Information Administration (EIA). (2016). Commercial Buildings Energy Consumption Survey (CBECS)-Table B6. Building size, number of buildings 2012.

UN-Environment. (2017). Towards a zero-emission, efficient, and resilient buildings and construction sector-global status report 2017. 45 pages

United Nations Educational, Scientific and Cultural Organization UNESCO. (2017). More Than One-Half of Children and Adolescents Are Not Learning Worldwide. Fact sheet No.6.

Uribe, D., Vera, S., Bustamante, W., et al. (2019). Impact of different control strategies of perforated curved louvers on the visual comfort and energy consumption of office buildings in different climates. Solar Energy. 190, 495-510.

Valeria, DG, Osvaldo, DP, Michele, DC. (2012). Indoor environmental quality and pupil perception in Italian primary schools. Building and Environment. 56: 335–345.

Valitabar, M., Moghimi, M., Mahdavinejad, M., et al. (2018). Design optimal responsive facade based on visual comfort and energy performance. 23rd International Conference on Computer-Aided Architectural Design Research in Asia: Learning, Prototyping and Adapting, CAADRIA, 2, Beijing, China. 93-102

Vanhoutteghem, L., Skarning, G.C.J., Hviid, C.A.,et al. (2015). Impact of Façade Window Design on Energy, Daylighting and Thermal Comfort in Nearly Zero-Energy Houses. Energy and Buildings. 102,149-156.

Vikhar, P. A. (2016). Evolutionary algorithms: A critical review and its future prospects. Proceedings of the 2016 International Conference on Global Trends in Signal Processing, Information Computing and Communication (ICGTSPICC). 261–265

Ville de Montréal. (2017). Climate Change Adaptation Plan for The Montreal Urban Agglomeration 2015-2020. 245 pages.

Virk, G., Jansz, A., Mavrogianni, A., et al. (2014) The effectiveness of retrofitted green and cool roofs at reducing overheating in a naturally ventilated office in London: Direct and indirect effects in current and future climates. 23,504-520

Vrac, M., Friederichs, P. (2015) Multivariate-intervariable, spatial, and temporal-bias correction. Journal of Climate. 28, 218–237

Vuuren, D., Edmonds, J., Kainuma, M., et al. (2011a). The representative concentration pathways: an overview. Climatic Change. 109, 22-50

Vuuren, D., Stehfest, E., Elzen, M., et al. (2011). RCP2.6: exploring the possibility to keep global mean temperature increase below 2 °C. Climatic Change. 109, 95-116.

Wang, L., Liu, X., Brown, H. (2017). Prediction of the impacts of climate change on energy consumption for a medium-size office building with two climate models. Energy and Buildings. 175, 218-226

Ward, R. (1925). The Climates of the United States. Creative Media Partners publisher. 544 page.

Wargocki, P. Wyon, P. (2013). Providing better thermal and air quality conditions in school classrooms would be cost- effective. Building and Environment. 59, 581-589.

Wargocki, P., Wyon, P. (2017). Ten questions concerning thermal and indoor air quality effects on the performance of office work and schoolwork. Building and Environment. 112, 359-366.

Watts, N., Amann, M., Arnell, N., et al. (2018). The 2018 Report of the Lancet Countdown on health and climate change: Shaping the Health of Nations for Centuries to Come. Lancet. 392. 2479–2514

WCRP (2014). WCRP Coupled Model Inter-comparison Project (CMIP). URL: https://www.wcrp-climate.org/wgcm-cmip (accessed January 24, 2022).

WCRP. (2021). CMIP6-endorsed MIPs. URL: https://www.wcrp-climate.org/modelling-wgcm-mip-catalogue/modelling-wgcm-cmip6-endorsed-mips (accessed January 24, 2021).

Weedon, G.P., Balsamo, G., Bellouin, N., et al. (2014). The WFDEI meteorological forcing data set: WATCH forcing data methodology applied to ERA-interim reanalysis data. Water Resources Researcher. 50, 505-7514. URL: https://cds.climate.copernicus.eu/#!/search?text=era5 (accessed January 24, 2021).

Westphal, F.S., Lamberts, R. (2005). Building Simulation Calibration Using Sensitivity Analysis. In Proceedings of the Ninth International IBPSA Conference, Montréal, QC, Canada. 1331–1338

White, L., Wright, G. (2019). Assessing resiliency and passive survivability in multifamily buildings. Thermal performance of the exterior envelopes of whole buildings XIV international conference. 123-134

White-Newsome, J. L., Sanchez, B. N., Jolliet, O., et al. (2012). Climate change and health: indoor heat exposure in vulnerable populations. Environmental Research. 112, 20-27

Wilcke RAI, Mendlik T, Gobiet A. (2013) Multi-variable error correction of regional climate models. Climate Change. 120, 871–887.

Wilson, A. (2015). LEED Pilot Credits on Resilient Design Adopted. U.S. Green Building Council (USGBC). http://www.resilientdesign.org/leed-pilot-credits-on-resilient-design-adopted/ (accessed January 24, 2021).

Winkler, J., Horowitz, S., DeGraw, J., Merket, N. (2016). Evaluating EnergyPlus Airflow Network Model for Residential Ducts, Infiltration, and Interzonal Airflow. NREL National renewable energy laboratory. PR-550-70230

Woodward, P. (2011). Bayesian analysis made simple: an excel GUI for WinBUGS. Taylor & Francis

Xu, C., Gertner, G. (2011). Understanding and comparisons of different sampling approaches for the Fourier Amplitudes Sensitivity Test (FAST). Computational statistics & data analysis. 55, 184-198.55 184-198

Yang, M.D., Lin, M.D., Lin, Y.H., et al. (2017). Multi-objective optimization design of green building envelope material using a non-dominated sorting genetic algorithm. Applied Thermal Engineering. 111, 1255-1264

Yang, S., Fiorito, F., Prasad, D., et al. (2021). A sensitivity analysis of design parameters of BIPV/T-DSF in relation to building energy and thermal comfort performances. Building Engineering. 41, 10242

Yang, T., Pan, Y., Mao, J., et al. (2016). An automated optimization method for calibrating building energy simulation models with measured data: Orientation and a case study. Apply Energy. 179, 1220–1231.

Zero Carbon Hub. (2015). Overheating in Homes, the Big Picture. Full Report91 pages; Zero Carbon Hub: London, UK.

Zeferina, V., Wood, F., Edwards, R. et al. (2021). Sensitivity analysis of cooling demand applied to a large office building. Energy and Buildings. 235, 110703

Zhai, Y.N., Wang, Y., Huang, Y.Q., et al. (2019). A multi-objective optimization methodology for window design considering energy consumption, thermal environment and visual performance. Renewable Energy. 134, 1190-1199

Zhai, Z., Johnson, M.H., Krarti, M. (2011). Assessment of natural and hybrid ventilation models in whole-building energy simulations. Energy and Buildings. 43, 2251-2261.

Zhang, A., Bokel, R., Dobbelsteen, A., et al. (2017). Optimization of thermal and daylight performance of school buildings based on a multi-objective genetic algorithm in the cold climate of China. Energy and Buildings. 139, 371-384

Zhang, X., Flato, G., Kirchmeier-Young, M., et al. (2019). Changes in Temperature and Precipitation Across Canada. In Canada's Changing Climate Report; Bush, E., Lemmen, D.S., Eds.; Government of Canada: Ottawa, ON, Canada. 112–193.

Zhang, Y. (2012). Use jEPlus as an Efficient Building Design Optimisation Tool. CIBSE ASHRAE Technical Symposium, Imperial College, London UK. URL: https://www.jeplus.org/wiki/doku.php?id=docs:jeplus_ea:start (accessed January 24, 2021).

Zhang, Y., Korolija, I. (2015). jEPlus - An EnergyPlus simulation manager for parametric. URL: http://www.jeplus.org/wiki/doku.php (accessed January 24, 2021).

Zhang, Y., Korolija, I. (2020). jEPlus+EA. URL: http://www.jeplus.org/wiki/doku.php?id=start (accessed January 24, 2021).

APPENDIX A:

A.1 FUTURE CLIMATE CODES

Extract data from multiple Nedcdf files Code

Python code:

```
import glob
from netCDF4 import Dataset
import pandas as pd
import numpy as np


# Record all the years of the netCDF files into a Python list
year1=2001
year2=year1+20


all_years = []


for file in glob.glob('*.nc'):
  #print(file)
   data = Dataset(file, 'r')
   time = data.variables['time']


for year in range(year1, year2):
   all_years.append(year)
```

```
#Creating an empty Pandas DataFrame covering the whole range of data
year_start = min(all_years)
end_year = max(all_years)
date_range = pd.date_range(start = str(year_start) + '-01-01',
                           end = str(end_year) + '-12-31 21:00:00',
                           freq = '3H')
df = pd.DataFrame(0.0, columns = ['tas'], index = date_range)

# Defining the lat, lon for the location of your interest
lat_place= 45.50
lon_place= -73.56

# Sorting the all_years python list
all_years.sort()

for yr in all_years:
    # Reading-in the data
    data = Dataset(str(yr)+'.nc', 'r')

    # Storing the lat and lon data of the netCDF file into variables
    lat = data.variables['rlat'][:]
    lon = data.variables['rlon'][:]

    # Squared difference between the specified lat,lon and the lat,lon of the netCDF
```

```
    sq_diff_lat = (lat - lat_place)**2
    sq_diff_lon = (lon - lon_place)**2

    # Identify the index of the min value for lat and lon
    min_index_lat = sq_diff_lat.argmin()
    min_index_lon = sq_diff_lon.argmin()

    # Accessing the average temparature data
    temp = data.variables['tas'][:]
    temp=temp-273.15

    # Creating the date range for each year during each iteration
    start = str(yr) + '-01-01'
    end = str(yr) + '-12-31 21:00:00'
    d_range = pd.date_range(start = start,
                            end = end,
                            freq = '3H')

    for t_index in np.arange(0, len(d_range)):
        print('Recording the value for: ' + str(d_range[t_index]))
        df.loc[d_range[t_index]]['tas'] = temp[t_index, min_index_lat, min_index_lon]

df.to_csv('Temperature'+str(year1)+'_'+str(year2)+'.csv')
```

Convert 3hr to 1 hr code

Python code:

```
import pvlib

from pvlib.location import Location

import glob

from netCDF4 import Dataset

import pandas as pd

import numpy as np


# you need 1. change path 2. the year in idx_30min 3. year in df and dbt_30min.plot()

path = r'C:\Users\umroot\Desktop\PhD\Future Climate\Annex80 Weather data workshop\Tas 2001-2020\Temperature2001_2021.csv'


df = pd.read_csv(path,index_col=0,header=0)

df.index = pd.to_datetime(df.index)



# Function to interpolate the temperature every 60 min


def interpolate_30min_poly_temp(s, idx_30min):


    # Redindexing the series to 30min time-step and interpolating to 30min time-step

    s_30min = s.reindex(idx_30min).interpolate('polynomial',order=7)
```

```
    # Filling the 1st and 2nd values with the 3rd and the last 3 values with the last 4th value
    last = s_30min.iloc[len(s_30min)-4]
    s_30min.iloc[len(s_30min)-3:len(s_30min)] = [last, last, last]
    first = s_30min[2]
    s_30min[0] = first
    s_30min[1] = first

    return s_30min

# Defining an index every 60 min dbt_30 min is the results
idx_30min = pd.date_range(start='1/1/2001', end='31/12/2020 21:00:00', freq='1h')
# Calling the function
dbt_30min = interpolate_30min_poly_temp(df['tas'], idx_30min)
bf=dbt_30min
#Plot of results: just change the year
df['tas']['2007-01-03'].plot(marker="*")
bf['2007-01-03'].plot()

bf.to_csv('Temperature 1996-2015 hourly.csv')
```

Calculate Bias Correlation

This code is develop by Dr. Abhishek Gaur

National Research Council Canada

Abhishek.Gaur@nrc-cnrc.gc.ca; +1-613-998-9799

R-studio code:

```
# A demonstration of bias correction for the city of Montreal is performed.
# set working directory to "demonstration package" folder
setwd("C:/Users/umroot/Desktop/PhD/Future Climate/Annex80 Weather data workshop")
# Data required are kept in "./input data" folder:
# 1. Observational data
# 2. RCM data for:
# a) observational time-period
# b) RCM: 2001-2020, 2041-2060, 2081-2100
library(lubridate) # for date time operations
obs_cal=read.csv("./Bias Correlation/obs_Singapora airport_1996_2015.csv")
rcm_cal=read.csv("./Bias Correlation/rcm_Singapora airport_1996_2015.csv")
rcm_2050s=read.csv("./Bias Correlation/rcm_Singapora airport 2041-2060.csv")
rcm_2090s=read.csv("./Bias Correlation/rcm_Singapora airport 2081-2100.csv")
# reframing data for bias correction
obs_cal=cbind(obs_cal$tas_degc,obs_cal$hurs_per,
              obs_cal$ps_pa,obs_cal$wsp_mpers)
rcm_cal=cbind(rcm_cal$tas_degc,rcm_cal$hurs_per,
              rcm_cal$ps_pa,rcm_cal$wsp_mpers)
#rcm_2010s=cbind(rcm_2010s$tas_degc,rcm_2010s$hurs_per,
#               rcm_2010s$ps_pa,rcm_2010s$wsp_mpers)
rcm_2050s=cbind(rcm_2050s$tas_degc,rcm_2050s$hurs_per,
              rcm_2050s$ps_pa,rcm_2050s$wsp_mpers)
rcm_2090s=cbind(rcm_2090s$tas_degc,rcm_2090s$hurs_per,
              rcm_2090s$ps_pa,rcm_2090s$wsp_mpers)
```

```
# dataframe of ratio and trace
ratio_trace_df=data.frame(varnames=c("tas_degc","hurs_per","ps_pa","wsp_mpers"),
                          ratio.seq=c("FALSE","TRUE","TRUE","TRUE"),
                          trace=c(Inf,0.0,10,0.1))
# MBCn model calibration and prediction
library(MBC)
# Apply the MBCn methods
set.seed(1)
MBCout_2050s=MBCn(o.c=obs_cal,
                  m.c=rcm_cal,
                  m.p=rcm_2050s,
                  ratio.seq=ratio_trace_df$ratio.seq,
                  trace=ratio_trace_df$trace)
set.seed(1)
MBCout_2090s=MBCn(o.c=obs_cal,
                  m.c=rcm_cal,
                  m.p=rcm_2090s,
                  ratio.seq=ratio_trace_df$ratio.seq,
                  trace=ratio_trace_df$trace)
# post-processing checks:
# ensure all variables are within the expected range
rcm_bc_cal=data.frame(MBCout_2050s[[1]])
colnames(rcm_bc_cal)=ratio_trace_df$varnames
# rain should be >=0.1
```

```
if(any(rcm_bc_cal$rain_mm<0.1))
  rcm_bc_cal$rain_mm[which(rcm_bc_cal$rain_mm<0.1)]=0
# wdr should be 0-360
if(any(rcm_bc_cal$wdr_deg<0))
rcm_bc_cal$wdr_deg[which(rcm_bc_cal$wdr_deg<0)]=360+rcm_bc_cal$wdr_deg[which(rcm_
bc_cal$wdr_deg<0)]
if(any(rcm_bc_cal$wdr_deg>=360))
rcm_bc_cal$wdr_deg[which(rcm_bc_cal$wdr_deg>=360)]=rcm_bc_cal$wdr_deg[which(rcm_b
c_cal$wdr_deg>=360)]-360
# wsp should be >=0
if(any(rcm_bc_cal$wsp_mpers<0))
  rcm_bc_cal$wsp_mpers[which(rcm_bc_cal$wsp_mpers<0)]=0
# no checks for tas
# rsds should be >=0
if(any(rcm_bc_cal$rsds_kjperm2<0))
  rcm_bc_cal$rsds_kjperm2[which(rcm_bc_cal$rsds_kjperm2<0)]=0

# ps should be >=0
if(any(rcm_bc_cal$ps_pa<0))
  rcm_bc_cal$ps_pa[which(rcm_bc_cal$ps_pa<0)]=0
# hurs should be 0-100
if(any(rcm_bc_cal$hurs_per<0))
  rcm_bc_cal$hurs_per[which(rcm_bc_cal$hurs_per<0)]=0
if(any(rcm_bc_cal$hurs_per>100))
  rcm_bc_cal$hurs_per[which(rcm_bc_cal$hurs_per>100)]=100
```

```
# clt should be 0-100
if(any(rcm_bc_cal$clt_per<0))
  rcm_bc_cal$clt_per[which(rcm_bc_cal$clt_per<0)]=0
if(any(rcm_bc_cal$clt_per>100))
  rcm_bc_cal$clt_per[which(rcm_bc_cal$clt_per>100)]=100
# snd should be >=1
if(any(rcm_bc_cal$snd_cm<1))
  rcm_bc_cal$snd_cm[which(rcm_bc_cal$snd_cm<1)]=0
rcm_bc_2010s=data.frame(MBCout_2010s[[2]])
colnames(rcm_bc_2010s)=ratio_trace_df$varnames
# rain should be >=0.1
if(any(rcm_bc_2010s$rain_mm<0.1))
  rcm_bc_2010s$rain_mm[which(rcm_bc_2010s$rain_mm<0.1)]=0
# wdr should be 0-360
if(any(rcm_bc_2010s$wdr_deg<0))
rcm_bc_2010s$wdr_deg[which(rcm_bc_2010s$wdr_deg<0)]=360+rcm_bc_2010s$wdr_deg[whi
ch(rcm_bc_2010s$wdr_deg<0)]
if(any(rcm_bc_2010s$wdr_deg>=360))
rcm_bc_2010s$wdr_deg[which(rcm_bc_2010s$wdr_deg>=360)]=rcm_bc_2010s$wdr_deg[whic
h(rcm_bc_2010s$wdr_deg>=360)]-360
# wsp should be >=0
if(any(rcm_bc_2010s$wsp_mpers<0))
  rcm_bc_2010s$wsp_mpers[which(rcm_bc_2010s$wsp_mpers<0)]=0
# no checks for tas
# rsds should be >=0
```

```
if(any(rcm_bc_2010s$rsds_kjperm2<0))
  rcm_bc_2010s$rsds_kjperm2[which(rcm_bc_2010s$rsds_kjperm2<0)]=0
# ps should be >=0
if(any(rcm_bc_2010s$ps_pa<0))
  rcm_bc_2010s$ps_pa[which(rcm_bc_2010s$ps_pa<0)]=0
# hurs should be 0-100
if(any(rcm_bc_2010s$hurs_per<0))
  rcm_bc_2010s$hurs_per[which(rcm_bc_2010s$hurs_per<0)]=0
if(any(rcm_bc_2010s$hurs_per>100))
  rcm_bc_2010s$hurs_per[which(rcm_bc_2010s$hurs_per>100)]=100
# clt should be 0-100
if(any(rcm_bc_2010s$clt_per<0))
  rcm_bc_2010s$clt_per[which(rcm_bc_2010s$clt_per<0)]=0
if(any(rcm_bc_2010s$clt_per>100))
  rcm_bc_2010s$clt_per[which(rcm_bc_2010s$clt_per>100)]=100
# snd should be >=1
if(any(rcm_bc_2010s$snd_cm<1))
  rcm_bc_2010s$snd_cm[which(rcm_bc_2010s$snd_cm<1)]=0
rcm_bc_2050s=data.frame(MBCout_2050s[[2]])
colnames(rcm_bc_2050s)=ratio_trace_df$varnames
# rain should be >=0.1
if(any(rcm_bc_2050s$rain_mm<0.1))
  rcm_bc_2050s$rain_mm[which(rcm_bc_2050s$rain_mm<0.1)]=0
# wdr should be 0-360
```

```
if(any(rcm_bc_2050s$wdr_deg<0))
rcm_bc_2050s$wdr_deg[which(rcm_bc_2050s$wdr_deg<0)]=360+rcm_bc_2050s$wdr_deg[which(rcm_bc_2050s$wdr_deg<0)]
if(any(rcm_bc_2050s$wdr_deg>=360))
rcm_bc_2050s$wdr_deg[which(rcm_bc_2050s$wdr_deg>=360)]=rcm_bc_2050s$wdr_deg[which(rcm_bc_2050s$wdr_deg>=360)]-360
# wsp should be >=0
if(any(rcm_bc_2050s$wsp_mpers<0))
  rcm_bc_2050s$wsp_mpers[which(rcm_bc_2050s$wsp_mpers<0)]=0
# no checks for tas
# rsds should be >=0
if(any(rcm_bc_2050s$rsds_kjperm2<0))
  rcm_bc_2050s$rsds_kjperm2[which(rcm_bc_2050s$rsds_kjperm2<0)]=0
# ps should be >=0
if(any(rcm_bc_2050s$ps_pa<0))
  rcm_bc_2050s$ps_pa[which(rcm_bc_2050s$ps_pa<0)]=0
# hurs should be 0-100
if(any(rcm_bc_2050s$hurs_per<0))
  rcm_bc_2050s$hurs_per[which(rcm_bc_2050s$hurs_per<0)]=0

if(any(rcm_bc_2050s$hurs_per>100))
  rcm_bc_2050s$hurs_per[which(rcm_bc_2050s$hurs_per>100)]=100
# clt should be 0-100
if(any(rcm_bc_2050s$clt_per<0))
  rcm_bc_2050s$clt_per[which(rcm_bc_2050s$clt_per<0)]=0
```

```
if(any(rcm_bc_2050s$clt_per>100))
  rcm_bc_2050s$clt_per[which(rcm_bc_2050s$clt_per>100)]=100
# snd should be >=1
if(any(rcm_bc_2050s$snd_cm<1))
  rcm_bc_2050s$snd_cm[which(rcm_bc_2050s$snd_cm<1)]=0
rcm_bc_2090s=data.frame(MBCout_2090s[[2]])
colnames(rcm_bc_2090s)=ratio_trace_df$varnames
# rain should be >=0.1
if(any(rcm_bc_2090s$rain_mm<0.1))
  rcm_bc_2090s$rain_mm[which(rcm_bc_2090s$rain_mm<0.1)]=0
# wdr should be 0-360
if(any(rcm_bc_2090s$wdr_deg<0))

rcm_bc_2090s$wdr_deg[which(rcm_bc_2090s$wdr_deg<0)]=360+rcm_bc_2090s$wdr_deg[whi
ch(rcm_bc_2090s$wdr_deg<0)]
if(any(rcm_bc_2090s$wdr_deg>=360))

rcm_bc_2090s$wdr_deg[which(rcm_bc_2090s$wdr_deg>=360)]=rcm_bc_2090s$wdr_deg[whic
h(rcm_bc_2090s$wdr_deg>=360)]-360
# wsp should be >=0
if(any(rcm_bc_2090s$wsp_mpers<0))
  rcm_bc_2090s$wsp_mpers[which(rcm_bc_2090s$wsp_mpers<0)]=0
# no checks for tas
# rsds should be >=0
if(any(rcm_bc_2090s$rsds_kjperm2<0))
```

```
 rcm_bc_2090s$rsds_kjperm2[which(rcm_bc_2090s$rsds_kjperm2<0)]=0
# ps should be >=0
if(any(rcm_bc_2090s$ps_pa<0))
 rcm_bc_2090s$ps_pa[which(rcm_bc_2090s$ps_pa<0)]=0
# hurs should be 0-100
if(any(rcm_bc_2090s$hurs_per<0))
 rcm_bc_2090s$hurs_per[which(rcm_bc_2090s$hurs_per<0)]=0
if(any(rcm_bc_2090s$hurs_per>100))
 rcm_bc_2090s$hurs_per[which(rcm_bc_2090s$hurs_per>100)]=100
# clt should be 0-100
if(any(rcm_bc_2090s$clt_per<0))
 rcm_bc_2090s$clt_per[which(rcm_bc_2090s$clt_per<0)]=0
if(any(rcm_bc_2090s$clt_per>100))
 rcm_bc_2090s$clt_per[which(rcm_bc_2090s$clt_per>100)]=100
# snd should be >=1
if(any(rcm_bc_2090s$snd_cm<1))
 rcm_bc_2090s$snd_cm[which(rcm_bc_2090s$snd_cm<1)]=0
# has bias correction worked?
obs_cal=data.frame(obs_cal)
colnames(obs_cal)=ratio_trace_df$varnames
rcm_cal=data.frame(rcm_cal)
colnames(rcm_cal)=ratio_trace_df$varnames
summary(obs_cal)
summary(rcm_cal)
```

```
summary(rcm_bc_cal)
#Export to CSV
write.csv(rcm_bc_2050s,file="./outputs/RCM Bias Correlation-2050.csv" )
write.csv(rcm_bc_2090s,file="./outputs/RCM Bias Correlation-2090.csv" )
# comparison of PDFs
library(ggplot2)
ggplot()+
  geom_density(data=obs_cal,aes(x=tas_degc),color="grey50",size=6)+
  geom_density(data=rcm_cal,aes(x=tas_degc),color="blue",size=2)+
  geom_density(data=rcm_bc_cal,aes(x=tas_degc),color="red",size=2)+
  xlab("Temperature (ɨC)")+ylab("Density")+theme_bw()+
  theme(legend.position = "none")+
  theme(axis.title.x = element_text(size=21,face = "bold",vjust=1),
        axis.title.y = element_text(size=21,face = "bold"),
        axis.text.x = element_text(size=21),
        axis.text.y = element_text(size=21),
        legend.title = element_text(size=21,face = "bold"),
        legend.text=element_text(size=21),text = element_text(size=21))
ggsave("./outputs/PDFs_tas_degc_obs_rcm_bcrcm.png",width=12,height=10)
ggplot()+
  geom_density(data=obs_cal,aes(x=wsp_mpers),color="grey50",size=6)+
  geom_density(data=rcm_cal,aes(x=wsp_mpers),color="blue",size=2)+
  geom_density(data=rcm_bc_cal,aes(x=wsp_mpers),color="red",size=2)+
  xlab("wind speed (m/s)")+ylab("Density")+theme_bw()+
```

```
  theme(legend.position = "none")+
  theme(axis.title.x = element_text(size=21,face = "bold",vjust=1),
        axis.title.y = element_text(size=21,face = "bold"),
        axis.text.x = element_text(size=21),
        axis.text.y = element_text(size=21),
        legend.title = element_text(size=21,face = "bold"),
        legend.text=element_text(size=21),text = element_text(size=21))
ggsave("./outputs/PDFs_wsp_mpers_obs_rcm_bcrcm.png",width=12,height=10)
# impact on projected changes
#summary(rcm_bc_2010s)
summary(rcm_bc_2050s)
summary(rcm_bc_2090s)



ggplot()+
  #geom_density(data=rcm_bc_2010s,aes(x=tas_degc),color="black",size=2)+
  geom_density(data=rcm_bc_2050s,aes(x=tas_degc),color="blue",size=2)+
  geom_density(data=rcm_bc_2090s,aes(x=tas_degc),color="red",size=2)+
  xlab("Temperature (C)")+ylab("Density")+theme_bw()+
  theme(legend.position = "none")+
  theme(axis.title.x = element_text(size=21,face = "bold",vjust=1),
        axis.title.y = element_text(size=21,face = "bold"),
        axis.text.x = element_text(size=21),
        axis.text.y = element_text(size=21),
```

```
      legend.title = element_text(size=21,face = "bold"),
      legend.text=element_text(size=21),text = element_text(size=21))
ggsave("./outputs/PDFs_tas_degc_2010s_2050s_2090s.png",width=12,height=10)
ggplot()+
  #geom_density(data=rcm_bc_2010s,aes(x=wsp_mpers),color="black",size=2)+
  geom_density(data=rcm_bc_2050s,aes(x=wsp_mpers),color="blue",size=2)+
  geom_density(data=rcm_bc_2090s,aes(x=wsp_mpers),color="red",size=2)+
  xlab("Wind speed (m/s)")+ylab("Density")+theme_bw()+
  theme(legend.position = "none")+
  theme(axis.title.x = element_text(size=21,face = "bold",vjust=1),
      axis.title.y = element_text(size=21,face = "bold"),
      axis.text.x = element_text(size=21),
      axis.text.y = element_text(size=21),
      legend.title = element_text(size=21,face = "bold"),
      legend.text=element_text(size=21),text = element_text(size=21))
ggsave("./outputs/PDFs_wsp_mpers_2010s_2050s_2090s.png",width=12,height=10)
```

Detect RSWY

```
from __future__ import division
import pandas as pd
import numpy as np
import matplotlib.pyplot as plt
from matplotlib.patches import Circle
from matplotlib.collections import PatchCollection
```

```
#  These data (path_hist) MUST BE 20 YEARS OF BIAS-ADJUSTED DATA
path_hist = r'C:\Users\umroot\Desktop\PhD\Future Climate\Annex80 Weather data workshop\Heat waves\RCM Bias Correlation-2090.csv'
path= r'C:\Users\umroot\Desktop\PhD\Future Climate\Annex80 Weather data workshop\Heat waves\RCM Bias Correlation-2090.csv'

df_hist = pd.read_csv(path_hist, index_col=0)
df_hist.index = pd.to_datetime(df_hist.index)

df_future = pd.read_csv(path, index_col=0)
df_future.index = pd.to_datetime(df_future.index)

#temp_hist = df_hist['1986':'2005'].squeeze().resample('24H').mean() # Keeping only 20 years and calculating daily temperature means
# If data imported are already 20 years, please use this line instead of above line:
temp_hist = df_hist.squeeze().resample('24H').mean()
temp_future = df_future['tas'].squeeze().resample('24H').mean()

# Temperature thresholds to characterize heatwaves
spic = temp_hist.quantile(0.990)
sdeb = temp_hist.quantile(0.970)
sint = temp_hist.quantile(0.940)

# This function detects heatwaves over a 20 years dataset.
```

```
# It returns a list of heatwaves, the heatwaves, a list of their severities a list of their duration, and a list of their Tmax


def get_dict_hws(daily_temp, spic, sdeb, sint):


    # Creating result, an empty dataframe with a series of 20 years daily temperatures

    result = pd.DataFrame({'Daily_Temp': daily_temp, 'sup_SPIC':"", '>SDEB':"", 'cons_SDEB':""})

    result['month']=result.index.month


    # Analysing only months from June to September included. !!! These must be replaced according to the summer period of the city of interest !!!

    filter_mask = (result['month'] > 5) & (result['month'] < 10)

    df = result[filter_mask]

    df.index = pd.to_datetime(df.index)

    del df['month']


    # Finding where the daily temperature exceeds the threshold SPIC

    df['sup_SPIC'] = np.where(df['Daily_Temp']>spic,df['Daily_Temp'],int(0))


    # Finding where the daily temperature exceeds the threshold SDEB

    df['>SDEB'] = np.where(df['Daily_Temp']>sdeb,df['Daily_Temp'],int(0))


    # Adding all the temperatures above the SDEB threshold to temp_sdeb

    temp_sdeb = df['>SDEB'].tolist()
```

```
    # Analyzing if temperatures are consecutive with a minimum of 3 days gap. If yes, filling the 'in between' days wit h1
    for i in range(0,len(temp_sdeb)-4):

        if ((temp_sdeb[i]!=0) and (temp_sdeb[i+4]!=0)):
            temp_sdeb[i+1]=1
            temp_sdeb[i+2]=1
            temp_sdeb[i+3]=1

        if ((temp_sdeb[i]!=0) and (temp_sdeb[i+3]!=0)):
            temp_sdeb[i+1]=1
            temp_sdeb[i+2]=1

        if ((temp_sdeb[i]!=0) and (temp_sdeb[i+2]!=0)):
            temp_sdeb[i+1]=1


    # Adding the list temp_sdeb to the dataframe column 'cons_SDEB'
    df['cons_SDEB'] = temp_sdeb

    # Replacing the 1 values with the temperature
    df['cons_SDEB'] = np.where(df['cons_SDEB']==1,df['Daily_Temp'],df['cons_SDEB'])
```

```
# Filling with 0 if the heatwaves temperatures fall under the SINT threshold
df['cons_SDEB'] = np.where(df['cons_SDEB']<sint,int(0),df['cons_SDEB'])

# Keeping only the heatwaves temperatures where there is no 0
df_reduit = df.loc[(df['cons_SDEB']!=0)]
del df_reduit['Daily_Temp']
del df_reduit['>SDEB']

# Storing in hws a list of heatwaves (sorting through consecutive days)
hws_idx = []

for i in range(0, len(df_reduit)):
    if (df_reduit.index.dayofyear[i]-df_reduit.index.dayofyear[i-1])!=1:
        hws_idx.append(int(np.where(df_reduit.index==df_reduit.index[i])[0]))

hws = []
for i in range(0, len(hws_idx)-1):
    hws.append(df_reduit.iloc[hws_idx[i]:hws_idx[i+1]])

for i in range(len(hws_idx)-1, len(hws_idx)):
    hws.append(df_reduit.iloc[hws_idx[i]:len(df_reduit)])

## Keeping in hws2 only the hws for which there is a temp > SPIC
hws2 = []
```

```
for i in range(0, len(hws)):
    for a in range(0, len(hws[i])):
        if (hws[i]['sup_SPIC'][a]) > 1:
            hws2.append(hws[i])
            break


## Keeping in hws3 only the hws that are min 5 days long
hws3 = []
for i in range(0, len(hws2)):
    if len(hws2[i])>=5:
        hws3.append(hws2[i])


# Calculating for each heatwave the severity and adding it to the list severities
severities=[]
for i in range(0, len(hws3)):
    b=0
    for j in range(0, len(hws3[i])):
        if (hws3[i]['cons_SDEB'][j])>sdeb:
            x = (hws3[i]['cons_SDEB'][j])-sdeb
            b=b+x


    severity=b/(spic-sdeb)
    severities.append(severity)
```

```
    # Calculating for each heatwave the length and adding it to the list lenghts
    lenghts=[]
    for i in range(0, len(hws3)):
        lenghts.append(len(hws3[i]))

    # Calculating for each heatwave the Tmax and adding it to the list maxs
    maxs=[]
    for i in range(0, len(hws3)):
        maxs.append(hws3[i]['sup_SPIC'].max())

    # Creating liste_hws, a list of lists containing all heatwaves characteristics
    liste_hws = []
    for (e, f, g, h) in zip(hws3, lenghts, maxs, severities):
         liste_hws.append([e,f,g,h])

    return liste_hws, hws3, severities, lenghts, maxs

# Calling the function


list_hws_hist = get_dict_hws(temp_hist,spic,sdeb,sint)
list_hws_future = get_dict_hws(temp_future,spic,sdeb,sint)

print(list_hws_hist)
```

```
#bf=pd.DataFrame(list_hws_hist, columns = ['','sup_SPIC','cons_SDEB'], index=0.0)
#bff=pd.DataFrame(0.0, columns = ['heat wave'], index = list_hws_future)



#bf.to_csv('heat wave hist.csv')
#bff.to_csv('heat wave 2050.csv')

c='red'
ec='chocolate'

# Creating patches (circles)
patches = []

# For each heatwave:
# x is the lenght
# y is the tmax
# bubblesize is the severity

# Historical heatwaves
for i in range(0, len(list_hws_hist[2])):
    fig_x_hist = list_hws_hist[3][i]
    fig_y_hist = list_hws_hist[4][i]
```

```
        fig_bubblesize_hist = list_hws_hist[2][i]/5
        circle_hist = Circle((fig_x_hist, fig_y_hist), fig_bubblesize_hist, color=c)
        patches.append(circle_hist)

# Future heatwaves
for i in range(0, len(list_hws_future[2])):
        fig_x_future = list_hws_future[3][i]
        fig_y_future = list_hws_future[4][i]
        fig_bubblesize_future= list_hws_future[2][i]/20
        circle_future = Circle((fig_x_future, fig_y_future), fig_bubblesize_future, color=ec)
        patches.append(circle_future)

### `PLOT  ####
p = PatchCollection(patches, match_original=True, edgecolor='black') ## this means that the colors given to the patches will be used
p.set_alpha(0.8) ## SET TRANSPARENCY OF BUBBLES
fig, ax = plt.subplots(figsize=(16, 12))
ax.add_collection(p)
ax.set_aspect('equal') ## keep the circles round
plt.legend([circle_hist, circle_future], ['Historical','Future'],fontsize=18)
plt.ylim(top=60,bottom=0)
plt.xlim(right=100, left=0)
plt.xlabel("Duration (number of days)", fontsize=18)
plt.ylabel("Maximum daily mean Temperature [°C]", fontsize=18)
```

```
plt.title('Heatwaves in Paris: Historical, and Future 2081-2100', fontsize=18)
plt.tight_layout()
plt.show()
```

A.2 CALIBRATION CODE

Determine objectives of calibration

```
{

    "notes" : "Some notes about this RVX",

    "rvis" : [
        {
            "fileName" : "my.rvi",
            "tableName" : "HourlyMeters",
            "frequency" : "Hourly",
            "usedInCalc" : false
        }
    ],

    "sqls" : [
    ],

    "scripts" : [
        {
            "fileName" : "MaxDifference.py",
```

```
                "pythonVersion" : "phython3",
                "onEachJob" : true,
                "arguments" : "HourlyMeters;ref.csv",
                "tableName" : "RMSE"
        }
],

"userVars" : [

],

"constraints" : [
],

"objectives" : [
        {
                "identifier" : "t1",
                "formula" : "(c1)",
                "caption" : "MaxDiff R208 Z5 [C]",
                "scaling" : false,
                "min" : "0",
                "max" : "100000",
                "weight" : "1.0"
        },
```

```
{
        "identifier" : "t2",
        "formula" : "(c3)",
        "caption" : "RMSE R208 Z5 [%]",
        "scaling" : false,
        "min" : "0",
        "max" : "100000",
        "weight" : "1.0"
},
{
        "identifier" : "t3",
        "formula" : "(c5)",
        "caption" : "MaxDiff R203 Z9 [%]",
        "scaling" : false,
        "min" : "0",
        "max" : "100000",
        "weight" : "1.0"
},
{
        "identifier" : "t4",
        "formula" : "(c7)",
        "caption" : "RMSE R203 Z9 [%]",
        "scaling" : false,
        "min" : "0",
```

```
        "max" : "100000",
        "weight" : "1.0"
},
{
        "identifier" : "t5",
        "formula" : "(c9)",
        "caption" : "MaxDiff R200 Z14 [%]",
        "scaling" : false,
        "min" : "0",
        "max" : "100000",
        "weight" : "1.0"
},
{
        "identifier" : "t6",
        "formula" : "(c11)",
        "caption" : "RMSE R200 Z14 [%]",
        "scaling" : false,
        "min" : "0",
        "max" : "100000",
        "weight" : "1.0"
},
{
        "identifier" : "t7",
        "formula" : "(c13)",
```

```
                "caption" : "MaxDiff R212 Z4 [%]",
                "scaling" : false,
                "min" : "0",
                "max" : "100000",
                "weight" : "1.0"
            },
            {
                "identifier" : "t8",
                "formula" : "(c15)",
                "caption" : "RMSE R212 Z4 [%]",
                "scaling" : false,
                "min" : "0",
                "max" : "100000",
                "weight" : "1.0"
            }

        ]
}
```


Calculate evaluation criteria

```
import pandas as pd
import numpy as np
import csv
import sys
import re
```

```
# function which calculates the cv(rmse)
def diff_function(observed, predicted, N):
    error = observed - predicted
    abserror = np.abs(error);
    return np.max(abserror)

# function which calculates the cv(rmse)
def cvrmse_function(observed, predicted, N):
    error = observed - predicted
    sqerror = error ** 2
    sumsqerror = np.sum(sqerror)
    meansqerror = sumsqerror / N
    rmse = np.sqrt(meansqerror)
    cvrmse = 100 * rmse / np.mean(observed);
    return cvrmse

def rmse_function(observed, predicted, N):
        error = observed - predicted
        sqerror = error ** 2
        sumsqerror = np.sum(sqerror)
        meansqerror = sumsqerror / N
        rmse = np.sqrt(meansqerror)
        return rmse
```

```
# function which calculates the normalized mean bias error
def nmbe_function(observed, predicted, N):
    error = predicted - observed
    sbe = np.sum(error)
    mbe = sbe / N
    nmbe = 100 * mbe / np.mean(observed)
    return nmbe



# This script takes
args = sys.argv[4].split(';')

refdata = pd.read_csv(sys.argv[1] + args[1]) #read data from the reference file (path passed from the script)

in_file = sys.argv[2] + args[0] + ".csv"
indata = pd.read_csv(in_file)

rowcolno = indata.shape

#take heading row from the reference file
heading = list(refdata.ix[:1])
newheading = heading[0:1]
```

```
for h in heading [1:]:
    newheading += ['CVRMSE:' + re.sub('\\s*\[.*\].*', '[%]', h)]
    newheading += ['Diff:' + re.sub('\\s*\[.*\].*', '[%]', h)]
    newheading += ['NMBE:' + re.sub('\\s*\[.*\].*', '[%]', h)]
    newheading += ['RMSE:' + re.sub('\\s*\[.*\].*', '[%]', h)]
outname = sys.argv[3] # output file name from the parameter passed to the script

rmsedata = ["NA"]

for column in range(1, rowcolno[1]):
    observed = np.array(refdata.iloc[:, column])
    predicted = np.array(indata.iloc[:, column])
    rmsedata.append(cvrmse_function(observed, predicted, rowcolno[0]))
    rmsedata.append(diff_function(observed, predicted, rowcolno[0]))
    rmsedata.append(nmbe_function(observed, predicted, rowcolno[0]))
    rmsedata.append(rmse_function(observed, predicted, rowcolno[0]))

with open(outname, "w", newline='') as outfile:
    output=csv.writer(outfile)
    output.writerow(newheading)
    output.writerow(rmsedata)
```